

Dissertation ETH number 26666

EMERGING PULSED ELECTRIC FIELD PROCESS DEVELOPMENT FOR BIO-
BASED APPLICATIONS

A thesis submitted to attain the degree of
DOCTOR OF SCIENCES of ETH ZURICH
(Dr. sc. ETH Zurich)

presented by

LEANDRO BUCHMANN

MSc in Food Sciences, ETH Zurich, Zurich, Switzerland

born on 14.12.1991

citizen of Hinwil ZH, Switzerland

accepted on the recommendation of:

Prof. Dr. Alexander Mathys, examiner

Prof. Dr. Erich J. Windhab, co-examiner

Prof. Dr. Damijan Miklavčič, co-examiner

2020

Copyright © 2020 Leandro Buchmann

Laboratory of Sustainable Food Processing (ETH Zurich)

All rights reserved.

EMERGING PULSED ELECTRIC FIELD PROCESS DEVELOPMENT FOR BIO-
BASED APPLICATIONS

ISBN: 978-3-906916-92-7

Sustainable Food Processing series no. 01

Published and distributed by:

Laboratory of Sustainable Food Processing

Institute of Food, Nutrition and Health

ETH Zurich

ETH Zentrum, LFO

8092 Zurich

Switzerland

<http://www.sfp.ethz.ch/>

Printed in Switzerland by:

ETH Print + Publish

HG D 34.1

Rämistrasse 101

8092 Zürich

*Wo kämen wir hin,
wenn alle sagten,
wo kämen wir hin,
und niemand ginge,
um zu sehen,
wohin wir kämen,
wenn wir gingen.*

Kurt Marti (1921-2017), Schweizer Pfarrer, Schriftsteller und Lyriker

Acknowledgements

I would like to genuinely thank Prof. Dr.-Ing. Alexander Mathys for giving me the opportunity to conduct my thesis and being a great mentor, supporter and friend throughout the journey. I'll never forget my interview for the Master's thesis and me saying I would never do a PhD. I'm glad you were persistent and enabled me this phantastic opportunity.

I am grateful for the constant support of Prof. Dr. Erich J. Windhab. It was a great pleasure to discuss my research with you and experience from your great scientific knowledge. A special thank you also enabling the establishment of the PEF Lab in the bunker.

I wish to thank Prof. Dr. Damijan Miklavčič for his constant support throughout my PhD, starting at EBTT 2016 through to my request of being a co-examiner for my exam. It was a great honour to be recognized by such a great researcher in the field.

Sincere thanks to Prof. Dr. Christian Franck. I still can not believe how much support I received from you. You always had an open door for a Food Scientist trying to understand Electrical Engineering and I highly valued your input and guidance.

I wish to express my gratitude to Dr. Hans-Jürg Weber and Dr. Mostafa Refaey, it was an incredible experience to profit from your extensive knowledge and your openness to discuss and implent my ideas.

I wish to thank Dr. Simon Kuster for his encouraging and supportive personality that helped me through some major struggles in my journey.

Sincere thanks to Prof. Dr. Hierlemann and his team around Dr. Mario M. Modena and Paolo S. Ravaynia for their support with the EIS measurements and great discussions.

Very special thanks to Markus Nyffeler for his constant support. You opened up a completely new world to me and guided me in my first steps to measure my first nanosecond pulse and the subsequent achievements. It was always a pleasure to

work with you and I highly appreciated how you welcomed me in your family.

Many thanks to all my students, Robin, Ursina, Ivraina, Jsmea, Daniel and Arnaud, shared students Michèle and Isabelle, research assistants Daniele and Cosima as well as my intern Jana it was a great pleasure to work with you and without your great work I would not be where I am today.

Thank you very much to the whole sustainable food processing and food process engineering group. It was an amazing journey with all of you and I truly appreciated the great atmosphere and constant support.

Special thanks to the LFO F24.2 office and the incredible time we had. I gonna miss the after lunch cute animals and the Friday afternoon tea sessions.

I wish to thank all my collaborators. It was a great experience working with you and I am truly thankful for your constant support of a young researcher.

A special thanks goes to Dani, Bruno, Peter, Bernie, Horst and Jan, this journey would not have been possible without you. I know I was not always the easiest PhD, but you always had an open ear for my crazy ideas and I received a level of support I could not have dreamed off. I will always be grateful for your constant support.

I wish to express my sincerest thanks to my family and friends. Thank you very much for being there when I needed you most. Your support is invaluable and I would not be the person I am today without you. I am sincerely grateful to have you in my life.

Last but not least, thank you very much Maya for always having my back. No matter what, I know you would support me and always be there for me. I could not have done it without you.

TABLE OF CONTENTS

Notation.....	IX
Latin Letters.....	IX
Greek Letters.....	XI
Abbreviations.....	XII
Summary.....	XI
Zusammenfassung.....	XIII
Introduction	1
1. Pulsed Electric Field Fundamentals	2
1.1. Pulse generation	3
1.2. Treatment chamber design	5
2. Flow Field Analysis.....	8
2.1. Importance of flow field analysis	8
2.2. Numerical simulations in PEF research	10
2.3. Physics underlying fluid dynamics simulations.....	10
2.4. Non-invasive flow field measurement	12
2.5. Rheological analysis	13
3. Biological Applications.....	15
3.1. PEF applications in the food- and bioprocessing industry.....	20
References	28
Manuscript 1.....	36
Abstract	37

1.	Introduction.....	38
1.1.	Electrical principles of nsPEF.....	39
1.2.	Energy input calculations in nsPEF systems	40
1.3.	Potential of nsPEF for microalgae applications.....	41
2.	Materials and methods	43
2.1.	Experimental equipment	43
2.2.	Cuvette holder configuration	43
2.3.	Treatment media.....	44
2.4.	Numerical and experimental set up.....	44
2.5.	<i>Chlorella vulgaris</i> cultivation and nsPEF treatment.....	45
2.6.	Data analysis	47
3.	Results and discussion.....	48
3.1.	System characterization and optimization.....	48
3.2.	Novel theoretical relation	50
3.3.	Microbial contamination control within <i>Chlorella vulgaris</i> culture	54
4.	Conclusions	57
	References	59
	Manuscript 2.....	62
	Abstract	63
	Graphical Abstract.....	63
1.	Introduction.....	64
2.	Materials and methods	66

TABLE OF CONTENTS

2.1.	Experimental setup	66
2.2.	<i>Arthrospira platensis</i> suspensions	66
2.3.	Measuring mass flow rate	66
2.4.	UVP measurements	67
2.5.	Rheological measurements	67
2.6.	Computational fluid dynamics simulation	69
2.7.	Data analysis	70
3.	Results and discussion	71
3.1.	Flow behavior of <i>Arthrospira platensis</i> suspensions	71
3.2.	Experimental validation of flow fields	73
3.3.	Simulation based comprehensive system analysis	75
3.4.	Energy input comparison between different treatment chambers	77
4.	Conclusions	81
	References	82
	Manuscript 2 – Unpublished Results	85
1.	Introduction	86
2.	Materials and Methods	87
2.1.	Numerical simulations	87
2.2.	Model systems for PEF system optimization	87
2.3.	Results evaluation	88
3.	Results and discussion	89
4.	Conclusions	91

References	92
Manuscript 3.....	93
Abstract	94
Graphical Abstract.....	94
1. Introduction.....	95
2. Material and methods	97
2.1. Nanosecond pulsed electric field (nsPEF) treatment	97
2.2. <i>Arthrospira platensis</i> cultures.....	98
2.3. Microalgae growth and pigment assessment.....	99
2.4. Single cell electrical impedance spectroscopy.....	99
2.5. Proteomic analysis.....	100
3. Results and discussion.....	103
3.1. Analysis of nsPEF treatment mechanisms.....	106
4. Conclusions.....	110
References	111
Manuscript 4.....	114
Abstract	115
Graphical Abstract.....	115
1. Introduction.....	116
2. Material and methods	119
2.1. Raw materials	119
2.2. Nanosecond pulsed electric field (nsPEF) treatment	119

TABLE OF CONTENTS

2.3.	Extraction procedure.....	120
2.4.	ζ -potential measurement.....	120
2.5.	Bubble pressure tensiometry	120
2.6.	Foam processing and characterization	121
2.7.	Bubble size distribution	122
2.8.	Statistical analysis.....	123
3.	Results and discussion.....	124
3.1.	ζ -potential of the <i>Arthrospira platensis</i> isolate.....	124
3.2.	Adsorption kinetics at air/water interfaces.....	124
3.3.	Overrun and stability of foams	128
3.4.	Macroscopic foam properties.....	132
4.	Conclusions	134
	References	135
	Manuscript 5.....	138
	Abstract	139
	Graphical Abstract.....	139
1.	Introduction.....	140
2.	Material and methods.....	142
2.1.	Raw materials	142
2.2.	Sample preparation.....	142
2.3.	Pulsed electric field (PEF) treatment.....	143
2.4.	Protein extraction by high-pressure homogenization	143

2.5.	Protein quantification	143
2.6.	Microalgae revitalization	144
2.7.	Proteomic analysis.....	144
2.8.	Statistical analysis.....	145
3.	Results and discussion.....	146
3.1.	Optimization of PEF-based protein extraction.....	147
3.2.	Protein extraction by PEF in dependency of microalgae growth phase	148
3.3.	Cellular origin of PEF- and HPH-based extracted proteins	150
3.4.	Continuous microalgae cultivation with PEF-assisted protein extraction	151
3.5.	Influence of the incubation and treatment fluid on the protein extraction and microalgae recovery rates.....	153
4.	Conclusions	157
	Appendix A. Supplementary data	158
	References	159
	Perspective	162
	Abstract	163
1.	Introduction.....	164
2.	Pulsed electric field treatment in the bio-based industry.....	166
2.1.	Basic principles of pulsed electric field processing	166
2.2.	Microbial inactivation by PEF	168
2.3.	Extraction of cellular compounds by PEF processing	170

TABLE OF CONTENTS

2.4. nsPEF induced growth stimulation.....	172
3. Conclusions.....	174
References	176
Conclusions and Outlook	180
List of Figures.....	184
List of Tables.....	189
Curriculum Vitae.....	191
Education	191
Publications.....	192

NOTATION

LATIN LETTERS

Symbol	Unit	Definition
A	m ²	Area
a _m	m	Cell radius
B	S	Susceptance
C	F	Electrical capacity
C _m	F	Membrane capacitance
c	mol L ⁻¹	Concentration
D	m	Diameter
D _H	m	Hydraulic diameter
D _{in}	m	Inner diameter
d	m	Distance
E	V m ⁻¹	Electric field strength
E _{crit}	V m ⁻¹	Critical electric field strength
e	C	Electric charge e = 1,60217656510 ⁻¹⁹ C
F	kg m s ⁻²	Volumetric force vector
f	Hz	Frequency
f	-	Form factor
f _c	Hz	Cutoff Frequency
G	S	Conductance
I	A	Electric current
I	-	Identity matrix
J	A m ⁻²	Current density gradient
J _e	A m ⁻²	Displacement current
K	Pa s ⁿ	Flow consistency index
k _B	J K ⁻¹	Boltzmann constant
L	m	Length
L _{entr}	m	Hydrodynamic entry length
ṁ	Kg s ⁻¹	Mass flow rate
n	-	Applied number of pulses
n	-	Flow behavior index
p	Pa	Pressure
p ₀	Pa	Hydrostatic pressure
p _{max}	Pa	Maximum pressure
Q	C	Electric charge
R	Ω	Electrical resistance
r _c	m	Radius of curvature
T	K	Temperature
T _{ref}	K	Reference temperature

NOTATION

t	s	Treatment time
t_c	s	Charging time
U	V	Electric potential
U_H	V	Applied voltage
U_R	V	Reflected voltage
u	$m\ s^{-1}$	Flow velocity
u_0	$m\ s^{-1}$	Inlet velocity
$u(t)$	V	Differential voltage
V	V	Electric potential
ΔV_L	V	Voltage decrease
V	m^3	Volume
\dot{V}	$m^3\ s^{-1}$	Volumetric flow rate
V_0	m^3	Treatment chamber's volume
W_s	$J\ kg^{-1}$	Specific energy input
X	Ω	Reactance
X_C	Ω	Capacitive reactance
X_L	Ω	Inductive reactance
Y	S	Admittance
Y_c	S	Admittance of the system
Z	Ω	Impedance
Z_1	Ω	Impedance of the generator
Z_2	Ω	Impedance of the load
Z_L	Ω	Impedance of the load
Z_{tot}	Ω	Total impedance

GREEK LETTERS

Symbol	Unit	Definition
α	K^{-1}	Temperature coefficient
Γ	-	Reflection coefficient
γ	$m V^{-1}$	Electric field dependence factor
$\dot{\gamma}$	s^{-1}	Shear rate
$\dot{\gamma}_0$	s^{-1}	Zero shear rate
ϵ	$F m^{-1}$	Permittivity
ϵ_0	$F m^{-1}$	Electric constant $\epsilon_0 = 8,854 \cdot 10^{-12} F m^{-1}$
ϵ_r	-	Relative permittivity
θ	$^\circ$	Angle with respect to the angle of the electric field
μ	$Pa s$	Dynamic viscosity
μ_r	-	Relative viscosity of the suspensions
μ_s	$Pa s$	Viscosity of the suspending medium
$[\mu]$	-	Intrinsic viscosity of suspended particles
π	-	Pi
ρ	$kg m^{-3}$	Density of the fluid
ρ	Ωm	Electrical resistivity
ρ_0	Ωm	Reference resistivity
ρ_v	$C m^{-2}$	Electric charge density
σ	$N m^{-1}$	Surface tension
σ	$S m^{-1}$	Electric conductivity
σ_e	$S m^{-1}$	Extracellular media conductivity
σ_i	$S m^{-1}$	Intracellular media conductivity
τ	Pa	Shear stress
τ_0	Pa	Yield stress
τ_c	S	Capacitor charging/discharging time
τ_p	S	Pulse width
τ_m	S	Membrane charging time
ϕ_{max}	-	Maximum volume fraction
ϕ_v	-	Volume fraction
Ψ	Wb	Magnetic flux
$\Delta\Psi_m$	V	Induced membrane potential
$\Delta\Psi_{m, crit}$	V	Critical transmembrane potential
ω	$rad s^{-1}$	Angular frequency

ABBREVIATIONS

Abbreviation	Meaning
AAA	Amino acid analysis
API	<i>A. platensis</i> isolate
aPC	Allophycocyanin
BPT	Bubble pressure tensiometer
BSD	Bubble size distribution
CfU	Colony-forming units
CP	Crude <i>Arthrospira platensis</i> powder
cPC	C-phycocyanin
DS	Dry substance
DW	Dry weight
EIS	Electrical impedance spectroscopy
ESI	Electrospray ionization
FDR	False discovery rate
FGCZ	Functional Genomics Center Zurich
FS	Foaming stability
HPH	High-pressure homogenization
KIT	Karlsruhe Institute of Technology
LC	Liquid chromatography
LCC	Living cell counts
nsPEF	Nanosecond pulsed electric field
OD	Optical density
OLS	Ordinary least squares
OR	Overrun
MOSFET	Metal oxide semiconductor field-effect transistor
MS	Mass spectrometry
PBS	Phosphate buffered saline
PCB	Printed circuit board
PDMS	Polydimethylsiloxane
PEF	Pulsed electric field
PPFD	Photosynthetically active photon flux density
PRF	Pulse repetition frequency
Re	Reynolds number
RPM	Revolutions per minute
RT	Room temperature
SAG	Culture collection of algae Goettingen
TCA	Trichloroacetic acid
UV	Ultraviolet
UVP	Ultrasonic Doppler velocity profiling
Vis	Visible
WPI	Whey protein isolate

SUMMARY

The bio-based industry is urged to find solutions to meet the demands of a growing world population. In this context, increased resource efficiency is a major goal. Pulsed electric field (PEF) processing is a promising technological solution. Conventional PEF and the emerging area of nanosecond PEF (nsPEF) processing have been shown to induce various biological effects, which could provide solutions for currently faced challenges. Based on the flexibility and continuous operation of PEF / nsPEF processing, the technology can be integrated into many existing cultivation systems, while its modularity has the potential to induce specific effects. However, the application of PEF and nsPEF in the food- and bioprocessing industry is scarce due to several challenges around reproducibility and scalability of results and technology.

Pulse measurement in the domain of PEF processing can be related to a sole Ohmic response of the load, however for nsPEF processing, this relation does not hold any longer and a novel theoretical relation had to be derived integrating the frequency-dependent complex impedance of the load, allowing for matched load conditions.

Moreover, in continuous PEF/nsPEF processing, the flow field is of utmost importance in order to induce targeted cellular effects and allow for a scalable system. Therefore, the flow field in continuous PEF/nsPEF processing and its influencing factors were analyzed and energy input distributions in PEF treatment chambers were investigated. The results were obtained using an interdisciplinary approach that combined multiphysics simulations with ultrasonic Doppler velocity profiling (UVP) and rheological measurements. Thereby, a comprehensive PEF system characterization and control was enabled. Based on the system characterization a first amendment of the treatment homogeneity focused on turbulent flow conditions, thereby, a facilitated scale-up of the technology might be possible in the future.

In addition, to the comprehensive PEF/nsPEF system analysis, promising applications within the bio-based industry including targeted inactivation, the cyclic extraction of bioactive compounds, and the stimulation of cell growth and/or cellular compounds without negatively influencing interfacial properties of the protein fraction were achieved. Moreover, several potential mechanisms for the induced effects were derived based on proteomic analysis and electrical impedance spectroscopy of single cells. Thus, the presented concepts bear the potential to be key processing steps toward more sustainable and efficient supply chains.

ZUSAMMENFASSUNG

Die biobasierte Industrie ist gefordert, Lösungen für die steigenden Anforderungen einer wachsenden Weltbevölkerung zu finden. Dabei ist die Steigerung der Ressourceneffizienz ein wichtiges Ziel. Eine vielversprechende technologische Lösung ist die gepulste elektrische Feldprozessierung (PEF). Konventionelle PEF und der aufkommende Bereich der Nanosekunden-PEF (nsPEF) haben gezeigt, dass sie verschiedene biologische Effekte hervorrufen, die Lösungen für die aktuellen Herausforderungen ermöglichen könnten. Aufgrund der Flexibilität und des kontinuierlichen Betriebs der PEF- und nsPEF-Prozessierung kann die Technologie in viele bestehende Kultivierungssysteme integriert werden, während ihre Modularität das Potenzial hat, spezifische Effekte zu induzieren. Die Anwendung von PEF und nsPEF in der Lebensmittel- und Bioprozessindustrie ist jedoch aufgrund verschiedener Herausforderungen in Bezug auf Reproduzierbarkeit und Skalierbarkeit der Ergebnisse und der Technologie nur selten zu finden.

Die Pulsmessung im Bereich der PEF-Prozessierung kann auf eine alleinige ohmsche Antwort der Last bezogen werden, für die nsPEF-Prozessierung gilt diese Beziehung jedoch nicht mehr und es musste eine neue theoretische Beziehung abgeleitet werden, die die frequenzabhängige komplexe Impedanz der Last integriert und angepasste Lastbedingungen ermöglicht.

Darüber hinaus ist bei der kontinuierlichen PEF/nsPEF-Prozessierung das Strömungsfeld von größter Bedeutung, um gezielte zelluläre Effekte zu induzieren und ein skalierbares System zu ermöglichen. Daher wurden das Strömungsfeld bei der kontinuierlichen PEF/nsPEF-Prozessierung und seine Einflussfaktoren analysiert und die Energieeintragsverteilungen in PEF-Behandlungskammern untersucht. Die Ergebnisse wurden in einem interdisziplinären Ansatz erzielt, der Multiphysik-Simulationen mit Ultraschall-Doppler-Geschwindigkeitsprofilung (UVP) und rheologischen Messungen kombinierte. Dadurch wurde eine umfassende Charakterisierung und Kontrolle des PEF-Systems ermöglicht. Basierend auf der Systemcharakterisierung wurde eine erste Optimierung der Behandlungshomogenität mit Fokus auf turbulente Strömungsverhältnisse durchgeführt, wodurch ein Scale-up der Technologie in Zukunft erleichtert werden sollte.

Zusätzlich zu der umfassenden PEF/nsPEF-Systemanalyse wurden vielversprechende Anwendungen innerhalb der biobasierten Industrie, einschließlich

der gezielten Inaktivierung, der zyklischen Extraktion bioaktiver Verbindungen und der Stimulation von Zellwachstum und/oder zellulären Verbindungen ohne negative Beeinflussung der Grenzflächeneigenschaften der Proteinfraction, erreicht. Darüber hinaus wurden verschiedene potentielle Mechanismen für die induzierten Effekte basierend auf der Proteomanalyse und der Elektroimpedanzspektroskopie einzelner Zellen abgeleitet. Die vorgestellten Konzepte haben somit das Potential, Schlüsselprozesse für eine nachhaltigere und effizientere Wertschöpfungskette zu werden.

INTRODUCTION

Studies in the field of bioengineering around reversible permeabilization of cells and subsequent findings regarding underlying kinetics, as well as process parameters and equipment design, provided the backbone for pulsed electric field (PEF) applications in the food- and bioprocessing industry. In the past centuries, several studies utilizing electricity for the inactivation of microbes and treatment of food and bio-products were executed.

In 1749 a French abbot observed that electricity increases the germination and overall growth of plants (Nollet 1749). Bertholon (1783), who used electrified water to grow crops, further approved the growth-enhancing properties of electricity. These initial findings resulted in the application of electricity in agriculture around the end of the 19th century, with applications of an electrical discharge treatment to different agricultural crops (Leicester 1889; Lemström 1904). Despite, agricultural crops, the effect of electrical stimulation based on weak currents in bacteria and yeast was observed by Stone (1909). Research on growth stimulation by electrical applications has a long history; positive effects have been established in several relevant cells.

Despite these studies on reversible applications of electricity, the inactivation of bacteria (irreversible) by electricity was determined in a so-called “electro-pure process” (Anderson and Finkelstein 1919). Moreover, the low cost and efficient process of electrical cooking was investigated (Sater 1935). In the 1960s Heinz Doevenspeck explored the effect of PEF on the disintegration and fractionation of biological material (Doevenspeck 1960). Around the same time, research conducted by Zagorulko (1958), reported an enhanced extraction of juice from sugar beets via the application of AC and DC electric fields.

These observations were the foundation for today’s extensive research and applications of PEF in the food- and bioprocessing industry.

1. PULSED ELECTRIC FIELD FUNDAMENTALS

PEF processing is based on the formation of a potential difference across a conductive biological material between two electrodes resulting in an applied electric field. The electric field is dependent on the applied electric potential, the gap between the electrodes and pulse waveform and width (Eq. (1)). The electric field strength E (V m^{-1}) over time can be calculated according to Eq. (1) with applied voltage over time $u(t)$ (V) and the gap between the electrodes d (m).

$$E(t) = 1/d * \int_0^t u(t) dt \quad (1)$$

Besides the electric parameters, the PEF treatment is dependent on reactor parameters such as the design of the treatment chamber and media parameters such as the thermophysical properties of the medium (Fig. 1). Within the whole process, all the parameters depicted in Fig. 1 are directly or indirectly linked to each other and influence the energy input into the system. Thereby, isolated studies of the effect of individual parameters on the treatment outcome/ efficiency are not possible.

The specific energy input W_s (J kg^{-1}) over time can be calculated according to Eq. (2) with the pulse width τ_p (s), the electric conductivity σ (S m^{-1}) and the applied number of pulses n (-).

$$W_s = E(t)^2 \cdot \tau_p \cdot \sigma \cdot n \quad (2)$$

The number of pulses can be derived from Eq. (3) with frequency f (Hz) and residence or treatment time t (s).

$$n = f \cdot t \quad (3)$$

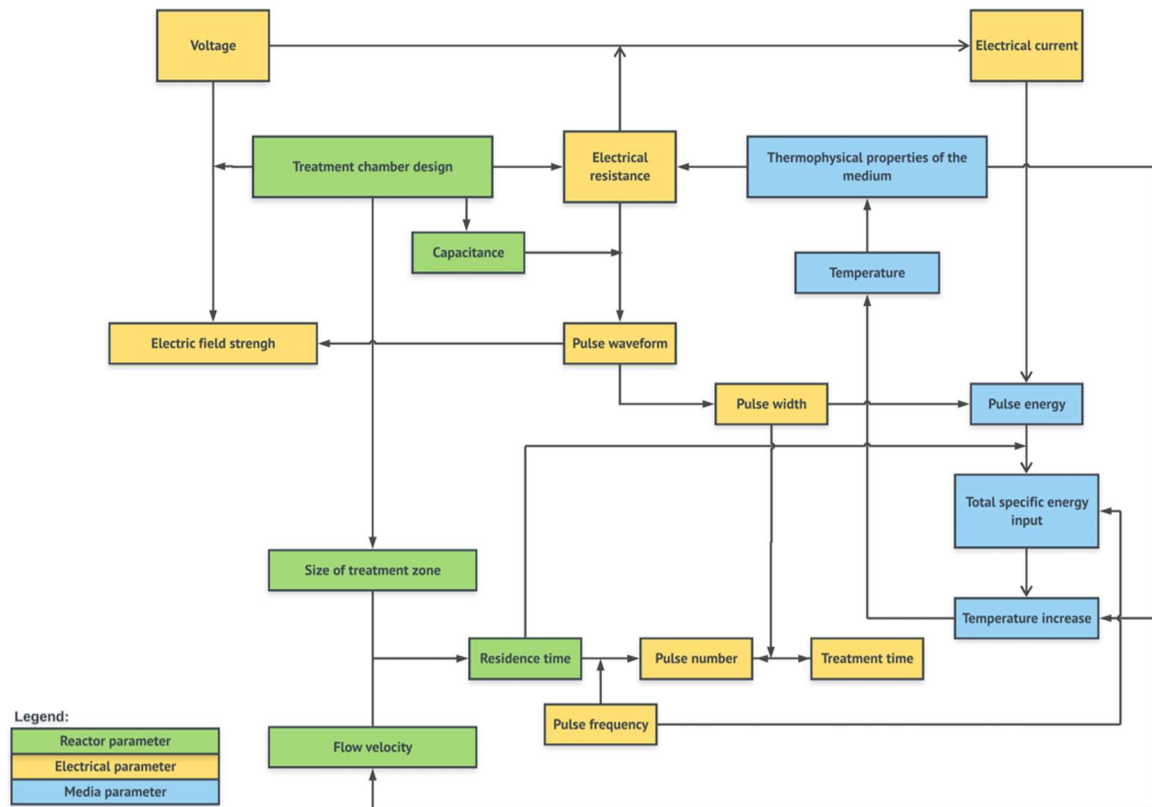


Figure 1: PEF parameter interconnectivity, adapted from (Jaeger, 2012). Reactor (green), electrical (yellow) and media (blue) parameters are shown. Within the whole process, all parameters are directly or indirectly linked to each other.

In PEF applications conventional PEF processing in the range of micro- to milliseconds and nsPEF processing in the range of nanoseconds can be divided (Beebe and Schoenbach, 2005; Mahnič-Kalamiza et al., 2014). The process referred to as nsPEF processing typically includes high electric fields ($10\text{-}100\text{ kV cm}^{-1}$) applied for 1-300 ns per pulse (Beebe and Schoenbach, 2005). In either case, electropermeabilization results in an increased mass transfer of molecules and ions (Toepfl et al., 2006b). Nevertheless, the mechanisms underlying the PEF/nsPEF induced effects are still the subject of intensive research (Teissie, 2017). Moreover, especially for nsPEF processing, the pulse measurement is regarded as challenging and thus there is a strong need for electrical process characterization and control.

1.1. Pulse generation

Different waveforms are possible based on pulse generator construction. In order to achieve microsecond pulses, exponential decay (Fig. 2, A) and rectangular pulse circuits (Fig. 2, B) are possible approaches. Nanosecond pulses can be achieved by Blumleingenerators (Fig. 2, C) and diode opening generators (Fig. 2, D). There are

other methods to generate electric pulses, but the stated once are the most relevant.

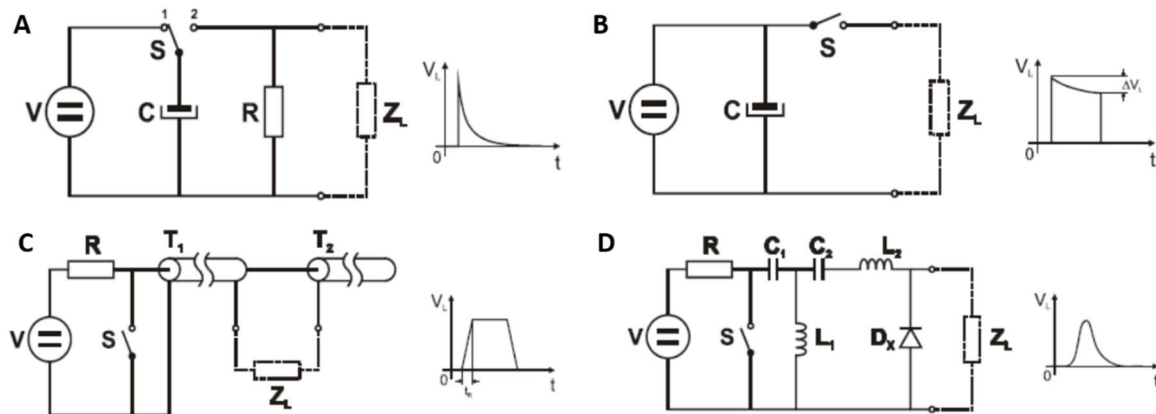


Figure 2: Electrical reference circuits and resulting pulse waveform for A) exponential decay pulse generator B) rectangular pulse generator C) Blumleingenerator and D) diode opening switch generator (Rebersek and Miklavčič, 2011).

Exponential decay pulse generators (Fig. 2, A) are a two-stage process based on the charge and discharge of a capacitor C (F). The discharge phase will result in an exponential decay pulse delivered to the load Z_L (Ω). The pulse width τ_p (s) of such pulses is defined, as the time required to reach 37% of the initial voltage (Barsotti et al., 1999; Ho and Mittal, 2000).

Rectangular pulse generators (Fig. 2, B) are closely linked to the concept of exponential decay pulses. The rectangular pulse shape is achieved by a constant charging of the capacitor and more advanced switches in the circuit, such as MOSFETs (metal oxide silicon field-effect transistors) or IGBTs (insulate gate bipolar transistors). Thereby, the pulse duration can be controlled. Rectangular pulses maintain a defined voltage for the most part of the pulse and a slight voltage decrease is primarily due to a lack of energy supply. Given that the actual voltage decrease ΔV_L (V) is proportional to the pulse width divided by the time constant of discharge ($Z_L \cdot C$ (s)), quite large capacitors are needed to minimize this voltage drop (Bertacchini et al., 2007).

The nanosecond pulse generation was primarily achieved by utilizing transmission line generators such as the Blumlein generator (Deng et al., 2001; Kolb et al., 2006) (Fig. 2, C). Such pulse generators are based on equally long transmission lines. During the charging step, the transmission line is charged to the set voltage and then discharged through the load. It is required that the load has an impedance twice as large as the impedance of the transmission line. Otherwise, mismatched load conditions will result in reflections within the system (Eq. (4) (Bluhm, 2006; K uchler,

2018; Schwab, 1981).

$$\Gamma = U_R/U_H = (Z_1 - Z_2)/(Z_1 + Z_2) \quad (4)$$

The reflection coefficient Γ (-) is equal to the reflected voltage U_R (V) divided by the applied voltage U_H (V). Z_1 (Ω) is the impedance of the generator and Z_2 (Ω) the impedance of the load. In the case of a perfectly matched reactor $Z_1 = Z_2$, Γ is equal to zero and no reflections occur.

In an ideal case, the pulse width of such Blumlein generators is equal to the electric length of the transmission line. Hence, the design and manufacturing of such generators are rather simple, yet limited in flexibility. For such pulse generators mostly Spark gaps switches are used, given their short rise time and ability to withstand high voltages. In the case of synchronized switch control, variable amplitudes, pulse widths and polarities can be achieved (Rebersek et al., 2009).

A more advanced and versatile nanosecond pulse generator is the diode opening switch generator concept (Fig. 2, D). These two-step pulse generators generate Gaussian-like pulses (Sanders et al., 2009). In the case of a charged capacitor, the LC oscillator starts to oscillate and the diode stack forms the pulse on the load itself. Thereby, the commutated current and induced voltage on the load are high. Further increasing the commutated current can be achieved by saturable-core inductors instead of air-core inductors. Nevertheless, nowadays thyristors or semiconductor-based diodes are used to manufacture such pulse generators (Blume et al., 2014). Given the vast possibilities of pulse generator designs, a detailed study of the sample's impedance could increase PEF treatment reproducibility. Most research in that area was based on cumulative signals (Silve et al., 2011; Toepfl, 2006). Electro impedance spectroscopy of single cells enabled in that context detailed information of the cells' frequency behavior and thus cellular composition (de Araujo et al., 2018). This information might be useful to further tailor PEF processing based on the detailed characterization of the electric equivalent circuit of biological cells (Fig. 7) and the resulting consequences depending on the used pulse generator concept and the respective Fourier transform thereof.

1.2. Treatment chamber design

PEF processing can be divided into batch and continuous processing. Due to a homogeneous electric field, parallel plate treatment chambers are mostly used for

batch processing. In continuous PEF processing, relevant for scale-up approaches and industrial implementation, there are three main treatment chamber concepts that have been studied (Fig. 3). As shown in Fig.1 the reactor parameters and thus treatment efficiency greatly depends on the treatment chamber design (Jaeger, 2012).

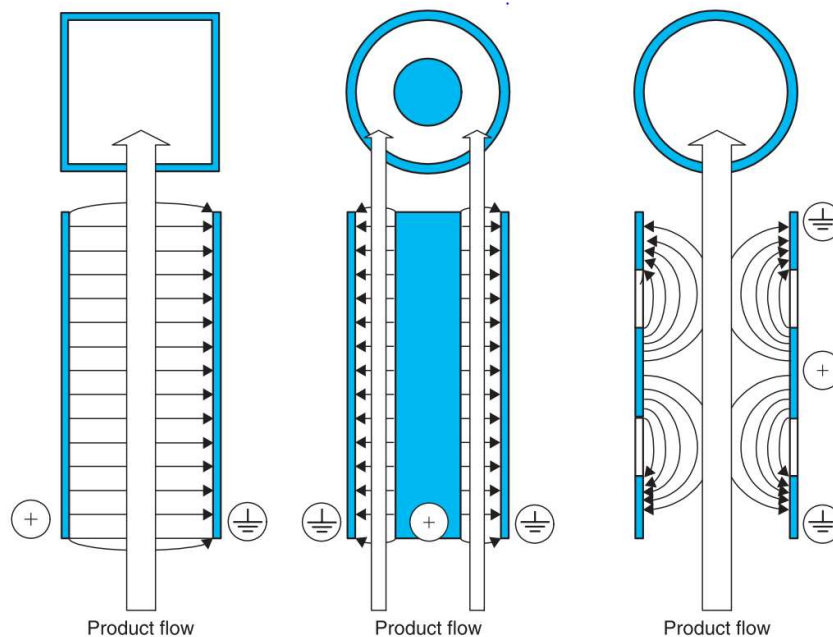


Figure 3: The three main types of continuous PEF treatment chamber designs; parallel plate, co-axial and co-linear from left to right. The black arrows indicate the direction of the electric field whereas the white arrow indicates the flow direction (Toepfl et al., 2005).

Within the continuous treatment chambers, two design categories can be differentiated, namely cross-field and co-field chambers. Cross-field treatment chambers are characterized by an electric field perpendicular to the fluid flow. The most commonly used cross-field chamber is the so-called parallel plate or plate-plate geometry, in which the treatment takes place in a rectangular channel with two electrodes and two insulating walls (Van den Bosch, 2007). The main advantage of parallel plate treatment chambers is the homogeneous electric field distribution, however, it is stated that due to stagnant zones within the treatment chamber and the low resistance thereof, the treatment chamber is not suitable for industrial applications of PEF.

Besides the parallel plate treatment chamber, the co-axial treatment chamber configuration is another example of a cross-field chamber. Within a co-axial treatment chamber, the product flows through a gap between two concentric cylinders (Jaeger, 2012). Similar to parallel plate treatment chambers the co-axial treatment chambers

violate hygienic design requirements of the food- and bioprocessing industry, making it unsuitable for industrial applications (Góngora-Nieto et al., 2002; Jaeger, 2012; Toepfl, 2006).

In co-field treatment chamber configurations, the electric field lines run in parallel to the product flow. The most commonly used treatment chamber is the co-linear configuration. This configuration is the currently most used and investigated PEF treatment chamber setup (Buckow et al., 2010; Jaeger et al., 2009a; Knoerzer et al., 2012). The co-linear treatment chamber is a modular pipe with integrated insulators separating the ground and high voltage electrodes from the residual process. The main advantage of these geometries is convenient cleanability, making them especially suitable for industrial processing (Góngora-Nieto et al., 2002; Jaeger, 2012; Toepfl, 2006). However, the inhomogeneous electric field distribution poses challenges towards a homogeneous energy input distribution. Yet by modulating and optimizing the insulator geometry, the electric field distribution was optimized based on numerical simulations (Gerlach et al., 2008; Meneses et al., 2011d). For example, reducing the diameter of the insulator compared to the residual pipe diameter allowed for an increased electric field homogeneity in the constricted/ pinched treatment area (Toepfl et al., 2007).

Based on the PEF parameter interconnectivity, current treatment chamber optimization was neglecting the flow field distribution and its influence on the specific energy input. Consequently, a comprehensive PEF system analysis was required in order to understand the difficulties in PEF treatment chambers and as a result optimize the treatment chamber with respect to homogeneous energy inputs.

2. FLOW FIELD ANALYSIS

The low commercial use of PEF processing can be attributed mainly to the lack of homogeneity and issues around the reproducibility of PEF research (Buckow et al., 2010; Gerlach et al., 2008; Jaeger et al., 2009a; Raso et al., 2016).

The numerous parameters that need to be considered for PEF processing can be summarized in three distinct groups. Firstly, there are media parameters such as composition, pH, product temperature, ionic strength, and water activity. Secondly, the treatment effect depends on biological factors such as microorganism species, growth phase, and cell size and shape. Thirdly, there are reactor parameters such as treatment chamber design, electric field strength, pulse shape, pulse duration, pulse repetition frequency, pulse number, temperature and treatment time (Barbosa-Cánovas and Altunakar, 2006; Mittal and Griffiths, 2005; Toepfl, 2011). Several of these factors are interconnected and influence the specific energy input into a volume element. The PEF parameter interconnectivity is illustrated in Fig. 1 (adapted from Jaeger (2012)).

Many recent publications have focused on the optimization of PEF processing considering above mentioned influencing factors (Alkhafaji and Farid, 2007; Fiala et al., 2001; Knoerzer et al., 2012; Meneses et al., 2011a, 2011d). Nonetheless, there is still a large potential for PEF system optimization, especially with regard to continuous PEF processing and thus consideration of flow field inhomogeneities.

2.1. Importance of flow field analysis

In recent years, the main focus of the PEF process development was on the optimization of the electric field distribution (Jaeger et al., 2009a; Knoerzer et al., 2012; Lindgren et al., 2002a; Meneses et al., 2011d). In order to increase PEF treatment homogeneity, this focus was a reasonable approach, however, the flow field and thus residence time distribution is certainly an equally crucial factor. The residence time distribution within the treatment chamber determines the number of pulses per volume element at a given pulse repetition frequency and hence the spatial energy input. This aspect results in potentially over-treated volume elements towards the walls and potentially under-treated volume elements towards the center of the treatment chamber.

This aspect was already highlighted by Zhang et al. (1995), which mentioned the flow rate as one of the five most important parameters to be addressed for the successful

scale-up of the PEF technology. However, even more than 20 years later, research papers based on continuous PEF treatments lack a standard deviation or any measure of uncertainty for the residence time in the treatment chamber and thus energy input into the system. A study by Min et al. (2007), reviewing more than 40 experimental studies that were published on PEF, reported that residence time and energy input if reported at all were always given as averages. However, the residence time distribution within the treatment chamber is not only crucial for targeted PEF treatments but further of utmost importance for the scale-up of the technology.

Several researchers have investigated measures to increase the flow field homogeneity in PEF processing. A design in which the fluid is forced through small holes in an insulating plate generating a mixing effect and focusing the electric field in a small gap was proposed already in 1991 (Matsumoto et al., 1991). However, this approach results in stagnant zones in the corners of the chamber potentially leading to overheating or biofouling (Huang and Wang, 2009). Conically shaped electrodes and insulators in combination with orifice channeling the liquid were analyzed to prevent stagnant zones (Sensoy et al., 1997). Yet, this modification had the drawback of an inhomogeneous electric field distribution (Huang and Wang, 2009). Integrating meshed electrodes and a narrow treatment zone potentially allowing for an optimization of the flow field, had the drawback that they were not suitable for products with an inhomogeneous composition or containing large suspended particles (Alkhafaji and Farid, 2007). In a patent from 2013, the authors elaborated on how a longitudinal insert at the beginning of a co-linear treatment chamber could optimize the flow field in the treatment area (Mathys et al., 2013). This was an interesting approach, and similar ideas could also be useful in other geometries or settings. Nonetheless, all these system optimizations were deficient in a common aspect. The PEF parameters were analyzed independently and the correlation of electric and flow field inhomogeneity on the spatial specific energy input was neglected. Thereby, not only the treatment homogeneity could be increased but also more targeted cellular effects could be induced. Moreover, the efficiency of PEF processing was mostly analyzed on a product/ output level without further analysis of the specific energy input, resulting in difficulties during up-scaling ultimately hindering further PEF process implementations in industrial relevant scales.

Hence, there is a need for an in-depth characterization of residence time distributions in lab-, pilot- and industrial-scale systems.

2.2. Numerical simulations in PEF research

PEF system optimization is regarded as a challenging process solely based on experimental analysis, as the process at lab-scales might be affected and disturbed by measuring equipment (Buckow et al., 2010; Gerlach et al., 2008; Meneses et al., 2011b). Therefore, local information during PEF processing has been extensively studied utilizing numerical simulations and thereby improving, for example, the PEF treatment chamber through an iterative process (Buckow et al., 2010; Meneses et al., 2011a). In addition, numerical simulations can be used to estimate treatment outcomes and thus optimizing treatment designs prior to tedious, expensive or time-consuming experiments (Fiala et al., 2001; Gerlach et al., 2008; Lindgren et al., 2002b; Wölken et al., 2017). Moreover, computational approaches can be utilized to gain a thorough understanding of different PEF processing factors and their influence on the treatment (Meneses et al., 2011d).

Even though simulations have numerous advantages and the model might seem plausible, their solutions, especially for complex problems, might not always be accurate. Hence, it is vital to experimentally validate the simulations, whenever possible (Barbosa-Cánovas et al., 2011). In the past decade, a variety of papers focused on the basic, physics, principles and equations underlying simulations of PEF processing (Buckow et al., 2010; Gerlach et al., 2008; Meneses et al., 2011b, 2011a). The main focus of research in this field was on optimization of the electric field homogeneity in co-linear treatment chambers targeting an increased overall treatment homogeneity. Thus various modified treatment chamber designs were analyzed with the focus on increased electric field homogeneity (Fiala et al., 2001; Meneses et al., 2011d; Qin. et al., 1995).

2.3. Physics underlying fluid dynamics simulations

Two governing equations underlie fluid dynamic simulations. First, The Navier-Stokes equation also described as Newton's second law of motion for fluids, describing the conservation of momentum for incompressible fluids (Eq. (5)). Second, the principle of mass conservation needs to be incorporated via a continuity equation (Eq. (6)),

$$\rho(u \cdot \nabla)u = \nabla[-pI + \mu(\nabla u + (\nabla u)^T)] + F \quad (5)$$

$$\rho \nabla \cdot (u) = 0 \quad (6)$$

where ρ (kg m^{-3}) stands for the density of the fluid, u (m s^{-1}) denotes the flow velocity vector, I (-) represents the identity matrix, μ (Pa s) is the dynamic viscosity, p (Pa) represents the pressure, and F (kg m s^{-2}) denotes the volumetric force vector. These equations are solved during fluid dynamic simulations incorporating certain boundary conditions such as inlets, walls, outlets to predict the fluid velocity and pressure (COMSOL, 2018).

In the case of the finite element method as used in COMSOL multiphysics® the whole geometry is divided into small elements via a mesh and the governing equations are solved for every individual mesh element (Heinz et al., 2002). Based on these local results, the result for the whole geometry is re-assembled. Thus, the mesh size is a crucial element in finite element simulations in order to achieve a solution as accurate as possible without an exorbitant high computational effort.

Despite the mesh size, the adequate physics interface is important for fluid dynamics simulations and requires analysis of the flow regime. Typically, the flow regime can be divided into laminar, transitioning and turbulent flow. The present flow profile can be assessed by the dimensionless Reynolds number, which for a channel or pipe can be calculated according to Eq. (7). The critical Reynolds number for the onset of laminar flow changing into transitioning and later turbulent flow is at 2300 (Schlichting and Gersten, 2017).

$$Re = \rho u D_H / \mu \quad (7)$$

with u (m s^{-1}) denoting the mean velocity and D_H (m) representing the hydraulic diameter, which can be replaced by the diameter D (m) for circular pipes.

Laminar flow is characterized by a highly ordered layered flow without mixing thereof. This flow regime typically occurs in lab-scale installations given the relatively small geometry and fluid velocity in such installations. On the contrary, the random three-dimensional motion of fluid elements resulting in lateral mixing characterizes turbulent flow (Bergman and Incropera, 2011). This flow regime is more likely to occur in industrial applications as relatively large characteristic lengths and flow velocities occur.

Besides the above mentioned, the two boundary conditions hydrodynamic length and inlet velocity need to be defined for accurate fluid dynamics simulations. It is generally considered that the fluid will enter a pipe with a uniform velocity (Bergman and Incropera, 2011). Within a pipe, fluid elements will interact with the wall surface

ultimately resulting in a boundary layer. In the case of laminar flow, after a certain distance defined as the hydrodynamic entry length L_{entr} (m) (Eq. (8)) the fluid profile will reach a parabolic shape and can be referred to as fully developed. In a fully developed flow, the profile will not change any longer, provided that there is no change in geometry or no externally applied force. In the case of a turbulent flow profile characterized by a random flow pattern, the hydrodynamic entry length can be approximated by Eq. (9).

$$L_{entr} = 0.05 \cdot D \cdot Re \quad (8)$$

$$L_{entr} = 4.4 \cdot D \cdot Re^{1/6} \quad (9)$$

2.4. Non-invasive flow field measurement

In order to validate numerical simulations in experimental settings, non-invasive measuring techniques are crucial. Measuring the flow profile in a closed entity in a non-invasive way can be achieved by either particle image velocimetry (PIV) or ultrasonic Doppler velocity profiling (UVP). Whereas PIV is based on a laser source, UVP is based on ultrasound as emitted and analyzed signal. Both measurements are based on reflections of the emitted signal from particles present in the fluid. Analysis of fluids without intrinsic particles can be enabled by the incorporation of inert reflector beads. The main advantage of UVP over PIV is the ability to measure in opaque liquids, whereas PIV has the advantage of directly analyzing the three-dimensional flow pattern in a cavity (Takeda, 1995; van Doorne and Westerweel, 2007; Wiklund et al., 2007). The underlying principle of UVP is based on the time delay between the ultrasound burst emission and the recording thereof. This time difference provides information on the position of reflection, which then based on the Doppler shift frequency, can be converted to the instantaneous velocity of the reflecting particle (Takeda and Tasaka, 2012). The possibility to cover the whole velocity profile makes UVP especially suitable for comparisons to numerical simulations. In addition, UVP could be combined with the measurement of the pressure difference to enable in-line rheological measurements (Dufour, 2018).

Up to now, non-invasive flow field measurements were neglected in PEF research and the focus was on sole numerical simulations. Given that the flow field was in any way severely neglected and its influence on the resulting energy input underestimated in present literature, this aspect does not come as a surprise. For the

first time, the electric- and flow field inhomogeneity was analyzed and the resulting specific energy input determined. This comprehensive analysis will allow for a facilitated scale-up of the technology and overall increasing continuous PEF processing comparability and reproducibility. Moreover, concepts based on in-line rheological analyses could be integrated into future process controls. The underlying potential for such a process control will be elucidated below.

2.5. Rheological analysis

The rheological analysis is an important tool to characterize the flow behavior of fluids, which can then be integrated into numerical simulations (Juliano et al., 2011). Rheological measurements allow for the determination of the fluids' viscosity in dependence of the applied force or shear rate. It can be differentiated between Newtonian and non-Newtonian fluids. Newtonian fluids are characterized by a shear rate independent viscosity whereas the viscosity depends on the shear rate for non-Newtonian fluids (Mewis and Macosko, 1994).

In the case of Newtonian fluids, a constant viscosity can be integrated into numerical simulations. On the contrary, non-Newtonian fluids require a viscosity function in order to account for the shear rate dependency. Mostly the flow behavior of a liquid can be approximated by a rheological equation. The commonly used equations for non-Newtonian fluids are either the Herschel-Bulkley equation (Eq. (10)) or the non-Newtonian power-law (Eq. (11)), also referred to as Ostwald-de Waele relationship (Mezger, 2015; Spagnolie, 2015).

$$\tau = \tau_0 + K\dot{\gamma}^n \quad (10)$$

$$\tau = K\dot{\gamma}^n \quad (11)$$

with shear stress τ (Pa), yield stress τ_0 (Pa), shear rate $\dot{\gamma}$ (s^{-1}), flow consistency index K (Pa s^n) and flow behavior index n (–). Incorporation of the generalized Newtonian law ($\mu(\dot{\gamma}) = \tau / \dot{\gamma}$), allows Eq. (9) to be rewritten. The resulting equation gives the dynamic viscosity of the non-Newtonian fluid as a function of the shear rate, given a shear rate equal to or greater than the zero shear rate $\dot{\gamma}_0$ (s^{-1}) (Eq. (12)).

$$\mu = \tau_0|\dot{\gamma}|^{-1} + K|\dot{\gamma}|^{n-1}, |\dot{\gamma}| \geq \dot{\gamma}_0 \quad (12)$$

This function can now be applied to rheological data to obtain values for the yield stress, flow consistency index, and flow behavior index. The resulting viscosity

function can then be used in numerical simulations and thereby real data can be linked to numerical simulations.

The rheological results can further be used to derive an equation for a suspension's viscosity as a function of its concentration, using the Krieger-Dougherty relation (Eq. (13)). The Krieger-Dougherty relation (Eq. (13)) can be used to express the suspension's viscosity as a function of the particle concentration (Krieger and Dougherty, 1959).

$$\mu_r = \mu/\mu_s = (1 - \Phi_V/\Phi_{max})^{-[\mu]\Phi_{max}} \quad (13)$$

where $\mu_r(-)$ denotes the relative viscosity of the suspensions, μ (Pa s) represents the effective viscosity of the suspensions, μ_s (Pa s) represents the viscosity of the suspending medium, $\phi_{max}(-)$ is the maximum volume fraction, $\phi_v(-)$ represents the volume fraction, and $[\mu](-)$ denotes the intrinsic viscosity of the suspended particles. The Krieger-Dougherty relation is mainly useful for the bioprocessing industry where biological variations in the cultivation process can result in significant changes in the final concentration, influencing the subsequent viscosity and thus resulting in the need for PEF treatment adjustments in order to induce homogeneous effects. Applications of PEF in the food industry require the consideration of the matrix's individual viscosity function. Neglecting this aspect hampers the ubiquitous application of PEF, as individual processing windows for different applications in different products may not be achieved and therefore wrong conclusions are drawn about the efficiency and suitability of PEF processing.

3. BIOLOGICAL APPLICATIONS

The application of PEF to biological cells is based on the principle of electropermeabilization due to an induced transmembrane potential (Pauly and Schwan, 1959; Schoenbach et al., 2004; Zimmermann et al., 1974b). The applied electric field accumulates charges at the cell membrane and therefore alters the transmembrane potential. The induced transmembrane potential $\Delta\psi_m$ (V) is given by Eq. (14) with the applied electric field, the form factor f (-) (1.5 for spherical cells) the cell radius a_m (m), the angle with respect to the angle of the electric field θ ($^\circ$), treatment time and the membrane charging time τ_m (s) from Eq. (15) (Kinosita et al., 1988; Pauly and Schwan, 1959),

$$\Delta\psi_m(t) = f \cdot E(t) \cdot a_m \cdot \cos\theta (1 - e^{-t/\tau_m}) \quad (14)$$

$$\tau_m = a_m \cdot C_m (1/2\sigma_e + 1/\sigma_i) \quad (15)$$

where C_m (F) is the membrane capacitance, σ_e the extracellular conductivity and σ_i the intracellular conductivity (Fig. 7 B).

In order to permeabilize a biological cell the transmembrane potential needs to exceed a critical value. According to literature this critical transmembrane potential $\Delta\psi_{m, crit}$ (V) is in the range of 0.1 - 1V (Teissie and Tsong, 1981; Zimmermann et al., 1974a, 1976). The critical transmembrane potential is often referred to as critical electric field strength E_{crit} ($V m^{-1}$). The greater the difference between the applied and the critical electric field strength the more severe are the induced effects, resulting in irreversible ($E \gg E_{crit}$) or reversible ($E > E_{crit}$) permeabilization of the cell (Fig. 4). Reversible pores re-seal within seconds (Glaser et al., 1988). Irreversible permeabilization results in loss of turgor, leakage of cytoplasmic content and lysis (Fuller, 1898).

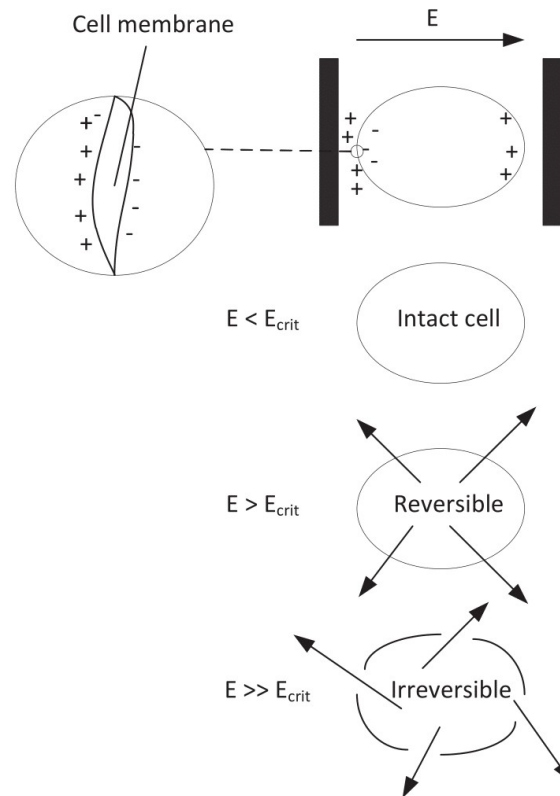


Figure 4: PEF principle of action. A critical electric field has to be exceeded in order to induce permeabilization of the cells. The severity of PEF treatments depends on the difference between the critical electric field and the applied electric field (adapted from Toepfl, 2006).

Depending on the pulse duration and amplitude of the applied electric field, different results can be achieved. Fig. 5 illustrates the possible treatment regimes based on the modification of the pulse duration and amplitude. By increasing the pulse amplitude, reversible electroporation can result in irreversible electroporation (Fig. 5, A -> B). A subsequent reduction of the pulse duration however, still enables a reversible PEF application (Fig. 5, B -> C). This aspect was emphasized in the conducted experiments and resulted in the presented concepts of selective inactivation, growth stimulation and cyclic protein extraction, where the interchange of pulse duration and amplitude allowed the achievement of completely different effects (Buchmann and Mathys, 2019).

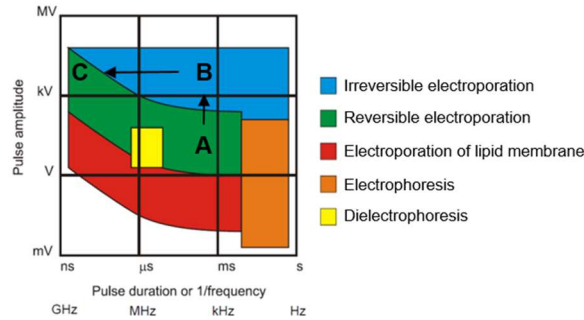


Figure 5: Influence of pulse duration and amplitude on the induced effects ranging from electrophoresis (orange), electroporation of lipid membranes (red), dielectrophoresis (yellow) to reversible electroporation (green) and irreversible electroporation (blue) (adapted from Rebersek and Miklavčič, 2010).

Research conducted at the Karlsruhe Institute of Technology (KIT), focused on the application high voltage (kV) and short-time pulses (ns) (Fig. 5, C) and found for 100 pulses at 5 kV cm^{-1} and 10 ns a significant increase in leaf area of *Arabidopsis thaliana*. They attributed the growth-stimulating nature of nanosecond pulsed electric field treatment (nsPEF), to an intracellular release of calcium affecting the free cytosolic calcium concentration, resulting in an abiotic sub-lethal stress response (Eing et al., 2009) (Table 1).

The hypothesis of intracellular abiotic sub-lethal stress induction by nsPEF is supported by a theoretical evaluation of the cells' membrane and organelles' membrane potential (Fig. 6) (Kotnik and Miklavčič, 2006). The authors found an increased effect on the organelle membrane for frequencies above 10 MHz corresponding to a 100 ns pulse and the highest subcellular effects for frequencies around 100 MHz. This observed response of the investigated cellular compartments could be an explanation for the reversible permeabilization on a subcellular level.

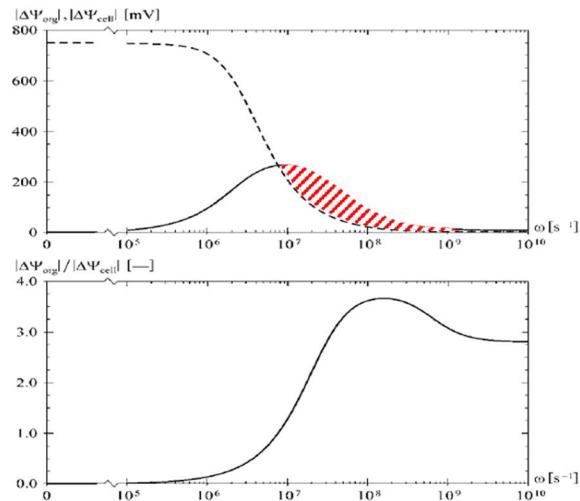


Figure 6: Theoretical evaluation of the cells' membrane and organelles' membrane potential at different frequencies, the red area indicated the range in which the organelles' membrane potential exceeds the cells' membrane potential (adapted from Kotnik and Miklavčič, 2006). The results were obtained assuming a trapezoidal pulse shape with an electric field strength of 500 V/cm and an angle with respect to the angle of the electric field $\theta = 0$, for a cell diameter of 10 μm .

This phenomenon of increased intracellular effects of the applied electric field can be explained by looking at a biological cell as an electric equivalent circuit (Fig. 7). In such a schematic view, cell membranes represent a capacitor with a low conductance between the extracellular fluid and the cytoplasm (Fig. 7). This structure is responsible for an electrical potential difference commonly allied with the membrane potential. Multiple cellular functions depend on changes in the membrane potential such as the transmission of an action potential in excited cells or transport across a membrane among them. The application of an electric field results in charge accumulation at the membrane resulting in conductance changes (Rettinger et al., 2016). For conventional PEF applications in the microsecond to millisecond domain, the present RC-element assembled of extracellular fluid (resistor) and cell membrane (capacitor) is charged resulting in reversible or irreversible electroporation dependent on the chosen parameter settings. The intracellular effects, in that case, will be negligible due to the insulating behavior of the charged membrane. In the case of pulse durations below the charging time of the RC-element the cells' organelles' membrane are exposed to the electric field with similar behavior as the cells' plasma membrane (Chiabrera et al., 1984; Schoenbach et al., 2004).

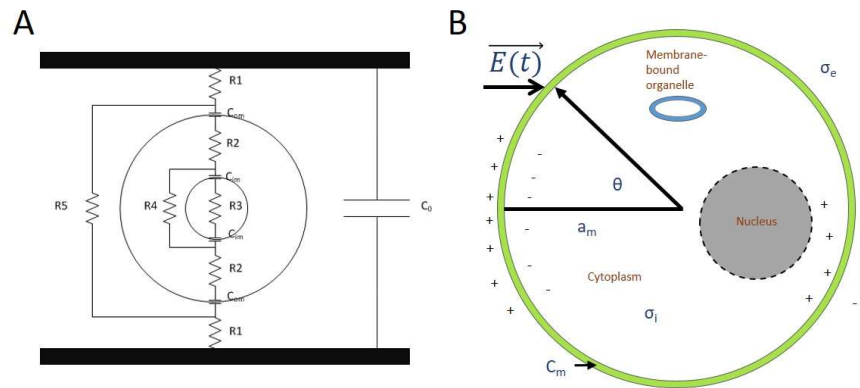


Figure 7: Underlying cell properties explaining various cellular responses to different pulse length and amplitude configurations. A) A biological cell as an electric equivalent circuit between two electrodes. Membranes can be viewed as a capacitor whereas intra- and extracellular fluid represent a resistor (adapted from Schoenbach et al., 2004). B) Cellular properties affecting the transmembrane potential and thus PEF treatment outcome.

As previously stated, PEF can either result in reversible or irreversible permeabilization of the cell. However, most research and current PEF applications in the food- and bioprocessing industry are focused on irreversible micro- to millisecond pulses targeting the cell membrane with focus on tissue softening, enhanced drying rates or inactivation of microorganisms (Barba et al., 2015; Golberg et al., 2016; Toepfl et al., 2006a). However, the constant growth of the human population poses new challenges regarding energy supply, food security, human health and biodiversity. Agriculture accounts for 30% of global greenhouse gas emissions and 85% of the water footprint. Biorefinery concepts, implementation of innovative technologies as well as a shift from animal toward more plant-based food are possible solutions to tackle these challenges. In this context, the exploitation of unicellular organisms e.g. microalgae has become a field of great interest. They can serve as raw material for biofuels or agricultural biostimulants, but at the same time are a promising source for food and feed production due to their high proportion of proteins and micronutrients. Besides these, unicellular organisms can be cultivated on non-arable land and fixate CO_2 if cultivated photoautotrophically. Therefore, microalgae have huge market potential. For example, according to Transparency Market Research (accessed on www.algaeindustrymagazine.com, October 29th 2018), a new market report entitled “Algae market, by application, by cultivation technology, and geography—global industry analysis, size, share, growth, trends, and forecast—2016–2024”, reported that the global algae market had a value of US\$608 million in 2015 and is projected to reach US\$1.143 billion with a volume of 27,552 tons by 2024. However, the cultivation of photoautotrophic unicellular organisms e.g.

microalgae is currently not competitive in comparison to other established sources. High production costs resulting from the growth medium, the energy supply and the extraction of valuable compounds demand a further improvement in the up- and downstream processing thereof. In this context, PEF/nsPEF are promising technologies to increase the viability of cultivation systems.

Nevertheless, implementation of nsPEF processing in the food- and bioprocessing industry needs an improved process characterization and control. The accurate pulse measurement as one of the main challenges faced in this regime. Moreover, there is a gap in process characterization in continuous PEF/nsPEF systems, allowing the transferability of findings to industrially relevant quantities. Thereby, the technology readiness level can be improved overall and the potential of PEF and nsPEF processing in the food- and bioprocessing industry can be leveraged. This will allow for innovative concepts, targeted on urgent matters in that sector, such as growth stimulation, selective inactivation and continuous extraction to be implemented in future food- and bioprocessing concepts (Fig. 8).

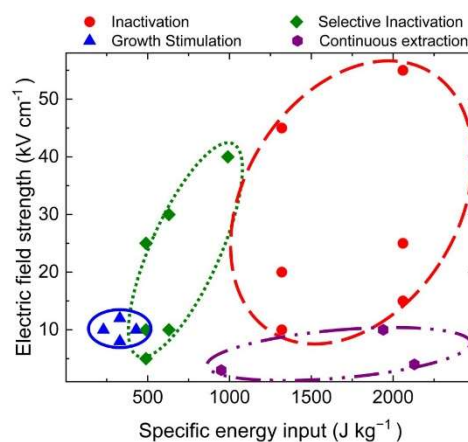


Figure 8: A case study of the microalgae *Chlorella vulgaris* SAG 211-12, illustrating treatment windows for selective inactivation, inactivation of microbial flora and *C. vulgaris*, continuous extraction of high value-added ingredients, and growth stimulation (Buchmann and Mathys, 2019).

3.1. PEF applications in the food- and bioprocessing industry

PEF applications in the food- and bioprocessing industry are numerous. Most current applications are focused on irreversible electroporation, including non (minimal)-thermal pasteurization, enhanced drying rates, increased extraction yields, and tissue softening (Barba et al., 2015; Golberg et al., 2016; Toepfl et al., 2006a). With regard to emerging PEF applications, selective inactivation of microorganisms, cyclic protein extraction and growth/ compound stimulation were recently shown in

lab-scale systems. Despite the PEF application on biological cells, the process can induce structural/functional modification of e.g. proteins as well (Mikhaylin et al., 2017; Sui et al., 2011). Given the huge potential of the technology, it is surprising to realize the scarce use thereof. This aspect is mainly attributed to the lack of treatment homogeneity, reproducibility and reporting of PEF research (Buckow et al., 2010; Gerlach et al., 2008; Jaeger et al., 2009a; Raso et al., 2016).

An overview of research articles on PEF applications in the food- and bioprocessing industry with a focus on reported process parameters is provided in Table 1. Patents within the field are excluded from the overview since specific process parameters cannot be determined.

Table 1: Literature overview of pulsed electric field applications in the food- and bioprocessing industry, focused on main research areas and reported PEF parameters and different organisms within the investigated research fields of this thesis.

Organism/ raw material	Application	PEF system	PEF parameter	Results	Source
<i>Auxenochlorella protothecoides</i> SAG 211-7a	Extraction	Continuous parallel-plate	32 kV cm ⁻¹ , 4 Hz, 6 mL min ⁻¹ , 1µs square wave pulse	Increased extraction of soluble compounds (around 30%)	(Goettel et al., 2013)
<i>Neochloris oleoabundans</i> UTEX 1185	Extraction	Continuous co-linear	20 kV cm ⁻¹ , 964 Hz, 14 pulses, 1476 kJ kg _{DW} ⁻¹ , 13 mL min ⁻¹ , 2µs square wave pulse	2.5% extracted protein	(Lam et al., 2017)
<i>Chlorella vulgaris</i> SAG 211-11b	Extraction	Continuous co-linear	20 kV cm ⁻¹ , 964 Hz, 14 pulses, 1476 kJ kg _{DW} ⁻¹ , 13 mL min ⁻¹ , 2µs square wave pulse	3.2% extracted protein	(Lam et al., 2017)
<i>Chlorella vulgaris</i> SAG 211-11b	Extraction	Continuous co-linear	20 kV cm ⁻¹ , 200 Hz, 27.75 Wh L ⁻¹ , 33mL min ⁻¹ , 5µs square wave pulse	3.6% extracted protein	(Postma et al., 2016)
<i>Haematococcus pluvialis</i>	Extraction	Batch parallel-plate	1 kV cm ⁻¹ , 1 Hz, 10 pulses, 50 kJ kg ⁻¹ , 5ms square wave pulse	Extraction of 96% of the total carotenoid content	(Martínez et al., 2019)
<i>Chlorella vulgaris</i> CCAP 211	Extraction	Continuous co-linear	20 kV cm ⁻¹ , 100 kJ kg ⁻¹ , 33mL min ⁻¹ , 5µs square wave pulse	Selective extraction of 36% w/w carbohydrates and 5.2% w/w proteins	(Carullo et al., 2018)
<i>Vaccinium myrtillus</i> L.	Extraction	Batch parallel-plate	1 kV cm ⁻¹ , 10Hz, 1 kJ kg ⁻¹ , 20µs square wave pulse	Increased juice yield and quality	(Bobinaité et al., 2015)
<i>Camellia sinensis</i>	Extraction	Batch parallel-plate	1 kV cm ⁻¹ , 0.2Hz, 100 pulses, 22 kJ kg ⁻¹ , 100µs	Enhanced polyphenol extraction after pre-treatment	(Liu et al., 2019)
<i>Chlamydomonas reinhardtii</i> SAG-34.98	Extraction	Batch parallel-plate	5.5 kV cm ⁻¹ , 5Hz, 10 pulses, 5µs square wave pulse	Increased lipid extraction after pre-treatment	(Bensalem et al., 2018)
Carrots, Apple	Extraction	Batch parallel-plate	0.8 kV cm ⁻¹ , 2kHz, 50 pulses, 765.5 kJ kg ⁻¹ , 10µs exponential decay pulse	Increased juice yield (10% carrots, 5% apple)	(Mannozi et al., 2018)

Organism	Application	PEF system	PEF parameter	Results	Source
<i>Escherichia coli</i> K12 TOP10	Extraction	Batch parallel-plate	20 kV cm ⁻¹ , 1 kHz, 8 pulses, 129.28 kJ L ⁻¹ , 100µs square wave pulse	16 µg mL ⁻¹ extracted protein	(Haberl Meglic et al., 2015)
Red beetroot	Extraction	Batch parallel-plate	1 kV cm ⁻¹ , 50 Hz, 270 pulses, 129.28 kJ L ⁻¹ , 10µs square wave pulse	About 90% of the total red pigments extracted	(Fincan et al., 2004)
<i>Escherichia coli</i> ATCC 11229	Inactivation	Continuous parallel-plate	25 kV cm ⁻¹ , 0.5 Hz, 25 pulses, 45 mL s ⁻¹ , 1.8µs exponential decay pulse	>2 log ₁₀ reduction	(Martín et al., 1997)
<i>Escherichia coli</i> K12DH5a	Inactivation	Continuous co-linear	35 kV cm ⁻¹ , 35 Hz, 5.3 pulses, 55 kJ kg ⁻¹ , 5 L h ⁻¹ , 3µs square wave pulse	4.4 log ₁₀ reduction	(Jaeger et al., 2010)
<i>Saccharomyces cerevisiae</i> S288	Inactivation	Continuous co-linear	20 kV cm ⁻¹ , 10.4 pulses, 2µs bipolar square wave pulse	3.9 log ₁₀ reduction	(Cserhalmi et al., 2002)
<i>Lactobacillus delbrueckii</i> ATCC 11842	Inactivation	Batch parallel-plate	16 kV cm ⁻¹ , 60 pulses, 200-300µs exponential decay pulse	4-5 log ₁₀ reduction	(Pothakamury et al., 1995)
<i>Lactobacillus rhamnosus</i> E522	Inactivation	Continuous co-linear	30 kV cm ⁻¹ , 56 Hz, 116 kJ kg ⁻¹ , 5 L h ⁻¹ , 3µs square wave pulse	5.5 log ₁₀ reduction	(Jaeger et al., 2009b)
<i>Listeria innocua</i> ATCC 33090	Inactivation	Continuous co-linear	32 kV cm ⁻¹ , 159.6 kJ kg ⁻¹ , 7.1 kg h ⁻¹ , 3µs square wave pulse	6.51 log ₁₀ reduction	(Schottroff et al., 2019)
<i>Bacillus subtilis</i> PS832	Inactivation	Continuous co-linear	10.26 kV cm ⁻¹ , 100 Hz, 163.1 kJ kg ⁻¹ , 6.4 L h ⁻¹ , 8µs square wave pulse	3.5 ± 0.3 log ₁₀ reduction	(Reineke et al., 2015)
<i>Geobacillus stearothermophilus</i> ATCC 7953	Inactivation	Continuous co-linear	10.26 kV cm ⁻¹ , 200 Hz, 180 kJ kg ⁻¹ , 6 L h ⁻¹ , 6µs square wave pulse	3.2 ± 0.4 log ₁₀ reduction	(Reineke et al., 2015)
<i>Bacillus subtilis</i> ATCC 9372 cells	Inactivation	Batch parallel-plate	30 kV cm ⁻¹ , 5 Hz, 100 pulses, 2.06 ± 0.289 kJ kg ⁻¹ , 80µs square wave pulse	4 log ₁₀ reduction	(Heinz and Knorr 2000)
<i>Zygosaccharomyces bailii</i> ATCC 36947	Inactivation	Continuous co-axial	35 kV cm ⁻¹ , 2 pulses, 2.3µs exponential decay pulse	5 log ₁₀ reduction	(Raso et al., 2006)

Organism	Application	PEF system	PEF parameter	Results	Source
<i>Total mesophilic aerobic counts</i>	Inactivation	Continuous co-linear	42 kV cm ⁻¹ , 2.4 L h ⁻¹ , 1.5µs exponential decay pulse	2.5 log ₁₀ reduction	(Walkling-Ribeiro et al., 2011)
<i>Escherichia coli</i> K12DH5a	Inactivation	Continuous co-linear	20 kV cm ⁻¹ , 50 Hz, 6 pulses, 80 kJ kg ⁻¹ , 5 kg h ⁻¹ , 6.2µs exponential decay pulse	5 log ₁₀ reduction	(Toepfl et al., 2007)
<i>Naegleria lovaniensis</i> Ar9M-1	Inactivation	Continuous co-linear	2 kV cm ⁻¹ , 10 pulses, 1 Hz, 10ms square wave pulses	100% inactivation of amoebae in fresh water	(Vernhes et al., 2002)
Protozoa	Inactivation	Continuous co-linear	0.9 kV cm ⁻¹ , 50 Hz, 65µs square wave pulse	100% Inactivation of protozoa in viable microalgae culture	(Rego et al., 2015)
Total microorganisms of raw skim milk and <i>Salmonella enteritidis</i> 9066.94	Inactivation	Continuous co-axial	55 kV cm ⁻¹ , 120Hz, 100 kJ kg ⁻¹ , 5 L h ⁻¹ , 250ns square wave pulse	1.4 log ₁₀ reduction of total microflora and <i>S. enteritidis</i>	(Floury et al., 2006)
Polyphenoloxidase (PPO)	Inactivation	Batch parallel-plate	25 kV cm ⁻¹ , 30Hz, 100 pulses, 207.61 kJ kg ⁻¹ , 3.4µs exponential decay pulse	PPO activity at anode reduced to around 45%	(Meneses et al., 2011c)
Platelets	Modification	Batch parallel-plate	30 kV cm ⁻¹ , 1 pulse, 300ns	Platelete activation/ aggregation	(Zhang et al., 2008)
β-lactoglobulin	Modification	Batch parallel-plate	80 kV cm ⁻¹ , 750 pulses, 10µs	80% Improvement of the enzymatic hydrolysis	(Mikhaylin et al., 2017)
Whey protein isolate	Modification	Continuous co-linear	30 kV cm ⁻¹ , 100 Hz, 131.9 kJ L ⁻¹ , 60mL min ⁻¹ , 2µs bipolar square wave pulse	Reduced gel strength	(Sui et al., 2011)
Carrots, Potatoes and Apples.	Modification	Batch parallel-plate	1.1 kV cm ⁻¹ , 100 Hz, 1000 pulses, 10µs square wave pulse	Tissue softening	(Lebovka et al., 2004)
Potatos	Modification	Batch parallel-plate	0.5 kV cm ⁻¹ , 90 pulses, 10µs square wave pulse	Tissue softening	(Fincan and Dejmek, 2003)

Organism	Application	PEF system	PEF parameter	Results	Source
Apple	Modification	Batch parallel-plate	1.07 kV cm ⁻¹ , 2 Hz, 0.5 kJ kg ⁻¹ , 40ms exponential decay pulse	Enhanced quality after drying	(Lammerskitten et al., 2019)
Organic strawberries	Modification	Batch parallel-plate	0.2 kV cm ⁻¹ , 100 Hz, 200 pulses, 10μs square wave pulse	Enhanced stability of anthocyanins during gastrointestinal in vitro digestion	(Oliveira et al., 2019)
β-lactoglobulin and ovalbumin	Modification	Batch parallel-plate	33 kV cm ⁻¹ , 1 Hz, 1000 pulses, 1.4μs exponential decay pulse	No significant unfolding or aggregation of protein solutions	(Barsotti et al., 2001)
Strawberries	Modification	Batch parallel-plate	0.85 kV cm ⁻¹ , 1 kHz, 5 pulses, 100μs bipolar square wave pulse	Higher cell viability in epidermal layer and 30% more red color retention	(Velickova et al., 2018)
<i>Lactobacillus plantarum</i> WCFS1	Modification	Batch parallel-plate	7.5 kV cm ⁻¹ , 0.2 Hz, 16.2 kJ kg ⁻¹ , 0.1ms square wave pulse	Increased intracellular trehalose content	(Vaessen et al., 2018)
<i>Arabidopsis thaliana</i> Columbia-0	Stimulation	Batch parallel-plate	5 kV cm ⁻¹ , 10 pulses, 100ns square wave pulse	Enhanced leaf area	(Eing et al., 2009)
<i>Arabidopsis thaliana</i> Columbia-0	Stimulation	Batch parallel-plate	10 kV cm ⁻¹ , 100 pulses, 10ns square wave pulse	80% increased leaf area	(Songnuan and Kirawanich, 2012)
<i>Saccharomyces cerevisiae</i> Actiflore F33	Stimulation	Batch parallel-plate	6 kV cm ⁻¹ , 10 Hz, 1000 pulses, 100μs square wave pulse	3.98 times increased Fructose consumption after lag phase	(Mattar et al., 2014)
<i>Chlamydomonas reinhardtii</i> 137c	Stimulation	Continuous parallel-plate	40 kV cm ⁻¹ , 4 Hz, 2 kJ kg ⁻¹ , 6.36 mL min ⁻¹ , 50ns square wave pulse	Stable cellular differentiation in palmella stage	(Bai et al., 2017)
Stem cells	Stimulation	Batch parallel-plate	10 kV cm ⁻¹ , 1 Hz, 5 pulses, 100ns	Enhanced chondrogenic potential of mesenchymal stem cells	(Ning et al., 2019)
Rat liver epithelial WB-F344 cells	Stimulation	Batch parallel-plate	20 kV cm ⁻¹ , 20 pulses, 100ns	Stimulation of the respiratory activity	(Steuer et al., 2018)
<i>Taxus chinensis</i>	Stimulation	Batch parallel-plate	0.01 V cm ⁻¹ , 50 Hz, 20 pulses, 20μs	Significant increase in intracellular accumulation of taxuyunnanine	(Ye et al., 2004)

The literature overview of pulsed electric field applications in the food- and bioprocessing industry (Table 1) emphasized the strong need for more homogeneous and accurate PEF treatment parameters (Raso et al., 2016). Despite the evident difficulties of the technology to develop into a widespread benchmark process for its promising applications, with regard to plant tissue modification and juice production, the advantage of PEF has been proven and found industrial applications (Table 1) (Toepfl, 2012).

However, the extraction efficiency of soluble substances from e.g. microalgae was limited and was not even close to the benchmark process of high-pressure homogenization (HPH). Nevertheless, PEF processing showed promising results with regard to pigment and polyphenol extraction. For non-soluble substances PEF has shown potential as pre-treatment method, enhancing lipid yields with subsequent solvent extraction (Table 1). Yet, an interesting aspect that was so far overlooked was the cells' morphology after the treatment. Due to the increased ion transfer, cell swelling or shrinking can occur after the treatment, yet for cell wall containing cells the process is not able to fully disintegrate the cells. Hence, a limited soluble compound extraction is realistic if the cells' morphology is more or less kept intact, as major e.g. protein fractions can be found within the structural parts of a cell e.g. membrane (Safi et al., 2014). However, the question that was not yet answered was whether the overall intact cells are actually still viable and subsequently could be cultivated again, allowing a cyclic protein extraction which can be compared to the conventional milking of animals.

With regard to the inactivation results (Table 1), it is observable that different microorganisms have a different susceptibility to the treatment. This concept is not surprising as different inactivation kinetics are known for other processes e.g. thermal processing as well (Kessler, 2002). Yet most inactivation trials focused either on non-(minimal) thermal preservation or specific inactivation of larger target organisms, which are naturally assumed to be more susceptible to an electric field, as shown in Eq. (14). However, the results indicate that selective inactivation of an undesirable flora within prokaryotic/eukaryotic consortia might be possible.

With regard to the different results as shown in Table 1 it is eminent that throughputs and consequently energy inputs are mostly stated as absolute values. Treatment inhomogeneities were analyzed throughout the years, however, the impact of electric and flow field distributions on subsequent treatment homogeneity was neglected.

Based on such a comprehensive PEF system analysis, the current limitations such as the lack of treatment homogeneity and thus reproducibility of PEF research might be overcome. For example, it was shown throughout that the effect of growth/compound stimulation occurs in a narrow processing window (Table 1). Therefore, without proper process characterization and control continuous processing is not achievable. Certainly, overprocessing of the cells can be considered, however the stress response of the cells will be different, e.g. cell differentiation into stagnant cell cycle e.g. palmella stage, during which pigments such as astaxanthin are accumulated. This stress response might be desired in certain cases, however, it does not allow for simultaneous growth and/or compound stimulation.

Despite the application of PEF/nsPEF on biological cells focusing on extraction, inactivation or stimulation, the technology has shown to induce modifications of certain macromolecules and tissue. Subsequently, novel techno-functional properties of treated macromolecules might be obtained as well as favoured structures of certain tissue. Based on the possibly occurring protein modification during PEF processing, the influence thereof on techno-functional properties of extracted compounds has not been considered so far. This aspect was recently studied in dairy products where the elimination of microorganisms was reported while the activity of bioactive components found in dairy products was conserved (Mathys et al., 2013). However, with regard to extracted compounds from biological cells/tissue this aspect was not yet analyzed.

REFERENCES

1. 't Lam, G.P., Vermuë, M.H., Eppink, M.H.M., Wijffels, R.H., van den Berg, C., 2017. Multi-product microalgae biorefineries: From concept towards reality. *Trends Biotechnol.* 36, 216–227.
2. Alkhafaji, S.R., Farid, M., 2007. An investigation on pulsed electric fields technology using new treatment chamber design. *Innov. Food Sci. Emerg. Technol.* 8, 205–212.
3. Anderson, A. K., Finkelstein, R., 1919. A study of electro-pure process of treating milk. *J Dairy Sci* 2:374–406.
4. Bai, F., Gusbeth, C., Frey, W., Nick, P., 2017. Nanosecond pulsed electric fields trigger cell differentiation in *Chlamydomonas reinhardtii*. *Biochim. Biophys. Acta - Biomembr.* 1859, 651–661.
5. Barba, F.J., Galanakis, C.M., Esteve, M.J., Frigola, A., Vorobiev, E., 2015. Potential use of pulsed electric technologies and ultrasounds to improve the recovery of high-added value compounds from blackberries. *J. Food Eng.* 167, 38–44.
6. Barbosa-Cánovas, G. V., Ghani Albaali, A., Juliano, P., Knoerzer, K., 2011. Introduction to innovative food processing technologies: Background, advantages, issues, and need for multiphysics modeling. *Innov. Food Process. Technol. Adv. Multiphysics Simul.* 3–21.
7. Barbosa-Cánovas, G. V., Altunakar, B., 2006. Pulsed Electric Fields Processing of Foods: An Overview, in: Raso, J., Heinz, V. (Eds.), *Pulsed Electric Fields Technology for the Food Industry: Fundamentals and Applications*. Springer US, Boston, pp. 3–26.
8. Barsotti, L., Dumay, E., Mu, T.H., Fernandez Diaz, M.D., Cheftel, J.C., 2001. Effects of high voltage electric pulses on protein-based food constituents and structures. *Trends Food Sci. Technol.* 12, 136–144.
9. Barsotti, L., Merle, P., Cheftel, J.C., 1999. Food processing by pulsed electric fields. I. Physical aspects. *Food Rev. Int.* 15, 163–180.
10. Beebe, S.J., Schoenbach, K.H., 2005. Nanosecond pulsed electric fields: A new stimulus to activate intracellular signaling. *J. Biomed. Biotechnol.* 2005, 297–300.
11. Bensalem, S., Lopes, F., Bodénès, P., Pareau, D., François, O., Le Pioufle, B., 2018. Understanding the mechanisms of lipid extraction from microalga *Chlamydomonas reinhardtii* after electrical field solicitations and mechanical stress within a microfluidic device. *Bioresour. Technol.* 257, 129–136.
12. Bergman, T.L., Incropera, F.P., 2011. *Fundamentals of heat and mass transfer*. Wiley.
13. Bertacchini, C., Margotti, P.M., Bergamini, E., Lodi, A., Ronchetti, M., Cadossi, R., Ph, D., Ronchetti, M., Cadossi, R., 2007. Design of an irreversible electroporation system for clinical use. *Technol Cancer Res Treat* 6, 313–320.
14. Bertholon, P., 1783. *De l'électricité des végétaux*. Paris: Imprimerie de Didot Jeune.
15. Bluhm, H., 2006. *Pulsed Power Systems*. Springer-Verlag Berlin.
16. Blume, S., Gerber, D., Jaritz, M., Carstensen, C., 2014. State-of-the-Art Solid State Pulse Modulators, in: *CERN Accelerator School on Power Converters*.
17. Bobinaitė, R., Pataro, G., Lamanauskas, N., Šatkauskas, S., Viškelis, P., Ferrari, G., 2015. Application of pulsed electric field in the production of juice and extraction of bioactive compounds from blueberry fruits and their by-products. *J. Food Sci. Technol.* 52.
18. Buchmann, L., Bertsch, P., Böcker, L., Krähenmann, U., Fischer, P., Mathys, A., 2019a. Adsorption kinetics and foaming properties of soluble microalgae fractions at the air/water interface. *Food Hydrocoll.* 97, 105182.
19. Buchmann, L., Bloch, R., Mathys, A., 2018a. Comprehensive pulsed electric field (PEF) system analysis for microalgae processing. *Bioresour. Technol.* 265, 268–274.
20. Buchmann, L., Böcker, L., Frey, W., Haberkorn, I., Nyffeler, M., Mathys, A., 2018b. Energy input assessment for nanosecond pulsed electric field processing and its application in a case study with

- Chlorella vulgaris*. *Innov. Food Sci. Emerg. Technol.* 47, 445–453.
21. Buchmann, L., Brändle, I., Haberkorn, I., Hiestand, M., Mathys, A., 2019b. Pulsed electric field based cyclic protein extraction of microalgae towards closed-loop biorefinery concepts. *Bioresour. Technol.* 291, 121870.
 22. Buchmann, L., Frey, W., Gusbeth, C., Ravaynia, P.S., Mathys, A., 2019c. Effect of nanosecond pulsed electric field treatment on cell proliferation of microalgae. *Bioresour. Technol.* 271, 402–408.
 23. Buchmann, L., Mathys, A., 2019. Perspective on Pulsed Electric Field Treatment in the Bio-based Industry. *Front. Bioeng. Biotechnol.* 7, 265.
 24. Buckow, R., Schroeder, S., Berres, P., Baumann, P., Knoerzer, K., 2010. Simulation and evaluation of pilot-scale pulsed electric field (PEF) processing. *J. Food Eng.* 101, 67–77.
 25. Carullo, D., Abera, B.D., Casazza, A.A., Donsì, F., Perego, P., Ferrari, G., Pataro, G., 2018. Effect of pulsed electric fields and high pressure homogenization on the aqueous extraction of intracellular compounds from the microalgae *Chlorella vulgaris*. *Algal Res.* 31, 60–69.
 26. Chiabrera, A., Grattarola, M., Viviani, R., 1984. Interaction between electromagnetic fields and cells: Microelectrophoretic effect on ligands and surface receptors. *Bioelectromagnetics* 5, 173–191.
 27. COMSOL: multiphysics CYCLOPEDIA - Navier-Stokes Equations, 2018. <https://www.comsol.com/multiphysics/navier-stokes-equations>, accessed on 2018-02-06.
 28. Cserhalmi, Z., Vidács, I., Beczner, J., Czukor, B., 2002. Inactivation of *Saccharomyces cerevisiae* and *Bacillus cereus* by pulsed electric fields technology. *Innov. Food Sci. Emerg. Technol.* 3, 41–45.
 29. de Araujo, A.L.A., Claudel, J., Nadi, M., Kourtiche, D., 2018. Detection and characterization of biological cells by impedance spectroscopy, in: 12th International Conference on Sensing Technology (ICST). IEEE, pp. 309–314.
 30. Deng, J., Stark, R.H., Schoenbach, K.H., 2001. A compact, nanosecond pulse generator with water as dielectric and as switch medium. *PPPS 2001 - Pulsed Power Plasma Sci.* 2001 2, 1587–1590.
 31. Dufour, D., 2018. Ultrasound Doppler Flow Measurement in Food Production and Digestion Processes. Ph.D. thesis, ETH Zürich.
 32. Eing, C., Bonnet, S., Pacher, M., Puchta, H., Frey, W., 2009. Effects of nanosecond pulsed electric field exposure on *Arabidopsis thaliana*. *IEEE Trans. Dielectr. Electr. Insul.* 16, 1322–1328.
 33. Fiala, A., Wouters, P.C., van den Bosch, E., Creyghton, Y.L., 2001. Coupled electrical-fluid model of pulsed electric field treatment in a model food system. *Innov. Food Sci. Emerg. Technol.* 2, 229–238.
 34. Fincan, M., Dejmek, P., 2003. Effect of osmotic pretreatment and pulsed electric field on the viscoelastic properties of potato tissue. *J. Food Eng.* 59, 169–175.
 35. Fincan M., DeVito F., Dejmek P., 2004. Pulsed electric field treatment for solid-liquid extraction of red beetroot pigment. *J Food Eng* 64:381–388.
 36. Floury, J., Grosset, N., Leconte, N., Pasco, M., Madec, M.-N., Jeantet, R., 2006. Continuous raw skim milk processing by pulsed electric field at non-lethal temperature: effect on microbial inactivation and functional properties. *Lait* 86, 43–57.
 37. Fuller, G.W., 1898. Report on the investigations into the purification of the Ohio river water at Louisville Kentucky. D. Van Nostrand Company, New York.
 38. Gerlach, D., Alleborn, N., Baars, A., Delgado, A., Moritz, J., Knorr, D., 2008. Numerical simulations of pulsed electric fields for food preservation: A review. *Innov. Food Sci. Emerg. Technol.* 9, 408–417.
 39. Giteru, S.G., Oey, I., Ali, M.A., 2018. Feasibility of using pulsed electric fields to modify biomacromolecules: A review. *Trends Food Sci. Technol.* 72, 91–113.
 40. Glaser, R.W., Leikin, S.L., Chernomordik, L. V., Pastushenko, V.F., Sokirko, A.I., 1988. Reversible electrical breakdown of lipid bilayers: formation and evolution of pores. *BBA - Biomembr.* 940, 275–287.

41. Goettel, M., Eing, C., Gusbeth, C., Straessner, R., Frey, W., 2013. Pulsed electric field assisted extraction of intracellular valuables from microalgae. *Algal Res.* 2, 401–408.
42. Golberg, A., Sack, M., Teissie, J., Pataro, G., Pliquett, U., Saulis, G., Stefan, T., Miklavcic, D., Vorobiev, E., Frey, W., 2016. Energy-efficient biomass processing with pulsed electric fields for bioeconomy and sustainable development. *Biotechnol. Biofuels* 9, 94.
43. Góngora-Nieto, M.M., Sepúlveda, D.R., Pedrow, P., Barbosa-Cánovas, G. V., Swanson, B.G., 2002. Food Processing by Pulsed Electric Fields: Treatment Delivery, Inactivation Level, and Regulatory Aspects. *LWT - Food Sci. Technol.* 35, 375–388.
44. Haberl Meglic, S., Marolt, T., Miklavcic, D., 2015. Protein Extraction by Means of Electroporation from *E. coli* with Preserved Viability. *J. Membr. Biol.* 248, 893–901.
45. Heinz, V., Álvarez, I., Angersbach, A., Knorr, D., 2002. Preservation of liquid foods by high intensity pulsed electric fields-basic concepts for process design. *Trends Food Sci. Technol.* 12, 103–111.
46. Heinz, V., Knorr, D., 2000. Effect of pH, ethanol addition and high hydrostatic pressure on the inactivation of *Bacillus subtilis* by pulsed electric fields. *Innov. Food Sci. Emerg. Technol.* 1, 151–159.
47. Ho, S., Mittal, G.S., 2000. High Voltage Pulsed Electrical Field for Liquid Food Pasteurization. *Food Rev. Int.* 16, 395–434.
48. Huang, K., Wang, J., 2009. Designs of pulsed electric fields treatment chambers for liquid foods pasteurization process: A review. *J. Food Eng.* 95, 227–239.
49. Jaeger, H., 2012. Process Performance Analysis of Pulsed Electric Field (PEF) Food Applications. Ph.D. thesis, Technol. Univ. Berlin.
50. Jaeger, H., Meneses, N., Knorr, D., 2009a. Impact of PEF treatment inhomogeneity such as electric field distribution, flow characteristics and temperature effects on the inactivation of *E. coli* and milk alkaline phosphatase. *Innov. Food Sci. Emerg. Technol.* 10, 470–480.
51. Jaeger, H., Meneses, N., Moritz, J., Knorr, D., 2010. Model for the differentiation of temperature and electric field effects during thermal assisted PEF processing. *J. Food Eng.* 100, 109–118.
52. Jaeger, H., Schulz, A., Karapetkov, N., Knorr, D., 2009b. Protective effect of milk constituents and sublethal injuries limiting process effectiveness during PEF inactivation of *Lb. rhamnosus*. *Int. J. Food Microbiol.* 134, 154–161.
53. Juliano, P., Javier Trujillo, F., Barbosa-Cánovas, G. V., Knoerzer, K., 2011. The Need for Thermophysical Properties in Simulating Emerging Food Processing Technologies, in: Knoerzer, K., Juliano, P., Roupas, P., Versteeg, C. (Eds.), *Innovative Food Processing Technologies: Advances in Multiphysics Simulation*. Blackwell Publishing Ltd, pp. 23–38
54. Kessler, H., 2002. *Food and Bio Process Engineering: Dairy Technology*, 5th ed. Verlag A. Kessler, Muenchen, Germany.
55. Kinoshita, K.J., Ashikawa, I., Saita, N., Yoshimura, H., Itoh, H., Nagayama, K., Ikegami, A., 1988. Electroporation of cell membrane visualized under a pulsed-laser fluorescence microscope. *Biophys. J.* 53, 1015–9.
56. Knoerzer, K., Baumann, P., Buckow, R., 2012. An iterative modelling approach for improving the performance of a pulsed electric field (PEF) treatment chamber. *Comput. Chem. Eng.* 37, 48–63.
57. Kolb, J.F., Kono, S., Schoenbach, K.H., 2006. Nanosecond pulsed electric field generators for the study of subcellular effects. *Bioelectromagnetics* 27, 172–187.
58. Kotnik, T., Miklavčič, D., 2006. Theoretical evaluation of voltage inducement on internal membranes of biological cells exposed to electric fields. *Biophys. J.* 90, 480–491.
59. Krieger, I.M., Dougherty, T.J., 1959. A Mechanism for non-newtonian flow in suspensions of rigid spheres. *Trans. Soc. Rheol.* 3, 137–152.
60. Küchler, A., 2009. *Hochspannungstechnik*. Springer International Publishing AG.
61. Lammerskitten, A., Wiktor, A., Siemer, C., Toepfl, S., Mykhailyk, V., Gondek, E., Rybak, K., Witrowa-

- Rajchert, D., Parniakov, O., 2019. The effects of pulsed electric fields on the quality parameters of freeze-dried apples. *J. Food Eng.* 252, 36–43.
62. Lebovka, N.I., Praporscic, I., Vorobiev, E., 2004. Effect of moderate thermal and pulsed electric field treatments on textural properties of carrots, potatoes and apples. *Innov. Food Sci. Emerg. Technol.* 5, 9–16.
63. Leicester, J., 1892. Action of electric currents upon the growth of seeds and plants. *Scientific American*, 33, 13505–13506.
64. Lemström, S., 1904. *Electricity in Agriculture and Horticulture*. London: The Electrician Printing & Publishing Company Ltd.
65. Lindgren, M., Aronsson, K., Galt, S., Ohlsson, T., 2002. Simulation of the temperature increase in pulsed electric field (PEF) continuous flow treatment chambers. *Innov. Food Sci. Emerg. Technol.* 3, 233–245.
66. Liu, Z., Esveld, E., Vincken, J.P., Bruins, M.E., 2019. Pulsed Electric Field as an Alternative Pre-treatment for Drying to Enhance Polyphenol Extraction from Fresh Tea Leaves. *Food Bioprocess Technol.* 12, 183–192.
67. Mahnič-Kalamiza, S., Vorobiev, E., Miklavčič, D., 2014. Electroporation in Food Processing and Biorefinery. *J. Membr. Biol.* 247, 1279–1304.
68. Mannozi, C., Fauster, T., Haas, K., Tylewicz, U., Romani, S., Dalla Rosa, M., Jaeger, H., 2018. Role of thermal and electric field effects during the pre-treatment of fruit and vegetable mash by pulsed electric fields (PEF) and ohmic heating (OH). *Innov. Food Sci. Emerg. Technol.* 48, 131–137.
69. Martín, O., Qin, B.L., Chang, F.J., Barbosa-Cánovas, G. V., Swanson, B.G., 1997. Inactivation of *Escherichia coli* in skim milk by high intensity pulsed electric fields HIGH. *J. Food Process Eng.* 20, 317–336.
70. Martínez, J.M., Gojkovic, Z., Ferro, L., Maza, M., Álvarez, I., Raso, J., Funk, C., 2019. Use of pulsed electric field permeabilization to extract astaxanthin from the nordic microalga *Haematococcus pluvialis*. *Bioresour. Technol.* 289, 121694.
71. Mathys, A., Toepfl, S., Siemer, C., Favre, L., Benyacoub, J., Hansen, C.E., 2013. Pulsed electric field treatment process and dairy product comprising bioactive molecules obtainable by the process. WO2013/007620A1.
72. Matsumoto, Y., Satake, T., Shioji, N., Sakuma, A., 1991. Inactivation of micro-organisms by pulsed high voltage applications, in: Conference Recordings of IEEE Industrial Applications Society Annual Meeting. pp. 652–659.
73. Mattar, J.R., Turk, M.F., Nonus, M., Lebovka, N.I., El Zakhem, H., Vorobiev, E., 2014. Electro-stimulation of *S. cerevisiae* wine yeasts by pulsed electric field and its effects on fermentation capacity. *Food Bioprocess Technol.* 7, 3328–3335.
74. Meneses, N., Jaeger, H., Knorr, D., 2011a. Minimization of Thermal Impact by Application of Electrode Cooling in a Co-linear PEF Treatment Chamber. *J. Food Sci.* 76, E536–E543.
75. Meneses, N., Jaeger, H., Knorr, D., 2011. Basics for Modeling of Pulsed Electric Field Processing of Foods, in: Knoerzer, K., Juliano, P., Roupas, P., Versteeg, C. (Eds.), *Innovative Food Processing Technologies: Advances in Multiphysics Simulation*, John Wiley & Sons, Ltd., pp. 171–191.
76. Meneses, N., Jaeger, H., Knorr, D., 2011c. pH-changes during pulsed electric field treatments --- Numerical simulation and in situ impact on polyphenoloxidase inactivation. *Innov. Food Sci. Emerg. Technol.* 12, 499–504
77. Meneses, N., Jaeger, H., Moritz, J., Knorr, D., 2011d. Impact of insulator shape, flow rate and electrical parameters on inactivation of *E. coli* using a continuous co-linear PEF system. *Innov. Food Sci. Emerg. Technol.* 12, 6–12.
78. Mewis, J., Macosko, C.W., 1994. Suspension Rheology, in: Macosko, C.W. (Ed.), *Rheology: Principles, Measurements, and Applications*. Wiley-VCH, pp. 425–474.

79. Mezger, T.G., 2015. Applied Rheology, 1st ed. Anton Paar GmbH, Graz.
80. Mikhaylin, S., Boussetta, N., Vorobiev, E., Bazinet, L., 2017. High voltage electrical treatments to improve the protein susceptibility to enzymatic hydrolysis. ACS Sustain. Chem. Eng. 5.
81. Min, S., Evrendilek, G.A., Zhang, Q.H., 2007. Pulsed Electric Fields: Processing System, Microbial and Enzyme Inhibition, and Shelf Life Extension of Foods. IEEE Trans. Plasma Sci. 35, 59–73.
82. Mittal, G.S., Griffiths, M.W., 2005. Pulsed Electric Field Processing of Liquid Foods and Beverages, in: Sun, D.-W. (Ed.), Emerging Technologies for Food Processing. Elsevier Ltd, pp. 99–139.
83. Ning, T., Guo, J., Zhang, K., Li, K., Zhang, J., Yang, Z., Ge, Z., 2019. Nanosecond pulsed electric fields enhanced chondrogenic potential of mesenchymal stem cells via JNK / CREB- STAT3 signaling pathway. Stem Cell Res. Ther. 10, 45.
84. Nollet, J. A., 1749, Recherches Sur Les Causes Particulieres des Phenomenes Electriques, les Freres Guerin, Paris.
85. Oliveira, G., Tylewicz, U., Dalla Rosa, M., Andlid, T., Alminger, M., 2019. Effects of pulsed electric field-assisted osmotic dehydration and edible coating on the recovery of anthocyanins from in vitro digested berries. Foods 8, 505.
86. Pavlin, M.M., Kandušer, M., Reberšek, M., Pucihar, G., Hart, F.X., Magjarević, R., Miklavčič, D., Kanduser, M., Reberšek, M., Pucihar, G., Hart, F.X., Magjareciv, R., Miklavčič, D., 2005. Effect of cell electroporation on the conductivity of a cell suspension. Biophys. J. 88, 4378–4390.
87. Postma, P.R., Pataro, G., Capitoli, M., Barbosa, M.J., Wijffels, R.H., Eppink, M.H.M., Olivieri, G., Ferrari, G., 2016. Selective extraction of intracellular components from the microalga *Chlorella vulgaris* by combined pulsed electric field-temperature treatment. Bioresour. Technol. 203, 80–88.
88. Pothakamury, U.R., Monsalve-González, A., Barbosa-Cánovas, G. V., Swanson, B.G., 1995. Inactivation of *Escherichia coli* and *Staphylococcus aureus* in model foods by pulsed electric field technology. Food Res. Int. 28, 167–171.
89. Qin, B., Zhang, Q.H., Barbosa-Canovas, G. V., Swanson, B.G., Pedrow, P.D., 1995. Pulsed electric-field treatment chamber design for liquid food pasteurization using a finite-element method. Trans. Am. Soc. Agric. Eng. 38, 557–565.
90. Raso, J., Calderón, M.L., Góngora, M., Barbosa-Cánovas, G. V., Swanson, B.G., 2006. Inactivation of *Zygosaccharomyces Bailii* in fruit juices by heat, high hydrostatic pressure and pulsed electric fields. J. Food Sci. 63, 1042–1044.
91. Raso, J., Frey, W., Ferrari, G., Pataro, G., Knorr, D., Teissie, J., Miklavčič, D., 2016. Recommendations guidelines on the key information to be reported in studies of application of PEF technology in food and biotechnological processes. Innov. Food Sci. Emerg. Technol. 37, 312–321.
92. Rebersek, M., Kranjc, M., Pavliha, D., Batista-Napotnik, T., Vrtanik, D., Amon, S., Miklavcic, D., 2009. Blumlein configuration for high-repetition-rate pulse generation of variable duration and polarity using synchronized switch control. IEEE Trans. Biomed. Eng. 56, 2642–2648.
93. Rebersek, M., Miklavčič, D., 2011. Advantages and disadvantages of different concepts of electroporation pulse generation. Automatika 52, 12–19.
94. Rebersek, M., Miklavčič, D., 2010. Concepts of Electroporation Pulse Generation and Overview of Electric Pulse Generators for Cell and Tissue Electroporation, in: Pakhomov, A.G., Miklavčič, D., Markov, M.S. (Eds.), Advanced Electroporation Techniques in Biology and Medicine. Boca Raton: CRC Press, pp. 431–496.
95. Rego, D., Redondo, L.M., Geraldés, V., Costa, L., Navalho, J., Pereira, M.T., 2015. Control of predators in industrial scale microalgae cultures with pulsed electric fields. Bioelectrochemistry 103, 60–64.
96. Reineke, K., Schottroff, F., Meneses, N., Knorr, D., 2015. Sterilization of liquid foods by pulsed electric fields-an innovative ultra-high temperature process. Front. Microbiol. 6.
97. Rettinger, J., Schwarz, S., Schwarz, W., 2016. Electrophysiology: Basics, Modern Approaches and Applications. Springer, Cham.

98. Safi, C., Zebib, B., Merah, O., Pontalier, P.Y., Vaca-Garcia, C., 2014. Morphology, composition, production, processing and applications of *Chlorella vulgaris*: A review. *Renew. Sustain. Energy Rev.* 35, 265–278
99. Sanders, J.M., Kuthi, A., Wu, Y.H., Vernier, P.T., Gundersen, M.A., 2009. A linear, single-stage, nanosecond pulse generator for delivering intense electric fields to biological loads. *IEEE Trans. Dielectr. Electr. Insul.* 16, 1048–1054.
100. Sater, L. E., 1935. Passing an alternating electric current through food and fruit juices. *Research Bulletin, Information Systems Division, National Agricultural Library* 181:275–312.
101. Schlichting, H., Gersten, K., 2017. *Boundary-Layer Theory*, 9th ed. Springer-Verlag Berlin Heidelberg.
102. Schoenbach, K.H., Joshi, R.P., Kolb, J.F., Chen, N., Stacey, M., Blackmore, P.F., Buescher, E.S., Beebe, S.J., 2004. Ultrashort electrical pulses open a new gateway into biological cells, in: *Proceedings of the IEEE*. pp. 1122–1137.
103. Schottroff, F., Gratz, M., Krottenthaler, A., Johnson, N.B., Bédard, M.F., Jaeger, H., 2019. Pulsed electric field preservation of liquid whey protein formulations – Influence of process parameters, pH, and protein content on the inactivation of *Listeria innocua* and the retention of bioactive ingredients. *J. Food Eng.* 243, 142–152.
104. Schwab, A.J., 1981. *Hochspannungsmesstechnik*. Springer-Verlag Berlin.
105. Schwan, H. P., 1957. Electrical properties of tissue and cell suspensions. *Adv.Biol.Med.Phys.*, 147-209.
106. Sensoy, I., Zhang, Q.H., Sastry, S.K., 1997. Inactivation kinetics of *Salmonella dublin* by pulsed electric field. *J. Food Process Eng.* 20, 367–381.
107. Silve, A., Ivorra, A., Mir, L.M., 2011. Detection of permeabilisation obtained by micropulses and nanopulses by means of bioimpedance of biological tissues. *EuCAP* 3164–67.
108. Songnuan, W., Kirawanich, P., 2012. Early growth effects on *Arabidopsis thaliana* by seed exposure of nanosecond pulsed electric field. *J. Electrostat.* 70, 445–450.
109. Spagnolie, S.E. (Ed.), 2015. *Complex Fluids in Biological Systems*. Springer Science+Business Media New York 2015.
110. Steuer, A., Wolff, C.M., von Woedtke, T., Weltmann, K.-D., Kolb, J.F., 2018. Cell stimulation versus cell death induced by sequential treatments with pulsed electric fields and cold atmospheric pressure plasma. *PLoS One* 13, e0204916.
111. Stone, G. E., 1909. Influence of electricity on micro-organisms. *Bot. Gaz.*, 48:359-379.
112. Sui, Q., Roginski, H., Williams, R.P.W., Versteeg, C., Wan, J., 2011. Effect of pulsed electric field and thermal treatment on the physicochemical and functional properties of whey protein isolate. *Int. Dairy J.* 21, 206–213.
113. Takeda, Y., 1995. Velocity profile measurement by ultrasonic doppler method. *Exp. Therm. Fluid Sci.* 10, 444–453.
114. Takeda, Y., Tasaka, Y., 2012. Ultrasonic Wave for Fluid Flow, in: Takeda, Y. (Ed.), *Ultrasonic Doppler Velocity Profiler for Fluid Flow*. Springer Japan, Tokyo, pp. 21–42.
115. Teissie, J., 2017. Critical Electric Field and Transmembrane Voltage for Lipid Pore Formation in Experiments, in: Miklavčič, D. (Ed.), *Handbook of Electroporation*. Springer International Publishing AG 2017, pp. 25–43.
116. Teissie, J., Tsong, T.Y., 1981. Electric field induced transient pores in phospholipid bilayer vesicles. *Biochemistry* 20, 1548–1554.
117. Toepfl, S., 2012. Pulsed electric field food processing -industrial equipment design and commercial applications. *Stewart Postharvest Rev.* 8.
118. Toepfl, S., 2011. Pulsed Electric Field food treatment - scale up from lab to industrial scale. *Procedia Food Sci.* 1, 776–779.

119. Toepfl, S., 2006. Pulsed Electric Fields (PEF) for Permeabilization of Cell Membranes in Food- and Bioprocessing. Applications, Process and Equipment Design and Cost Analysis. Ph.D. thesis, Technol. Univ. Berlin.
120. Toepfl, S., Heinz, V., Knorr, D., 2007. High intensity pulsed electric fields applied for food preservation. *Chem. Eng. Process. Process Intensif.* 46, 537–546.
121. Toepfl, S., Heinz, V., Knorr, D., 2006a. Applications of Pulsed Electric Fields Technology for the Food Industry, in: Raso, J., Heinz, V. (Eds.), *Pulsed Electric Fields Technology for the Food Industry*. Springer, Boston, MA, pp. 197–221.
122. Toepfl, S., Heinz, V., Knorr, D., 2005. Overview of Pulsed Electric Field Processing for Food, in: Sun, D.-W. (Ed.), *Emerging Technologies for Food Processing*. Elsevier Ltd, pp. 69–97.
123. Toepfl, S., Mathys, A., Heinz, V., Knorr, D., 2006b. Review: Potential of high hydrostatic pressure and pulsed electric fields for energy efficient and environmentally friendly food processing. *Food Rev. Int.* 22, 405–423.
124. Vaessen, E.M.J., den Besten, H.M.W., Patra, T., van Mossevelde, N.T.M., Boom, R.M., Schutyser, M.A.I., 2018. Pulsed electric field for increasing intracellular trehalose content in *Lactobacillus plantarum* WCFS1. *Innov. Food Sci. Emerg. Technol.* 47, 256–261.
125. Van den Bosch, H.F.M., 2007. Chamber Design and Process Conditions for Pulsed Electric Field Treatment of Food, in: Lelieveld, H.L.M., Notermans, S., de Haan, S.W.H. (Eds.), *Food Preservation by Pulsed Electric Fields*, Woodhead Publishing Series in Food Science, Technology and Nutrition. Woodhead Publishing, pp. 70–93.
126. van Doorne, C.W.H., Westerweel, J., 2007. Measurement of laminar, transitional and turbulent pipe flow using Stereoscopic-PIV. *Exp. Fluids* 42, 259–279.
127. Velickova, E., Tylewicz, U., Dalla Rosa, M., Winkelhausen, E., Kuzmanova, S., Romani, S., 2018. Effect of pulsed electric field coupled with vacuum infusion on quality parameters of frozen/thawed strawberries. *J. Food Eng.* 233, 57–64.
128. Vernhes, M., Benichou, A., Pernin, P., Cabanes, P., Teissié, J., 2002. Elimination of free-living amoebae in fresh water with pulsed electric fields. *Water Res.* 36, 3429–3438.
129. Walkling-Ribeiro, M., Rodríguez-González, O., Jayaram, S., Griffiths, M.W., 2011. Microbial inactivation and shelf life comparison of “cold” hurdle processing with pulsed electric fields and microfiltration, and conventional thermal pasteurisation in skim milk. *Int. J. Food Microbiol.* 144, 379–386.
130. Wiklund, J., Shahram, I., Stading, M., 2007. Methodology for in-line rheology by ultrasound Doppler velocity profiling and pressure difference techniques. *Chem. Eng. Sci.* 62, 4277–4293.
131. Wölken, T., Sailer, J., Maldonado-Parra, F.D., Horneber, T., Rauh, C., 2017. Application of Numerical Simulation Techniques for Modeling Pulsed Electric Field Processing, in: Miklavčič, D. (Ed.), *Handbook of Electroporation*. Springer International Publishing AG 2017, pp. 1237–1267.
132. Ye, H., Huang, L.-L., Chen, S.-D., Zhong, J.-J., 2004. Pulsed electric field stimulates plant secondary metabolism in suspension cultures of *Taxus chinensis*. *Biotechnol. Bioeng.* 88, 788–795.
133. Zagorulko A. Y., 1958 Obtaining of Diffusion Juice with the Help of Electropasmolysis. Ph.D. thesis, Central Research Institute of Sugar Industry (TsNII saharnoy promyshlennosti), Kiev
134. Zhang, J., Blackmore, P.F., Hargrave, B.Y., Xiao, S., Beebe, S.J., Schoenbach, K.H., 2008. Nanosecond pulse electric field (nanopulse): A novel non-ligand agonist for platelet activation. *Arch. Biochem. Biophys.* 471, 240–248.
135. Zhang, Q., Barbosa-Canovas, G. V, Swanson, B.G., 1995. Engineering aspects of pulsed electric field pasteurization. *J. Food Eng.* 25, 261–281.
136. Zimmermann, U., Pilwat, G., Beckers, F., Riemann, F., 1976. Effects of external electrical fields on cell membranes. *Bioelectrochemistry Bioenerg.* 3, 58–83.

137. Zimmermann, U., Pilwat, G., Bresgen, D., 1974. Dielectric breakdown of cell membranes. *Biophys. Struct. Mech.* 6, 113.

MANUSCRIPT 1

Energy input assessment for nanosecond pulsed electric field processing and its application in a case study with *Chlorella vulgaris*

Leandro Buchmann^a, Lukas Böcker^a, Wolfgang Frey^b, Iris Haberkorn^a, Markus Nyffeler^c, Alexander Mathys^{a,*}

^a *ETH Zurich, Department of Health Sciences and Technology, Institute of Food, Nutrition and Health, IFNH, Sustainable Food Processing Laboratory, Schmelzbergstrasse 9, Zurich 8092, Switzerland*

^b *Karlsruhe Institute of Technology, KIT, Institute for Pulsed Power and Microwave Technology, Hermann-von-Helmholtz-Platz 1, Eggenstein-Leopoldshafen 76344, Germany*

^c *Swiss Federal Office for Defence Procurement, Institute of High Power Electromagnetics, Feuerwerkstrasse 39, Thun 3602, Switzerland*

**Corresponding author*

Innovative Food Science and Emerging Technologies 47 (2018) 445–453

ABSTRACT

Arising challenges in the bio-based industry caused by population growth, seek sustainable solutions to increase productivity with the given resources. Nanosecond pulsed electric field (nsPEF) processes provide a promising tool to tackle these challenges. Among the possible applications of nsPEF are the following: sub-lethal stress induction, targeted release of intracellular valuables and induced cell apoptosis. However, without accurate pulse measurement and control, nsPEF processes are not readily applicable within the bio-based industry. The present research undertook an in-depth analysis of the process parameters and their influences on pulse measurements to address this shortcoming. These findings regarding the system enabled calculation of an accurate energy input from pulse measurement based on a novel theoretical relationship. The acquired comprehensive understanding of the system dependency enabled applications of nsPEF in the bio-based industry. A case study with *Chlorella vulgaris* allowed microbial contamination control applying nsPEF while retaining the viability of microalgae cells. Industrial relevance: Pulsed electric field (PEF) technologies are rapidly developing because of their promising applications, continuous operability, short processing times and low energy requirements. Nanosecond PEF (nsPEF) as emerging field can be applied for sub-lethal stress induction, targeted release of intracellular valuables and induced cell apoptosis. However, process characterization and control are limited so far. The acquired comprehensive understanding of the system dependency in this research enables improved applications of nsPEF in the bio-based industry.

1. INTRODUCTION

Electric signals affect biological cells, as John Walsh and Sieu Seignette first demonstrated in 1773 (Walsh & Seignette, 1773). Subsequent studies in the field of bioengineering and their findings regarding process parameters, equipment design and kinetics of permeabilization are the basis for food applications of pulsed electric fields (PEF) (Galvani, 1791).

Heinz Doevenspeck investigated the impact of PEF on the disintegration of biological material in the 1960s (Doevenspeck, 1960, 1961). Mechanical and/or electrical mechanisms are stated to cause the effects from PEF applications (Chiabrera, Grattarola, & Viviani, 1984; Coster, 1965; Silve, Leray, Poignard, & Mir, 2016). Numerous applications of PEF have arose in the food, pharmaceutical, medical and biotech industry (Casciola & Tarek, 2016; Heinz, Alvarez, Angersbach, & Knorr, 2001; Knorr, Geulen, Grahl, & Sitzmann, 1994; Mathys et al., 2013; Raso, Calderón, Góngora, Barbosa-Cánovas, & Swanson, 2006; Raso & Heinz, 2006; Yarmush, Golberg, Serša, Kotnik, & Miklavčič, 2014). PEF allows a more sustainable and less harsh production of microbiologically safe and qualitative food, as it is a non-thermal technique (Toepfl, Heinz, & Knorr, 2005; Toepfl, Mathys, Heinz, & Knorr, 2006).

Currently, nanosecond PEF (nsPEF) applications are of major interest for the bio-based industry because of the ability to induce biological effects while reducing the energy input compared to conventional PEF processes. Cell apoptosis, sub-lethal stress induction and a targeted release of intracellular valuables are among the possible applications (Bai, Gusbeth, Frey, & Nick, 2017; Buescher & Schoenbach, 2003; Goettel, Eing, Gusbeth, Straessner, & Frey, 2013). Schoenbach, Beebe, and Buescher (2001) further reported the possibility to target cells selectively on a subcellular level employing nsPEF.

The electrical nature of a cell, which is composed of resistors (cell plasma) and capacitors (membranes), results in increased electropermeabilization effects on cell organelles compared to membranes for angular frequencies ω (rad s⁻¹) above 10⁷ (Kotnik & Miklavčič, 2006). Therefore, applying nanosecond pulses to biological cells will result in pronounced intracellular electro effects (Buescher & Schoenbach, 2003). Intracellular electro effects could be conformational changes of membrane-bound proteins and stimulation of DNA damage (Schoenbach et al., 2007; Stacey et al., 2003).

Despite the high potential of nsPEF, its applications remain scarce in the bio-based

industry because of the lack of accurate measurements and control of nanosecond pulses.

1.1. Electrical principles of nsPEF

Aspects regarding the electrical principles applicable for nsPEF treatments are derived from the relevant literature (Bluhm, 2006; K uchler, 2017; Schwab, 1981). Ohm's law, which is the underlying principle for PEF applications, states that the applied voltage U_H (V) is equal to electrical resistance R (Ω) times the current I (A) Eq. (1).

$$U_H = R \cdot I \quad (1)$$

Batch process PEF applications are widely executed in plate-plate based electroporation cuvettes. The electrical resistance for such a treatment chamber is expressed as

$$R = 1/\sigma \cdot d/A = \rho \cdot d/A \quad (2)$$

where σ is the media conductivity ($S\ m^{-1}$); d is the electrode distance (m); A is the electrode surface area (m^2) and ρ is the electrical resistivity (Ωm). However, for nsPEF applications Ohm's law Eq. (1) must be modified to Eq. (3). Instead of the resistance being independent of frequency f (s^{-1}), the frequency-dependent impedance Z (Ω) should be used.

$$U_H = Z \cdot I \quad (3)$$

Equal generator Z_1 (Ω) and treatment chamber Z_2 (Ω) impedance allow direct application of Ohm's law (Eq. (3)). Impedance disparities result in reflections within the system, which require consideration (Eq. (4)). The reflection coefficient Γ (–) corresponds to the reflected voltage U_R (V) divided by the applied voltage. The equation is a result of current and voltage continuity.

$$\Gamma = U_R/U_H = (Z_2 - Z_1)/(Z_2 + Z_1) \quad (4)$$

In the case of matched load conditions $Z_1 = Z_2$, the reflection factor is equal to zero and no reflections occur. A reduced pulse amplitude will result for the case $Z_1 > Z_2$, whereas the case $Z_1 < Z_2$ results in an increased amplitude. Analyzing the nsPEF system components, the treatment setup appears to be an RLC circuit (Fleming,

1891). The generator output cable and the plate-plate based treatment chamber build such an RLC element. The impedance for an RLC element is shown in Eq. (5), with the complex reactance X (Ω) being composed of the inductive X_L (Ω) and capacitive X_C (Ω) reactance.

$$Z = R + jX \rightarrow |Z| = \sqrt{R^2 + (X_L - X_C)^2} \quad (5)$$

R is the resistance given by Eq. (2). The inductive and capacitive reactances are shown in Eqs. (6) & (7) with the inductance L (H m^{-1}) Eq. (10) and the capacitance C (F m^{-1}) Eq. (9), respectively. The angular frequency ω (s^{-1}) for the reactance is equal to $2\pi \cdot f$.

$$X_L = j\omega L \quad (6)$$

$$X_C = -1/j\omega C \quad (7)$$

The reciprocal of the impedance, called the admittance Y (S), is calculated from the sum of the conductance G (S) and the complex susceptance B (S) Eq. (8).

$$Y = G + jB \quad (8)$$

Laboratory scale experiments mostly rely on plate-plate geometries owing to a homogenous applied electric field. Plate-plate treatment chambers have a given capacitance, with a permittivity ε (F m^{-1}) being calculated from the permittivity of free space ε_0 (F m^{-1}) and the relative permittivity ε_r (-) of the dielectric medium Eq. (9).

$$C = \varepsilon \cdot A/d = \varepsilon_0 \cdot \varepsilon_r \cdot A/d \quad (9)$$

The resulting inductance can be derived from Eq. (10) with the magnetic flux Ψ (Wb).

$$L = \Psi/I \quad (10)$$

1.2. Energy input calculations in nsPEF systems

Applications of nsPEF require a precise energy input measurement and control to increase the accessibility of the technology in the biobased industry. The electric field E (V m^{-1}) is of high importance for these calculations Eq. (11).

$$E = U_H/d \quad (11)$$

Multiplication of the squared electric field Eq. (11) with the pulse width τ_p (s), the

external media conductivity and number of applied pulses n (–) results in the system specific energy input W_s (kJ kg^{-1}) Eq. (12). For batch systems, the number of applied pulses can be expressed as the product of treatment duration t (s) and frequency. For continuous systems, the treatment duration is expressed as the treatment chamber's volume V_0 (m^3) divided by the volumetric flow rate \dot{V} ($\text{m}^3 \text{s}^{-1}$) at constant temperature Eq. (13).

$$W_s = E^2 \cdot \tau_p \cdot \sigma \cdot n \quad (12)$$

$$n = f \cdot t = f \cdot V_0 / \dot{V} \quad (13)$$

The specific energy input Eq. (12) depends strongly on the media composition and treatment chamber geometry. Therefore, a profound system characterization is crucial for accurate pulse measurement and control. Incorporation of electrochemical changes allow for a comprehensive system characterization. The relative permittivity Eq. (9) depends on the ion-concentration within the solution. Blüh (1924) derived values for saline solutions on the basis of the Born approximation (Born, 1920). Changes in media conductivity caused by the external applied electric field can be approximated by Eqs. (14) & (15), with electric field dependence factor γ (m V^{-1}), electric charge e (C), Boltzmann constant k_B (J K^{-1}) and temperature T (K) (Park, Ryu, Kim, & Kang, 2009).

$$\sigma = \sigma(1 + \gamma E) \quad (14)$$

$$\gamma = e^3 / 16\pi \cdot \varepsilon \cdot k_B^2 \cdot T^2 \quad (15)$$

Nonetheless, process requirements impair optimal conditions for electric measurements. Multiphysics simulations are a powerful tool to elucidate the influence of reactor designs on the obtained results (Knoerzer, Buckow, Trujillo, & Juliano, 2014; Meneses, Jaeger, & Knorr, 2011a, 2011b; Wölken, Sailer, Maldonado-Parra, Horneber, & Rauh, 2017). In this study, we aim at an optimized reactor configuration based on multiphysics simulations for accurate high voltage measurement and control, enabling a ubiquitously applicable system to be devised.

1.3. Potential of nsPEF for microalgae applications

Industrial boundaries and microalgae production conditions commonly result in a non-axenic and non-sterile cultivation. A stable cultivation relies on microbial

contamination control during cultivation. Furthermore, the bio-based industry is urged to find novel resources for sustainable energetic and material utilization, making *Chlorella vulgaris* a suitable reference organism (Golberg et al., 2016; Posten & Feng Chen, 2016). A case study on targeted microbial contamination control during cultivation of *C. vulgaris* was performed to test the transferability of the findings regarding system characterization to bio-based applications.

2. MATERIALS AND METHODS

2.1. Experimental equipment

The experimental setup for the batch pulsed electric field measurements consisted of a cuvette holder and a plate-plate electroporation cuvette (BTX Cuvette, Harvard Apparatus, Holliston MA, USA). Electrode distances of 2 and 4mm allowed varying ohmic resistances from 25 to 155 Ω , applying Eq. (2) and media properties shown in Table 1.

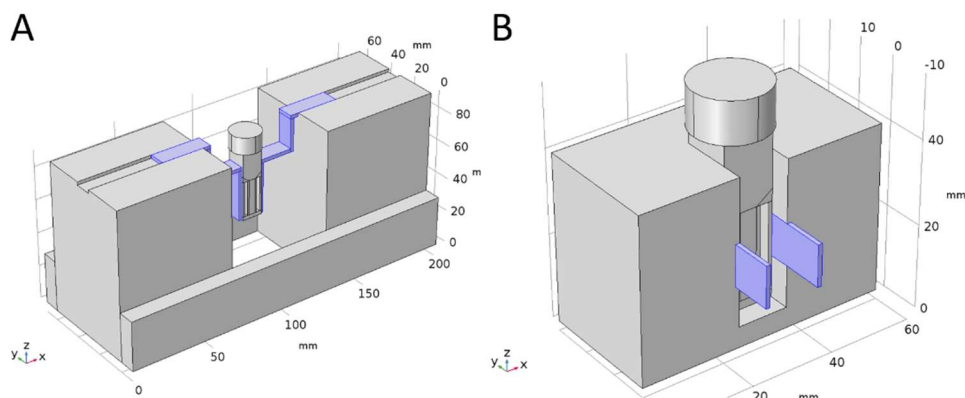
Two different pulse generators were analyzed NPG-18/3500 (Megaimpulse Ltd., St. Petersburg, Russia) and FPG 10-1NL100 (FID GmbH, Burbach, Germany). Both pulse generators were diode opening switch generators. Those generators allowed applications of rectangular pulses from 2 to 100 ns. The voltage level was adjustable from 2 to 20 kV, resulting in electric field strengths from 5 to 100 kV cm⁻¹. The repetition rate was adjustable from 1 to 3.5 kHz. The NPG-18/3500 had an internal impedance of 75 Ω and the FPG 10-1NL100 of 50 Ω . Both generators were analyzed using the same saline solutions according to Table 1 to obtain comparable results. A matched load condition was achieved for all types of cuvettes.

The system behavior after a single pulse was analyzed. Prior to a second pulse application, the whole setup was grounded to ensure steady-state conditions preceding pulse application. Applied voltage and current were measured using a calibrated high voltage probe P6015A (Tektronix Inc., Beaverton OR, USA) and current monitor type 6585 (Pearson Electronics Inc., Paolo Alto CA, USA), respectively. The high voltage probe was attached directly after the transition from the generator output cable to the copper electrodes contacting the cuvette. The current monitor was placed perpendicular to the current flow on the anode side of the generator. A WaveSurfer 10 1-GHz oscilloscope (Teledyne LeCroy, Chestnut Ridge NY, USA) was used to monitor the signals.

2.2. Cuvette holder configuration

Different cuvette holder configurations were analyzed to assess the influence of distorting electric fields within the measuring circuit. The conductive surface area surrounded by air was 48.80 cm² for the broad configuration (Fig. 1 A). System optimization studies resulted in a conductive, air surrounded, surface area of 5.60 cm² for the narrow configuration (Fig. 1 B). For both cases, cuvette contacting was realized by copper electrodes directly attached to the core and shield of the

generators output cable.



M1 - Figure 1: Cuvette holder configuration with air surrounded conductive surface area (purple) of 48.80 cm² for the broad setup A) and 5.60 cm² for the narrow setup B), resulting from multiphysics simulation based optimization studies.

2.3. Treatment media

Solutions of either NaCl or KCl (Sigma-Aldrich, Merck KGaA, Darmstadt, Germany) were used as treatment media to investigate the system behavior. Investigation of two alkali salts allowed comparable results because of their similar chemical behavior. The conductivity was measured using a Seven compact conductivity meter (Mettler-Toledo International Inc., Columbus OH, USA). Measurements were conducted at three different concentrations to broaden the covered impedance range (Table 1).

M1 - Table 1: Resulting conductivity σ for NaCl and KCl solutions used to assess system behavior resulting from nanosecond pulsed electric field applications, based on saline concentration c differences.

	NaCl		KCl	
	c (mmol L ⁻¹)	σ (mS cm ⁻¹)	c (mmol L ⁻¹)	σ (mS cm ⁻¹)
Solution I	28.01	3.15 ± 0.016	26.05	3.16 ± 0.005
Solution II	22.24	2.01 ± 0.001	16.27	2.21 ± 0.005
Solution III	10.69	1.23 ± 0.004	7.17	1.02 ± 0.004

2.4. Numerical and experimental set up

The complete system was simulated by use of COMSOL Multiphysics® (Comsol Inc., Burlington MA, USA) simulation software version 5.3. The electric current (ec) and electrostatics (es) physics interface were used to assess the system behaviors. A

current conservation equation Eq. (16) based on Ohm's law Eq. (17) was applied in the ec physics interface. Current conservation is expressed as the current density gradient J (A m^{-2}) equal to the electric charge Q (C). The current conservation is based on the sum of a time dependent Ohm's law $J = (\sigma + \varepsilon\partial/\partial t)E$ (A m^{-2}) and the displacement current J_e (A m^{-2}).

$$\nabla J = Q_{j,v} \quad (16)$$

$$J = (\sigma + \varepsilon\partial/\partial t)E + J_e \quad (17)$$

The es physics interface solves Gauss's law for the electric field. Gauss's law in a differential form is shown in Eq. (18), with the divergence of the electric displacement field $\varepsilon_0\varepsilon_r E$ (C m^{-2}) equal to the electric charge density ρ_v (C m^{-2}).

$$\nabla \cdot (\varepsilon_0 \varepsilon_r E) = \rho_v \quad (18)$$

For both physics interfaces the scalar electric potential $-\nabla V$ (V) was used as the dependent variable Eq. (19).

$$E = -\nabla V \quad (19)$$

The system was simulated stationary as well as time dependent. A combination of the waveform (wv) and analytic (an) function allowed for an incorporation of the actual pulse shape into the simulation. The temperature dependency of the conductivity was simulated by use of a linearized model. This model depends on the reference resistivity ρ_0 (Ωm) and the temperature coefficient α (K^{-1}) multiplied by the temperature difference $T - T_{Ref}$ (K) Eq. (20).

$$\sigma = 1/\rho_0(1 - \alpha(T - T_{Ref})) \quad (20)$$

In accordance with the experimental setup, only one pulse was applied to analyze the system behavior.

2.5. *Chlorella vulgaris* cultivation and nsPEF treatment

Three independent *C. vulgaris* SAG 211-12 cultivations were prepared in triplicates. An aliquot of 20 mL of *C. vulgaris* suspension was diluted in 40 mL DSN medium (Pohl, Kohlhase, Krautwurst, & Baasch, 1987) to obtain an optical density (OD) of 2.5 at 750 nm. The cultures were incubated at 25 ± 0.2 °C, 70% relative humidity, 150 rpm, ambient CO_2 , and continuous illumination with a mean photosynthetically active

photon flux density (PPFD) of $36 \mu\text{mol photons m}^{-2} \text{s}^{-1}$ using warm white LED lamps in a shaking incubator (Multitron Pro shaking incubator, Infors AG, Bottmingen, Switzerland). The growth of *C. vulgaris* was monitored by OD measurements at 750 nm and 680 nm using disposable 1.5 mL semi-microcuvettes (Brand GmbH, Wertheim, Germany) in an UV/VIS spectrophotometer (Cary 100, Agilent Technologies, Santa Clara CA, USA).

Application of three different electric field strengths resulted in three differently treated *C. vulgaris* cultures (Table 2). The treatments consisted of 100 pulses with a pulse width $\tau_p = 5.56 \text{ ns}$ and a frequency $f = 3 \text{ Hz}$, resulting in a treatment duration of 33.3 s. The specific energy input was calculated based on the energy per pulse in accordance with Eqs. (12) & (13).

The treatment of *C. vulgaris* cultures with nanosecond pulses was performed in a batch mode using electroporation cuvettes with an electrode distance of 4 mm. Pulse waveform, electrical conductivity and temperature were controlled for all treatments.

M1 - Table 2: Resulting conductivity σ for NaCl and KCl solutions used to assess system behavior resulting from nanosecond pulsed electric field applications, based on saline concentration c differences.

	$\sigma \text{ (mS cm}^{-1}\text{)}$	$E \text{ (kV cm}^{-1}\text{)}$
Treatment T1	1.28 ± 0.02	32.75
Treatment T2	1.15 ± 0.01	40.88
Treatment T3	1.24 ± 0.02	49.00

The effect of nsPEF treatment on bacterial counts was analyzed by plate count. Serial dilutions between 10^{-2} to 10^{-6} were prepared in sterile maximum recovery medium (Oxoid Limited, Thermo Fisher Scientific Inc., Waltham MA, USA) from all samples. Aliquots of 100 μL of the dilutions were plated on BHI (Oxoid Limited, Thermo Fisher Scientific Inc., Waltham MA, USA) (3.7% BHI and 1.5% agar in dH_2O) and bacterial colony forming units (CfU) (g^{-1}) were determined after 2 days of incubation at $30 \text{ }^\circ\text{C}$. Vitality of *C. vulgaris* was assessed using Eosin Y staining (Merck KGaA, Darmstadt, Germany) for living cells. Each sample was diluted with dH_2O to obtain an OD of around 2. Subsequently, 500 μL of the diluted algal suspension were mixed with 500

μL of Eosin Y disodium salt solution (20 mg mL^{-1}). Following an incubation period of 20 min in the dark, a washing step was performed by adding 4 mL of dH_2O to the mixture, followed by centrifugation (1300 rpm, 2 min) (Hermle Labortechnik GmbH, Wehingen, Germany). In total, three washing steps were performed. After the third washing step, all remaining water was removed and the resulting pellet was diluted in dH_2O to obtain an OD of 1. An aliquot of 10 μL of the stained suspension was used for the determination of the vitality of *C. vulgaris*. A Thoma cell counting chamber (Karl Hecht GmbH & Co KG, Sondheim v. d. Roehn, Germany) and DM 6 light microscope (Leica Microsystems GmbH, Wetzlar, Germany) were used to determine the vitality of *C. vulgaris* based on living cell counts (LCC), according to the manufacturer's instructions. In accordance with Eq. (21), the recorded OD was converted into dry substance (DS) (g L^{-1}).

$$DS = 0.424 \cdot OD_{750} \quad (21)$$

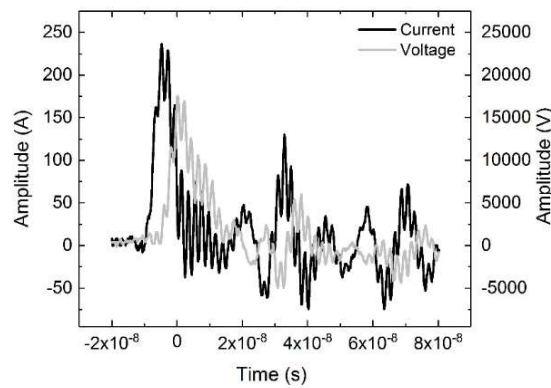
2.6. Data analysis

Data analysis was conducted by an independent t-test. The confidence interval was 95% for microbial contamination control trials and 99% for pulse measurements. Statistical results were obtained using the software IBM SPSS Statistics (IBM Corp., Armonk NY, USA).

3. RESULTS AND DISCUSSION

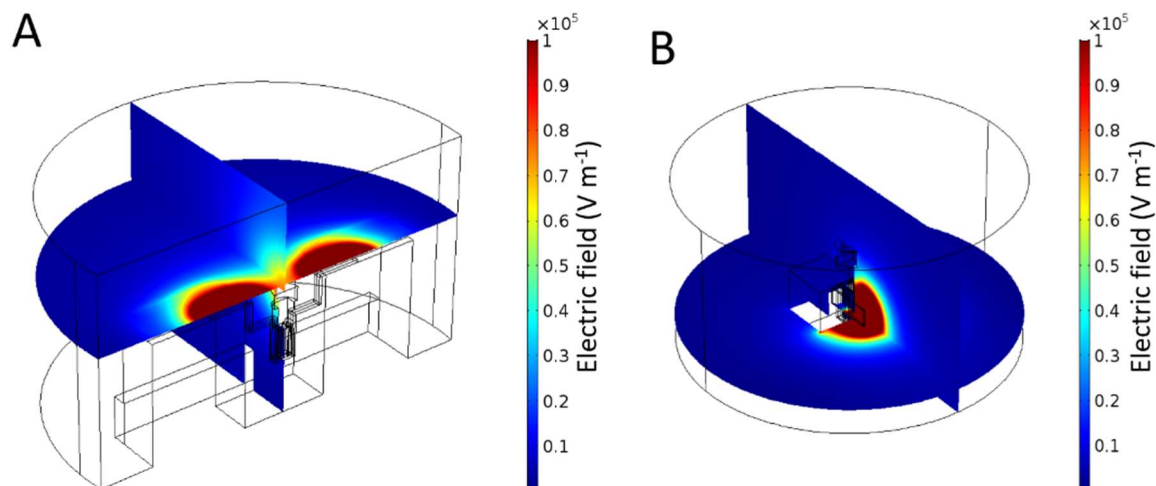
3.1. System characterization and optimization

Pulse measurements were conducted with the broad and narrow cuvette holder configuration (Fig. 1 A/B). For the broad cuvette holder, the pulse measurements resulted in distorted signals. Voltage and current measurements are biased, and no distinct pulse shape was detectable (Fig. 2). Thus, determination of the pulse parameters was not possible, and the measured voltage contradicted Eq. (4). The voltage amplitude increased, although for $Z_1 > Z_2$, the applied voltage should be lower. The treatment chamber's resistance was assessed with respect to Eq. (2). All saline solutions (Table 1) resulted in a congruent system behavior.



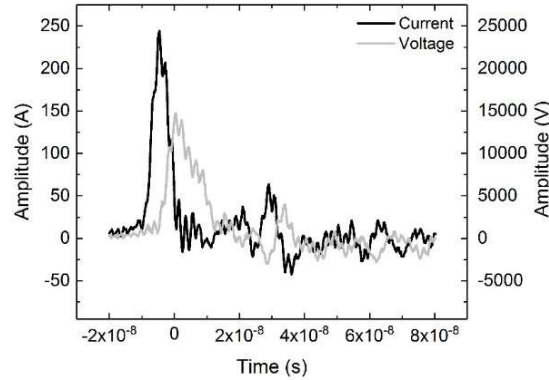
M1 - Figure 2: Voltage and current measurement obtained using the NPG-18/3500 generator with a pulse width of 5.56 ns and the broad cuvette holder configuration (Figure 1 A) using a 4 mm cuvette filled with NaCl solution I (Table 1).

Multiphysics simulation revealed a possible explanation for the distorted signals and the resulting measurement error (Fig. 3 A). The electric field strength within the measurement area exceeds values of $1 \cdot 10^5 \text{ V m}^{-1}$. This electric field paired with the pulse width of 5.56 ns appears to cause an interfering signal.



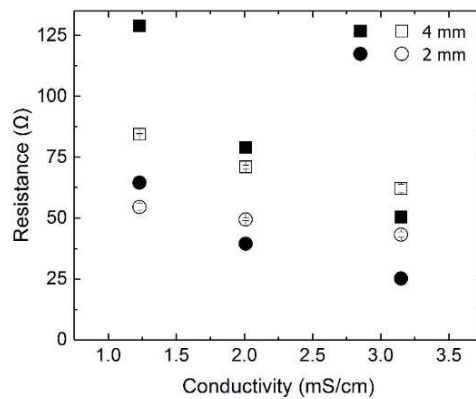
M1 - Figure 3: Electric field strength simulated for the broad cuvette holder A) (Figure 1 A) and the narrow cuvette holder configuration B) (Figure 1 B) using electrostatic (es) physic interface in COMSOL multiphysics® simulation.

Multiphysics simulation based system analysis aimed for a reduction of the interfering signal. It was hypothesized that by minimizing the air surrounded conductive surface area, this interfering signal can be reduced. System analysis by multiphysics simulation resulted in the narrow cuvette holder configuration (Fig. 3 B). The maximum electric field values are similarly high for the broad and narrow configuration (Fig. 3 A/B); see also Fig. 1 A/B. However, the narrow configuration (Fig. 1 B) allowed for a reduction of the air surrounded conductive surface area from 48.80 cm^2 to 5.60 cm^2 . The minimization of the conductive surface area resulted in a decreased interfering signal. The measured current displayed the output pulse of the NPG-18/3500 using the optimized narrow configuration (Fig. 1 B), as shown in Fig. 4. In contrast, voltage measurements were still biased, resulting in detection of a wider pulse (Fig. 4). These misleading voltage measurements might be explained by consideration of the electric field simulations; see also Fig. 3 A/B. Derived from electric field simulations, the voltage measurements occur in the region of the highest external electric field. A measuring point outside this area was not achievable because of the system components.



M1 - Figure 4: Voltage and current measurement obtained by use of NPG-18/3500 generator with a pulse width of 5.56 ns and the narrow cuvette holder configuration (Figure 1 B) using a 4 mm cuvette filled with NaCl solution I (Table 1).

Nevertheless, Ohm's law must be obeyed; dividing voltage by current should result in the commonly used theoretical resistance Eq. (2). For matched load conditions, Ohm's law was found to be obeyed regarding absolute errors (Fig. 5). However, the results for matched load conditions exhibited a mean percentage difference of $-14.89 \pm 4.25\%$. A comparable and scalable system relies on accurate measurements. Therefore, the current measurement was further analyzed for nanosecond pulse characterization and control, as this is crucial to achieve reproducible results.



M1 - Figure 5: Resistance obtained by applying Ohm's law to the current and voltage measured (empty) using the narrow cuvette holder configuration compared to the theoretical resistance Eq. (2) (full). The pulses were delivered by use of the NPG 18-3500 generator with a pulse width of 5.56 ns. The values are derived for 4 mm and 2 mm electroporation cuvettes filled with NaCl solutions, as shown in Table 1, and the narrow cuvette holder configuration (Figure 1 B).

3.2. Novel theoretical relation

In Section 3.1, the commonly used theory of Eq. (2) for nsPEF system characterization was analyzed. It was demonstrated that the mean percentage error

impairs reproducible bio-based applications. Therefore, novel mathematical considerations for accurate measurements are necessary. With regard to the pulse voltage and current measurements (Fig. 4), the system is observed to behave as a pure RC element. A pure capacitive behavior is characterized by a phase shift $\varphi = -90^\circ$ between current and voltage. Therefore, in accordance with an adjusted Eq. (5), the impedance of the system ($|Z_C| = R^2 + X_C^2$) was calculated assuming a relative permittivity of water ($\epsilon_r = 81.1$). Regarding frequency, the first peak frequency from a Fourier transform of the applied pulses was assessed. This adjustment did not improve the evaluation of the measured results. Furthermore, incorporation of the reflection factor Eq. (4), characterized by the resistance Eq. (2), did not improve the obtained results. It appeared that the system behavior was following a non-ideal RC element behavior. Consideration of the pulse shape (which for all cases is rectangular) led to a novel equivalent circuit with an assumption of a parallel capacitive and resistive system. Therefore, Eq. (2) was extended for high-frequency applications, as shown in Eq. (22):

$$Z_{tot} = 1/(\sigma \cdot A/d + Y_C) \quad (22)$$

with the total impedance $Z_{tot}(\Omega)$ equal to the fraction of the inverse resistance added by the system's admittance $Y_C(S)$. For conventional PEF applications in the μs range, Eq. (22) correlates with the common resistance Eq. (2). Decreasing the pulse width increases the influence of the parallel impedance.

The measured treatment chamber's impedances for NaCl (A) and KCl (B) after application of one 5.56 ns pulse are shown in Fig. 6. The applied voltage used for system analysis was adjusted in accordance to the parallel impedance Eq. (22) incorporating the reflection factor Eq. (4). Furthermore, to incorporate electrochemical changes, the relative permittivity was adapted based on the correlation derived from Blüh, 1924 (Table 3).

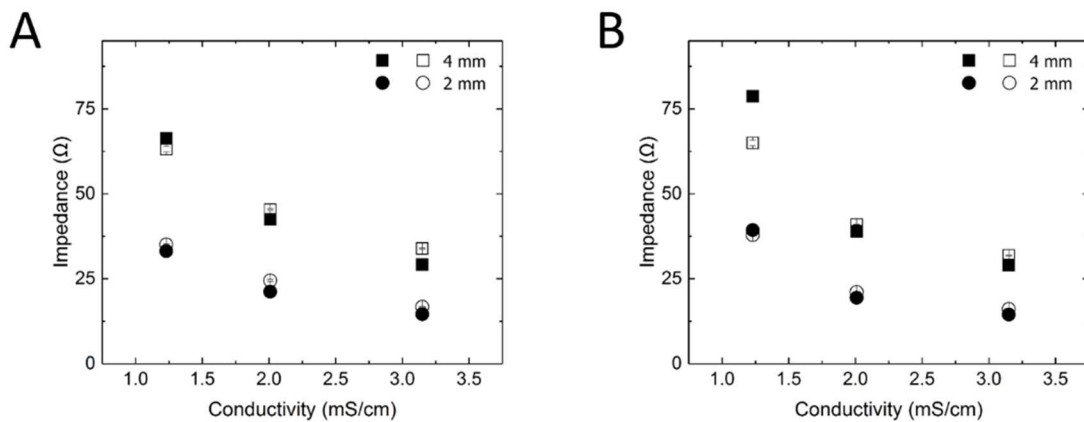
M1 - Table 3: Electric conductivity σ and resulting relative permittivity ϵ_r for saline solutions of NaCl and KCl based on (Blüh, 1924)

	NaCl		KCl	
	σ (mS cm ⁻¹)	ϵ_r (-)	σ (mS cm ⁻¹)	ϵ_r (-)
Solution I	3.15 ± 0.015	68.95 ± 0.050	3.16 ± 0.005	68.94 ± 0.019
Solution II	2.01 ± 0.010	73.21 ± 0.033	2.21 ± 0.005	72.48 ± 0.019
Solution III	1.23 ± 0.003	76.11 ± 0.163	1.02 ± 0.003	76.88 ± 0.003

Adjustment of the treatment chamber impedance in accordance to Eq. (22) led to correlating results for cases given $Z_1 > Z_2$ (Fig. 6) and could therefore increase the measurement accuracy. The angular frequency was calculated assuming a frequency given by Eq. (23).

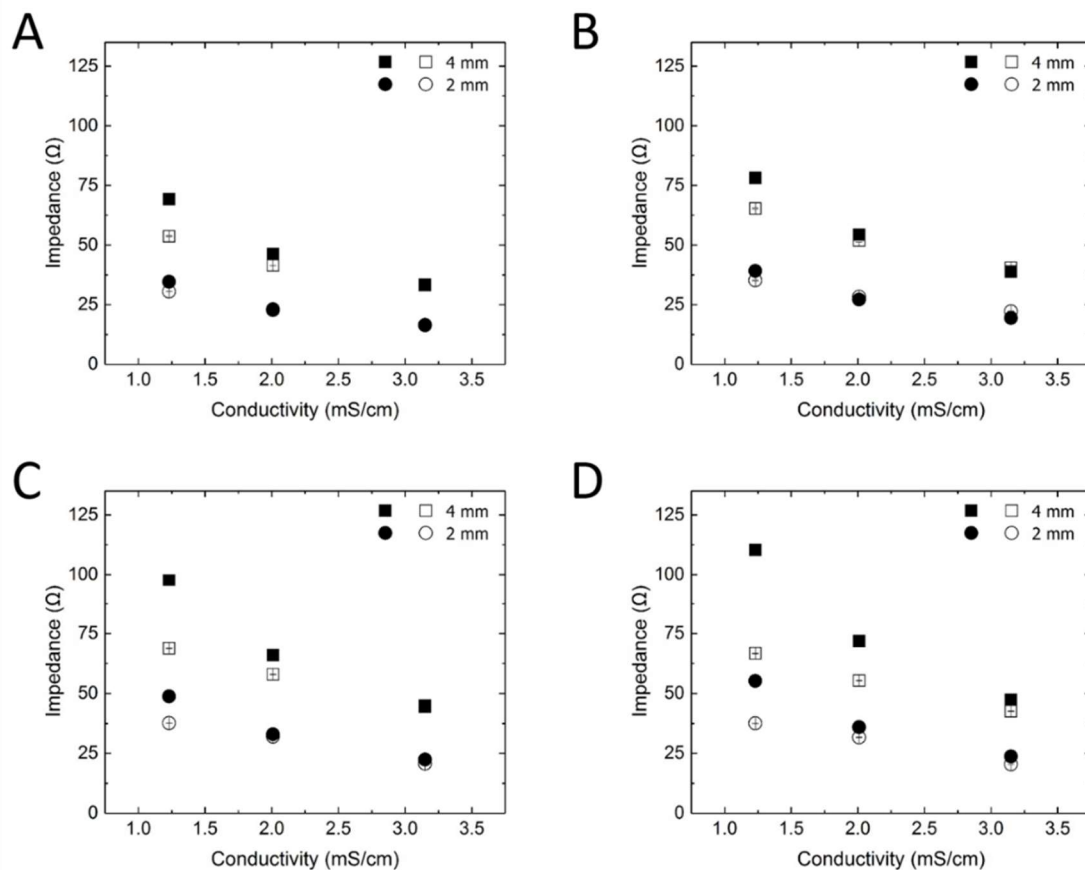
$$f = 1/(2 \cdot \tau_p) \tag{23}$$

The inclusion of the electric field strength dependent conductivity, as stated by Park et al. (2009), did not increase the accuracy of measured pulse analysis. Therefore, this intermediate step is not necessary for single-phase systems; however, for colloidal systems and DC fields, Park et al. (2009) found it to be relevant. The treatments of cell suspensions with μ s-ms pulse widths may require this adaption for precise pulse measurements, energy input calculations and system characterization, as well as control.



M1 - Figure 6: Theoretical impedance (full) values derived by consideration of Eq. (21) compared with the measured results (empty) for 4 mm and 2 mm electroporation cuvettes filled with A) NaCl and B) KCl solutions according to Table 1 utilizing the NPG18-3500 pulse generator with a pulse width of 5.56 ns and the narrow cuvette holder configuration (Figure 1 B).

The significance of the novel theoretical relation Eq. (22) was evaluated for pulse widths from 10 to 100 ns using the FPG 10-1NL100 pulse generator. The results for NaCl (Fig. 7) and KCl (see Supplementary material) solutions (Table 1) were determined to be similar. Adjustment of the treatment chamber impedance Eq. (22) and voltage amplitude Eq. (4) enabled correlation of the measurements. Based on consideration of the absolute error results for cases given $Z_1 > Z_2$, a correlation was observed with the novel theoretical relation Eq. (22) for pulses from 5.56 to 100 ns Eq. (22).



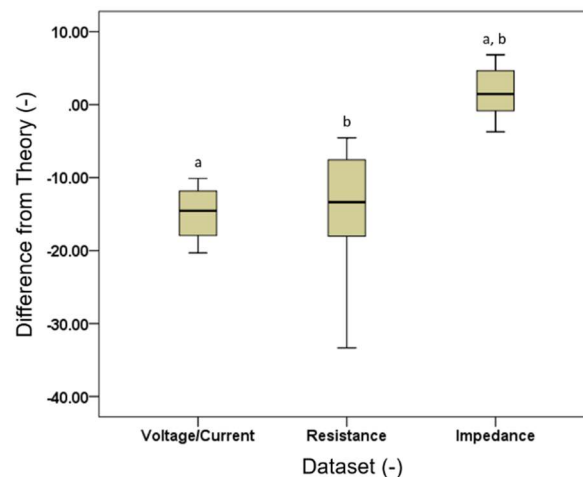
M1 - Figure 7: Theoretical impedance (full) values derived by considering Eq. (22) compared with the measured results (empty) for 4 mm and 2 mm electroporation cuvettes filled with NaCl solutions, as shown in Table 1. The pulse generator FPG 10-1NL100 and pulse widths of 10 ns A), 20 ns B), 50 ns C) and 100 ns D), utilizing the narrow cuvette holder configuration (Fig. 1 B) were analyzed.

Increasing the pulse width reduced the effect of the parallel impedance Eq. (22) concerning Eqs. (7) & (23). The parallel impedance is valid as long as the frequency according to Eq. (23) is lower than the cutoff frequency f_c (Hz) of the RC element ($f_c = 1/2\pi RC$). In addition, the capacitors charging and discharging time τ_c (s) ($\tau_c = R \cdot C$)

must be considered.

Regarding the dependence of the pulse width and charging time, different current parameters are relevant. After a charging time t_c (s) of $5 \cdot \tau_c$, the capacitor is charged to 99%. Achieving a steady-state system requires a fully charged and discharged capacitor, which is the case for $\tau_p > 10 \cdot \tau_c$. For cases of $\tau_p > 10 \cdot \tau_c$, the current satisfying Eq. (22) is the measured peak to peak current. In the case of $\tau_p < 10 \cdot \tau_c$ the maximum current results in correlating values according to Eq. (22). The proposed current most suitable for nanosecond pulse characterization is in accordance with literature (Pirc, Reberšek, & Miklavčič, 2017; Reberšek, Miklavčič, Bertacchini, & Sack, 2014).

In our study, based on current measurements, the parallel impedance Eq. (22) and resistance Eq. (2) showed a significant difference ($p < 0.01$) regarding system characterization. In addition, a significant difference between the parallel impedance and the impedance, derived from voltage and current measurements, was obtained by satisfying Ohm's law Eq. (3) ($p < 0.01$). The relative error is based on the resistance Eq. (2) equal to -0.14 ± 0.08 and the parallel impedance Eq. (22) equal to 0.02 ± 0.03 . The results were obtained for matched load conditions. In the case of an unmatched system, the error increased. However, the relative error for the parallel impedance (Eq. (22)) was for all cases lower compared to any other evaluated theory.



M1 - Figure 8: Boxplot data for matched load conditions using 4 mm and 2 mm cuvettes filled with NaCl and KCl solutions in accordance with Table 1 for pulse widths below cutoff frequency of the RC element; the same letters indicate statistical significance ($p < 0.01$).

3.3. Microbial contamination control within *Chlorella vulgaris* culture

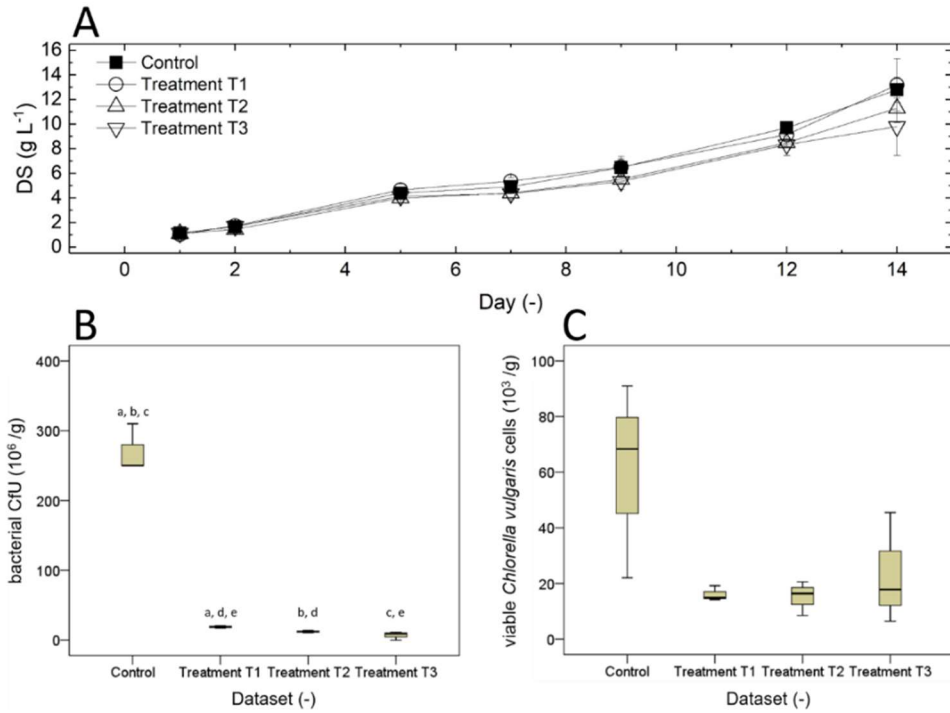
The transferability of findings regarding system characterization and control was

investigated by a case study on targeted microbial contamination control during cultivation of *C. vulgaris*. The full potential of microalgae in the bio-based industry can be revealed with a stable cultivation system. Due to industrial production conditions and boundaries it is common to use non-axenic and non-sterile microalgae to produce high value added functional ingredients, food, feed, and bioenergy. A stable cultivation system requires measures for microbial contamination control in the presence of a viable algae culture.

Applying the novel theoretical relation Eq. (22), the energy input Eq. (12) for the inactivation trials was calculated. The energy input was 0.53 kJ kg^{-1} (Treatment T1), 0.99 kJ kg^{-1} (Treatment T2), and 1.69 kJ kg^{-1} (Treatment T3), with a relative error of -0.0003 ± 0.072 . This relative error is greater than that obtained for the matched case ($Z_2 = Z_1$) (Fig. 8); however, it is still lower than for the resistance model Eq. (2). Using the former equation for energy input calculations Eq. (2) corresponds to a 4-times higher energy input with 1.99 kJ kg^{-1} (Treatment T1), 3.81 kJ kg^{-1} (Treatment T2) and 6.43 kJ kg^{-1} (Treatment T3) with a relative error of 0.445 ± 0.111 . Therefore, applying the novel theoretical relation significantly increases the accuracy of treatment controls.

A significant difference regarding bacterial CfU was found between the control and all treatments ($p < 0.05$) (Fig. 9 B). Inter treatment significance was found between treatment T1 and T2 as well as treatment T1 and T3. There was no statistical significance observable between treatment T2 and T3 ($p = 0.211$). For all treatments, no changes were observed in the external media conductivity and in the sample's temperature.

Eosin Y staining of the living cells determined the immediate vitality of *C. vulgaris*. There was no significant difference regarding vitality of *C. vulgaris* (Fig. 9 C). These findings enable a microalgae cultivation system by-passed with an nsPEF treatment chamber, which allows continuous microbial contamination control during cultivation.



M1 - Figure 9: Resulting effects of nsPEF treatments at electric field strengths of $E_1 = 27.43 \text{ kV cm}^{-1}$ (Treatment T1), $E_2 = 39.64 \text{ kV cm}^{-1}$ (Treatment T2), and $E_3 = 49.79 \text{ kV cm}^{-1}$ (Treatment T3) of *Chlorella vulgaris* SAG 211-12. The effects were based on a 14 days revitalization ability of *C. vulgaris* according to Eq. (21) A), determination of CfU after 2 days of incubation B) and immediate vitality assessment of *C. vulgaris*, as determined by Eosin Y staining C); for figure B) the same letters indicate statistical significance ($p < 0.05$) and for figure C) no statistical significant difference was found.

4. CONCLUSIONS

The study aimed at an optimized reactor configuration based on multiphysics simulations for accurate high voltage measurement and control. Multiphysics simulation allowed comprehensive analysis of the cuvette holder configurations used for nsPEF applications. As a result, the accuracy of nanosecond pulse measurements was improved. Experimental analysis results led to the derivation of a novel theoretical relationship for the calculation of the treatment chamber resistance. The theoretical relationship is based on a parallel system impedance Eq. (22). Extension of the commonly used equation for the treatment chamber resistance Eq. (2) to the nanosecond range Eq. (22) resulted in a significant decrease of the measurement signal disparities ($p < 0.01$). The relative error for matched load conditions ($Z_2 = Z_1$) was 0.02 ± 0.03 . Thus, nanosecond pulses can be measured and controlled, thereby improving the utility of nsPEF for bio-based applications.

A case study for nsPEF applications in the bio-based industry demonstrated a statistically significant reduction of microbial contamination within a *C. vulgaris* culture. The detected total bacterial count reduction of $>1 \log_{10}$ without compromising the eukaryotic microalgae strain is a promising phenomenon that has not been thoroughly elucidated to date. The continuous operability of nsPEF enables novel cultivation systems with an integrated nsPEF treatment chamber, allowing for simultaneous contamination control and cultivation of relevant organisms. Further detailed analysis is required to optimize the targeted microbial contamination control. An in-depth understanding of the biological response might enable tailored microbial inactivation in the future.

Applying the novel theoretical relation (Eq. (22)) enabled a more accurate energy input calculation (Eqs. (12) & (13)). This improvement will enhance comparability of the results from different laboratories and hence facilitate research in the area of nsPEF processing. Further research is necessary to optimize the pulse measurement for mismatched load conditions ($Z_2 \neq Z_1$). Derivation of a complete system characterization will promote the utilization of nsPEF in the bio-based industry.

ACKNOWLEDGEMENT

The authors gratefully acknowledge the World Food System Center (Project "NewAlgae", Grant number: 2-72235-17), the ETH Zürich Foundation, Switzerland and the ETH Zürich Food Process Engineering workshop (Daniel Kiechl and Bruno Pfister) for their support.

CONFLICT OF INTEREST STATEMENT

The authors declare no conflict of interest.

REFERENCES

1. Bai, F., Gusbeth, C., Frey, W., & Nick, P. (2017). Nanosecond pulsed electric fields trigger cell differentiation in *Chlamydomonas reinhardtii*. *Biochimica et Biophysica Acta (BBA) - Biomembranes*, 1859(5), 651–661.
2. Blüh, O. (1924). Die Dielektrizitätskonstanten von Elektrolytlösungen. *Zeitschrift für Physikalische Chemie*, 220–229.
3. Bluhm, H. (2006). *Pulsed power systems: Principles and applications*. Berlin: Springer-Verlag.
4. Born, M. (1920). Über die Beweglichkeit der elektrolytischen Ionen. *Zeitschrift für Physik*, 1(3), 221–249.
5. Buescher, E. S., & Schoenbach, K. H. (2003). Effects of submicrosecond, high intensity pulsed electric fields on living cells - Intracellular electromanipulation. *IEEE Transactions on Dielectrics and Electrical Insulation*, 10(5), 788–794.
6. Casciola, M., & Tarek, M. (2016). A molecular insight into the electro-transfer of small molecules through electropores driven by electric fields. *Biochimica et Biophysica Acta - Biomembranes*, 1858(10), 2278–2289.
7. Chiabrera, A., Grattarola, M., & Viviani, R. (1984). Interaction between electromagnetic fields and cells: Microelectrophoretic effect on ligands and surface receptors. *Bioelectromagnetics*, 5(2), 173–191.
8. Coster, H. G. L. (1965). A quantitative analysis of the voltage-current relationships of fixed charge membranes and the associated property of "punch-through". *Biophysical Journal*, 5(5), 669.
9. Doevenspeck, H. (1960). Verfahren und Vorrichtung zur Gewinnung der einzelnen Phasen aus dispersen Systemen. Patent No. DE 1237541, Germany.
10. Doevenspeck, H. (1961). Influencing cells and cell walls by electrostatic impulses. *Fleischwirtschaft*, 13(12), 968–987.
11. Fleming, J. A. (1891). On some effects of alternating current flow in circuits having capacity and self-induction. *Journal of the Institution of Electrical Engineers*, 20(94), 362–408.
12. Galvani, L. (1791). Viribus electricitatis in motu musculari. *De Bononiensi Scientiarum et Artium Instituto atque Academia Commentarii*, 7, 363–418.
13. Goettel, M., Eing, C. J., Gusbeth, C., Straessner, R., & Frey, W. (2013). Pulsed electric field assisted extraction of intracellular valuables from microalgae. *Algal Research*, 2(4), 401–408.
14. Golberg, A., Sack, M., Teissie, J., Pataro, G., Pliquett, U., Saulis, G., ... Frey, W. (2016). Energy-efficient biomass processing with pulsed electric fields for bioeconomy and sustainable development. *Biotechnology for Biofuels*, 9(1), 94.
15. Heinz, V., Alvarez, I., Angersbach, A., & Knorr, D. (2001). Preservation of liquid foods by high intensity pulsed electric fields-basic concepts for process design. *Food Science and Technology*, 12, 103–111.
16. Knoerzer, K., Buckow, R., Trujillo, F. J., & Juliano, P. (2014). Multiphysics simulation of innovative food processing technologies. *Food Engineering Reviews*, 7(2), 64–81.
17. Knorr, D., Geulen, M., Grahl, T., & Sitzmann, W. (1994). Food application of high electric field pulses. *Trends in Food Science & Technology*, 5(3), 71–75.
18. Kotnik, T., & Miklavčič, D. (2006). Theoretical evaluation of voltage inducement on internal membranes of biological cells exposed to electric fields. *Biophysical Journal*, 90(2), 480–491.
19. Küchler, A. (2017). *Hochspannungstechnik: Grundlagen, Technologie, Anwendungen. Vol. 4*. Berlin: Springer-Verlag.
20. Mathys, A., Toepfl, S., Siemer, C., Favre, L., Benyacoub, J., & Hansen, C. E. (2013). Pulsed electric field treatment process and dairy product comprising bioactive molecules obtainable by the process. Patent application. EP 2543254(A1). NESTEC S.A.

21. Meneses, N., Jaeger, H., & Knorr, D. (2011a). Computational fluid dynamics applied in pulsed electric field preservation of liquid foods. In K. Knoerzer, P. Juliano, P. Roupas, & C. Versteeg (Eds.). *Innovative food processing technologies: Advances in multiphysics simulation* (pp. 193–207). West Sussex: Wiley-Blackwell and IFT Press.
22. Meneses, N., Jaeger, H., & Knorr, D. (2011b). pH-changes during pulsed electric field treatments - Numerical simulation and in situ impact on polyphenoloxidase inactivation. *Innovative Food Science & Emerging Technologies*, 12(4), 499–504.
23. Park, J. K., Ryu, J. C., Kim, W. K., & Kang, K. H. (2009). Effect of electric field on electrical conductivity of dielectric liquids mixed with polar additives: DC conductivity. *The Journal of Physical Chemistry B*, 113(36), 12271–12276.
24. Pirc, E., Reberšek, M., & Miklavčič, D. (2017). Dosimetry in electroporation-based technologies and treatments. In M. Markov (Ed.). *Dosimetry in bioelectromagnetics* (pp. 233–268). Taylor & Francis Group, LLC.
25. Pohl, P., Kohlhase, M., Krautwurst, S., & Baasch, K.-H. (1987). An inexpensive inorganic medium for the mass cultivation of freshwater microalgae. *Phytochemistry*, 26(6), 1657–1659.
26. Posten, C., & Feng Chen, S. (Vol. Eds.), (2016). *Advances in biochemical engineering/biotechnology: Vol. 153*. Berlin: Springer-Verlag.
27. Raso, J., Calderón, M. L., Góngora, M., Barbosa-Cánovas, G. V., & Swanson, B. G. (2006). Inactivation of *Zygosaccharomyces bailii* in fruit juices by heat, high hydrostatic pressure and pulsed electric fields. *Journal of Food Science*, 63(6), 1042–1044.
28. Raso, J., & Heinz, V. (Eds.). (2006). *Pulsed electric fields technology for the food industry: Fundamentals and applications*. Berlin: Springer-Verlag.
29. Reberšek, M., Miklavčič, D., Bertacchini, C., & Sack, M. (2014). Cell membrane electroporation - Part 3: The equipment. *IEEE Electrical Insulation Magazine*, 30(3), 8–18.
30. Schoenbach, K. H., Beebe, S. J., & Buescher, E. S. (2001). Intracellular effect of ultrashort electrical pulses. *Bioelectromagnetics*, 22(6), 440–448.
31. Schoenbach, K. H., Hargrave, B., Joshi, R. P., Kolb, J. F., Nuccitelli, R., Osgood, C., ... Buescher, E. S. (2007). Bioelectric effects of intense nanosecond pulses. *IEEE Transactions on Dielectrics and Electrical Insulation*, 14(5), 1088–1107.
32. Schwab, A. J. (1981). *Hochspannungsmesstechnik: Messgeräte und Messverfahren*. Berlin: Springer-Verlag.
33. Silve, A., Leray, I., Poignard, C., & Mir, L. M. (2016). Impact of external medium conductivity on cell membrane electropermeabilization by microsecond and nanosecond electric pulses. *Scientific Reports*, 6, 19957.
34. Stacey, M., Stickley, J., Fox, P., Statler, V., Schoenbach, K., Beebe, S. J., & Buescher, S. (2003). Differential effects in cells exposed to ultra-short, high intensity electric fields: Cell survival, DNA damage, and cell cycle analysis. *Mutation Research, Genetic Toxicology and Environmental Mutagenesis*, 542, 65–75.
35. Toepfl, S., Heinz, V., & Knorr, D. (2005). Overview of pulsed electric field processing for food. In D.-W. Sun (Ed.). *Emerging technologies for food processing* (pp. 69–97). Oxford, UK: Elsevier Ltd.
36. Toepfl, S., Mathys, A., Heinz, V., & Knorr, D. (2006). Review: Potential of high hydrostatic pressure and pulsed electric fields for energy efficient and environmentally friendly food processing. *Food Reviews International*, 22(4), 405–423.
37. Walsh, J., & Seignette, S. (1773). *Of the electric property of the torpedo. In a letter from John Walsh to Benjamin Franklin*.
38. Wölken, T., Sailer, J., Maldonado-Parra, F. D., Horneber, T., & Rauh, C. (2017). Application of numerical simulation techniques for modeling pulsed electric field processing. In D. Miklavčič (Ed.). *Handbook of electroporation* (pp. 1237–1267). Berlin: Springer-Verlag.

39. Yarmush, M. L., Golberg, A., Serša, G., Kotnik, T., & Miklavčič, D. (2014). Electroporation-based technologies for medicine: Principles, applications, and challenges. *Annual Review of Biomedical Engineering*, 16(1), 295–320.

MANUSCRIPT 2

Comprehensive pulsed electric field (PEF) system analysis for microalgae processing

Leandro Buchmann, Robin Bloch, Alexander Mathys*

*ETH Zurich, Department of Health Sciences and Technology, Institute of Food,
Nutrition and Health, IFNH, Sustainable Food Processing Laboratory,
Schmelzbergstrasse 9, Zurich 8092, Switzerland*

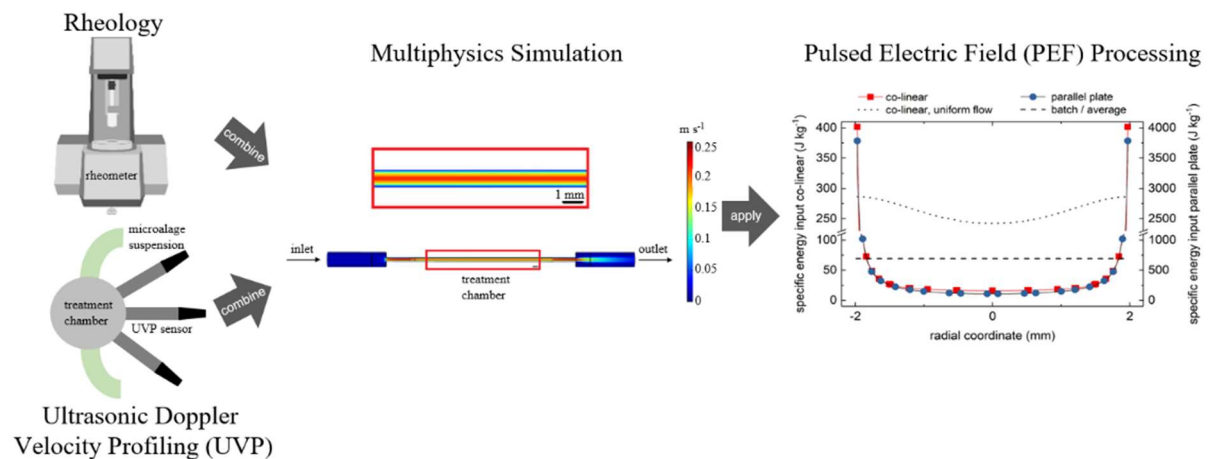
**Corresponding author*

Bioresource Technology 265 (2018) 268–274

ABSTRACT

Pulsed electric field (PEF) is an emerging nonthermal technique with promising applications in microalgae biorefinery concepts. In this work, the flow field in continuous PEF processing and its influencing factors were analyzed and energy input distributions in PEF treatment chambers were investigated. The results were obtained using an interdisciplinary approach that combined multiphysics simulations with ultrasonic Doppler velocity profiling (UVP) and rheological measurements of *Arthrospira platensis* suspensions as a case study for applications in the biobased industry. UVP enabled non-invasive validation of multiphysics simulations. *A. platensis* suspensions follow a non-Newtonian, shear-thinning behavior, and measurement data could be fitted with rheological functions, which were used as an input for fluid dynamics simulations. Within the present work, a comprehensive system characterization was achieved that will facilitate research in the field of PEF processing.

GRAPHICAL ABSTRACT



1. INTRODUCTION

Nonthermal processes such as pulsed electric field (PEF) can be used to effectively process biomass (Mahnič-Kalamiza et al., 2014; Rocha et al., 2018; Vorobiev and Lebovka, 2008). For instance, PEF could be used to gently pasteurize heat-sensitive liquids (Mathys et al., 2013; Raso et al., 2006) or efficiently extract valuable compounds from microalgae (Goettel et al., 2013; 't Lam et al., 2017; Kempkes et al., 2011; Parniakov et al., 2015; Postma et al., 2016). Apart from these focus areas, many other applications and advantages of PEF can be considered. Toepfl et al. (2006) note the potential to use PEF to improve environmental sustainability while saving energy and costs. Overall, PEF has many promising applications for microalgae processing, such as lipid extraction, stress inductions and contamination control within microalgae cultures (Bensalem et al., 2018; Buchmann et al., 2018; Eing et al., 2009; Rocha et al., 2018). Despite the long history of PEF research and the apparent advantages of PEF, it is not yet widely used commercially. Researchers mainly attribute this to the lack of treatment homogeneity, comparability, and reproducibility of PEF research results (Buckow et al., 2010; Jaeger et al., 2009; Raso et al., 2016; Buchmann et al., 2018). In fact, limited comparability and reproducibility of PEF research has been reported as the main underlying problem and is viewed by Raso et al. (2016) as a barrier for the development and wide use of the technology. Buckow et al. (2010) discusses the high monetary costs caused by the nonuniformity of PEF treatments and the high energy use resulting thereof. Consequently, many researchers have rightly focused on understanding PEF treatment inhomogeneities and on developing measures to reduce such inhomogeneities. However, experimental validation of simulated results is a challenging task (Buckow et al., 2010; Gerlach et al., 2008).

The ultrasonic Doppler velocity profiling (UVP) method can be utilized to noninvasively determine velocity profiles and therefore to validate flow field simulations. The method was developed at the Paul Scherrer Institute in Switzerland (Takeda, 1995). UVP uses ultrasonic echography and the Doppler shift frequency to measure the instantaneous velocity profile of liquids (Takeda, 1995). The time delay between the initiation and reception of the ultrasound pulse gives information on the reflection position, allowing velocity determination by incorporation of the Doppler shift frequency (Takeda, 2012). Compared to other flow measuring methods, UVP can be used on opaque liquids, and since it is noninvasive, it does not influence the

velocity profile (Wiklund et al., 2007).

To link UVP measurements to simulation results, the characteristic suspension viscosities must be known. Analysis of characteristic suspension viscosities as used for flow field simulations and experiments can be conducted using rheological measurements (Ewoldt et al., 2015). Thereby, the viscosity of fluids as a function of the applied force or shear rate can be determined. Microalgae suspensions from *Arthrospira platensis* serve as a promising model system for such analysis since they are widely used in research and application. When simulating Newtonian fluids, a constant viscosity value can be assumed for the entire simulated process. On the other hand, simulations of non-Newtonian fluids are more complex and require a viscosity function as an input.

Noninvasive system analysis can be executed by integration of suspension characteristics into numerical simulations. Simulations can be used to improve PEF in an iterative process, for example, by constantly simulating and optimizing the treatment chamber geometry (Buckow et al., 2010). Furthermore, computational tools can aid in understanding the different process factors involved in PEF and how those influence the treatment (Fiala et al., 2001; Gerlach et al., 2008; Meneses et al., 2011c). For those reasons, numerical simulations are used in this work to gain a better understanding of flow fields in PEF processing. Although simulation models might seem plausible, their solutions might not always be accurate, especially for complex problems (Barbosa-Cánovas et al., 2011). Consequently, it is essential to validate the simulations with experimental data whenever possible. This principle is also accounted for in the experimental portion of this work. Multiple papers in the past decade have described or reviewed the basic physics laws, principles, equations and boundary conditions underlying numerical simulations of PEF (Buckow et al., 2010; Gerlach et al., 2008; Krauss et al., 2011; Meneses et al., 2011a; Wölken et al., 2017). The focus of research on PEF simulations has been on improving the electric field homogeneity (Álvarez et al., 2006; Fiala et al., 2001; Meneses et al., 2011b; Zhang et al., 1995). Within this study, a comprehensive approach is taken to achieve a homogenous and comparable energy input from PEF, considering electric and flow field inhomogeneities. This novel approach combines multiphysics simulation with noninvasive UVP measurement and rheological validation, enabling a comprehensive PEF system analysis and laying the foundation for improved microalgae processing.

2. MATERIALS AND METHODS

2.1. Experimental setup

Experiments were conducted using a 10 mm and 1 mm diameter polycarbonate treatment chamber (manufactured at ETH Zürich, Switzerland). The treatment chamber was clamped into a retainer with the flow aligned vertically. Polypropylene-based tubes with a 2.79 mm internal diameter (SC0319A, Cole-Parmer GmbH, Wertheim, Germany) were attached to the treatment chamber on both sides as an inlet and outlet for the treated liquid. A peristaltic pump (MS-4/12-100 ISMATEC®, Cole-Parmer GmbH, Wertheim, Germany) was used at the highest speed (99 rpm) to pump the liquid through the PEF treatment cell from the bottom up, as described elsewhere (Goettel et al., 2013). Prior to flow measurements, it was ensured that the treatment chamber was thoroughly filled with liquid so that there were no remaining air bubbles and the flow reached steady-state conditions.

2.2. *Arthrospira platensis* suspensions

Arthrospira platensis suspensions were used as a model system for conducting flow behavior experiments. *A. platensis* suspensions of four different concentrations in deionized water were prepared (5, 25, 60 and 100 g L⁻¹); using *A. platensis* powder (PREMIUM II, origin China, Institute for Food and Environmental Research ILU, Bergholz-Rehbruecke, Germany). The suspensions were thoroughly stirred and shaken in a flask to achieve a homogenous suspension. Flow experiments were conducted within two hours of production to minimize any decomposition of the suspension. In addition, a magnetic stirrer was used during the entire flow profiling experiment to prevent sedimentation.

2.3. Measuring mass flow rate

The mass flow rate through each parallel plate treatment chamber (10 mm and 1 mm gap) was measured for the water and *A. platensis* suspensions used in the flow field measurements. The liquids were pumped through the treatment cell as described in Section 2.1 and collected in a 50 mL falcon tube. The time for 20 mL to flow through the system was recorded. From the mass flow rate \dot{m} (kg s⁻¹), the cross-sectional area of the inlet A (m²), and the fluid density ρ (kg m⁻³), the average flow velocity u (m s⁻¹) in the inlet were calculated for different inlet diameters (Eq. (1)). These

measurements served as a guide for the selection range of the inlet velocity value u_0 (m s^{-1}) in the simulations. Using the actual experimental inlet velocity as a boundary condition in the simulation allowed an experimental validation.

$$\dot{m} = u \cdot A \cdot \rho \quad (1)$$

2.4. UVP measurements

A 10 mm lab-scale parallel plate continuous PEF system as described in Section 2.1 was used for the UVP experiments. An ultrasonic profiler (UB-Lab, UBERTONE, Strasbourg, France) was used for measurements, together with two 4 MHz and one 8 MHz ultrasound transducer (UBLab, UBERTONE, Strasbourg, France). Round holes approximately 6 mm deep with a diameter only marginally larger than the ultrasound transducer were drilled into the outer polycarbonate shell of the treatment cell at three incident angles θ_1 (-) (0° or perpendicular to the liquid flow, 45° , 60°) to hold the ultrasound transducers in place. Water as a reference medium, as well as three different concentrations of *A. platensis* suspensions, were used for the UVP measurements (see section 2.2). Inert copolyamide acoustic reflector beads (size 80–200 μm , density 1.07 g cm^{-3} , MET-FLOW S.A., Lausanne, Switzerland) were added to the suspensions and the water in order to facilitate the reflections of the ultrasound waves and to improve the measurement signal. The results were averaged over ten measurements for each investigated suspension and water. For an in-depth method description and experimental procedure, refer to Takeda (2012).

2.5. Rheological measurements

Rheological analyses were conducted on the *A. platensis* suspensions and water as described in Section 2.2. The flow behavior was analyzed using a stress-controlled rheometer (Physica MCR 501, Anton Paar, Graz, Austria) with double gap geometry (DG 26.7, Anton Paar, Graz, Austria). For each measurement, a liquid volume of 3.8 mL was loaded into the outer cylinder. Samples were sheared at shear rates $\dot{\gamma}$ (s^{-1}) of $500 \text{ s}^{-1} - 0.5 \text{ s}^{-1}$ and vice versa. By reversing the shear rate, it was ensured that a possible sedimentation of *A. platensis* during rheological measurements was accounted for. The resulting measurement points were visualized in a scatter plot showing the viscosity versus the shear rate. The best-fitting rheological equation was either the Herschel-Bulkley equation (Eq. (2)) or the non-Newtonian power law (Eq. (3)) (Mezger, 2015; Spagnolie, 2015).

$$\tau = \tau_0 + K\dot{\gamma}^n \quad (2)$$

$$\tau = K\dot{\gamma}^n \quad (3)$$

with shear stress τ (Pa), yield stress τ_0 (Pa), flow consistency index K (Pa sⁿ) and flow behavior index n (–). Incorporation of the generalized Newtonian law ($\mu(\dot{\gamma}) = \tau / \dot{\gamma}$), allows Eq. (2) to be rewritten. The resulting equation gives the viscosity μ (Pa s) of the non-Newtonian fluid as a function of the shear rate, given a shear rate equal to or greater than the zero shear rate $\dot{\gamma}_0$ (s⁻¹) (Eq. (4)).

$$\mu = \tau_0|\dot{\gamma}|^{-1} + K|\dot{\gamma}|^{n-1}, |\dot{\gamma}| \geq \dot{\gamma}_0 \quad (4)$$

This function can now be applied onto rheological data to obtain values for the yield stress, flow consistency index, and flow behavior index. The resulting functions were used as viscosity functions in the multiphysics simulations, as described in Section 2.6.

The rheological results were further used to derive an equation for the *A. platensis* suspension's viscosity as a function of its concentration, using the Krieger-Dougherty relation (Eq. (5)). The Krieger-Dougherty relation (Eq. (5)) can be used to express the suspension viscosity as a function of the particle concentration (Krieger and Dougherty, 1959). While this relation is strictly valid for the low shear Newtonian plateau, it can be used at the lower end of the measured shear rate range (Zhang et al., 2013).

$$\mu_r = \mu/\mu_s = (1 - \Phi_V/\Phi_{max})^{-[\mu]\Phi_{max}} \quad (5)$$

where μ_r (–) denotes the relative viscosity of the suspensions, μ (Pa s) represents the effective viscosity of the suspensions, μ_s (Pa s) represents the viscosity of the suspending medium, ϕ_{max} (–) is the maximum volume fraction, ϕ_v (–) represents the volume fraction, and $[\mu]$ (–) denotes the intrinsic viscosity of the suspended particles. Ciferri (1983) describe the morphology of *A. platensis* as helical filaments. Consequently, the shape of *A. platensis* filaments can be approximated as a cylinder with an aspect ratio of 1:10. This ratio was confirmed in microscopic images. Metzner (1985) gives values for the maximum packing fraction of short fibers with different aspect ratios. Pan (1993) provides a graph for the maximum volume fraction as a function of the aspect ratio. Both sources suggest that the value for maximum packing fraction of elongated structures with aspect ratios close to 1:10 can be approximated

at $\phi_{max} = 0.43$.

In the absence of a value for the volume fraction of *A. platensis* suspensions, the mass fraction was used instead. The mass fraction was approximated from the mass concentration using a value for the free water content in the *A. platensis* powder. The water content in the utilized *A. platensis* powder was determined to be at 6.56% by using a moisture analyzer (HR73/HA-P43, Mettler-Toledo International Inc., Columbus OH, USA). The water content of the powder was subtracted from the powder mass and added to the mass of the suspending medium water to calculate the mass fraction.

2.6. Computational fluid dynamics simulation

COMSOL multiphysics® software (version 5.3, Comsol Inc., Burlington MA, USA) was used to conduct multiphysics simulations of the flow field in PEF treatment chambers. The geometries of the parallel plate treatment chambers available at ETH Zurich, Sustainable Food Processing Laboratory were recreated in COMSOL multiphysics®. The simulations for parallel plate treatment chambers were conducted using a 3D model. The geometry of a co-linear treatment cell was simulated using a 2D axisymmetric approach.

The Reynolds numbers for the lab-scale geometries investigated in this work were all well below the critical Reynolds value of 2300, even at the highest velocities and lowest viscosities that were simulated. Thus, Reynolds numbers were sufficiently small that a laminar physics model was used to simulate the flow field. Boundary conditions for the fluid properties, i.e., the fluid density and the dynamic viscosity, were defined for every simulation. The density was set to equal the density of water for all simulations ($\rho = 1000 \text{ kg m}^{-3}$). To simulate the flow of water, the standard dynamic viscosity of water as deposited in the software was used ($\mu = 0.001 \text{ Pa s}$). The flow behavior of the *A. platensis* suspensions used for the experimental part of this work was measured in rheological trials as described in Section 2.5. The results of these experiments were used to construct viscosity functions for every concentration of *A. platensis* solution measured. The viscosity functions were then integrated into the simulation. The presented work only considered stationary solutions of the simulation, as the system had reached its equilibrium and was in a steady state. Therefore, investigating stationary solutions was sufficient to describe the situation present in most PEF research applications. Further, effects of

temperature on media parameters were neglected due to the low energy inputs studied.

2.7. Data analysis

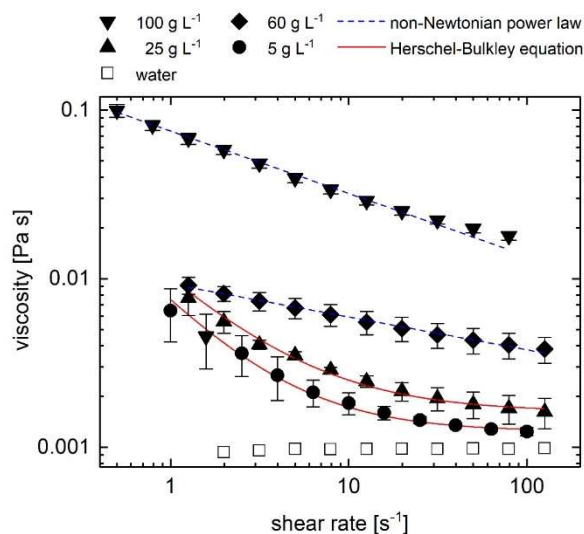
Data analysis was conducted by an independent t-test. The confidence interval was 95% for all experiments. Statistical results were obtained using the software IBM SPSS Statistics (IBM Corp., Armonk NY, USA).

3. RESULTS AND DISCUSSION

To set up the multiphysics simulations, the mass flow rate was determined prior to all other experiments. It was found that the mass flow rate was equal to $3.03 \cdot 10^{-7} \text{ kg s}^{-1}$, $2.94 \cdot 10^{-7} \text{ kg s}^{-1}$, $2.86 \cdot 10^{-7} \text{ kg s}^{-1}$ and $2.78 \cdot 10^{-7} \text{ kg s}^{-1}$ for water and for *A. platensis* suspension with concentrations of 5 g L^{-1} , 25 g L^{-1} and 100 g L^{-1} , respectively. Based on the mass flow rate, the inlet velocities were calculated for different inlet configurations using Eq. (1).

3.1. Flow behavior of *Arthrospira platensis* suspensions

Rheological measurements demonstrated that *A. platensis* suspensions showed a non-Newtonian, shear-thinning behavior, and measurement data could be fitted with rheological functions (Fig. 1). Lower-concentration suspensions (5 g L^{-1} , 25 g L^{-1}) were best fitted using the Herschel-Bulkley equation (Eq. (2)) whereas higher-concentration suspensions (60 g L^{-1} , 100 g L^{-1}) were best fitted with the non-Newtonian power law (Eq. (3)).



M2 - Figure 1: Rheological measurement results for water and different *A. platensis* suspension concentrations, fitted with rheological equations. The viscosity increased for increasing concentrations. The suspensions exhibited a non-Newtonian, shear thinning behavior. In comparison, water showed Newtonian behavior, characterized by the horizontal line at viscosity $\mu = 0.001 \text{ Pa s}$.

The flow consistency index and the flow behavior index of *A. platensis* suspensions, which together define the viscosity functions at the respective concentration, are shown in Table 1 in accordance with Eq. (4). The rheological results for *A. platensis* suspensions correspond well with findings by Bernaerts et al. (2017), who

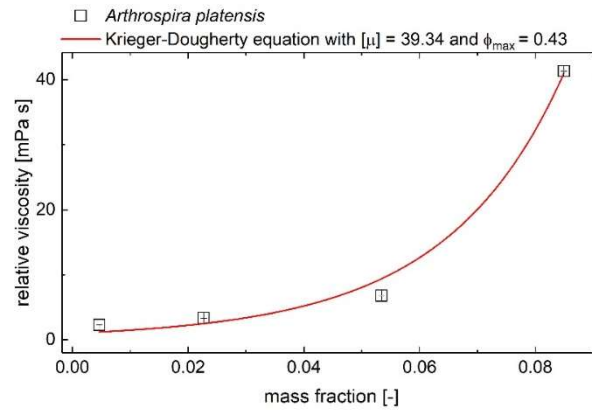
characterized rheological behavior for suspensions of seven different strains of microalgae, including *A. platensis*. The rheological behavior depends on the investigated strain and biopolymer composition; therefore, it must be analyzed for every strain independently.

M2 - Table 1: Values for yield stress τ_0 times shear rate $|\dot{\gamma}|^{-1}$, flow consistency index K , and flow behavior index n of *A. platensis* suspensions obtained from the Herschel-Bulkley and non-Newtonian power law fits on the rheological measurements.

	$\tau_0 \dot{\gamma} ^{-1}$ (Pa s)	K (Pa s ⁿ)	$n-1$ (-)
<i>A. platensis</i> 5 g·L ⁻¹	0.0012	0.0063	-0.1091
<i>A. platensis</i> 25 g·L ⁻¹	0.0016	0.0085	-0.0161
<i>A. platensis</i> 60 g·L ⁻¹	-	0.0093	-0.1952
<i>A. platensis</i> 100 g·L ⁻¹	-	0.0751	-0.3703

The investigated *A. platensis* suspensions showed an increasing viscosity with increasing concentration (Fig. 1). Therefore, the maximum packing fraction was integrated with the rheological results to obtain a Krieger-Dougherty plot illustrating the dependency of cell concentration on relative viscosity (Fig. 2). The viscosity increased exponentially with increasing concentration. Hence, the resulting plot illustrates that the empirical equation formulated by Krieger and Dougherty accurately approximates the viscosity of *A. platensis* suspensions as a function of their concentration. The maximum mass fraction was set to 0.43 in accordance with the literature. The data shown in Fig. 2 were obtained for a shear rate of 5 s⁻¹. In accordance with Eq. (5), a value for the intrinsic viscosity of 39.24 was obtained.

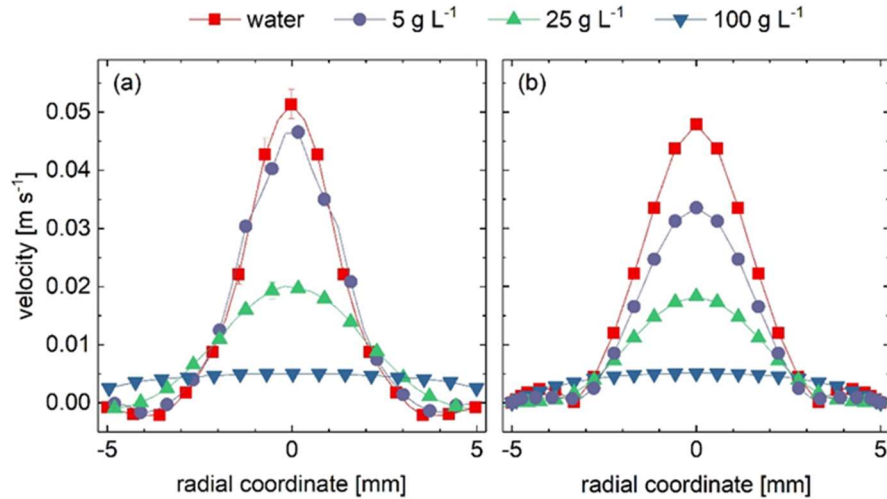
This value is significantly higher than the intrinsic viscosity of 24.7 for *Chlorella vulgaris* reported by Zhang et al. (2013). This observation means that the *A. platensis* cells contribute more to the viscosity of the suspension than *C. vulgaris* cells do. In view of the morphological differences between *C. vulgaris* and *A. platensis*, this difference is not surprising. The long filamentous structure of *A. platensis* interacts more strongly with the medium than the spherical cell of *C. vulgaris*, resulting in a higher viscosity of the suspended cells.



M2 - Figure 2: Relative viscosity $\mu_r = \mu / \mu_s$ of *A. platensis* suspensions as a function of their mass fractions, estimated by fitting the Krieger-Dougherty equation to the rheological data for shear rate $\dot{\gamma} = 5 \text{ s}^{-1}$, with the maximum mass fraction set to 0.43. The resulting intrinsic viscosity value $[\mu]$ equals 39.24. The relative viscosity increased exponentially as a function of its mass fraction.

3.2. Experimental validation of flow fields

Experimental validation of the fluid dynamic simulations was conducted using a parallel plate treatment chamber of 10 mm diameter applying UVP, as described in Section 2.4. The results of the measurements are presented in Fig. 3 and are compared with the simulation results for exactly the same treatment chamber geometry, using the viscosity functions obtained from the rheological measurements. The results of the experiments and simulations correlate. Based on an independent t-test, no significant difference between UVP and simulation results was found for water and 25 g L^{-1} and 100 g L^{-1} *A. platensis* solutions. Both in the simulation and in the flow profiling results, the velocity profile was narrow and pronounced at low viscosity but flattened to become more uniform at higher viscosity.



M2 - Figure 3: a) Ultrasonic Doppler velocity profiling (UVP) measurement and b) simulation results for water and suspensions with different *A. platensis* concentrations in the 10 mm diameter treatment chamber.

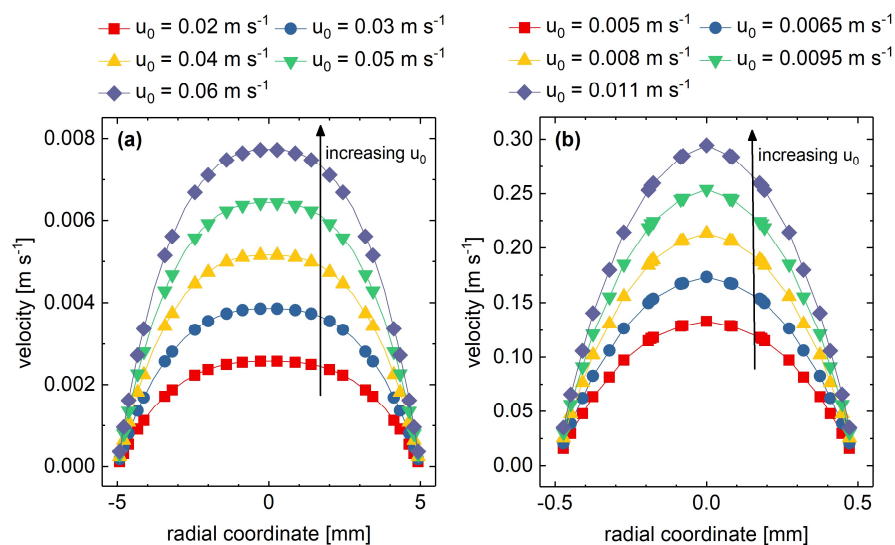
However, a statistically significant difference between the simulation and UVP occurred at suspension concentrations of 5 g L⁻¹ ($p < 0.05$). The reason for this deviation might be the sensitivity of the UVP method. As described in Section 2.4, the number of microalgae cells in the 5 g L⁻¹ suspension might simply be too low for the ultrasound transducer to receive a signal significantly different from that of water. Nevertheless, UVP validates the simulation results well and reinforces that simulations are a useful means to test the basic principles in processes such as PEF.

While the validity and value of the simulations has already been confirmed by other researchers who have used simulations for PEF (Buckow et al., 2010; Fiala et al., 2001; Gerlach et al., 2008; Meneses et al., 2011b), using the UVP method to validate the simulation results is a new approach. Some researchers have raised the concern that measuring equipment might disturb the flow and thus make an experimental validation of flow experiments difficult (Buckow et al., 2010; Gerlach et al., 2008). The UVP method addresses these concerns well, since it can be used on a broad range of liquids and suspensions, even opaque and non-Newtonian suspensions, without disturbing the flow field. However, when testing lab-scale equipment, it is necessary to increase the scale to a diameter in the range of 10mm or more in order to obtain sufficient data points during UVP measurements.

3.3. Simulation based comprehensive system analysis

3.3.1. Effect of inlet velocity

The effect of changing inlet velocity was investigated in both the treatment chamber geometries of 10 mm and 1 mm diameter and for fluids of different viscosity. Fig. 4 shows the velocity profiles in the center of the treatment chambers for different inlet velocities (u_0). In both geometries, the velocity profiles had a parabolic shape, as expected from laminar flow profiles. The velocity was at its maximum in the center of the treatment chamber and tended towards zero near the walls. The maximum velocity increased with increasing inlet velocity. Therefore, the differences in velocity across the treatment chamber became larger with increasing inlet velocity, assuming laminar flow. This basic principle was confirmed in simulations for all different medium viscosities and treatment chamber geometries tested. The influence of inlet velocity on the flow profile correlated for all tested viscosity and treatment chamber configurations. Therefore, reducing the inlet velocity would increase the treatment homogeneity in parallel plate treatment chambers, provided a laminar flow field.



M2 - Figure 4: Simulation results showing the effect of increasing inlet velocity u_0 on the velocity profiles in the parallel plate treatment chambers for a) *A. platensis* suspension of concentration 100 g L⁻¹ in the 10 mm diameter parallel plate chamber and b) water in the 1 mm diameter parallel plate chamber.

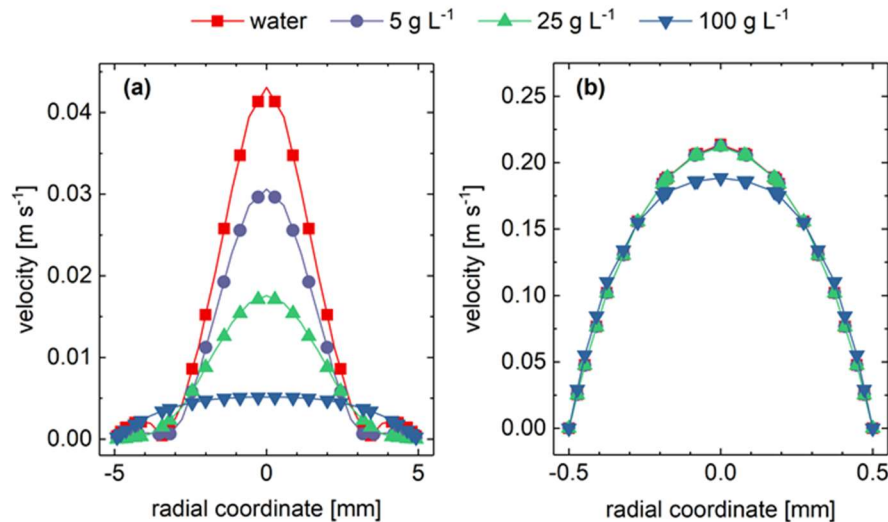
3.3.2. Effect of viscosity

Liquid flow in continuous PEF was simulated for different viscosities, using the viscosity functions determined in Section 3.1 for the different concentrations of *A. platensis*. The inlet velocities and all other parameters were kept constant to investigate the effect that viscosity alone had on the velocity profile. The simulation

results are displayed in Fig. 5 for both parallel plate treatment chamber geometries. In the 10 mm diameter parallel plate chamber, the effect of viscosity (Fig. 1) was clearly visible (Fig. 5a). At a low viscosity equal to that of water, the maximum velocity in the treatment chamber was the highest. There was a highly pronounced velocity profile and recirculation zones near the chamber walls. These recirculation zones could be reduced with an optimized treatment chamber inlet design. Nevertheless, with increasing viscosity, the peak velocity decreased and the velocity profile became flatter and more homogeneous overall. In the 1 mm diameter chamber, the velocity profile appeared to be almost independent from the viscosity (Fig. 5b). Within narrow treatment chambers, the friction from the walls and the interacting forces between the fluid and the walls dominated the fluid flow. The wall forces appear to have influenced the flow field all the way to the center of the treatment chamber. On the other hand, with larger geometries such as the 10 mm diameter chamber, the wall appeared to exert its effect on liquid fractions that were nearby, but the viscosity of the fluid governed the liquid flow in the center.

Goettel et al. (2013) observed that the conductivity of PEF-treated microalgae (*A. protothecoides* SAG 211-7a) suspensions increased with increasing biomass concentration, making the PEF treatments at higher concentrations more efficient. An increase in concentration led to an increase in viscosity, as illustrated in section 3.1. Therefore, based on the results presented in Fig. 5, an improvement in treatment homogeneity and energy efficiency accompanied the increased biomass concentration. This finding further emphasizes the importance of flow field considerations in continuous PEF systems.

Overall, the results showed that the medium viscosity does have an impact on the flow profiles, although this effect seems to be dependent on the size of the treatment chamber. Higher viscosities in general improved the flow field uniformity and reduced the peak viscosity in the center of the treatment chamber. When scaling up from a treatment chamber with one or only a few millimeters in diameter, one should be aware that the impact of viscosity might become more important with increasing scale.



M2 - Figure 5: Simulation results showing the effect of increasing viscosity, according to Fig. 1, on the velocity profiles in the treatment chambers for different concentrations of *A. platensis* suspensions for the a) 10 mm and b) 1 mm diameter parallel plate chambers.

3.4. Energy input comparison between different treatment chambers

In PEF treatments, the specific energy input is crucial to assess treatment effectivity and to compare results from different laboratories. In parallel plate treatment chambers where the electric field is uniform, variabilities in the flow fields account for the entire inhomogeneity in energy input. Therefore, only the flow field must be simulated without having to consider the electric field distribution. In contrast, with collinear treatment chambers, both the flow field and the electric field are inhomogeneous. Therefore, there are two independent factors that both contribute to potential treatment inhomogeneities. It may not be sufficient to only investigate one of these two factors. To make a conclusive statement on the overall treatment homogeneity, specific energy input distributions were calculated for both co-linear and parallel plate treatment chambers, combining the results from flow field and electric field simulations. To make the results as comparable as possible, a collinear cell with a 4mm gap between the insulators (the geometry utilized by Meneses et al. (2011c)) was compared to a parallel plate treatment chamber with a 4 mm electrode gap (the geometry utilized by Goettel et al. (2013)). All other parameters such as inlet velocity, viscosity, electric potential, pulse width, pulse repetition rate, and medium conductivity were kept equal for both treatment chambers (Table 2). The results for the energy input distribution are visualized in Fig. 6. Since there was a much larger treatment zone in the parallel plate chamber and the liquid was exposed to a higher

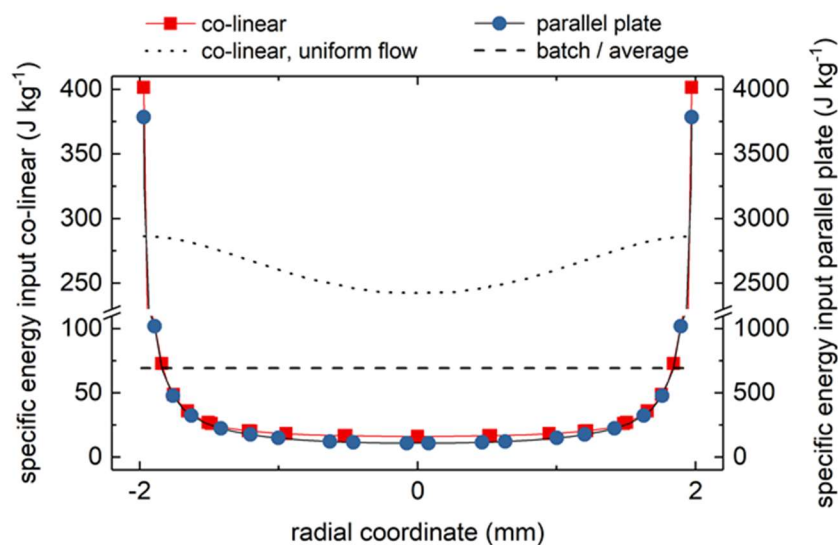
pulse number, the specific energy input was approximately ten times higher than that of the co-linear chamber. However, by reducing the pulse repetition frequency by the same factor of ten, the energy input for both treatment chambers correlated. The shape of the energy input distributions was almost the same for both geometries. Therefore, for the chosen parameters, both treatments were approximately equally nonuniform, with equal amounts of deviation from the average treatment effect. However, as illustrated by the dotted line (· ·) in Fig. 6, there was a significant difference between the actual energy input distribution in the co-linear chamber considering electric and flow field, and the energy distribution assuming a uniform flow field. This difference further underlines the necessity to consider the flow field in continuous PEF.

M2 - Table 2: Parameters used for the calculation of the energy input distribution in the parallel plate and co-linear treatment chamber geometries. The electric potential U , the pulse width τ_p , the medium conductivity σ , the pulse repetition frequency f and the treatment chamber diameter D_{in} were all defined the same for both treatment chamber geometries, providing the same conditions for both chambers in order to make the results comparable. Due to the differences in geometry, the treatment chamber length L was larger for the parallel plate chamber than for the co-linear chamber.

	U (V)	τ_p (μ s)	σ (mS cm ⁻¹)	f (s ⁻¹)	D_{in} (mm)	L (mm)
parallel plate	1000	1	4	9	4	28
co-linear	1000	1	4	9	4	5

The parameters of the energy input had to be examined more closely to understand what made up the inhomogeneities in both treatment chamber geometries and what was different between the two geometries. The parallel plate chamber had a uniform electric field but a nonuniform flow field. On the other hand, the co-linear chamber had a more uniform flow field due to its pinched geometry. However, the electric field of the co-linear chamber was nonuniform; it was stronger near the walls and weaker towards the center of the chamber. Therefore, the liquid near the walls that was already flowing more slowly experienced a higher field, while the fast-moving liquid in the center experienced a lower electric field. Consequently, the flow field was more uniform in the co-linear chamber, but the electric field nonuniformity exacerbated the effect of the inhomogeneous flow field. Overall, it is possible that under certain conditions, either the co-linear or the parallel plate chamber is more uniform concerning the energy input distribution. In the case simulated in Fig. 6, the effects

of electric field and flow field described above seemed to be in balance, resulting in correlating energy input profiles for both treatment chambers. However, any of the medium or process parameters can be modified, and the modifications might favor one of the two geometries more than the other. While for different reasons, both the co-linear and parallel plate treatment chambers exhibited a nonuniform energy input distribution. Therefore, it is important to calculate and compare the energy input distributions every time when changing between the two geometries, optimizing the treatment chamber designs, modifying process parameters, or scaling up the process.



M2 - Figure 6: Simulated distribution of specific energy input across treatment chambers for parallel plate and co-linear geometries, both with 4 mm diameter and assuming the viscosity of water. All other parameters (inlet velocity, electric potential, pulse width, pulse repetition rate, and medium conductivity) were also kept equal for both treatment chambers (Table 2). The dotted (· · ·) line represents the energy input distribution in the co-linear chamber when assuming an average or uniform flow field and only considering the nonuniform electric field. The dashed (- -) line represents the energy input in a batch parallel plate system with no flow and a uniform electric field.

The dashed line (- -) in Fig. 6 shows the specific energy input distribution of a batch parallel plate treatment chamber with the same dimensions as the continuous chamber. All other parameters such as the electric potential, conductivity, pulse width and frequency were kept the same as for the continuous process (Table 2). It became evident that the energy input in the continuous process deviated greatly from a batch process, even when using the otherwise exact same process parameters and geometry. To quantify the extent of the deviation, one can disregard the fluid adjacent to the wall, and focus on the 80 percent of fluid in the center of the chamber. In these middle 80 percent of the parallel plate chamber volume, the average specific energy

input was approximately 165 J kg^{-1} for the continuous system and three times higher for the batch system at approximately 700 J kg^{-1} . At the same time, the approximately 10 percent of liquid nearest to the walls displayed an extremely high energy input that was significantly beyond the energy input of 700 J kg^{-1} expected from the batch treatment and may have led to overtreated microalgae cells. This difference between batch and continuous PEF processes is striking, and it is highly relevant for improving reproducibility in PEF research. Considering the large deviations between batch and continuous PEF, one must be extremely cautious when transferring process knowledge or settings from batch to continuous processes during scale-up.

4. CONCLUSIONS

Sustainable and economically viable microalgae-based biorefinery concepts require cost-effective processing. PEF processing demonstrated relevant applications in microalgae valorization; however, the reproducibility of results was low. In continuous PEF processing electric and flow field, characterization is crucial. The novel approach to combine multiphysics simulation with noninvasive UVP measurements and rheological validation enabled a comprehensive PEF system characterization and control. The results presented in this work will allow for better reproducibility of results, facilitating the research on PEF and subsequent microalgae biorefinery approaches. Further research is required in the area of turbulent flow fields for scale-up considerations.

ACKNOWLEDGEMENTS

The authors gratefully acknowledge the ETH World Food System Center (Project “NewAlgae”, grant number: 2-72235-17), Dr. Wolfgang Frey and Dr. Christian Gusbeth from the Karlsruhe Institute of Technology (KIT), the ETH Zürich Foundation, as well as Prof. Dr. Erich J. Windhab, Dr. Damien Dufour, Pascal Bertsch, Daniel Kiechl and Bruno Pfister from the ETH Zürich Food Process Engineering Laboratory for their support.

CONFLICT OF INTEREST STATEMENT

The authors declare no conflict of interest.

REFERENCES

1. 't Lam, G.P., Postma, P.R., Fernandes, D.A., Timmermans, R.A.H., Vermuë, M.H., Barbosa, M.J., Eppink, M.H.M., Wijffels, R.H., Olivieri, G., 2017. Pulsed electric field for protein release of the microalgae *Chlorella vulgaris* and *Neochloris oleoabundans*. *Algal Res.* 24, 181–187.
2. Álvarez, I., Condón, S., Raso, J., 2006. Microbial inactivation by pulsed electric fields. In: Raso, J., Heinz, V. (Eds.), *Pulsed Electric Fields Technology for the Food Industry*. Food Engineering Series, Springer, Boston, MA, pp. 97–129.
3. Barbosa-Cánovas, G.V., Ghani Albaali, A., Juliano, P., Knoerzer, K., 2011. Introduction to innovative food processing technologies: Background, advantages, issues, and need for multiphysics modeling. In: Knoerzer, K., Juliano, P., Roupas, P., Versteeg, C. (Eds.), *Innovative Food Processing Technologies: Advances in Multiphysics Simulation*. John Wiley & Sons, Ltd., pp. 3–21.
4. Bensalem, S., Lopes, F., Bodénès, P., Pareau, D., Français, O., Le Pioufle, B., 2018. Understanding the mechanisms of lipid extraction from microalga *Chlamydomonas reinhardtii* after electrical field solicitations and mechanical stress within a microfluidic device. *Bioresour. Technol.* 257, 129–136.
5. Bernaerts, T.M.M., Panozzo, A., Doumen, V., Foubert, I., Gheysen, L., Goiris, K., Moldenaers, P., Hendrickx, M.E., Van Loey, A.M., 2017. Microalgal biomass as a (multi)functional ingredient in food products: rheological properties of microalgal suspensions as affected by mechanical and thermal processing. *Algal Res.* 25, 452–463.
6. Buchmann, L., Böcker, L., Frey, W., Haberkorn, I., Nyffeler, M., Mathys, A., 2018. Energy input assessment for nanosecond pulsed electric field processing and its application in a case study with *Chlorella vulgaris*. *Innov. Food Sci. Emerg. Technol.* 47, 445–453.
7. Buckow, R., Schroeder, S., Berres, P., Baumann, P., Knoerzer, K., 2010. Simulation and evaluation of pilot-scale pulsed electric field (PEF) processing. *J. Food Eng.* 101, 67–77.
8. Ciferri, O., 1983. Spirulina, the edible microorganism. *Microbiol. Rev.* 47, 551–578.
9. Eing, C.J., Bonnet, S., Pacher, M., Puchta, H., Frey, W., 2009. Effects of nanosecond pulsed electric field exposure on *Arabidopsis thaliana*. *IEEE Trans. Dielectr. Electr. Insul.* 16, 1322–1328.
10. Ewoldt, R.H., Johnston, M.T., Caretta, L.M., 2015. Experimental challenges of shear rheology: how to avoid bad data. In: Spagnolie, S.E. (Ed.), *Complex Fluids in Biological Systems*. Springer Science+Business Media, New York, pp. 207–241.
11. Fiala, A., Wouters, P.C., van den Bosch, E., Creyghton, Y.L., 2001. Coupled electrical-fluid model of pulsed electric field treatment in a model food system. *Innov. Food Sci. Emerg. Technol.* 2, 229–238.
12. Gerlach, D., Alleborn, N., Baars, A., Delgado, A., Moritz, J., Knorr, D., 2008. Numerical simulations of pulsed electric fields for food preservation: a review. *Innov. Food Sci. Emerg. Technol.* 9, 408–417.
13. Goettel, M., Eing, C., Gusbeth, C., Straessner, R., Frey, W., 2013. Pulsed electric field assisted extraction of intracellular valuables from microalgae. *Algal Res.* 2, 401–408.
14. Jaeger, H., Meneses, N., Knorr, D., 2009. Impact of PEF treatment inhomogeneity such as electric field distribution, flow characteristics and temperature effects on the inactivation of *E. coli* and milk alkaline phosphatase. *Innov. Food Sci. Emerg. Technol.* 10, 470–480.
15. Kempkes, M.A., Roth, I., Gaudreau, M.P.J., 2011. Pulsed Electric Field (PEF) Method for Continuous Enhanced Extraction of Oil and Lipids From Small Aquatic Plants. Patent Application. US2011/0107655 A1.
16. Krauss, J., Rauh, C., Delgado, A., 2011. Novel, multi – objective optimization of pulsed electric field processing for liquid food treatment. In: Knoerzer, K., Juliano, P., Roupas, P., Versteeg, C. (Eds.), *Innovative Food Processing Technologies: Advances in Multiphysics Simulation*. John Wiley & Sons, Ltd., pp. 209–231.
17. Krieger, I.M., Dougherty, T.J., 1959. A mechanism for non-newtonian flow in suspensions of rigid spheres. *Trans. Soc. Rheol.* 3, 137–152.
18. Mahnič-Kalamiza, S., Vorobiev, E., Miklavčič, D., 2014. Electroporation in food processing and

- biorefinery. *J. Membr. Biol.* **247**, 1279–1304.
19. Mathys, A., Toepfl, S., Siemer, C., Favre, L., Benyacoub, J., & Hansen, C. E., 2013. Pulsed Electric Field Treatment Process and Dairy Product Comprising Bioactive Molecules Obtainable by the Process. Patent Application. EP 2543254(A1). NESTEC S.A.
 20. Meneses, N., Jaeger, H., Knorr, D., 2011a. Minimization of thermal impact by application of electrode cooling in a co-linear PEF treatment chamber. *J. Food Sci.* **76**, 536–543.
 21. Meneses, N., Jaeger, H., Knorr, D., 2011b. Computational fluid dynamics applied in pulsed electric field preservation of liquid foods. In: Knoerzer, K., Juliano, P., Roupas, P., Versteeg, C. (Eds.), *Innovative Food Processing Technologies: Advances in Multiphysics Simulation*. John Wiley & Sons, Ltd., pp. 193–207.
 22. Meneses, N., Jaeger, H., Moritz, J., Knorr, D., 2011c. Impact of insulator shape, flow rate and electrical parameters on inactivation of *E. coli* using a continuous co-linear PEF system. *Innov. Food Sci. Emerg. Technol.* **12**, 6–12.
 23. Metzner, A.B., 1985. Rheology of suspensions in polymeric liquids. *J. Rheol.* **29**, 739–775.
 24. Mezger, T.G., 2015. *Applied Rheology*, first ed. Anton Paar GmbH, Graz, Austria.
 25. Pan, N., 1993. Theoretical determination of the optimal fiber volume fraction and fibermatrix property compatibility of short fiber composites. *Polym. Compos.* **14**, 85–93.
 26. Parniakov, O., Barba, F.J., Grimi, N., Marchal, L., Jubeau, S., Lebovka, N., Vorobiev, E., 2015. Pulsed electric field and pH assisted selective extraction of intracellular components from microalgae *Nannochloropsis*. *Algal Res.* **8**, 128–134.
 27. Postma, P.R., Pataro, G., Capitoli, M., Barbosa, M.J., Wijffels, R.H., Eppink, M.H.M.M., Olivieri, G., Ferrari, G., 2016. Selective extraction of intracellular components from the microalga *Chlorella vulgaris* by combined pulsed electric field-temperature treatment. *Bioresour. Technol.* **203**, 80–88.
 28. Raso, J., Calderón, M.L., Góngora, M., Barbosa-Cánovas, G.V., Swanson, B.G., 2006. Inactivation of *Zygosaccharomyces bailii* in fruit juices by heat, high hydrostatic pressure and pulsed electric fields. *J. Food Sci.* **63**, 1042–1044.
 29. Raso, J., Frey, W., Ferrari, G., Pataro, G., Knorr, D., Teissie, J., Miklavčič, D., 2016. Recommendations guidelines on the key information to be reported in studies of application of PEF technology in food and biotechnological processes. *Innov. Food Sci. Emerg. Technol.* **37**, 312–321.
 30. Rocha, C.M.R., Genisheva, Z., Ferreira-Santos, P., Rodrigues, R., Vicente, A.A., Teixeira, J.A., Pereira, R.N., 2018. Electric field-based technologies for valorization of bioresources. *Bioresour. Technol.* **254**, 325–339.
 31. Spagnolie, S.E. (Ed.), 2015. *Complex Fluids in Biological Systems*. Springer Science +Business Media, New York.
 32. Takeda, Y. (Ed.), 2012. *Ultrasonic Doppler Velocity Profiler for Fluid Flow*. Springer, Japan.
 33. Takeda, Y., 1995. Velocity profile measurement by ultrasonic Doppler method. *Exp Therm. Fluid Sci.* **10**, 444–453.
 34. Toepfl, S., Mathys, A., Heinz, V., Knorr, D., 2006. Review: Potential of high hydrostatic pressure and pulsed electric fields for energy efficient and environmentally friendly food processing. *Food Rev. Int.* **22**, 405–423.
 35. Vorobiev, E., Lebovka, N. (Eds.), 2008. *Electrotechnologies for Extraction from Food Plants and Biomaterials*. Springer Science+Business Media, New York.
 36. Wiklund, J., Shahram, I., Stading, M., 2007. Methodology for in-line rheology by ultrasound Doppler velocity profiling and pressure difference techniques. *Chem. Eng. Sci.* **62**, 4277–4293.
 37. Wölken, T., Sailer, J., Maldonado-Parra, F.D., Horneber, T., Rauh, C., 2017. Application of numerical simulation techniques for modeling pulsed electric field processing. In: Miklavčič, D. (Ed.), *Handbook of Electroporation*. Springer International Publishing AG, pp. 1237–1267.

38. Zhang, X., Jiang, Z., Chen, L., Chou, A., Yan, H., Zuo, Y.Y., Zhang, X., 2013. Influence of cell properties on rheological characterization of microalgae suspensions. *Bioresour. Technol.* *139*, 209–213.
39. Zhang, Q., Qin, B.L., Barbosa-Cánovas, G.V., Swanson, B.G., 1995. Inactivation of *E. coli* for food pasteurization by high-strength pulsed electric fields. *J. Food Proc. Pres.* *19*, 103–118.

MANUSCRIPT 2 – UNPUBLISHED RESULTS

Advanced pulsed electric field system optimization based on thorough process characterization

Leandro Buchmann, Robin Bloch, Jsmea Hug, Alexander Mathys

ETH Zurich, Department of Health Sciences and Technology, Institute of Food, Nutrition and Health, IFNH, Sustainable Food Processing Laboratory, Schmelzbergstrasse 9, Zurich 8092, Switzerland

1. INTRODUCTION

Treatment homogeneity is a crucial element in order to apply PEF/nsPEF in a targeted way. Given the almost fully homogenous electric field distribution (Diaz, 2005) in parallel-plate treatment chambers, they appear the most suitable ones to reach this goal. Nonetheless, co-linear treatment chambers are currently the most used systems in lab and industrial applications. One of the discussed advantages of co-linear chambers is the suitability for cleaning in place, however, liquid processing units such as plate-plate heat exchangers prove that hygienic operation in non-circular tubes is feasible (Góngora-Nieto et al., 2002; Toepfl, 2006; Jeurink 1994). A further discussed disadvantage of parallel-plate treatment chambers is the low electrical resistance, resulting in high peak currents and failures within the electric circuit (Jaeger et al., 2009; Toepfl, 2006). However, the electrical resistance of a treatment chamber mainly depends on the chosen geometrical parameters and can be adjusted according to Eq. (1)

$$R = 1/\sigma \cdot d/A = \rho \cdot d/A \quad (2)$$

where σ is the media conductivity (S m^{-1}); d is the electrode distance (m); A is the electrode surface area (m^2) and ρ is the electrical resistivity (Ωm).

Furthermore, an additional load in parallel or series to the integrated treatment chamber could be used to achieve matched load conditions and thereby operate the system safely.

Therefore, the industrial standard was challenged based on the comprehensive PEF system analysis, focusing on a thorough PEF system optimization, allowing for targeted treatments on a first pilot-scale level.

2. MATERIALS AND METHODS

2.1. Numerical simulations

COMSOL multiphysics® software (version 5.3a, Comsol Inc., Burlington MA, USA) was used to conduct multiphysics simulations of the flow field in PEF treatment chambers. The simulations for parallel plate treatment chambers were conducted using a 3D model. The geometry of a co-linear treatment cell was simulated using a 2D axisymmetric approach.

The Reynolds numbers for the lab-scale geometries investigated in this work were all well below the critical Reynolds value of 2300. For the system optimization, Reynolds numbers up to 4000 were reached. Depending on the expected flow regime, a laminar or turbulent flow model was chosen. Within this study, the turbulent *algebraic yPlus* model was used with the respective governing equations. Despite reduced accuracy close to the wall, the robust model results in a good approximation for internal flow and is less computationally expensive (Frei, 2019).

Boundary conditions for the fluid properties, i.e., the fluid density and the dynamic viscosity, were defined for every simulation. The density was set to the density of water for all simulations ($\rho = 1000 \text{ kg m}^{-3}$). The standard dynamic viscosity of water as deposited in the software was used ($\mu = 0.001 \text{ Pa s}$), to simulate the flow of water. The flow behavior of model suspensions was measured in rheological trials as described in Buchmann et al, (2018). The same viscosity functions were integrated as a model system into the optimization simulations. The presented work only considered stationary solutions of the simulation, which are sufficient to describe the situation present in most PEF research applications. Further effects of temperature on media parameters were neglected due to the low energy inputs.

2.2. Model systems for PEF system optimization

Based on the flow behavior characterization from Buchmann et al, (2018), three model systems were evaluated for strategies aiming at a more homogeneous energy input distribution within PEF/nsPEF processes. The optimization focused on the growth and/or cellular compound stimulation as shown by literature and a parallel scale-up approach thereof (Buchmann et al., 2019; Buchmann and Mathys, 2019; Haberkorn et al., 2019). Based on the equipment available at ETH Zürich, the maximum electrode distance was fixed at 10 mm due to the required electric field strength of 10 kV cm^{-1} .

M2U - Table 1: Evaluated parameters for nsPEF system optimization focused on growth stimulation according to Buchmann et al., (2019), with reference *Arthrospira platensis* concentrations of 0, 5 and 25 g L⁻¹ as a model system according to Buchmann et al., (2018). Different scale-up scenarios were analyzed for a throughput of around ≥ 100 L h⁻¹. In addition, a Reference treatment chamber was analyzed in order to have a direct comparison to the results obtained from Buchmann et al., (2018b).

	reference	0 g L ⁻¹	5 g L ⁻¹	25 g L ⁻¹
Treatment chamber				
Chamber diameter [mm]	4	5	5	10
Chamber length [mm]	28	28	28	28
Process parameter				
Inlet velocity [m s ⁻¹]	1	1.2	1.2	0.3
Average residence time [s]	0.028	0.023	0.023	0.093
Pulse repetition frequency [Hz]	107	88	88	22
Pulse number [-]	3	2.05	2.05	2.05
Pulse duration [ns]	1000	100	100	100
Applied Voltage [V]	1000	5115	5115	10230
Electric field strength [kV cm ⁻¹]	2.5	10.23	10.23	10.23
Energy input [J kg ⁻¹]	75	256	256	256
System parameter				
Flow regime [-]	turbulent	turbulent	turbulent	laminar
Throughput [L h ⁻¹]	57.6	108	108	108

2.3. Results evaluation

The optimization approach was validated based on a horizontal 3D cut line in the middle of the treatment chamber's height. Evaluation of the system's homogeneity was conducted by analyzing the specific energy input in percentage across 80% ($\Delta W_{spec,80}$ (%)) of the treatment chamber according to Eq. (1):

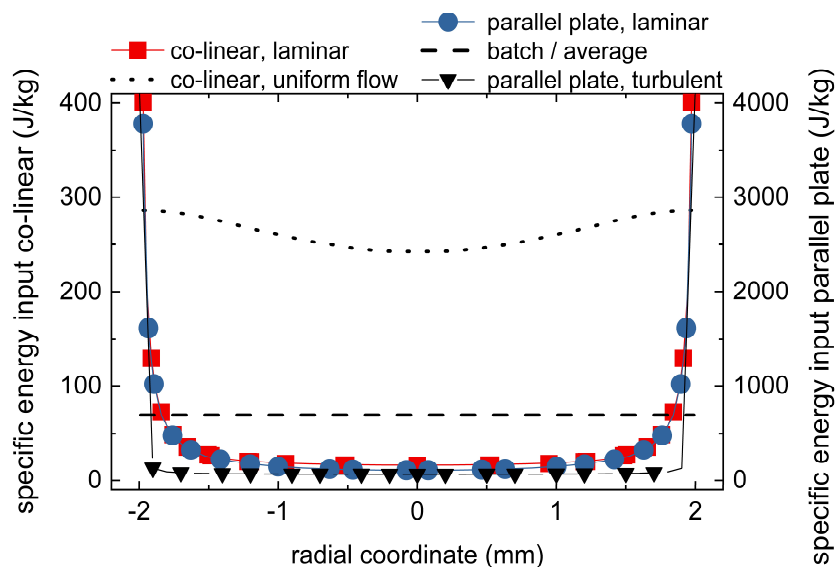
$$\Delta W_{spec,80} = W_{spec}(0.8r) / W_{spec}(0r) \quad (1)$$

with $\Delta W_{spec}(0.8r)$ (J kg⁻¹) being the specific energy input at 80 % of the radial coordinate and $\Delta W_{spec}(0r)$ (J kg⁻¹) the specific energy input on the chamber's centerline.

3. RESULTS AND DISCUSSION

Based on the results of Buchmann et al. (2018), the optimized co-linear and non-optimized parallel-plate treatment chamber are not suitable for homogeneous energy inputs. The specific energy input deviation over 80% of the radial coordinate was 96.27% for the optimized co-linear chamber and 173.28% for the non-optimized parallel plate treatment chamber.

The investigation of the optimized co-linear treatment chamber, considering uniform flow with respect to the $\Delta W_{spec,80}$, allowed for an evaluation of the electric field inhomogeneity within the optimized system ((Meneses et al. (2011)). The relative deviation across 80% of the chamber thereby corresponded to 15.75% (Fig. 1). The electric field inhomogeneity in a co-linear system is thus similar to the total deviation, considering electric and flow field inhomogeneity, in a parallel-plate treatment chamber assuming turbulent flow ($\Delta W_{spec,80} = 15.87\%$) (Fig. 1; Table 1). Given that in the parallel-plate system a uniform electric field is present, the deviation within the system derives mostly from the flow field distribution. Hence, the treatment homogeneity in the co-linear system appears to be inferior to the parallel-plate system, as electric and flow field inhomogeneity sum up to the total treatment inhomogeneity. Thus, the co-linear treatment chamber was not considered in the approach to developing a treatment chamber suitable for homogeneous and specific PEF treatments on a pilot-scale level.



M2U - Figure 1: Distribution of the specific energy input across parallel-plate and co-linear treatment chambers, all with a diameter of 4 mm. The reference simulation (parallel-plate turbulent) is thereby compared to previous simulations conducted by Buchmann et al. (2018). In all simulations, the viscosity of water (0.001 Pas) was assumed and electric potential, pulse width, pulse repetition rate, medium conductivity were kept constant. Corresponding values are listed in Table 1, column reference.

The treatment chamber optimization was conducted for a system suitable for treating a 300 L cultivation system with the protocol for growth stimulation established by Buchmann et al (2019). Therefore, the throughput of the whole system needed to be $\geq 100 \text{ L h}^{-1}$ and was set to 108 L h^{-1} (Table 1). Thereby, low viscous fluids, in our case microalgae concentration up to 5 g L^{-1} achieved Reynolds numbers beyond the critical Reynolds number of 2300. High viscous fluids, however, resulted in a laminar flow profile. Based on the comprehensive system analysis, two strategies are proposed in order to increase treatment homogeneity on the tested scale.

In the case of low viscous fluids, achieving a stable turbulent flow must be the aim. High viscous fluids, however, show a quite homogeneous flow profile in the laminar case. Thus increasing the chamber diameter, allowing for a reduced flow velocity without compromising on the throughput, appeared to be a suitable approach. In all cases, the inlet had the same diameter as the treatment chamber in order to reduce high peak velocities in the chamber's center. Based on the increased inlet velocity and chamber diameter the $\Delta W_{spec,80}$ was reduced to 13.84%, 14,22% and 47,33% for a model system of 0 g L^{-1} , 5 g L^{-1} and 25 g L^{-1} respectively.

Based on the increased cell growth achieved in a system with deviations in the specific energy input of 173.28% (Buchmann et al, 2019), the optimization of the flow field and thus increased energy input homogeneity, bears the potential to further increase the efficiency of the growth stimulation process enabling an increased resource efficiency in bio-based applications.

4. CONCLUSIONS

PEF system optimization bears the potential to drastically increase the system's efficiency due to an increased treatment homogeneity. Based on the comprehensive PEF system analysis, the co-linear system was found to be inferior to a parallel-plate system. Thereby, optimization focused on the parallel-plate system were a treatment deviation of 13.84% across 80% of the chamber was found for water-like systems. Thus, the overall deviation in the parallel-plate system is lower compared to an optimized co-linear system's deviation in the electric field only (15.75%). Further improvements of the treatment homogeneity are possible with regard to mixing elements prior to the treatment chamber and/or structural modifications of the wall.

REFERENCES

1. Buchmann, L., Bloch, R., Mathys, A., 2018. Comprehensive pulsed electric field (PEF) system analysis for microalgae processing. *Bioresour. Technol.* 265, 268–274.
2. Buchmann, L., Frey, W., Gusbeth, C., Ravaynia, P.S., Mathys, A., 2019. Effect of nanosecond pulsed electric field treatment on cell proliferation of microalgae. *Bioresour. Technol.* 271, 402–408.
3. Buchmann, L., Mathys, A., 2019. Perspective on Pulsed Electric Field Treatment in the Bio-based Industry. *Front. Bioeng. Biotechnol.* 7, 265.
4. Diaz, R.E., 2005. Electrostatics. *Electr. Eng. Handb.* 499–512.
5. Frei, W. (2019). COMSOL Blog - Which Turbulence Model Should I Choose for My CFD Application?. <https://www.comsol.com/blogs/which-turbulence-model-should-choose-cfd-application>, accessed on 2019-05-19.
6. Góngora-Nieto, M.M., Sepúlveda, D.R., Pedrow, P., Barbosa-Cánovas, G. V., Swanson, B.G., 2002. Food processing by pulsed electric fields: Treatment delivery, inactivation level, and regulatory aspects. *LWT - Food Sci. Technol.* 35, 375–388.
7. Haberkorn, I., Buchmann, L., Hiestand, M., Mathys, A., 2019. Continuous nanosecond pulsed electric field treatments foster the upstream performance of *Chlorella vulgaris*-based biorefinery concepts. *Bioresour. Technol.* 293, 122029.
8. Jaeger, H., Meneses, N., Knorr, D., 2009. Impact of PEF treatment inhomogeneity such as electric field distribution, flow characteristics and temperature effects on the inactivation of *E. coli* and milk alkaline phosphatase. *Innov. Food Sci. Emerg. Technol.* 10, 470–480.
9. Jeurnink, T.J.M., Brinkman, D.W., 1994. The cleaning of heat exchangers and evaporators after processing milk or whey. *Int. Dairy J.* 4, 347–368.
10. Meneses, N., Jaeger, H., Moritz, J., Knorr, D., 2011. Impact of insulator shape, flow rate and electrical parameters on inactivation of *E. coli* using a continuous co-linear PEF system. *Innov. Food Sci. Emerg. Technol.* 12, 6–12.
11. Toepfl, S., 2006. Pulsed Electric Fields (PEF) for Permeabilization of Cell Membranes in Food- and Bioprocessing. Applications, Process and Equipment Design and Cost Analysis. Ph.D. thesis, Technol. Univ. Berlin.

MANUSCRIPT 3

Effect of nanosecond pulsed electric field treatment on cell proliferation of Microalgae

Leandro Buchmann^a, Wolfgang Frey^b, Christian Gusbeth^b, Paolo S. Ravaynia^c,
Alexander Mathys^{a,*}

^a *ETH Zurich, Department of Health Sciences and Technology, Institute of Food, Nutrition and Health, IFNH, Sustainable Food Processing Laboratory, Schmelzbergstrasse 9, Zurich 8092, Switzerland*

^b *Karlsruhe Institute of Technology, KIT, Institute for Pulsed Power and Microwave Technology, IHM, Hermann-von-Helmholtz-Platz 1, Eggenstein-Leopoldshafen 76344, Germany*

^c *ETH Zurich, Department of Biosystems Science and Engineering, Bio Engineering Laboratory, Mattenstrasse 26, Basel 4058, Switzerland*

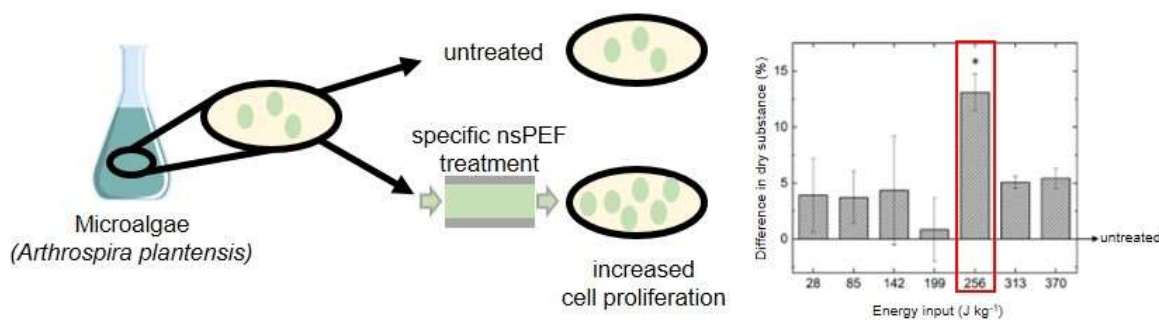
**Corresponding author*

Bioresource Technology 271 (2019) 402–408

ABSTRACT

Photoautotrophic microalgae based biorefinery concepts are currently not competitive compared to other established production systems. Therefore, innovative upstream processes need to be developed to increase the competitiveness of photoautotrophic microalgae biorefinery concepts. Abiotic sub-lethal stress induction via nanosecond pulsed electric field (nsPEF) treatment might be a viable process to increase the efficiency of photoautotrophic microalgae cultivation. In this work, an increased cell growth after nsPEF treatment was observable. Application of nsPEF to highly proliferating cells in a repetitive process resulted in a statistical significant increase in cell growth ($p = 0.009$). The effect was most pronounced after five days wherefore cellular structures and processes were analyzed to reveal a possible mechanism. Within this work, a protocol for increased cell proliferation with a possible mechanism was derived, which improves competitiveness of photoautotrophic microalgae biorefineries in the future. However, based on the derived mechanism, the results are also relevant for other microorganisms.

GRAPHICAL ABSTRACT



1. INTRODUCTION

The constant growth of human population causes new challenges regarding energy supply, food security, human health and biodiversity. Agriculture causes 30% of global greenhouse gas emission and 85% of the water footprint (Smetana et al., 2015). Biorefinery concepts, implementation of innovative technologies as well as a shift from animal toward more plant-based foods are possible solutions to tackle those challenges (Chaudhary et al., 2018). In this context, the exploitation of microalgae have become a field of great interest (Golberg et al., 2016; Rocha et al., 2018). They can serve as raw material for biofuels or agricultural biostimulants but at the same time are a promising source for food and feed production due to their high proportion of proteins and micronutrients (Colla et al., 2007). Besides these, microalgae can be cultivated on non-arable land and fixate CO₂ if cultivated photoautotrophically (Jacob-lobes et al., 2018). However, the cultivation of photoautotrophic microalgae is currently not competitive in comparison to many other plant sources (Smetana et al., 2017). High production costs resulting from the growth medium, energy supply and extraction of valuable compounds demands further improvement in the up- and down-stream processing of microalgae (Golberg et al., 2016).

Nanosecond pulsed electric fields (nsPEF) are a promising technology to increase the viability of microalgae cultivation systems. Among the possible applications of nsPEF are sub-lethal stress induction as well as targeted microbial flora control (Buchmann et al., 2018b; Buescher and Schoenbach, 2003; Eing et al., 2009). In nsPEF applications on eukaryotic cells, an increased growth was observable after the treatment (Eing et al., 2009; Gusbeth et al., 2013).

The underlying theory assumes an abiotic stress induction on a subcellular level. Based on mathematical models an increased electropermeabilization effect on intracellular structures compared to the cell membrane was observed for angular frequencies ω (rad s⁻¹) above 10⁷ (Kotnik and Miklavčič, 2006; Vernier et al., 2006). The double-shell model of a biological cell and its resulting reference circuit supports this theoretical analysis (Schoenbach et al., 2004). Hence, nsPEF treatments affect sub-cellular compartments. This aspect results from the charging time constant of the plasma membrane (Vernier et al., 2006). The charging time constant is dependent on the conductive (intra- and extracellular fluids) and the dielectric (cell membrane) properties of a cell in an electric reference circuit (Vernier et al., 2006). A pulse

duration below the charging time constant will result in an electric field conveyed through the intracellular space (Schoenbach et al., 2004). In addition, intracellular effects are most pronounced in proliferating cells compared to stationary phase cells (Schoenbach et al., 1997).

Induced intracellular effects could be Ca^{2+} release from internal storages, formation of radical oxygen species and release of cytochrome c from mitochondria among others (Batista Napotnik et al., 2016; Schoenbach et al., 2007).

The induced effects are confirmed by numerical simulation in which nsPEF increased the number of minimum size pores compared to conventional PEF (Gowrishankar et al., 2006). Hence, nsPEF treatments enable the transport of primarily small molecules across the membrane by either direct transport or voltage gating of channels (Casciola and Tarek, 2016; Stewart et al., 2004).

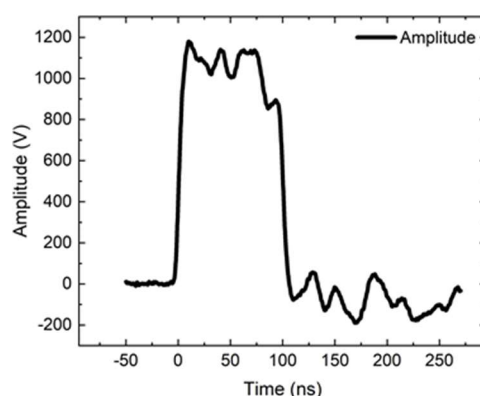
However, the fundamental process characteristic to induce intracellular electro effects is not yet understood. The influence of pulse repetition frequency (PRF), ionic strength of the medium and cell composition are currently investigated. Silve et al. (2014) introduced the concept of electro-desensitization, where an increased PRF results in reduced electroporation effects. This principle is based on different dynamics of membrane resealing (Lamberti et al., 2015). A study from Sridhara and Joshi (2014) focused on the influence of external medium conductivity and found that high ionic strengths in the medium locally increase the electroporation process, resulting in much faster pore formation. Napotnik et al. (2012), could further demonstrate that nsPEF lead to an increase in the inner mitochondrial membrane permeability.

The lipid composition between the inner mitochondrial membrane and the prokaryotic membrane was shown to be similar (Fontanesi, 2015). Hence, the concept of electropulsation, oxidation of membrane phospholipids, could play an important role in the underlying mechanisms of pulsed electric field application (Breton and Mir, 2018). Therefore, the effects of nsPEF on mitochondrial structures might be transferrable to prokaryotic cells, and vice versa with regard to the endosymbiotic theory. However, the exploitation of nsPEF induced effects on prokaryotic cells is a new area of research.

2. MATERIAL AND METHODS

2.1. Nanosecond pulsed electric field (nsPEF) treatment

The nsPEF treatments were executed in triplicates using a Blumlein generator (manufactured at the Karlsruhe Institute of Technology (KIT), Germany), for further information refer to Kolb et al. (2006). The cable length of 20,8 m resulted in a rectangular pulse with a pulse duration of 100 ns. A metal oxide semiconductor field-effect transistor (MOSFET) switch (manufactured at the Karlsruhe Institute of Technology (KIT), Germany) was connected to the Blumlein and triggered with a frequency generator (YOKOGAWA FG 300, Yokogawa, Musashino, Japan). The system was charged to 1 kV by incorporating a high voltage power supply (Model 205A-05R, Spellmann High Voltage Electronics Ltd., Pulborough, UK) (Fig. 1).



M3 - Figure 1: Reference 100 ns pulse as applied in the experiments.

The resulting electric field strength E (kV cm^{-1}) was 10 kV cm^{-1} as experiments were conducted using a plate-plate 1 mm polycarbonate treatment chamber (manufactured at the Karlsruhe Institute of Technology (KIT), Germany), for further information regarding the experimental setup refer to Goettel et al. (2013). The pulse duration and electric field were kept constant due to experience from previous studies (Eing et al., 2009) and processing capabilities. The microalgae suspension was pumped through polypropylene-based tubes (SC0319A, Cole-Parmer GmbH, Wertheim, Germany) connected to the treatment chamber. A peristaltic pump (MS-4/12-100 ISMATEC®, Cole-Parmer GmbH, Wertheim, Germany) was used at 15 rpm to pump the suspension through the treatment chamber. The electrical efficiency of the process is around 90% and higher, in dependence of the treatment homogeneity

(Buchmann et al., 2018a,b). In order to achieve matched load conditions the plate treatment chamber was adjusted to the conductivity σ (mS cm⁻¹) of the microalgae suspensions. The relation between conductivity and impedance can be derived from Eq. (1), with the total impedance Z_{tot} (Ω) equal to the fraction of the inverse resistance, with the conductivity σ (mS cm⁻¹), electrode surface area A (m²) and electrode distance d (m), added by the system's admittance Y_c (S).

$$Z_{tot} = 1/(\sigma \cdot A/d + Y_c) \quad (1)$$

The specific energy input W_s (J kg⁻¹) can be calculated according to Eq. (2), with the electric field E (kV cm⁻¹), pulse width τ_p (ns), conductivity σ (mS cm⁻¹), and pulse number n (-).

$$W_s = E^2 \cdot \tau_p \cdot \sigma \cdot n \quad (2)$$

The pulse number can be derived from Eq. (3), with the frequency f (Hz) and the residence time t (s), which itself can be expressed as the treatment chamber's volume V_0 (m³) divided by the volumetric flow rate V (m³ s⁻¹).

$$n = f \cdot t = f \cdot V_0/\dot{V} \quad (3)$$

Further information on these theoretical backgrounds could be found elsewhere (Buchmann et al., 2018a,b; Pirc et al., 2017; Reberšek et al., 2014). Based on an in-depth nsPEF system characterization (Buchmann et al., 2018a,b), the specific energy input could be calculated for all experiments.

2.2. *Arthrospira platensis* cultures

The strain *Arthrospira platensis* SAG 21.99 was cultivated in a modified Zarrouk medium (Aiba and Ogawa, 1977). The cultures were incubated at 25 ± 0.2 °C, 70% relative humidity, 150 rpm, ambient CO₂, and continuous illumination with a mean photosynthetically active

photon flux density (PPFD) of 32 $\mu\text{mol photons m}^{-2} \text{s}^{-1}$ using warm white LED lamps in a shaking incubator (Multitron Pro shaking incubator, Infors AG, Bottmingen, Switzerland). The growth of *A. platensis* was monitored by OD measurements at 750 nm.

Prior and after every experiment, the conductivity and pH of the *A. platensis* suspensions were measured using a Seven compact conductivity meter (Mettler-

Toledo International Inc., Columbus OH, USA) and pH meter (827 pH lab, Metrohm, Herisau, Switzerland) that was connected to a primatrode (Metrohm, Herisau, Switzerland), respectively.

2.3. Microalgae growth and pigment assessment

Assessing microalgae growth was done by gravimetical determination of the dry substance (DS) (g L^{-1}) using an analytical balance (LA 214i, VWR, Leuven, Belgium). The gravimetical analysis was conducted after microalgae harvesting by use of a vacuum filtration system (SciLabware Ltd., Staffordshire, UK). Glass microfiber filters with a pore size of $1.2 \mu\text{m}$ (GF/C, GE Healthcare, Chicago IL, USA), were used to collect the dry substance. Based on the gravimetical analysis a conversion factor to the optical density (OD) at 750 nm was determined. OD measurements were conducted in triplicates with a UV/VIS spectrophotometer (Cary 100, Agilent Technologies, Santa Clara CA, USA).

The conversion of OD to DS was conducted in accordance with Eq. (4)

$$DS = 0.689 \pm 0.039 \cdot OD_{750} \quad (4)$$

where the conversion factor (0.689 ± 0.039) was obtained empirically. The C-phycoerythrin (cPC) and allophycocyanin (aPC) content of the *A. platensis* suspensions was assessed by correcting the measured absorption values with the absorption at 750 nm. Based on Yoshikawa and Belay, (2008) aPC and cPC concentrations (g L^{-1}) could be determined according to Eqs. (5) and (6):

$$aPC = 0.180 \cdot A_{650} - 0.042 \cdot A_{620} \quad (5)$$

$$cPC = 0.162 \cdot A_{620} - 0.098 \cdot A_{650} \quad (6)$$

An independent T-test at a confidence interval of either 95% or 99% was used to assess statistical significance of the results. The results were obtained using the software IBM SPSS Statistics (IBM Corp., Armonk NY, USA).

2.4. Single cell electrical impedance spectroscopy

Impedance measurements of microalgae cells were conducted using a custom-made electrical impedance spectroscopy (EIS) platform for single cell analysis. The platform is composed of a microfluidic chip made of polydimethylsiloxane (PDMS) and bonded to a glass substrate with patterned platinum electrodes. The PDMS chip

consists of an inlet and outlet connected by a 3 mm straight channel of $300 \cdot 50 \mu\text{m}^2$ (width \cdot height) dimensions. The channel features a constriction at the center with $50 \mu\text{m}$ width and height. The 150 nm thick platinum electrodes are deposited on a glass substrate patterned via a lift-off process. A pair of coplanar electrodes of $150 \mu\text{m}$ width and spacing between the electrodes is aligned within the channel's constriction to enable EIS measurements of single flowing cells. The solution was injected with a flow rate of $2.5 \mu\text{L min}^{-1}$ using a syringe pump (Pump 11 Elite, Harvard Apparatus, Holliston MA, USA) connected to the inlet port. The chip was contacted via a custom-made printed circuit board (PCB) to route the connections from the impedance spectroscopy to the electrodes. Impedance measurements were performed using a HF2-LI impedance spectroscopy (Zurich Instruments AG, Zurich, Switzerland). EIS measurements were taken at six frequencies logarithmically spaced between 100 kHz and 10 MHz . An AC voltage of 300 mV at each selected frequency was applied between the coplanar electrodes. The current flowing through the system was then converted to voltage through a trans-impedance amplifier with $1 \text{ k}\Omega$ feedback resistor and sampled by the HF2-LI with a sampling frequency of 225 Hz . The signal was post processed in Matlab (MATLAB 2016b, The Mathworks Inc., Natick MA, USA). The passage of each microalgae cell induces a transient reduction of the voltage-converted current between the electrodes pair resulting in a peak. The transient peak height was extracted by measuring the local peak-to-baseline value for all simultaneously recorded frequencies. Untreated as well as nsPEF treated *A. platensis* cells were analyzed. More than 100 cells per condition were analyzed to provide significant statistics for measuring the average peak-to-baseline signal variations caused by the passage of the cells over the electrodes. All measurements were carried out in the same modified Zarrouk medium (Aiba and Ogawa, 1977) to avoid signal differences caused by different medium conductivity.

2.5. Proteomic analysis

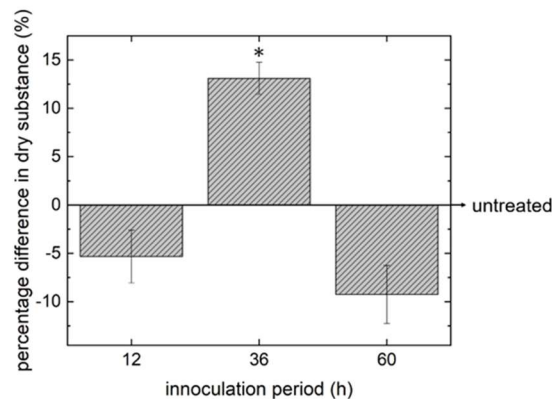
A shotgun analysis liquid chromatography and mass spectrometry (LC-MS) was conducted at the Functional Genomics Center Zurich (FGCZ), Switzerland. Protein/peptide identification and characterization was performed using liquid chromatography-electrospray ionization- tandem mass spectrometry (LC/ESI/MS/MS). Sample preparation was conducted by precipitation and proteolytic digestion. The nsPEF treated *A. platensis* cells were harvested and the pellet was

resuspended (10 g L^{-1}) in a 1:5 diluted solution I of the Zarrouk medium (Aiba and Ogawa, 1977). In a next step trichloroacetic acid (TCA, Sigma-Aldrich, St. Louis MO, USA) precipitation was conducted using $10 \mu\text{L}$ of sample with $90 \mu\text{L}$ of water and $100 \mu\text{L}$ 20% TCA. The sample was washed twice with cold acetone. The dried pellets were afterwards dissolved in $45 \mu\text{L}$ buffer (10mM Tris + 2mM CaCl_2 at pH 8.2) and $5 \mu\text{L}$ trypsin ($100 \text{ ng } \mu\text{L}^{-1}$ in 10mM HCl) for digestion, which was carried out in a microwave instrument (Discover System, CEM, Matthews NC, USA) for 30 min at 5W and $60 \text{ }^\circ\text{C}$. Subsequent samples were dried in a Savant SpeedVac (Thermo Fisher Scientific, Waltham MA, USA). For LC-MS/MS analysis the samples were dissolved in 0.1% formic acid (Romil Ltd., Cambridge, UK) and an aliquot of 4% was analyzed on a nanoAcquity UPLC (Waters Inc., Milford MA, USA) connected to a Q Exactive mass spectrometer (Thermo Fisher Scientific, Waltham MA, USA) equipped with a Digital PicoView source (New Objective, Woburn MA, USA). Peptides were trapped on a Symmetry C18 trap column ($5 \mu\text{m}$, $180 \mu\text{m} \cdot 20 \text{ mm}$, Waters Inc., Milford MA, USA) and separated on a BEH300 C18 column ($1.7 \mu\text{m}$, $75 \mu\text{m} \cdot 150 \text{ m}$, Waters Inc., Milford MA, USA) at a flow rate of 250 nl min^{-1} using a gradient from 1% solvent B (0.1% formic acid in acetonitrile, Romil Ltd., Cambridge, UK) / 99% solvent A (0.1% formic acid in water, Romil Ltd., Cambridge, UK) to 40% solvent B/60% solvent A within 90 min. Mass spectrometer settings were: Data dependent analysis. Precursor scan range $350\text{--}1500\text{mz}^{-1}$, resolution 70'000, maximum injection time 100 ms, threshold 3e^6 . Fragment ion scan range $200\text{--}2000\text{mz}^{-1}$, resolution 35'000, maximum injection time 120 ms, threshold 1e^5 . Proteins were identified using the Mascot search engine (version 2.5.1.3, Matrix Science, Boston MA, USA). Mascot was set up to search the SwissProt and the Trembl (bacteria only) database assuming the digestion enzyme trypsin. Mascot was searched with a fragment ion mass tolerance of 0.030 Da and a parent ion tolerance of 10.0 ppm. Oxidation of methionine was specified in Mascot as a variable modification. Scaffold (Proteome Software Inc., Portland OR, USA) was used to validate MS/MS based peptide and protein identifications. Peptide identifications were accepted if they achieved a false discovery rate (FDR) of less than 0.1% by the Scaffold Local FDR algorithm. Protein identifications were accepted if they achieved an FDR of less than 1.0% and contained at least 2 identified peptides. Subsequent results are based on the Trembl (bacteria) search. The database contains around 80 million different proteins and a fully sequenced *A. platensis* strain with 6630 open reading frames (NIES-39, National Institute of Technology and

Evaluation, Tokyo, Japan). The data was analyzed applying very stringent settings, (protein threshold 99%, min # peptides 2 and peptide threshold 95%). Statistical analysis was conducted by a T-test with normalization, on a 99% confidence interval.

3. RESULTS AND DISCUSSION

According to the theory of an increased nsPEF effect on fast proliferating cells (Schoenbach et al., 1997), the influence of cell growth stage on the increased cell proliferation was investigated. Based on literature data different inoculation intervals were analyzed. The effect of nsPEF treatments after 12, 36 and 60 h of inoculation was assessed (Fig. 2).



M3 - Figure 2: Percentage difference in dry substance five days after the nsPEF treatment between treated and untreated *Arthrospira platensis* solutions with varying time intervals between inoculation and nsPEF treatment. The illustrated results were obtained for an energy input of $3 \cdot 256.22 \pm 67.53 \text{ J kg}^{-1}$ as shown in Table 1 and the experimental procedure stated in Section 2.1.

The obtained results (Fig. 2) correspond with the theory where an increased effect was expected on highly proliferating cells (Schoenbach et al., 1997). Therefore, experiments were conducted within the exponential phase using a time interval of 36 h between inoculation and nsPEF treatment.

Based on the concept of electrosensitization (Pakhomova et al., 2011), the nsPEF treatment was applied repetitively. A single treatment did not result in a statistical significant effect and neither did a single repetition of the treatment. The increased cell proliferation was observable if the treatment was repeated three times as described in the methods Section 2.1. In-between the single nsPEF treatment was a time interval of three hours.

Based on the obtained results, the assessment of the influence of treatment energy on the cell proliferation was examined after 36 h and after three subsequent nsPEF treatments. We found that nsPEF treatments lead to an increase in DS in *A. platensis* suspensions. The various analyzed energy inputs were achieved by increasing the PRF while maintaining all other pulse parameters (Table 1).

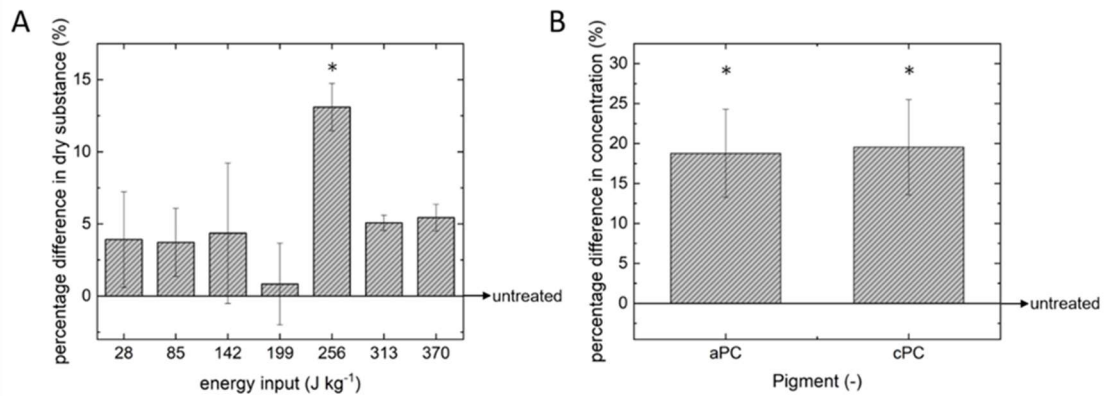
M3 - Table 1: Experimental parameters used in the analyzed nsPEF treatments. With electric field strength E (kV cm^{-1}), pulse duration τ_p (ns), conductivity σ (mS cm^{-1}), frequency f (s^{-1}), residence time t (s), number of applied pulses n (-), and specific energy input W_s (J kg^{-1}). The specific energy input is stated for a single treatment.

E	τ_p	σ	f	t	n	W_s
(kV cm^{-1})	(ns)	(mS cm^{-1})	(s^{-1})	(s)	(-)	(J kg^{-1})
10.23 ± 0.0050	100	11.93 ± 0.98	1.00	0.23 ± 0.06	0.23 ± 0.06	28.40 ± 7.49
10.23 ± 0.0050	100	11.95 ± 1.01	3.00	0.23 ± 0.06	0.68 ± 0.18	85.34 ± 22.49
10.23 ± 0.0050	100	11.95 ± 1.01	5.00	0.23 ± 0.06	1.14 ± 0.30	142.23 ± 37.49
10.23 ± 0.0050	100	11.97 ± 1.03	7.00	0.23 ± 0.06	1.59 ± 0.42	199.45 ± 52.57
10.23 ± 0.0050	100	11.96 ± 1.02	9.00	0.23 ± 0.06	2.05 ± 0.54	256.22 ± 67.53
10.23 ± 0.0050	100	11.96 ± 1.05	11.00	0.23 ± 0.06	2.50 ± 0.66	313.16 ± 82.54
10.23 ± 0.0050	100	11.96 ± 1.05	13.00	0.23 ± 0.06	2.96 ± 0.78	370.10 ± 97.55

Based on findings from Buchmann et al. (2018a), varying only the PRF ensured an reproducible nsPEF treatment. Furthermore allowed this alteration of the system to analyze the effects of PRF and energy input on the obtained results.

A PRF of 9 Hz resulting in an energy input of $256.22 \pm 67.53 \text{ J kg}^{-1}$ was found to be most effective (Fig. 3A) ($p = 0.009$). The increase in DS was $13.1 \pm 1.6 \%$. The other tested energy inputs did not increase cell proliferation significantly ($p > 0.05$). The treatment energy is always stated for an individual replication of the nsPEF treatment (Fig. 3A). The energy input in-between experiments did not vary significantly, as no influence on external medium conductivity was detectable.

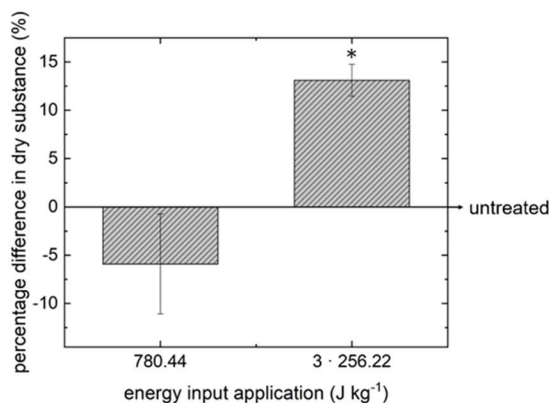
With regard to aPC and cPC, an even increased difference between treated and untreated samples was found (Fig. 3B). The increase was $18.8 \pm 5.5 \%$ and $19.5 \pm 6 \%$ for aPC and cPC, respectively. The observation was in accordance with the overall results. Energy inputs resulting in a non-significant cell proliferation increase did also not affect phycocyanin concentrations significantly.



M3 - Figure 3: Percentage difference in dry substance A) between treated and untreated *Arthrospira platensis* solutions after 5 days of cultivation. The stated energy input is only depending on the pulse repetition frequency and represents a single treatment (Table 1), which was repeated three times, with time intervals of three hours. The allophycocyanin (aPC) and C-phycoyanin (cPC) concentration difference on the fifth day for $256.22 \pm 67.53 \text{ J kg}^{-1}$ is shown in B).

Based on the experimental procedure the effect of PRF and energy input on the nsPEF induced effect was studied. The obtained results indicate that the effect of nsPEF on the cell proliferation of *A. platensis* is primary energy dependent. Alternatively, an increased cell proliferation would have to be observed with PRFs of 11 and 13 Hz (Table 1). As illustrated in Fig. 3A, this dependency on PRF was not detectable.

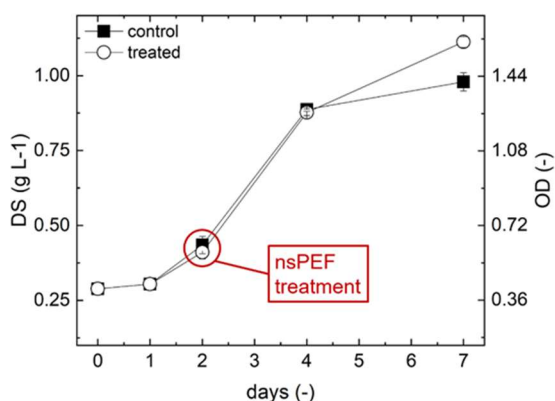
However, regarding the importance of the repetitive nsPEF application the concept of electrosensitization (Pakhomova et al., 2011) appears to be valid for nsPEF induced effects on cell proliferation. This concept was further tested by applying the energy input equal to a repetitive experiment in one single experiment. These experiments resulted in a significant difference in DS ($p = 0.000003$) if the energy was applied in a single, compared to a repetitive treatment (Fig. 4). Hence, the repetitive abiotic stress induction appears to be critical for increased cell proliferation due to nsPEF. However, even the application of the whole energy input did not statistically significant reduce the DS of *A. platensis* ($p > 0.05$). Further studies should focus on the optimized treatment repetition/ frequency to use the full potential of nsPEF treatments based on the concept of electrosensitization.



M3 - Figure 4: Percentage difference in dry substance after application of the same energy input by single treatment ($780.44 \pm 206.74 \text{ J kg}^{-1}$) compared to three uniform treatments ($3 \cdot 256.22 \pm 67.53 \text{ J kg}^{-1}$) performed as in Section 2.1. The single energy application was achieved by a reduction of the residence time t (s), while keeping all other parameters constant (Table 1).

3.1. Analysis of nsPEF treatment mechanisms

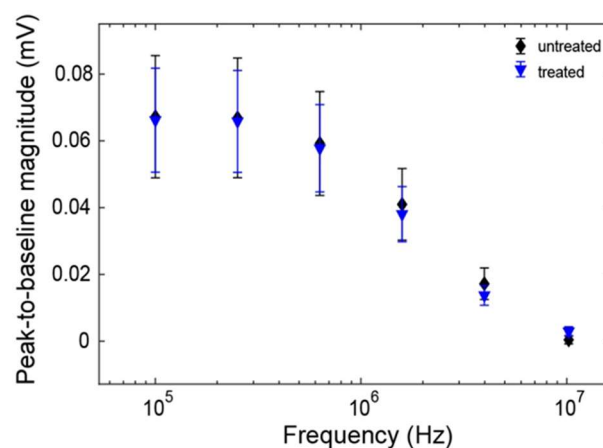
Prior and after every experiment, the conductivity of the *A. platensis* cultures was measured. There was no significant difference detectable between treated and untreated cultures. In addition, no cell swelling was observable for the *A. platensis* cells during the experimental period. Moreover, there was no difference in the pH of *A. platensis* solutions detectable. Concisely, short-term electroporation effects were not detectable by these analytical methods. However, as already described by Bai et al. (2017), the effect of nsPEF was most pronounced 5 days after the nsPEF treatment (Fig. 5).



M3 - Figure 5: Growth monitoring of *Arthrospira platensis* culture during experimental procedure, by measuring DS and OD measurement at 750 nm.

Detectable changes after 5 days let to the hypothesis that cellular structures/

processes were altered by the nsPEF treatment. Therefore, the cellular structure was analyzed after 5 days using a non-invasive technique, such as EIS. Impedance cytometers, realized by integrating a set of electrodes within a microfluidic channel, have been used for multi-parametric assessments across different frequencies for differentiation of single cells, based on cell size, membrane integrity and internal properties of cells (Sun and Morgan, 2010). Impedance characterization at low frequencies (< 1 MHz) provides information on cell volume/ size due to the non-conducting cell membrane barrier, while intermediate frequencies (0.5–10 MHz) are used to investigate membrane capacitance due to increases in capacitive coupling across the cell barrier (Cheung et al., 2005; McGrath et al., 2017). EIS can therefore be used to assess morphological variations of *A. platensis* after exposure to different treatments. The acquired EIS spectra did not show significant differences ($p > 0.05$) between treated and untreated cells in the tested frequency range (Fig. 6). EIS characterization therefore supports the hypothesis that nsPEF treatment does not induce morphological changes on a plasma membrane level. Hence, the applied rectangular 100 ns pulses seem to primarily affect the subcellular structures (Kotnik and Miklavčič, 2006). Given the similarity between mitochondrial cell membranes and prokaryotic cell membranes (Fontanesi, 2015), prokaryotes may allow for analysis of nsPEF induced subcellular effects. Thereby, the increased cell proliferation in prokaryotic cells might be transferable to eukaryotic cells.



M3 - Figure 6: Peak-to-baseline voltage amplitude of untreated and treated *Arthrospira platensis* cells measured between 100 kHz and 10 MHz.

This hypothesis was tested with a shotgun LC-MS analysis of the harvested biomass.

Thereby, 956 proteins were identified corresponding to 12'268 peptide spectra. Based on the database search as described in Section 2.5, two significant different proteins were determined. The first protein is the Na-Ca exchanger/integrin-beta4 OS=*Arthrospira* sp. PCC 8005 OX=376219 GN=ARTHRO_430061 PE=4 SV=1 (p=0.0069). The heterodimeric protein integrin is involved in transmembrane cell communication and regulation of cell behavior (Rédei, 2008). The protein is present in the cytoplasmic domain of Na-Ca exchangers and mediates the bi-directional transfer of signals (Schwarz and Benzer, 1997). Thereby, integrins have been attributed to growth promotion as they signal to guanine nucleotide-binding proteins (Harburger and Calderwood, 2009). The overexpression of these proteins correlates with the abiotic stress response of plants, which involves Ca^{2+} as an essential second messenger in the signaling pathway (Zhu, 2016).

The second overexpressed protein is the elongation factor Tu OS=*Halomonas daqingensis* OX=419596 GN=tuf PE=3 SV=1 (p=0.0073) belonging to the cluster of Elongation factor Tu OS=*Arthrospira platensis* (strain NIES-39/IAM M-135) OX=696747 GN=tuf PE=3 SV=1 (D4ZUX7_ARTPN). The cluster is assembled using protein cluster analysis based on shared evidence. The elongation factor (EF) TU binds aminoacyl-tRNA to the ribosomal acceptor site (Zvereva et al., 2001). Aminoacyl-tRNA is an amino acid-charged tRNA at the 3' end (Rédei, 2008). The prokaryotic EF-TU is a guanine nucleotide-binding Ras-like protein (Paduch et al., 2001; Wuichet and Søggaard-Andersen, 2014). The Ras superfamily are proto-oncogenes with various cellular functions, for example they are one of the most important turnstiles in signal transduction (Dong et al., 2007; Wuichet and Søggaard-Andersen, 2014).

The proteomics result correspond well with the observed macroscopic change in cell proliferation. Integrin signaling to a Ras-like protein is strongly related to increased cell proliferation. However, the proteomics results are only indicating a possible nsPEF induced abiotic stress response pathway, as the proteome was solely analyzed on the fifth day. Furthermore, there was no correction for multiple comparisons executed. Nevertheless, the results were obtained in triplicates and there are only two distinct proteins overexpressed with the applied boundary conditions.

Given that the observed effect is only detectable after 5 days might also correlate with the cell doubling time. With respect to Fig. 5, the doubling time is around three

days after the nsPEF treatment. Therefore, the cell number is quite low to detect significant differences from the beginning and need to increase, to recognize the macroscopic effect after 5 days.

The obtained results are in good agreement with literature. A repetitive nsPEF treatment led to increased effects, which corresponds well with the concept of electrosensitization (Pakhomova et al., 2011). Furthermore, the increase in cell proliferation was most pronounced in fast proliferating cells (Schoenbach et al., 1997). Moreover, the outer cellular structure of treated and untreated *A. platensis* did not change. This aspect might be surprising as prokaryotes and mitochondria are similar in cell membrane composition (Fontanesi, 2015) and therefore, subcellular effects in eukaryotes should theoretically be expressed on a cellular level in prokaryotes. However, focusing the effect of nsPEF in eukaryotes on mitochondrial changes might still be valid. Prokaryotes and mitochondria are not only similar in cell membrane composition but further in the aspect that both contain similar molecular weight

ribosomes (Amunts et al., 2015; Ban et al., 2014; Rédei, 2008). Therefore, nsPEF induced growth-promoting effects might be linked back to organellar ribosomes and Ca^{2+} signaling. The involvement of Ca^{2+} signaling pathways might be a reason for the improved effects of nsPEF on highly proliferating cells. It was shown for *Arabidopsis thaliana* that highly proliferating cells have an increased Ca^{2+} channel activity compared to mature cells (Very and Davies, 2000). Hence, the proposed mode of action might even be valid for nsPEF induced effects in *Arabidopsis thaliana* (Eing et al., 2009).

The obtained results indicate that Ca^{2+} could play a crucial role in the nsPEF induced upregulation of cell proliferation. Therefore, further research should be conducted with labelled Ca^{2+} to analyze flux as well as relocation of the cation. In addition, a monitoring of the changes occurring in the cell's proteome throughout the cultivation might reveal the underlying mode of action of nsPEF induced abiotic stress.

4. CONCLUSIONS

Photoautotrophic microalgae based biorefinery concepts are currently not competitive compared to other established production systems. However, nsPEF treatment led to an increased cell proliferation in prokaryotic *A. platensis*. The increase was detectable after repeated nsPEF treatment in the exponential growth phase. The effect was most pronounced five days after the treatment, and besides dry substance; an increase in pigments was detectable. Proteomic analysis revealed a possible stress response pathway. However, the role of specific cellular processes in an nsPEF induced growth stimulation needs to be further analyzed. Thereby, nsPEF treatments might enable sustainable and economical microalgae based biorefineries.

ACKNOWLEDGEMENTS

The authors gratefully acknowledge the World Food System Center (Project “NewAlgae”, grant number: 2-72235-17), the ETH Zürich Foundation, Switzerland, Prof. Dr. Erich J. Windhab, Daniel Kiechl and Bruno Pfister from the ETH Zürich Food Process Engineering Laboratory, as well as Dr. Peter Hunziker and Simone Wüthrich from the Functional Genomics Center Zurich for their support.

CONFLICT OF INTEREST STATEMENT

The authors declare no conflict of interest.

REFERENCES

1. Aiba, S., Ogawa, T., 1977. Assessment of growth yield of a blue-green alga, *Spirulina platensis*, in axenic and continuous culture. *J. Gen. Microbiol.* 102, 179–182.
2. Amunts, A., Brown, A., Toots, J., Scheres, S.H.W., Ramakrishnan, V., 2015. The structure of the human mitochondrial ribosome. *Science* 348, 95–98.
3. Bai, F., Gusbeth, C., Frey, W., Nick, P., 2017. Nanosecond pulsed electric fields trigger cell differentiation in *Chlamydomonas reinhardtii*. *Biochim. Biophys. Acta—Biomembr.* 1859, 651–661.
4. Ban, N., Beckmann, R., Cate, J.H.D., Dinman, J.D., Dragon, F., Ellis, S.R., Lafontaine, D.L.J., Lindahl, L., Liljas, A., Lipton, J.M., McAlear, M.A., Moore, P.B., Noller, H.F., Ortega, J., Panse, V.G., Ramakrishnan, V., Spahn, C.M.T., Steitz, T.A., Tchorzewski, M., Tollervey, D., Warren, A.J., Williamson, J.R., Wilson, D., Yonath, A., Yusupov, M., 2014. A new system for naming ribosomal proteins. *Curr. Opin. Struct. Biol.* 24, 165–169.
5. Batista Napotnik, T., Reberšek, M., Vernier, P.T., Mali, B., Miklavčič, D., 2016. Effects of high voltage nanosecond electric pulses on eukaryotic cells (in vitro): a systematic review. *Bioelectrochemistry* 110, 1–12.
6. Breton, M., Mir, L.M., 2018. Investigation of the chemical mechanisms involved in the electropulsation of membranes at the molecular level. *Bioelectrochemistry* 119, 76–83.
7. Buchmann, L., Bloch, R., Mathys, A., 2018a. Comprehensive pulsed electric field (PEF) system analysis for microalgae processing. *Bioresour. Technol.* 265, 268–274.
8. Buchmann, L., Böcker, L., Frey, W., Haberkorn, I., Nyffeler, M., Mathys, A., 2018b. Energy input assessment for nanosecond pulsed electric field processing and its application in a case study with *Chlorella vulgaris*. *Innov. Food Sci. Emerg. Technol.* 47, 445–453.
9. Buescher, E.S., Schoenbach, K.H., 2003. Effects of submicrosecond, high intensity pulsed electric fields on living cells - Intracellular electromanipulation. *IEEE Trans. Dielectr. Electr. Insul.* 10, 788–794.
10. Casciola, M., Tarek, M., 2016. A molecular insight into the electro-transfer of small molecules through electropores driven by electric fields. *Biochim. Biophys. Acta - Biomembr.* 1858, 2278–2289.
11. Chaudhary, A., Gustafson, D., Mathys, A., 2018. Multi-indicator sustainability assessment of global food systems. *Nat. Commun.* 9, 848.
12. Cheung, K., Gawad, S., Renaud, P., 2005. Impedance spectroscopy flow cytometry: On-chip label-free cell differentiation. *Cytom. Part A* 65, 124–132.
13. Colla, L.M., Oliveira Reinehr, C., Reichert, C., Costa, J.A.V., 2007. Production of biomass and nutraceutical compounds by *Spirulina platensis* under different temperature and nitrogen regimes. *Bioresour. Technol.* 98, 1489–1493.
14. Dong, J.H., Wen, J.F., Tian, H.F., 2007. Homologs of eukaryotic Ras superfamily proteins in prokaryotes and their novel phylogenetic correlation with their eukaryotic analogs. *Gene* 396, 116–124.
15. Eing, C., Bonnet, S., Pacher, M., Puchta, H., Frey, W., 2009. Effects of nanosecond pulsed electric field exposure on *Arabidopsis thaliana*. *Dielectr. Electr. Insul. IEEE Trans.* 16, 1322–1328.
16. Fontanesi, F., 2015. Mitochondria: Structure and Role in Respiration. eLS. John Wiley & Sons Ltd, Chichester, UK, pp. 1–13.
17. Goettel, M., Eing, C.J., Gusbeth, C., Straessner, R., Frey, W., 2013. Pulsed electric field assisted extraction of intracellular valuables from microalgae. *Algal Res.* 2, 401–408.
18. Golberg, A., Sack, M., Teissie, J., Pataro, G., Pliquett, U., Saulis, G., Stefan, T., Miklavčič, D., Vorobiev, E., Frey, W., 2016. Energy-efficient biomass processing with pulsed electric fields for bioeconomy and sustainable development. *Biotechnol. Biofuels* 9, 94.

19. Gowrishankar, T.R., Esser, A.T., Vasilkoski, Z., Smith, K.C., Weaver, J.C., 2006. Microdosimetry for conventional and supra-electroporation in cells with organelles. *Biochem. Biophys. Res. Commun.* 341, 1266–1276.
20. Gusbeth, C., Eing, C., Goettel, M., Frey, W., 2013. Boost of algae growth by ultra short pulsed electric field treatment. In: 2013 Abstracts IEEE International Conference on Plasma Science (ICOPS), pp. 1.
21. Harburger, D.S., Calderwood, D.A., 2009. Integrin signalling at a glance. *J. Cell Sci.* 122, 1472–1472.
22. Jacob-lopès, E., Queiroz Zepka, L., Queiroz, M.I. (Eds.), 2018. *Energy from Microalgae*. Springer International Publishing AG, Cham, Switzerland.
23. Kolb, J.F., Kono, S., Schoenbach, K.H., 2006. Nanosecond pulsed electric field generators for the study of subcellular effects. *Bioelectromagnetics* 27, 172–187.
24. Kotnik, T., Miklavčič, D., 2006. Theoretical evaluation of voltage inducement on internal membranes of biological cells exposed to electric fields. *Biophys. J.* 90, 480–491.
25. Lamberti, P., Romeo, S., Sannino, A., Zeni, L., Zeni, O., 2015. The role of pulse repetition rate in nsPEF—Induced electroporation: A biological and numerical investigation. *IEEE Trans. Biomed. Eng.* 62, 2234–2243.
26. McGrath, J.S., Honrado, C., Spencer, D., Horton, B., Bridle, H.L., Morgan, H., 2017. Analysis of parasitic protozoa at the single-cell level using microfluidic impedance cytometry. *Sci. Rep.* 7 (2601), 1–11.
27. Napotnik, T.B., Wu, Y.-H., Gundersen, M.A., Miklavčič, D., Vernier, P.T., 2012. Nanosecond electric pulses cause mitochondrial membrane permeabilization in Jurkat cells. *Bioelectromagnetics* 33, 257–264.
28. Paduch, M., Jeleń, F., Otlewski, J., 2001. Structure of small G proteins and their regulators. *Acta Biochim. Pol.* 48, 829–850.
29. Pakhomova, O.N., Gregory, B.W., Khorokhorina, V.A., Bowman, A.M., Xiao, S., Pakhomov, A.G., 2011. Electroporation-induced electrosensitization. *PLoS One* 6, 36–38.
30. Pirc, E., Reberšek, M., Miklavčič, D., 2017. Dosimetry in electroporation-based technologies and treatments. In: Markov, M. (Ed.), *Dosimetry in Bioelectromagnetics*. Taylor & Francis Group, LLC, pp. 233–268.
31. Reberšek, M., Miklavčič, D., Bertacchini, C., Sack, M., 2014. Cell membrane electroporation - part 3: the equipment. *IEEE Electr. Insul. Mag.* 30 (3), 8–18.
32. Rédei, G.P., 2008. *Encyclopedia of Genetics, Genomics, Proteomics and Informatics*. Springer, Netherlands, Dordrecht.
33. Rocha, C.M.R., Genisheva, Z., Ferreira-Santos, P., Rodrigues, R., Vicente, A.A., Teixeira, J.A., Pereira, R.N., 2018. Electric field-based technologies for valorization of bioresources. *Bioresour. Technol.* 254, 325–339.
34. Schoenbach, K., Hargrave, B., Joshi, R., Kolb, J., Nuccitelli, R., Osgood, C., Pakhomov, A., Stacey, M., Swanson, R., White, J., Xiao, S., Zhang, J., Beebe, S., Blackmore, P., Buescher, E., 2007. Bioelectric effects of intense nanosecond pulses. *IEEE Trans. Dielectr. Electr. Insul.* 14, 1088–1109.
35. Schoenbach, K.H., Joshi, R.P., Kolb, J.F., Chen, N., Stacey, M., Blackmore, P.F., Buescher, E.S., Beebe, S.J., 2004. Ultrashort electrical pulses open a new gateway into biological cells. In: *Proceedings of the IEEE*, pp. 1122–1137.
36. Schoenbach, K.H., Peterkin, F.E., Alden, R.W., Beebe, S.J., 1997. The effect of pulsed electric fields on biological cells: Experiments and applications. *IEEE Trans. Plasma Sci.* 25, 284–292.
37. Schwarz, E.M., Benzer, S., 1997. Calx, a Na-Ca exchanger gene of *Drosophila melanogaster*. *Proc. Natl. Acad. Sci. USA* 94, 10249–10254.

38. Silve, A., Guimerà Brunet, A., Al-Sakere, B., Ivorra, A., Mir, L.M., 2014. Comparison of the effects of the repetition rate between microsecond and nanosecond pulses: electroporation-induced electro-desensitization? *Biochim. Biophys. Acta, Gen. Subj.* 1840, 2139–2151.
39. Smetana, S., Mathys, A., Knoch, A., Heinz, V., 2015. Meat alternatives – Life cycle assessment of most known meat substitutes. *Int. J. Life Cycle Assess.* 2050, 1254–1267.
40. Smetana, S., Sandmann, M., Rohn, S., Pleissner, D., Heinz, V., 2017. Autotrophic and heterotrophic microalgae and cyanobacteria cultivation for food and feed: Life cycle assessment. *Bioresour. Technol.* 245, 162–170.
41. Sridhara, V., Joshi, R.P., 2014. Evaluations of a mechanistic hypothesis for the influence of extracellular ions on electroporation due to high-intensity, nanosecond pulsing. *Biochim. Biophys. Acta, Biomembr.* 1838, 1793–1800.
42. Stewart, D.A.J., Gowrishankar, T.R., Weaver, J.C., 2004. Transport lattice approach to describing cell electroporation : Use of a local asymptotic model. *IEEE Trans. Plasma Sci.* 32, 1696–1708.
43. Sun, T., Morgan, H., 2010. Single-cell microfluidic impedance cytometry: A review. *Microfluid. Nanofluidics* 8, 423–443.
44. Vernier, P.T., Sun, Y., Gundersen, M.A., 2006. Nanoelectropulse-driven membrane perturbation and small molecule permeabilization. *BMC Cell Biol.* 7, 37.
45. Very, A.-A., Davies, J.M., 2000. Hyperpolarization-activated calcium channels at the tip of *Arabidopsis* root hairs. *Proc. Natl. Acad. Sci.* 97, 9801–9806.
46. Wuichet, K., Søgaard-Andersen, L., 2014. Evolution and diversity of the ras superfamily of small GTPases in prokaryotes. *Genome Biol. Evol.* 7, 57–70.
47. Yoshikawa, N., Belay, A., 2008. Single-laboratory validation of a method for the determination of c-phycocyanin and allophycocyanin in *Spirulina (Arthrospira)* supplements and raw materials by spectrophotometry. *J. AOAC Int.* 91, 524–529.
48. Zhu, J., 2016. Abiotic stress signaling and responses in plants. *Cell* 167, 313–324.
49. Zvereva, M.I., Ivanov, P.V., Teraoka, Y., Topilina, N.I., Dontsova, O.A., Bogdanov, A.A., Kalkum, M., Nierhaus, K.H., Shpanchenko, O.V., 2001. Complex of transfer-messenger RNA and elongation factor Tu. Unexpected modes of interaction. *J. Biol. Chem.* 276, 47702–47708.

MANUSCRIPT 4

Adsorption kinetics and foaming properties of soluble microalgae fractions at the air/water interface

Leandro Buchmann^a, Pascal Bertsch^b, Lukas Bocker^a, Ursina Krahenmann^a, Peter Fischer^b, Alexander Mathys^{a,*}

^a *ETH Zurich, Department of Health Sciences and Technology, Institute of Food Nutrition and Health, IFNH, Laboratory of Sustainable Food Processing, Schmelzbergstrasse 9, 8092, Zurich, Switzerland*

^b *ETH Zurich, Department of Health Sciences and Technology, Institute of Food Nutrition and Health, IFNH, Laboratory of Food Process Engineering, Schmelzbergstrasse 7, 8092, Zurich, Switzerland*

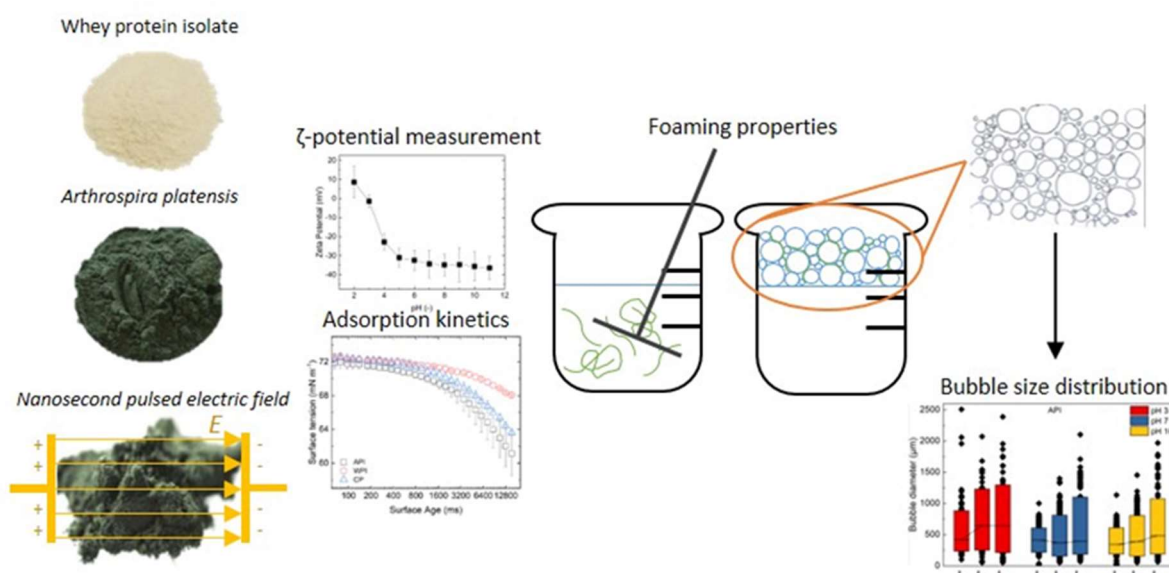
**Corresponding author*

Food Hydrocolloids 97 (2019) 105182

ABSTRACT

Microalgae as a novel food ingredient are of increasing interest as they can be grown on non-arable land and fixate CO₂ when grown photoautotrophically. Here, we employ proteins extracted from *Arthrospira platensis* biomass to be used for the stabilization of fluid interfaces, which is one of the most important techno-functional applications of proteins. Model foams were prepared from crude *A. platensis* powder and *A. platensis* isolate and whey protein isolate as a reference. The derived *A. platensis* isolate exceeded the overrun and the foam stability of whey protein isolate. The comparable low surface activity of crude *A. platensis* powder emphasizes the need for the extraction process. The neutral color of the *A. platensis* isolate indicates that the valuable natural pigments present in *A. platensis* were retained while achieving relevant techno-functional properties with the residual biomass. Physical treatment with nanosecond pulsed electric fields further increased the biomass yield without impeding the techno-functional properties of the derived isolates. Thus, protein extraction from microalgae biomass is an interesting approach to obtain techno-functional proteins and increase microalgae production efficiency.

GRAPHICAL ABSTRACT



1. INTRODUCTION

Microalgae-based food production systems can potentially meet the increasing demand for healthy and nutritious food due to the growing world population. Within the food industry, one of the main interests of microalgae is its protein content and the correlating high-quality amino acid composition. Therefore, microalgae are considered a source of alternative, vegetal proteins (Wong, Cheung, & Ang, Jr., 2004). Moreover, different protein-pigment complexes, bioactive peptides or surface active proteins are present in various species and are of interest from a technological perspective (Buono, Langellotti, Martello, Rinna, & Fogliano, 2014; Dai, Bergfreund, Reichert, Fischer, & Weiss, 2019; Matos, 2017).

The broad cultivation of microalgae is currently not competitive because of inefficient up- and downstream processing (Caporgno & Mathys, 2018; Smetana, Sandmann, Rohn, Pleissner, & Heinz, 2017). Nanosecond pulsed electric fields (nsPEF) have demonstrated potential in the upregulation of cell proliferation in eukaryotes (Eing, Bonnet, Pacher, Puchta, & Frey, 2009) and most recently in the prokaryotic microalgae *Arthrospira platensis* as well (Buchmann, Frey, Gusbeth, Ravaynia, & Mathys, 2019). Therefore, the cultivation efficiency of microalgae could be increase, yet the influence of nsPEF on technofunctional properties of microalgae is unknown. As an application, foaming properties were investigated as they are among the most important techno-functional properties of food proteins (Smith, 2017). Foams are a two-phase system, in which a gas is dispersed in a continuous liquid or solid. The creation of a stable foam is challenging because of rapidly occurring destabilization processes. Foams are thermodynamically unstable, which counteracts the foam volume and foam stability (Wilson, 1989). The three main processes involved in foam destabilization, coalescence, drainage, and Ostwald ripening, can be counteracted by the adsorption of proteins at the air/water interface forming a viscoelastic interfacial layer and partly by higher viscosity of the dispersed phase (Foegeding, Luck, & Davis, 2006; Pugh, 1996; Voorhees, 1985).

Foam stability is defined by the rate of loss of foam structure and is related to the ability to maintain bubble size. Overrun (OR) is defined as the ability to incorporate air into the continuous phase. Proteins can prevent the destabilization processes in foams (foam stability) and enhance overall foam formation (overrun) (Marinova et al., 2009; Wilson, 1989). Both properties are linked to interfacial tension and in particular to the viscoelastic interface between the gas bubbles and the continuous phase

(Hailing & Walstra, 1981; Nicorescu et al., 2011). Proteins present in the aqueous phase are able to adsorb at the air/water interface. They decrease surface tension and form viscoelastic interfacial layers, thereby counteracting coalescence and drainage (Dickinson, 1999; Dickinson, Murray, & Stainsby, 1988; Fischer, 2013; Foegeding et al., 2006). The reduction of surface tension by proteins depends on the protein concentration, the protein diffusion coefficient as well as the kinetic barrier of protein adsorption. In literature a reduction of surface tension to around 65 mN m^{-1} was found for β -casein and β -lactoglobulin at concentrations of $1 \cdot 10^{-7} \text{ mol L}^{-1}$ (Mitropoulos, Mütze, & Fischer, 2014). Given the protein's amphiphilic structure the adsorption at the interface is energetically driven (Beverung, Radke, & Blanch, 1999; Mezzenga & Fischer, 2013). The adsorption kinetics of proteins during foam formation at the newly generated air/water interface ultimately determine foam overrun and bubble size (Damodaran, 2006). Three different time regimes of proteins are commonly distinguished (Beverung et al., 1999). First, a diffusion-driven lag phase or induction phase with no observable changes in surface pressure is observed. The protein diffusion to the air/water interface is influenced by their solubility (Singhal, Stone, Vandenberg, Tyler, & Nickerson, 2016). Second, proteins start adsorbing at the air/water interface. Upon adsorption, proteins undergo structural changes resulting in a kinetic energy barrier which increases with the protein's thermodynamic stability and decreases with exposed hydrophobicity (Mitropoulos et al., 2014; Wierenga, Meinders, Egmond, Voragen, & de Jongh, 2003). Third, interfacial gelation occurs due to the ongoing rearrangement of adsorbed proteins as well as the formation of multiple layers in the water phase (Dickinson, 1999; Mezzenga & Fischer, 2013).

Other protein adsorption factors are ionic strength and pH. Adsorption is enhanced at an increasing ionic strength and near the isoelectric point. However, both may also induce protein aggregation, resulting in a larger hydrodynamic radius and lower effective concentration (Mezzenga & Fischer, 2013; Mitropoulos et al., 2014; Zhang & Sun, 2002). Moreover, in protein mixtures such as whey protein isolate, the different fractions may competitively adsorb (Zhang, Dalgleish, & Goff, 2004).

The aim of this study was to investigate the foaming properties of photoautotrophically grown *A. platensis*. The foaming properties of commercial *A. platensis* powder were compared with those of whey protein isolate (WPI) as a benchmark foaming agent. In addition, the techno-functional properties following

nsPEF treatment that upregulate cell proliferation (Buchmann et al., 2019) were evaluated and compared with *A. platensis* isolate (API).

2. MATERIAL AND METHODS

2.1. Raw materials

The strain *Arthrospira platensis* SAG 21.99 was cultivated in a modified Zarrouk medium (Aiba & Ogawa, 1977). The cultures were incubated at 25 ± 0.2 °C, 70% relative humidity, 150 rpm, ambient CO₂, and continuous illumination with a mean photosynthetically active photon flux density (PPFD) of $32 \mu\text{mol photons m}^{-2} \text{s}^{-1}$ using warm white LED lamps in a shaking incubator (Multitron Pro shaking incubator, Infors AG, Bottmingen, Switzerland). Growth of *A. platensis* was monitored by optical density (OD) measurements at 750 nm (Cary 100, Agilent, Santa Clara, USA).

In comparison to self-grown *A. platensis*, a commercially available *A. platensis* powder Premium II (PII) from China (Institut für Lebensmittel und Umweltforschung ILU, Nuthetal, Germany) was used. A spray drying process with a final protein content $>60 \text{ g L}^{-1}$ was used to manufacture the powder. As reference material for surface tension and foaming experiments whey protein isolate (WPI) with a protein content of $>90 \text{ g L}^{-1}$ (NZMP SureProtein WPI 8855, Fonterra, Auckland, New Zealand) was included in the experimental design (Table 1).

M4 - Table 1: Overview of the raw material name and source with the corresponding abbreviation.

Name	Abbreviation	Source
Crude <i>Arthrospira platensis</i> powder	CP	Commercial
<i>Arthrospira platensis</i> isolate	API	Commercial
Whey protein isolate	WPI	Commercial
untreated self-cultivated <i>Arthrospira platensis</i>	control	Self-cultivated
nsPEF treated self-cultivated <i>Arthrospira platensis</i>	treated	Self-cultivated

2.2. Nanosecond pulsed electric field (nsPEF) treatment

The nsPEF treatments of the fresh biomass were executed in biological triplicates. The generator output voltage was 1 kV, resulting in an electric field strength E (kV cm⁻¹) of 10 kV cm^{-1} , as a plate-plate 1mm polycarbonate continuous treatment chamber was used. For further information regarding the nsPEF treatment, refer to Buchmann et al. (2019). Regarding the treatment homogeneity, the electrical efficiency of the process was approximately 90% or higher (Buchmann, Böcker, et al., 2018; Buchmann, Bloch, & Mathys, 2018).

2.3. Extraction procedure

The extraction procedure for the production of *A. platensis* isolates (API) was based on an alkaline extraction, followed by acidic precipitation, and was comparable to that used by Benelhadj, Gharsallaoui, Degraeve, Attia, and Ghorbel (2016).

For the alkaline extraction, the Zarrouk growth medium (Aiba & Ogawa, 1977) served as a buffer. The solution was diluted at 1:5 with Milli-Q water (Zarrouk buffer 20%) reaching a final pH of 9.35. This dilution was necessary to decrease the buffer capacity and therefore minimize the amount of HCl during precipitation. A total of 12 g *A. platensis* was added to 600 mL of Zarrouk buffer 20% and placed on a magnetic stirrer (MST Basic C, Bioswisstec AG, Schaffhausen, Switzerland). After 24 h, the pH was controlled in order to detect contamination or fouling. The suspension was centrifuged for 60 min at 16,000 g (Sorvall LYNX 6000, Thermo Fisher Scientific, Waltham, USA). The supernatant was collected and stored at 4 °C. For more efficient extraction, this step was repeated again with the pellet. Therefore, the pellet was dissolved in 300 mL Zarrouk buffer 20%, agitated for 30 min at RT and 200 rpm and centrifuged. Both supernatants were combined and adjusted to a pH of 3 with HCl (1 M). The solution was agitated and centrifuged at 16,000 g for 30 min each. The pellet was recovered, shock-frozen in liquid nitrogen (< -196 °C) and freeze-dried for 36 h at 260 µbar (Bench Top Pro Manifold Freeze Dryer, SP Industries, Warminster, PA, USA). The final isolates were gravimetrically measured and nitrogen was quantified by using the Dumas method with a conversion factor of 5.03 based on mass balance determination (TruMac CN, LECO Coporation, St. Joseph, USA).

2.4. ζ -potential measurement

The ζ -potential was used to assess the net charge of the proteins as a function of pH. A Zetasizer Nano ZS (Malvern Instruments Ltd., Worcestershire, UK) was used to analyze the ζ -potential. The samples were dissolved at a concentration of 1 g L⁻¹ in 50mM phosphate buffer at a pH from 2 to 11. After 4 h of dissolution, ζ -potential was measured using a DTS 1060 cell (Malvern Instruments Ltd., Worcestershire, UK) at 22 °C.

2.5. Bubble pressure tensiometry

A bubble pressure tensiometer (BPT) (BP50, Krüss GmbH, Hamburg, Germany) with

a 0.05 mm capillary was used to assess the surface tension as a function of surface age. The BPT records the maximum internal pressure of a spherical gas bubble formed in a liquid. Based on the Young-Laplace equation (Eq. (1)) and the known radius of the capillary, the surface tension σ (mN m⁻¹) at a defined surface age is calculated from the BPT (Eq. (2)). The Young-Laplace equation (Eq. (1)) relates the internal pressure of a spherical gas bubble ρ (Pa) to the radius of curvature r_c (m) and the surface tension as follows:

$$\rho = 2\sigma/r_c \quad (1)$$

$$\sigma = (p_{max} - p_0) \cdot r_c/2 \quad (2)$$

with the maximum pressure p_{max} (Pa) and the hydrostatic pressure p_0 (Pa).

The time dependence of the surface tension was studied at a fixed concentration of 0.1% w/V under acidic (pH 3), neutral (pH 7), and alkaline (pH 10) conditions. Prior to the first measurement, the capillary was calibrated to 72.4 mN m⁻¹ using Milli-Q water. After each measurement, the capillary was purged using Milli-Q water. Measurements were performed using logarithmic time steps to record the surface tension of the bubbles from 15 ms to 16000 ms, resulting in 25 measurements. The results were graphically evaluated by plotting the surface age versus the surface tension.

2.6. Foam processing and characterization

The different raw materials were dissolved in phosphate buffer, and the pH was adjusted using HCl/NaOH solution. The working solutions were prepared by mixing 0.1 g or 0.01 g of *A. platensis* powder with 5 mL Milli-Q and additionally stirring for 30 min. This step facilitated the dissolution of the powder, particularly at a low pH. During the second step, aliquots of 50mM phosphate buffer (85 wt % in H₂O, Merck, Darmstadt, Germany) at pH values of 3, 7 or 10 were added, leading to a final buffer concentration of 25 mM. The samples were stirred for another 30 min and stored in a fridge at 4 °C.

Foaming experiments required a minimum concentration of 1% w/V. For each powder and pH combination, triplicate samples were prepared and simultaneously measured. Samples were whipped at 1500 rpm using a commercial milk frother (Cilio, Aerolatte, Leipzig, Germany). The frother blade was immersed in the liquid sample and foam was formed over 60 s at pH 3, 7 and 10.

The overrun (OR) was defined as the volume following 60 s of foaming V_{t0} (%) over the initial volume of the liquid V (mL) (Peng, Yang, Li, Tang, & Li, 2017). The 10 mL samples were foamed in 75 mL glassware and V_{t0} was determined by height measurement of the foam using a scale. The OR was calculated according to Eq. (3) as follows:

$$OR(\%) = (V_{t0}/V) \cdot 100 \quad (3)$$

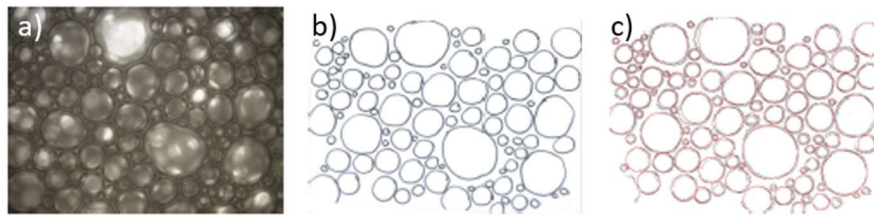
The mean and standard deviation of the replicates were used for evaluation. The foaming stability (FS) is defined in Eq. (4) and was determined by the difference in the volume at a specific time point V_t (%) compared to that at V_{t0} (%) over the initial sample volume, as follows:

$$FS(\%) = ((V_{t0} - V_t)/V) \cdot 100 \quad (4)$$

Volumes were recorded immediately after foaming (t_0), after 20 min (t_{20}) and after 60 min (t_{60}).

2.7. Bubble size distribution

The bubble size distribution (BSD) measurements were used to observe the foam microstructure over time. The BSD and surface tension experiments were executed in triplicate for each raw material and pH combination. The samples were analyzed immediately after foaming (t_0), after 20 min (t_{20}) and after 60 min (t_{60}). The foam microstructure was analyzed using an inverse light microscope (Nikon Diaphot TMD, Nikon Corporation, Japan). Following post-processing, using manual bubble recognition, which aims to increase the contrast of the microscopic images, the pictures were integrated into the software BubbleDetect (ETH Zurich, Switzerland, Müller-Fischer, Suppiger, and Windhab (2007)) (Fig. 1). Bubble Detect is able to automatically determine the number and diameter of spherical objects. As a control, images were evaluated one-by-one for bubble recognition and diameter size. Bubble Detect was calibrated using a recorded picture.



M4 - Figure 1: Process to determine bubble diameter and counts for bubble size distribution (BSD). The microscopic image a) was postprocessed b) and automatically analyzed by the software Bubble Detect c).

The bubble size distribution was evaluated using three different methods: 1) qualitatively by comparison of the pictures, 2) graphically by plotting the distributions in quantiles and 3) statistically by fitting an ordinary least squares (OLS) model. For the graphical evaluation, the replicates data points were combined and treated as if they were one observation. As response variables for the OLS, the median diameter (d_{50} , μm) and the span (see Eq. (5)) were calculated similarly to that in Nicorescu et al. (2011). The median is accurate for skewed distributions and less susceptible to outliers. The span is an estimate of the width of the distribution and was calculated from the 90th (d_{90} , μm) and 10th percentiles (d_{10} , μm) and normalized by division of the median, according to Eq. (5) as follows:

$$\text{span} = (d_{90} - d_{10})/d_{50} \quad (5)$$

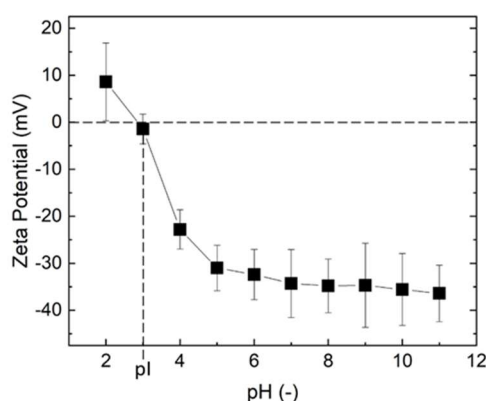
2.8. Statistical analysis

Statistical analysis was performed on the observations resulting from the foaming property experiments. It was assumed that the data are normally distributed and have a homogeneous variance. The model was developed based on a parametric linear regression, estimated using a mixed effect model and evaluated in the free software R and RStudio Version 3.4.4 (RStudio Inc., Boston, MA, USA) with ANOVA. Because of the significant interaction effect between “pH” and “Treatment”, a pairwise comparison between all levels of the factors was performed by using contrasts. The p-values of the pairwise comparison were adjusted using a Scheffé correction.

3. RESULTS AND DISCUSSION

3.1. ζ -potential of the *Arthrospira platensis* isolate

The ζ -potential of the API shown in Fig. 2 was measured to quantify the effect of the electrostatic interactions between the proteins in different pH regimes. As commercial and self-cultivated microalgae samples showed a similar ζ -potential, the results for the API are shown representatively. The API ζ -potential was constant at -40 mV at $\text{pH} > 5$. At a more acidic pH, the ζ -potential decreased with the charge inversion denoting the isoelectric point (pI) around $\text{pH}=3$. Given that the API is a mixture of several protein fractions, this corresponds to the net charge of all protein fractions. Therefore, it suggests that proteins present in the API are subjected to electrostatic repulsion at $\text{pH} > 4$. With respect to foaming, different adsorption kinetics and foam stabilities, are expected at $\text{pH} > 4$ compared to a more acidic pH, as assessed in detail later. The isoelectric point of the WPI as stated in literature is at $\text{pH} = 4.6$ (Anandharamakrishnan, Rielly, & Stapley, 2008; Gbassi et al., 2012).



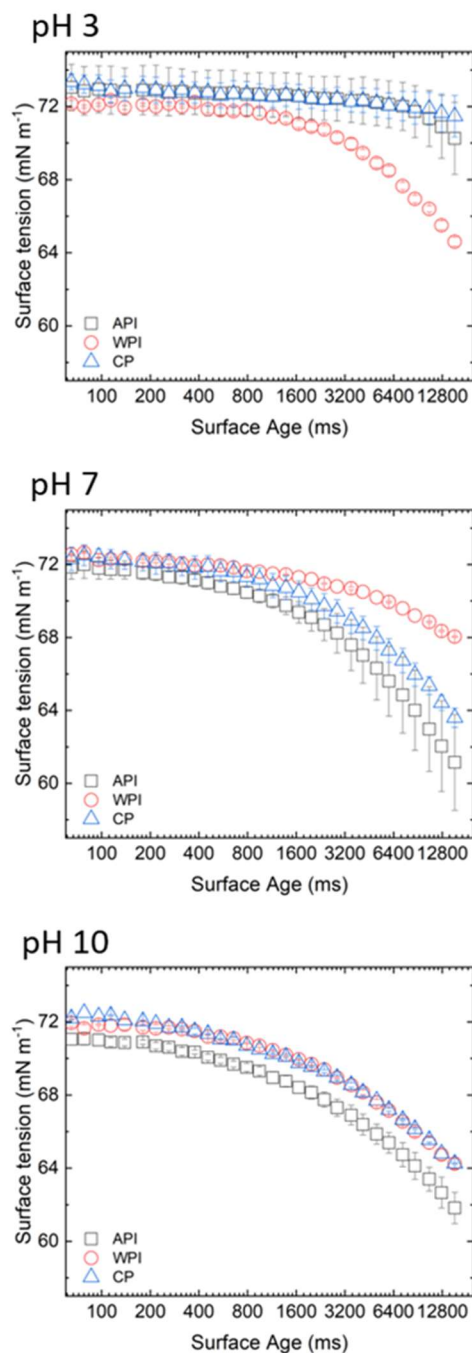
M4 - Figure 2: ζ -potential of the *Arthrospira platensis* isolate (API) extracted from commercial powder and dissolved in aliquots of 50mM phosphate buffer ranging from pH 2 to 11 at room temperature.

3.2. Adsorption kinetics at air/water interfaces

The measurement of surface tension was focused on the surface activity of different *A. platensis* fractions at the air/water (a/w) interface. The adsorption of the crude *A. platensis* powder (CP) and API in comparison to WPI is shown in Fig. 3. The *A. platensis* isolate adsorbed faster than CP and WPI, except at pH 3 (Fig. 3) as the WPI had a net charge of $+23.1$ mV (Gbassi et al., 2012). A rapid decrease in surface tension is related to the rapid adsorption at the interface and therefore stabilization of the dispersed air bubbles (Beverung et al., 1999; Wierenga et al., 2003). A pH equal

to the pI of the microalgae samples (Fig. 2) could have resulted in protein aggregation due to the hydrophobic attraction impeding the diffusion-limited adsorption at the a/w interface (Singhal et al., 2016; Wierenga et al., 2003).

For pH 7 and 10, the lowest decrease in surface tension was found for the WPI. The observation at pH 7 was not expected as the pI of WPI is at pH = 4.6 (Anandharamakrishnan et al., 2008; Gbassi et al., 2012). However, a possible explanation for the observation could be the composition of WPI. The pI of WPI corresponds to the net charge of all protein fractions and varies for the individual fractions. According to literature, immunoglobulins present in WPI have a pI between pH 5.5 to 6.8 (Bryant & McClements, 1998). A pH around the individual pI probably led to hydrophobic attraction, resulting in increased protein aggregation. The API showed superior surface activity in comparison to that of CP independent of pH. The results correlate with the ζ -potential measurement (Section 3.1) as a constant ζ -potential above pH > 5 was measured. These observations are in line with the results of Chronakis, Galatanu, Nylander, and Lindman (2000), who found a similar adsorption behavior for *A. platensis* isolates at a pH ranging from 4.5 to 11. Similar to this study, the authors observed faster adsorption at pH 7 than at pH 4.5.

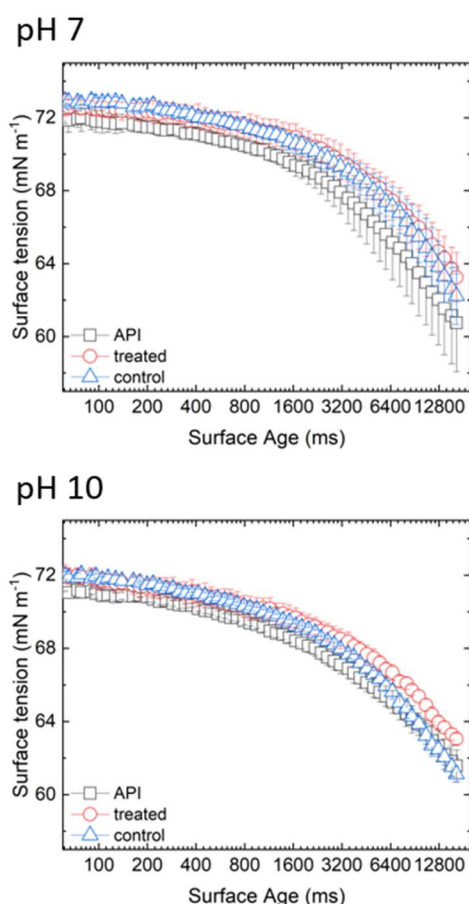


M4 - Figure 3: Surface tension over time for the *Arthrospira platensis* isolate (API), crude *Arthrospira platensis* powder (CP) and whey protein isolate (WPI) at a concentration of 0.1% weight per volume for pH 3, pH 7 and pH 10.

The surface activity of the self-cultivated nsPEF treated *A. platensis* samples was investigated and compared to untreated self-cultivated *A. platensis* samples and API in order to observe effects on microalgae constituent alterations induced by the nsPEF treatment (Fig. 4). Neither for pH 7 nor for pH 10, did the nsPEF treatment influence the surface activity as shown in Fig. 4. The self-cultivated samples had a similar surface activity compared to that of API (Fig. 4). For all samples at pH 7, the

lag phase lasted until 3000 ms and reached 62–67 mN m⁻¹ after 16000 ms. Similar to the results found during the surface tension experiments with commercial powders, the self-cultivated cultures did not show a significant pH dependence between pH 7 and 10, which is in agreement with the ζ -potential measurement (Section 3.1). Nevertheless, there was a slight trend for the untreated self-cultivated *A. platensis* samples (control, Fig. 4) to reach a lower surface tension at 16000 ms (61–62 mN m⁻¹) compared to that of the self-cultivated nsPEF treated *A. platensis* samples (treated, Fig. 4) samples (63–63.5 mN m⁻¹) at pH 10.

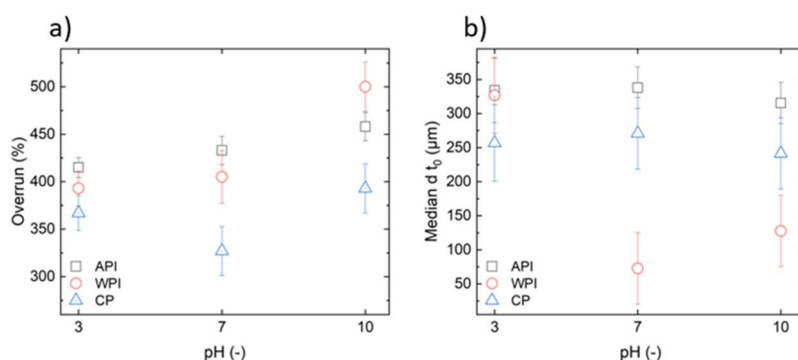
It was observed that the nsPEF treatment increased the biomass while maintaining high protein content, but its composition was influenced (Buchmann et al., 2019). However, based on the surface tension measurements, the quality of the isolate was not adversely affected, as the surface activity was comparable to that of the control and the API. Therefore, the nsPEF technology was able to increase the biomass yield while maintaining the foaming properties.



M4 - Figure 4: Surface activity of the nanosecond pulsed electric field treated self-cultivated *Arthrospira platensis* (treated) and untreated self-cultivated *Arthrospira platensis* (control) compared to *Arthrospira platensis* isolate (API) at a concentration of 0.1% weight per volume at pH 7 and 10.

3.3. Overrun and stability of foams

The overrun was characterized by the height measurement of the foam, calculated median (median d_{t_0}), and span of the foam bubble size distribution immediately after foaming (span t_0) (Fig. 5). At pH 3, the API showed the highest overrun followed by the WPI and CP with the lowest OR. The overrun at pH 7 was higher for the API compared to that of the CP with a tendency to increase from pH 7 to 10. However, the increase in the OR from pH 7 to 10 was more pronounced for the CP than for the isolate. These results are correlating with literature data of API where an increase in overrun was found from pH 3 to pH 10 (Benelhadj et al., 2016; Devi & Venkataraman, 1984). In comparison to the WPI, the overrun performance of the API was significantly different, higher at pH 7 but lower at pH 10, in which the WPI reached its maximum volume and minimal median, respectively (Fig. 5, Table 2). However, the median d_{t_0} did not correlate with the OR and did not considerably change over the different pH values for the microalgae samples (Fig. 5). Therefore, the adsorption process during our experiments can be regarded as mostly a kinetic-limited process (Beverung et al., 1999; Wierenga et al., 2003, Mezzenga & Fischer, 2013). The overrun at pH 3 indicates that shear-induced foaming by a rotor-stator device enabled insoluble protein adsorption (Smith, 2017). During a diffusion-limited adsorption process, the overrun should correlate with the decrease in surface tension (Fig. 3) (Beverung et al., 1999).



M4 - Figure 5: a) Overrun and b) median d_{t_0} immediately after foaming for the *Arthrospira platensis* isolate (API), crude *Arthrospira platensis* powder (CP) and whey protein isolate (WPI) over the investigated pH range.

A higher foam stability is achieved if the foam decay is decelerated and polydispersity is reduced (Marinova et al., 2009; Wilson, 1989). An increased polydispersity

decreases the foam stability as Ostwald ripening is increased. In addition to the immediate foaming properties, the foam stability and the bubble size distribution were assessed as a function of time (Fig. 6). The foam decay was characterized based on the evolution in median bubble diameter, indicated as slope t_{20} and t_{60} in Table 2.

M4 - Table 2: Foaming characteristics of different samples at pH 3, 7 and 10 at t_0 immediately after foaming, t_{20} after 20 min and t_{60} after 60 min, ^a means significantly different from whey protein isolate (WPI), ^b means significantly different from crude *Arthrospira platensis* powder (CP) on a Scheffé corrected p-value <0.05 after pairwise comparison with contrasts.

pH	Sample	OR	STD	Median d t_0	STD	span t_0	STD	Slope t_{20}	STD	Slope t_{60}	STD
		[%]	±	[μm]	±		±	[$\mu\text{m min}^{-1}$]	±	[$\mu\text{m min}^{-1}$]	±
3	API	415	10.5	333.94	47.08	1.89 ^{a,b}	0.11	12.38 ^{a,b}	2.95	5.97 ^a	0.97
	WPI	393.3	18.2	326.8	55.96	1.21	0.18	-4.76	4.18		
	CP	366.7	18.2	256.9	55.96	1.11	0.15	-0.25	2.74	2.24	1.68
7	API	433.3 ^a	14.9	337.96 ^a	30.25	1.16	0.15	2.27	4.03	0.53 ^a	1.37
	WPI	405	27.9	72.77	52.39	1.15	0.26	10.72	3.87	5.94	2.38
	CP	326.7 ^a	25.8	270.94 ^a	52.39	1.06	0.21	3.08	3.87	2.23	2.38
10	API	458.3 ^a	14.9	315.58 ^a	30.25	1.19	0.15	-2.31	4.74	2.9 ^a	1.37
	WPI	500	25.8	127.64	52.39	1.43	0.26	4.11	4.74	15.94	2.38
	CP	393.3 ^a	25.8	241.43	52.39	1.19	0.26	7.32	4.74	2.35 ^a	2.38

At pH 3, the box width of the API was lower than that for the CP, but it showed more outliers. Regarding the speed of the median increase (slope t_{20}), a significantly higher slope was observed for the API compared to that of the CP. However, the median increase decelerated comparing slope t_{20} to slope t_{60} . For the CP, the median increase is lower, but according to the box width, the disparity increases between t_{20} and t_{60} . Moreover, the distribution after 60 min (t_{60}) for the CP is skewed (median position compared to the whole box width). After all, CP and API exceeded the foam stability of the WPI at pH 3 as the foam completely disappeared after 60 min. Comparing the API to CP, the increased polydispersity could indicate an imminent collapse resulting from Ostwald ripening (Voorhees, 1985). The increased polydispersity indicates that the thermodynamically-driven Ostwald ripening is advanced and thereby close to the equilibrium state which is a two-phase system with a low curvature interfacial area. According to Voorhees (1985), these surface

energy driven morphological changes mostly correlate with the last phase of a first-order phase transformation process.

At pH 7 and 10, the widths of the boxplots are in a similar range for all the microalgae samples. Dense foams are observed at t_0 with a small distribution in the range of 200–600 μm . During the following 60 min, the distribution width increases to a greater extent than the median. Thus, the bubble size distributions are more skewed than at the beginning, indicating a higher polydispersity. An exception is the distribution observed for the CP at pH 10 after 60 min, where the disparity decreases again after 20 min. The foam stability of *A. platensis* derived foams over 60 min is in line with literature (Nirmala, Prakash, & Venkataraman, 1992). Regarding the ζ -potential measurement (Fig. 2), a similar behavior for the microalgae samples at pH > 5 was expected. However, there was a tendency to decelerate the bubble median increase at pH 7 compared to that at pH 10, and it was more pronounced for the API than for the CP. These results correlate well with the adsorption kinetics experiments, during which a faster adsorption was found for the API compared to that of the CP (Fig. 3). The presented data indicates higher OR and foam stability, which was less pH dependent than the results from the literature (Benelhadj et al., 2016; Devi, Subbulakshmi, Devi, & Venkataraman, 1981).

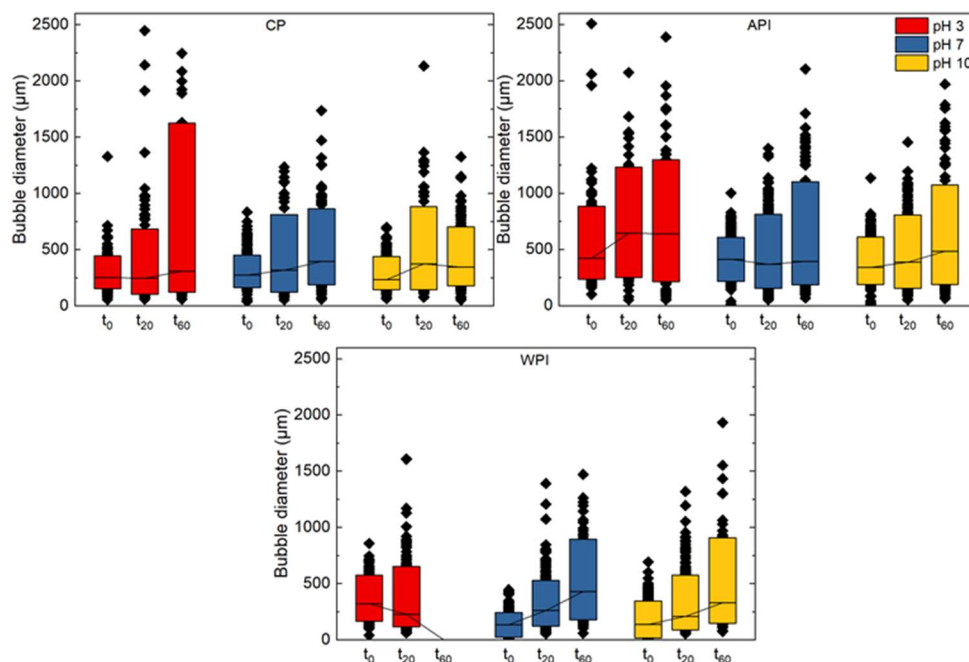
In addition, the pH dependency of the microalgae samples related to the BSD over time was less pronounced than that for the OR. The samples show a higher disparity at pH 3 compared to pH 7 and 10 and fewer structural changes according to the differences between slope t_{20} and t_{60} . At pH 7 and 10, the bubble size distributions are similar. The patterns of the microalgae samples are similar to the values observed for the WPI, in which the bubble size distribution also did not show a clear pH dependence, although the median increase between t_{20} and t_{60} of the microalgae samples is slower at pH 7 and 10 compared to that of the WPI. These result correlate with the surface tension measurements were an increased reduction of the surface tension was observed for the microalgae samples. Therefore, protein adsorption and the size of the viscoelastic interfacial layer could be increased, stabilizing the foam (Foegeding et al., 2006).

Overall, better foam stability in comparison to that of the WPI was observed for all microalgal samples at pH 3. The results were most pronounced for the CP as the span, and the median were smaller compared to those of the API; therefore, polydispersity was reduced. In fact, there was complete foam decay for the WPI at

pH 3, which agrees with observations from the bubble size distribution. The enhanced foam stability of the *A. platensis* samples at pH 3 can be associated with higher protein aggregation potential leading to more cross-linking and a more viscoelastic film at the interface (Lupatini, Colla, Canan, & Colla, 2017; Müller-Fischer et al., 2007; Wilson, 1989). The pH at the determined pI of the API probably led to hydrophobic attraction (Gbassi et al., 2012).

We found that CP and API had similar or even better foaming properties compared to those of WPI. Hence, the CP and API showed potential to be alternative foaming agents. The extracted API had a superior overrun at pH 3 and 7, and the foam stability was higher at all

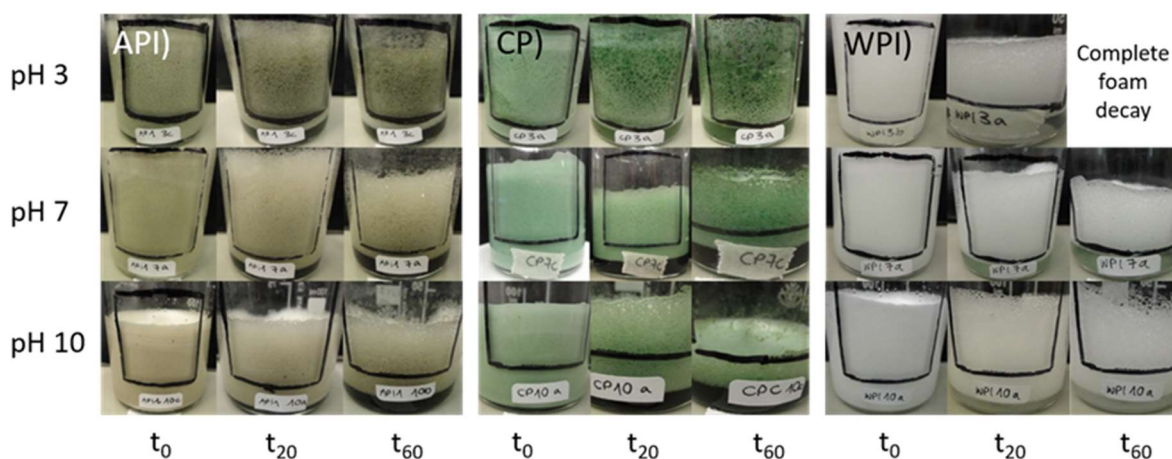
pH values compared to WPI. In contrast, there was higher decrease in surface tension for the API observed at pH 7 and 10, but lower decrease at pH 3 compared to that of the WPI. Therefore, the foaming process is not regarded as diffusion limited (Beverung et al., 1999). During the foaming process high shear rates are occurring in the system which results in a not diffusion limited process. Otherwise, surface tension measurements with concentration where a lag-phase is present (Fig. 3) and overrun should correlate (Fig. 5, Table 2). In fact, the WPI is widely used in the food industry because of its contribution to overrun and stability, as well as the ability to dissolve in an acidic pH, which is uncommon (Marinova et al., 2009; Norwood et al., 2016; Zayas, 1997). Thus, the isolate derived from *A. platensis* has the potential to reach the importance of that of WPI, with the benefit of coming from a vegetal source.



M4 - Figure 6: Bubble size distribution of crude *Arthrospira platensis* powder (CP), *Arthrospira platensis* isolate (API) and whey protein isolate (WPI) over time and at different pH values. Medians are estimated from all replicates at once and interconnected between the different time points. The box width includes all data points within the 10th and 90th percentiles. Time points correspond to t_0 immediately after foaming, t_{20} after 20 min and t_{60} after 60 min. The distribution for the WPI at t_{60} at pH 3 is not shown as the foam completely disappeared.

3.4. Macroscopic foam properties

Foaming properties are among the most important techno-functional properties that are provided by food ingredients. Images of the foamed *A. platensis* and WPI samples are shown in Fig. 7. A clear difference in color was visible for the *A. platensis* samples prior to (CP) and following extraction (API). The extraction procedure reduced the coloring agents leading to a yellowish/whitish foam color. For industrial applications, a coloring side effect of a foaming agent is generally undesirable. The isolated API was able to form foams with neutral color. This observation is in line with previous studies, including Waghmare, Salve, LeBlanc, and Arya (2016) who reported a less intense color for isolates compared to whole biomass derived from *Chlorella pyrenoidosa*. Therefore, the presented procedure enables the derivation of the high-value blue colorant phycocyanin, while utilizing the remaining cell constituents as promising food ingredients (Böcker et al., 2019; Caporgno & Mathys, 2018).



M4 - Figure 7. Macrostructure of foams created at pH 3, 7 and 10 at t_0 immediately after foaming, t_{20} after 20 min and t_{60} after 60 min for *Arthrospira platensis* isolate (API), crude *Arthrospira platensis* powder (CP), and whey protein isolate (WPI). A total of 10 mL algae with 50 mM phosphate buffer was foamed at a powder concentration of 1% weight per volume for 60 s using a milk frother.

Herein, we demonstrated the adsorption of soluble microalgae protein at air/water interfaces and the production of model foams. However, the same principles of adsorption and interfacial stabilization apply to oil/water interfaces and emulsions (Dalgleish, 1997; Fischer & Erni, 2007). Thus, soluble microalgae protein could further be employed for the stabilization of emulsions, although the adsorption kinetics and interfacial layer formation may vary depending on the nature of the used oil (Bergfreund, Bertsch, Kuster, & Fischer, 2018).

4. CONCLUSIONS

Photoautotrophic cultivation systems of microalgae bear great potential as an alternative source of food ingredients. Model foams were prepared from crude *A. platensis* powder (CP), *A. platensis* isolate (API) and whey protein isolate (WPI) to assess their foaming properties. The API showed better overrun and stability compared to that of the WPI and CP. The superior foaming properties of the API compared to those of the WPI were maintained even after nsPEF treatment. Therefore, nsPEF treatment presents a possible physical treatment to increase the biomass yield without compromising the investigated foaming properties. Moreover, the production of API leads to the separation of the economically important protein-pigment complex phycocyanin from the bulk biomass, enabling a cascade utilization of highly relevant cellular compounds derived from *A. platensis*. Thereby, microalgae biomass utilization could be improved. Further research should focus on the biochemical nature of *A. platensis* derived proteins with a foaming activity. In this regard, investigation of isolated protein and peptide fractions from the microalgal biomass with respect to their foaming activity would be beneficial.

ACKNOWLEDGMENTS

The authors gratefully acknowledge support from the World Food System Center (Project “NewAlgae”, grant number: 2-72235-17); the ETH Zürich Foundation, Switzerland; and Prof. Dr. Erich J. Windhab, Daniel Kiechl and Bruno Pfister from the ETH Zürich Food Process Engineering Laboratory.

CONFLICT OF INTEREST STATEMENT

The authors declare no conflict of interest.

REFERENCES

1. Aiba, S., & Ogawa, T. (1977). Assessment of growth yield of a blue-green alga, *Spirulina platensis*, in axenic and continuous culture. *Journal of General Microbiology*, 102, 179–182. <http://doi.org/10.1099/00221287-102-1-179>.
2. Anandharamakrishnan, C., Rielly, C. D., & Stapley, A. G. F. (2008). Loss of solubility of α -lactalbumin and β -lactoglobulin during the spray drying of whey proteins. *Lebensmittel-Wissenschaft und -Technologie- Food Science and Technology*, 41, 270–277. <http://doi.org/10.1016/J.LWT.2007.03.004>.
3. Benelhadj, S., Gharsallaoui, A., Degraeve, P., Attia, H., & Ghorbel, D. (2016). Effect of pH on the functional properties of *Arthrospira (Spirulina) platensis* protein isolate. *Food Chemistry*, 194, 1056–1063. <http://doi.org/10.1016/j.foodchem.2015.08.133>.
4. Bergfreund, J., Bertsch, P., Kuster, S., & Fischer, P. (2018). Effect of oil hydrophobicity on the adsorption and rheology of β -lactoglobulin at oil–water interfaces. *Langmuir*, 34, 4929–4936. <http://doi.org/10.1021/acs.langmuir.8b00458>.
5. Beverung, C. J., Radke, C. J., & Blanch, H. W. (1999). Protein adsorption at the oil/water interface: Characterization of adsorption kinetics by dynamic interfacial tension measurements. *Biophysical Chemistry*, 81, 59–80. [http://doi.org/10.1016/S0301-4622\(99\)00082-4](http://doi.org/10.1016/S0301-4622(99)00082-4).
6. Böcker, L., Ortmann, S., Surber, J., Leeb, E., Reineke, K., & Mathys, A. (2019). Biphasic short time heat degradation of the blue microalgae protein phycocyanin from *Arthrospira platensis*. *Innovative Food Science & Emerging Technologies*, 52, 116–121. <http://doi.org/10.1016/J.IFSET.2018.11.007>.
7. Bryant, C. M., & McClements, D. J. (1998). Molecular basis of protein functionality with special consideration of cold-set gels derived from heat-denatured whey. *Trends in Food Science & Technology*, 9, 143–151. [http://doi.org/10.1016/S0924-2244\(98\)00031-4](http://doi.org/10.1016/S0924-2244(98)00031-4).
8. Buchmann, L., Bloch, R., & Mathys, A. (2018a). Comprehensive pulsed electric field (PEF) system analysis for microalgae processing. *Bioresource Technology*, 265, 268–274. <http://doi.org/10.1016/j.biortech.2018.06.010>.
9. Buchmann, L., Böcker, L., Frey, W., Haberkorn, I., Nyffeler, M., & Mathys, A. (2018b). Energy input assessment for nanosecond pulsed electric field processing and its application in a case study with *Chlorella vulgaris*. *Innovative Food Science & Emerging Technologies*, 47, 445–453. <http://doi.org/10.1016/j.ifset.2018.04.013>.
10. Buchmann, L., Frey, W., Gusbeth, C., Ravaynia, P. S., & Mathys, A. (2019). Effect of nanosecond pulsed electric field treatment on cell proliferation of microalgae. *Bioresource Technology*, 271, 402–408. <http://doi.org/10.1016/j.biortech.2018.09.124>.
11. Buono, S., Langellotti, A. L., Martello, A., Rinna, F., & Fogliano, V. (2014). Functional ingredients from microalgae. *Food and Function*, 5, 1669–1685. <http://doi.org/10.1039/c4fo00125g>.
12. Caporgno, M. P., & Mathys, A. (2018). Trends in microalgae incorporation into innovative food products with potential health benefits. *Frontiers in Nutrition*, 5, 58. <http://doi.org/10.3389/fnut.2018.00058>.
13. Chronakis, I. S., Galatanu, A. N., Nylander, T., & Lindman, B. (2000). The behaviour of protein preparations from blue-green algae (*Spirulina platensis* strain Pacifica) at the air/water interface. *Colloids and Surfaces A: Physicochemical and Engineering Aspects*, 173, 181–192. [http://doi.org/10.1016/S0927-7757\(00\)00548-3](http://doi.org/10.1016/S0927-7757(00)00548-3).
14. Dai, L., Bergfreund, J., Reichert, C. L., Fischer, P., & Weiss, J. (2019). Shear rheological properties of acid hydrolyzed insoluble proteins from *Chlorella protothecoides* at the oil-water interface. *Journal of Colloid and Interface Science*, 551, 297–304. <http://doi.org/10.1016/J.JCIS.2019.05.029>.
15. Dalgleish, D. G. (1997). Adsorption of protein and the stability of emulsions. *Trends in Food Science & Technology*, 8, 1–6. [http://doi.org/10.1016/S0924-2244\(97\)01001-7](http://doi.org/10.1016/S0924-2244(97)01001-7).
16. Damodaran, S. (2006). Protein stabilization of emulsions and foams. *Journal of Food Science*, 70, 54–66. <http://doi.org/10.1111/j.1365-2621.2005.tb07150.x>.
17. Devi, M. A., Subbulakshmi, G., Devi, K. M., & Venkataraman, L. V. (1981). Studies on the proteins of mass-cultivated, blue-green alga (*Spirulina platensis*). *Journal of Agricultural and Food Chemistry*, 29,

- 522–525. <http://doi.org/10.1021/jf00105a022>.
18. Devi, M. A., & Venkataraman, L. V. (1984). Functional properties of protein products of mass cultivated blue-green alga *Spirulina platensis*. *Journal of Food Science*, 49, 24–27. <http://doi.org/10.1111/j.1365-2621.1984.tb13660.x>.
 19. Dickinson, E. (1999). Adsorbed protein layers at fluid interfaces: Interactions, structure and surface rheology. *Colloids and Surfaces B: Biointerfaces*, 15, 161–176. [http://doi.org/10.1016/S0927-7765\(99\)00042-9](http://doi.org/10.1016/S0927-7765(99)00042-9).
 20. Dickinson, E., Murray, B. S., & Stainsby, G. (1988). Coalescence stability of emulsion-sized droplets at a planar oil–water interface and the relationship to protein film surface rheology. *Journal of the Chemical Society, Faraday Transactions*, 84, 871–883. 1: *Physical Chemistry in Condensed Phases* <http://doi.org/10.1039/f19888400871>.
 21. Eing, C., Bonnet, S., Pacher, M., Puchta, H., & Frey, W. (2009). Effects of nanosecond pulsed electric field exposure on *Arabidopsis thaliana*. *IEEE Transactions on Dielectrics and Electrical Insulation*, 16(5), 1322–1328. <http://doi.org/10.1109/TDEI.2009.5293945>.
 22. Fischer, P. (2013). Rheology of interfacial protein-polysaccharide composites. *The European Physical Journal - Special Topics*, 222, 73–81. <http://doi.org/10.1140/epjst/e2013-01827-x>.
 23. Fischer, P., & Erni, P. (2007). Emulsion drops in external flow fields — the role of liquid interfaces. *Current Opinion in Colloid & Interface Science*, 12, 196–205. <http://doi.org/10.1016/J.COCIS.2007.07.014>.
 24. Foegeding, E. A., Luck, P. J., & Davis, J. P. (2006). Factors determining the physical properties of protein foams. *Food Hydrocolloids*, 20, 284–292. <http://doi.org/10.1016/J.FOODHYD.2005.03.014>.
 25. Gbassi, G. K., Yolou, F. S., Sarr, S. O., Atheba, P. G., Amin, C. N., & Ake, M. (2012). Whey proteins analysis in aqueous medium and in artificial gastric and intestinal fluids. *International Journal of Brain and Cognitive Sciences*, 6, 1828–1837. <http://doi.org/10.4314/ijbcs.v6i4.38>.
 26. Hailing, P. J., & Walstra, P. (1981). Protein-stabilized foams and emulsions. *CRC Critical Reviews in Food Science & Nutrition*, 15, 155–203. <http://doi.org/10.1080/10408398109527315>.
 27. Lupatini, A. L., Colla, L. M., Canan, C., & Colla, E. (2017). Potential application of microalga *Spirulina platensis* as a protein source. *Journal of the Science of Food and Agriculture*, 97, 724–732. <http://doi.org/10.1002/jsfa.7987>.
 28. Marinova, K. G., Basheva, E. S., Nenova, B., Temelska, M., Mirarefi, A. Y., Campbell, B., et al. (2009). Physico-chemical factors controlling the foamability and foam stability of milk proteins: Sodium caseinate and whey protein concentrates. *Food Hydrocolloids*, 23, 1864–1876. <http://doi.org/10.1016/J.FOODHYD.2009.03.003>.
 29. Matos, Â. P. (2017). The impact of microalgae in food science and technology. *Journal of the American Oil Chemists' Society*, 94, 1333–1350. <http://doi.org/10.1007/s11746-017-3050-7>.
 30. Mezzenga, R., & Fischer, P. (2013). The self-assembly, aggregation and phase transitions of food protein systems in one, two and three dimensions. *Reports on Progress in Physics*, 76, 046601 <http://doi.org/10.1088/0034-4885/76/4/046601>.
 31. Mitropoulos, V., Mütze, A., & Fischer, P. (2014). Mechanical properties of protein adsorption layers at the air/water and oil/water interface: A comparison in light of the thermodynamical stability of proteins. *Advances in Colloid and Interface Science*, 206, 195–206. <http://doi.org/10.1016/J.CIS.2013.11.004>.
 32. Müller-Fischer, N., Suppiger, D., & Windhab, E. J. (2007). Impact of static pressure and volumetric energy input on the microstructure of food foam whipped in a rotor–stator device. *Journal of Food Engineering*, 80, 306–316. <http://doi.org/10.1016/J.JFOODENG.2006.05.026>.
 33. Nicorescu, I., Vial, C., Talansier, E., Lechevalier, V., Loisel, C., Della Valle, D., et al. (2011). Comparative effect of thermal treatment on the physicochemical properties of whey and egg white protein foams. *Food Hydrocolloids*, 25, 797–808. <http://doi.org/10.1016/J.FOODHYD.2010.09.020>.
 34. Nirmala, C., Prakash, V., & Venkataraman, L. V. (1992). Physico-chemical and functional properties of proteins from spray dried algae (*Spirulina platensis*). *Food/Nahrung*, 36, 569–577.

- <http://doi.org/10.1002/food.19920360608>.
35. Norwood, E.-A., Le Floch-Fouéré, C., Briard-Bion, V., Schuck, P., Croguennec, T., & Jeantet, R. (2016). Structural markers of the evolution of whey protein isolate powder during aging and effects on foaming properties. *Journal of Dairy Science*, 99, 5265–5272. <http://doi.org/10.3168/jds.2015-10788>.
 36. Peng, D., Yang, J., Li, J., Tang, C., & Li, B. (2017). Foams stabilized by β -lactoglobulin amyloid fibrils: Effect of pH. *Journal of Agricultural and Food Chemistry*, 65, 10658–10665. <http://doi.org/10.1021/acs.jafc.7b03669>.
 37. Pugh, R. J. (1996). Foaming, foam films, antifoaming and defoaming. *Advances in Colloid and Interface Science*, 64, 67–142. [http://doi.org/10.1016/0001-8686\(95\)00280-4](http://doi.org/10.1016/0001-8686(95)00280-4).
 38. Singhal, A., Stone, A. K., Vandenberg, A., Tyler, R., & Nickerson, M. T. (2016). Effect of genotype on the physicochemical and functional attributes of faba bean (*Vicia faba* L.) protein isolates. *Food Science and Biotechnology*, 25, 1513–1522. <http://doi.org/10.1007/s10068-016-0235-z>.
 39. Smetana, S., Sandmann, M., Rohn, S., Pleissner, D., & Heinz, V. (2017). Autotrophic and heterotrophic microalgae and cyanobacteria cultivation for food and feed: Life cycle assessment. *Bioresource Technology*, 245, 162–170. <http://doi.org/10.1016/j.biortech.2017.08.113>.
 40. Smith, D. M. (2017). Protein separation and characterization procedures. In S. Nielsen (Ed.). *Food analysis*. Food science text series. (pp. 431–453). Cham: Springer. <https://doi.org/10.1007/978-3-319-45776-5>
 41. Voorhees, P. W. (1985). The theory of Ostwald ripening. *Journal of Statistical Physics*, 38, 231–252. <http://doi.org/10.1007/BF01017860>.
 42. Waghmare, A. G., Salve, M. K., LeBlanc, J. G., & Arya, S. S. (2016). Concentration and characterization of microalgae proteins from *Chlorella pyrenoidosa*. *Bioresources and Bioprocessing*, 3, 16. <http://doi.org/10.1186/s40643-016-0094-8>.
 43. Wierenga, P. A., Meinders, M. B. J., Egmond, M. R., Voragen, F. A. G. J., & de Jongh, H. H. J. (2003). Protein exposed hydrophobicity reduces the kinetic barrier for adsorption of ovalbumin to the air–water interface. *Langmuir*, 19, 8964–8970. <http://doi.org/10.1021/LA034868P>.
 44. Wilson, A. J. (Ed.). (1989). *Foams: Physics, chemistry and structure* London: Springer <http://doi.org/10.1007/978-1-4471-3807-5>.
 45. Wong, K. H., Cheung, P. C. K., & Ang, P. O., Jr. (2004). Nutritional evaluation of protein concentrates isolated from two red seaweeds: *Hypnea charoides* and *Hypnea japonica* in growing rats. *Hydrobiologia*, 512, 271–278. <http://doi.org/10.1023/B:HYDR.0000020337.13945.20>.
 46. Zayas, J. F. (1997). Foaming properties of proteins. In J. F. Zayas (Ed.). *Functionality of proteins in food* (pp. 262–309). Berlin, Heidelberg: Springer. http://doi.org/10.1007/978-3-642-59116-7_6.
 47. Zhang, Z., Dalgleish, D., & Goff, H. (2004). Effect of pH and ionic strength on competitive protein adsorption to air/water interfaces in aqueous foams made with mixed milk proteins. *Colloids and Surfaces B: Biointerfaces*, 34, 113–121. <http://doi.org/10.1016/j.colsurfb.2003.11.009>.
 48. Zhang, S., & Sun, Y. (2002). Ionic strength dependence of protein adsorption to dye-ligand adsorbents. *AIChE Journal*, 48, 178–186. <http://doi.org/10.1002/aic.690480118>.

MANUSCRIPT 5

Pulsed electric field based cyclic protein extraction of microalgae towards closed-loop biorefinery concepts

Leandro Buchmann, Ivrainia Brandle, Iris Haberkorn, Michele Hiestand, Alexander Mathys*

ETH Zurich, Department of Health Sciences and Technology, Institute of Food Nutrition and Health, IFNH, Laboratory of Sustainable Food Processing, Schmelzbergstrasse 9, Zurich 8092, Switzerland

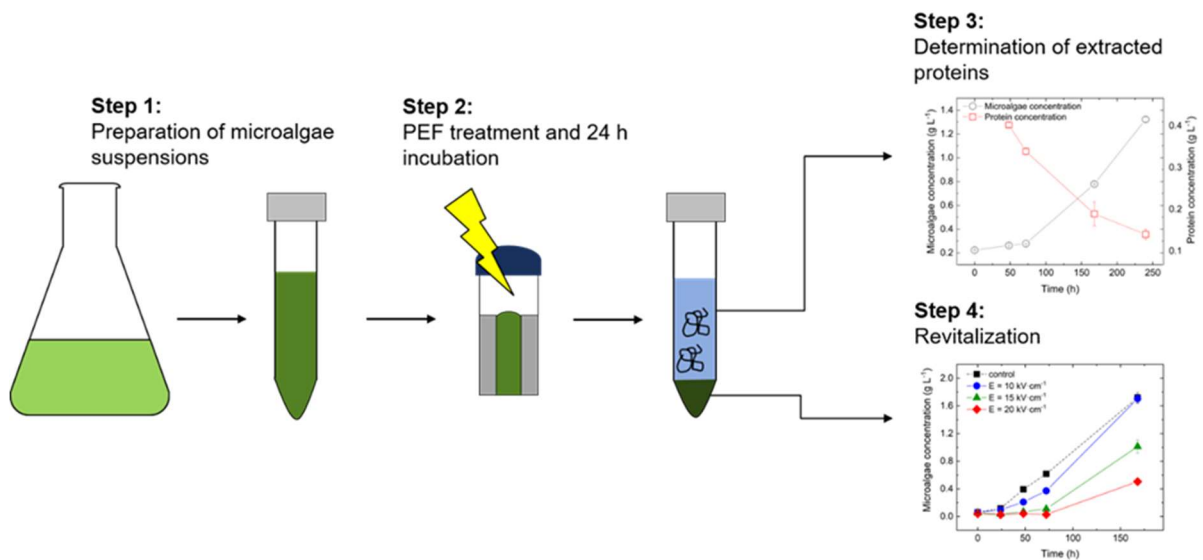
**Corresponding author*

Bioresource Technology 291 (2019) 121870

ABSTRACT

Microalgae-based biorefinery concepts can contribute to providing sufficient resources for a growing world population. However, the performance needs to be improved, which requires innovative technologies and processes. Continuous extraction from *Chlorella vulgaris* cultures via pulsed electric field (PEF) processing might be a viable process to increase the performance of microalgae-based biorefinery concepts. In this study, increasing protein extraction rates were observed with increasing electric field strength, up to $96.6 \pm 4.8\%$ of the free protein in the microalgae. However, increased extraction rates negatively influenced microalgae growth after PEF treatment. A free protein extraction rate up to $29.1 \pm 1.1\%$ without a significant influence on microalgal growth after 168 h was achieved ($p = 0.788$). Within the scope of this work, a protocol for continuous protein extraction during microalgae cultivation by PEF processing was developed. The incorporation of innovative downstream into upstream processing could be a viable future concept.

GRAPHICAL ABSTRACT



1. INTRODUCTION

The world population is expected to reach 9.8 billion people by 2050 (United Nations, 2017). Thereby, the demand for arable land independent sustainable resources is increasing (Alexandratos and Bruinsma, 2012; Chaudhary et al., 2018). Microalgae such as *Chlorella vulgaris* are possible resources to meet this demand.

C. vulgaris is a popular species in the bio-based industry because of its high protein and lipid content. *C. vulgaris* can not only be used for biofuel production but also as a novel food source (Becker, 2013; Brennan and Owende, 2010; Caporgno and Mathys, 2018). The annual production of *Chlorella* species amounts to approximately 5000 metric tons (Masojídek and Torzillo, 2014). However, current cultivation systems are not yet competitive compared with other established sources (Smetana et al., 2017). One way to increase the performance of microalgae-based biorefineries is growth stimulation or selective microbial inactivation via nanosecond pulsed electric field (nsPEF) processing, an innovative technology in microalgae upstream processing (Buchmann et al., 2019a,b, 2018a). However, further improvements in downstream processing are required to overcome limitations regarding the high production costs of microalgae derived from the growth medium, energy supply and intensive extraction procedures for valuable compounds (Enzing et al., 2014; Golberg et al., 2016).

C. vulgaris possesses a rigid cell wall, which protects the microalgae against harsh environmental conditions (Safi et al., 2014). However, this rigid cell wall causes low bioavailability of microalgae constituents for human digestion. Therefore, the disintegration of microalgae cells is necessary to release microalgal constituents (Becker, 2007). Currently, energy-intensive downstream processes, including the harvesting of biomass, cell disruption and drying of the extracted components, are required (Enzing et al., 2014; Golberg et al., 2016).

Pulsed electric field (PEF) processing of fresh microalgae biomass could be a potential solution to realize a closed loop biorefinery concept. PEF processing is extensively investigated as an innovative nonthermal technique to increase mass transfer across cellular membranes (Golberg et al., 2016; Toepfl et al., 2007). However, PEF-based extraction of cell constituents showed lower yields compared to other established extraction processes (Carullo et al., 2018; Grimi et al., 2014). Nevertheless, pulsed electric field processing can be applied reversibly or irreversibly, depending on the selected parameters (Luengo et al., 2015a). Reversible

electropermeabilization is widely used for the insertion of molecules into cells, whereas irreversible electropermeabilization is widely used for microbial inactivation and cancer treatment (Campana et al., 2016; Stacey et al., 2003). Applying PEF in a reversible way increases the mass transfer across the cell membrane without impeding the cell's physiological state (Luengo et al., 2015a). In addition, the extractable cell constituents after PEF processing depend on the suspending fluid (Goettel et al., 2013). Therefore, combining PEF processing with membrane technology could allow for continuous cascade processing of microalgae (Bleakley and Hayes, 2017; Goettel et al., 2013).

Based on these findings, the aim of this project was to assess the ability of PEF processing to extract microalgal proteins from viable cell cultures, towards the implementation of PEF processing in a closed-loop biorefinery concept.

2. MATERIAL AND METHODS

2.1. Raw materials

Chlorella vulgaris SAG 211-12 was obtained from the Culture Collection of Algae at Goettingen University (SAG, Goettingen, Germany). First, 50 mL of *C. vulgaris* was inoculated one week prior to experiments in 350 mL of DSN cultivation medium in a 1-L Erlenmeyer flask (Pohl et al., 1987). The initial dry weight (DW) of *C. vulgaris* was standardized to 0.3 g L⁻¹. *C. vulgaris* was cultivated under autotrophic and non-axenic growth conditions. The cultures were incubated at 25 ± 0.2 °C, 70% relative humidity, 150 rpm, 7% v/v CO₂, and continuous illumination with a mean photosynthetically active photon flux density (PPFD) of 36 μmol photons m⁻² s⁻¹ using warm white LED lamps in a shaking incubator (Multitron Pro shaking incubator, Infors AG, Bottmingen, Switzerland). The growth of *C. vulgaris* was monitored by optical density (OD) measurements at 750 nm (GENESYS™ 10S, Thermo Fischer Scientific Inc., Waltham, MA, USA). The correlation factor between OD and DW is shown in Eq. (1) (R² = 0.9971):

$$DW(g L^{-1}) = 0.3712 \cdot OD_{750nm} + 0.0672 \quad (1)$$

2.2. Sample preparation

Prior to the cell disruption processes, the concentration and conductivity of the microalgae cultures were standardized. For all PEF experiments, a microalgae concentration of 6 g L⁻¹ was used. Through centrifugation (1780 g, 5 min), the microalgae biomass was separated from the supernatant (Centrifuge Z 366 K, Hermle Labortechnik GmbH, Wehingen, Germany). Subsequently, the supernatant was removed and the microalgae biomass was resuspended in 151.7 mM phosphate buffered saline (PBS), adjusted to a conductivity σ (mS cm⁻¹) of 2 mS cm⁻¹ and pH = 7. The conductivity adjustment was necessary to achieve matched load conditions in subsequent PEF treatments. Directly after the preparation of the microalgae suspensions, the conductivity was measured and the pH of the microalgae suspension was monitored. Following a mixing step, 0.5 mL aliquots of the microalgae suspensions were transferred to electroporation cuvettes for PEF treatment.

In addition to this standard protocol, the influence of the treatment fluid on the protein extraction and recovery rate was analyzed. Therefore, the cultivation media DSN

(Pohl et al., 1987) was used as a treatment fluid without conductivity adjustment, after dry weight standardization. The resulting mismatched load conditions were accounted for in the energy input calculations (Buchmann et al., 2018b).

2.3. Pulsed electric field (PEF) treatment

The samples were treated batch wise in plate-plate electroporation cuvettes at 2 mm electrode distance, resulting in electric field strengths of up to 20 kV cm⁻¹ (BTX cuvettes, Harvard Apparatus, Holliston MA, USA). Hence, a homogenous treatment resulting in a homogenous energy input was achieved (Buchmann et al., 2018a,b). The experimental setup consisted of a cuvette holder connected to a TSS 500 pulse generator (EM Test, Reinach, Switzerland). The pulse generator was capable of exponential decay pulses with a pulse width of 50 µs and a varying pulse amplitude from 1 V to 4000 V. Pulse measurements were conducted with a P6015A voltage probe (Tektronix Inc., Beaverton OR, USA) connected to a Wave Surfer 10 oscilloscope (Teledyne LeCroy GmbH, Heidelberg, Germany). For further information regarding the experimental setup, refer to Buchmann et al. (2018b).

2.4. Protein extraction by high-pressure homogenization

Protein extraction by high-pressure homogenization (HPH) was carried out in order to compare two different extraction methods for microalgal cell constituents. According to Safi et al. (2015), high-pressure homogenization is one of the most efficient extraction methods. Thus, this method was selected as the reference process. For each sample, 2 mL of microalgae suspension were transferred to an HPH (Cell Disruptor, Constant Systems Limited, Daventry, UK). The microalgae cells were treated with 100 MPa.

Subsequent determination of the protein content was performed in accordance with the protocol described below (Section 2.5). However, the protein concentration was evaluated directly after the HPH process without an additional incubation period, as preliminary results indicated no increase in protein extraction with an extended incubation period.

2.5. Protein quantification

Following PEF treatment, the cuvettes were placed on a shaking plate (150 rpm) at ambient conditions for 24 h. The 24 h incubation period was derived from preliminary

results. Following the incubation period, proteins were quantified by a colorimetric protein assay kit (Bradford Reagent, VWR International, Radnor, PA, USA) (Bradford, 1976).

Protein quantification was conducted after centrifugation (5000 g, 5 min) of the microalgae suspensions, separating the biomass from the protein-containing supernatant. The standard manufacturer VWR protocol was followed, with an incubation time of 10 min. Subsequently, the absorbance at 595 nm was measured by UV–Vis spectroscopy (GENESYS™ 10S, Thermo Fischer Scientific Inc., Waltham, MA, USA). In addition to this standard protocol, the influence of the incubation fluid on the protein extraction and recovery rate was analyzed. Therefore, microalgae were transferred to DSN medium for the incubation period, instead of PBS. Directly after PEF treatment, microalgal samples were separated from PBS by centrifugation (5000 g, 5 min). Then, the PBS was removed and replaced by the same amount of DSN medium per sample. In the case of DSN as the treatment fluid, the incubation was directly carried out in DSN as well, equivalent to the sole PBS protocol, without an additional centrifugation step.

Determination of the total protein concentration was carried out by amino acid analysis (AAA) at the Functional Genomics Center Zurich (FGCZ), Switzerland. The AAA was carried out with a microalgae concentration of 6 g L⁻¹.

2.6. Microalgae revitalization

Microalgae revitalization was conducted by inoculation of the whole incubation volume in 10 mL of DSN medium in a sterilized 100-ml Erlenmeyer flask. Following DW determination, another 25 mL of DSN medium were added. This sequential DSN addition was necessary to reduce the dilution of the microalgae culture for DW determination. All samples were incubated at equal cultivation conditions as described above (Chapter 2.1). The growth curves of the revitalized samples were monitored over 168 h. The microalgae revitalization was assessed by the recovery rate (Eq. (2)):

$$\text{Recovery rate (\%)} = (\text{Treatment}_{\text{DW}} / \text{Control}_{\text{DW}}) \cdot 100. \quad (2)$$

2.7. Proteomic analysis

A shotgun analysis, liquid chromatography and mass spectrometry (LC-MS), of extracted proteins from *C. vulgaris* was conducted at the Functional Genomics Center

Zurich (FGCZ), Switzerland. Proteins extracted by PEF were compared to proteins extracted by high-pressure homogenization.

The subsequent results are based on the SWISS-PROT database search. The database contains approximately 560,000 different proteins and a sequenced *C. vulgaris* SAG 211-12 strain. *C. vulgaris* has approximately 7100 protein-coding genes (Zuñiga et al., 2016). The data were analyzed applying very stringent settings (protein threshold 1% FDR, min # peptides 2 and peptide threshold 0.1% FDR).

The total spectra with normalization and a minimum value of 0.5 were investigated. Further information regarding the proteomic analysis can be found in Buchmann et al. (2019b).

2.8. Statistical analysis

The statistical analysis was conducted using IBM SPSS Statistics® (Version 24.0., IBM Corp., Armonk NY, USA). The equality of variance for the compared groups was tested using Levene's test. Subsequently, one-way ANOVA was performed, followed by a post hoc Tukey's HSD test. A confidence interval of 95% for all statistical evaluations was used. Proteomic results were analyzed by an analysis of variance with a 95% confidence interval, including a Benjamini-Hochberg correction.

3. RESULTS AND DISCUSSION

The absolute protein concentration of the investigated *C. vulgaris* suspension obtained by the AAA amounted to 2.87 g L^{-1} and 2.71 g L^{-1} . Consequently, the microalgae culture used consisted of $46.46 \pm 0.01\%$ protein. This total protein concentration of *C. vulgaris* agrees with the literature, where a total protein content of *C. vulgaris* between 42 and 58 % was found (Safi et al., 2014).

The energy inputs of the PEF experiments performed in PBS or in DSN fluid are compared in Table 1. The theoretical applied electric field strength and the actual measured electric field strength must be distinguished. The actual measured electric field strength is lower than the theoretical. Furthermore, the measured electric field strength of experiments conducted in DSN is significantly lower compared to the experiments conducted in PBS. The higher conductivity of DSN results in mismatched load conditions. Consequently, for equal theoretical PEF parameters, the energy inputs of experiments performed with DSN as the treatment fluid are lower compared to the energy inputs of experiments performed with PBS as the treatment fluid. No temperature influence could be detected across all PEF parameters, with a temperature increase of $< 5 \text{ }^\circ\text{C}$ for all investigated conditions.

M5 - Table 1: Resulting energy inputs for different electric field strengths and incubation fluids in PEF treatments using a 2 mm electroporation cuvette, with electric field strength E (kV cm^{-1}), conductivity σ (mS cm^{-1}), number of pulses n (-) and energy input W ($\text{kJ kg}_{\text{Sus}}^{-1}$).

Incubation fluid	Theoretical E	Measured E	σ	n	ΔW
(-)	(kV cm^{-1})	(kV cm^{-1})	(mS cm^{-1})	(-)	($\text{kJ kg}_{\text{Sus}}^{-1}$)
PBS	10	9.24 ± 0.32	1.9 ± 0.1	2	1.94 ± 0.01
PBS	15	13.86 ± 0.48	1.9 ± 0.1	2	4.37 ± 0.02
PBS	20	18.47 ± 0.63	1.9 ± 0.1	2	7.76 ± 0.04
DSN	10	2.83 ± 0.01	9.7 ± 0.04	2	0.95 ± 0.001
DSN	15	4.24 ± 0.02	9.7 ± 0.04	2	2.13 ± 0.006
DSN	20	5.64 ± 0.02	9.7 ± 0.04	2	3.79 ± 0.01

For increased readability, the electric field strength is stated as the theoretical electric field strength in the manuscript. The energy input for the high-pressure homogenization was $400 \text{ kJ kg}_{\text{Sus}}^{-1}$ for each pass and two subsequent passes were

applied in order to ensure complete disintegration of the cells.

3.1. Optimization of PEF-based protein extraction

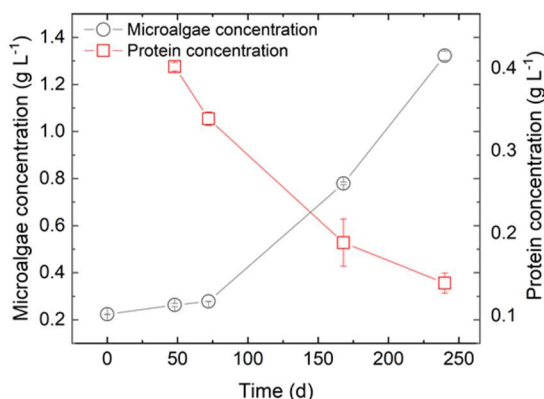
The influence of the electric field strength on protein extraction was analyzed in order to optimize the PEF-based protein extraction. Therefore, the number of pulses was adjusted to obtain an equal energy input ($7.76 \pm 0.04 \text{ kJ kg}_{\text{SUS}}^{-1}$) for both electric field strengths (10 and 20 kV cm^{-1}). Based on the energy input calculation, differences in the electric field strength can be accounted for by adjusting the number of applied pulses; for further information, refer to Buchmann et al. (2019b). The results indicate a dependency of the protein extraction on the electric field strength. An electric field strength of 10 kV cm^{-1} resulted in an average protein extraction of $0.55 \pm 0.01 \text{ g L}^{-1}$, whereas for an electric field strength of 20 kV cm^{-1} , a protein concentration of $0.80 \pm 0.04 \text{ g L}^{-1}$ was extracted. The results are in agreement with the common theory of electroporation, for which a critical electric field needs to be exceeded in order to cause PEF-based effects on biological cells (Grahl and Märkl, 1996; Teissie and Tsong, 1981; Zimmermann et al., 1974). Thereby, the size of the permeable structures is crucial for the extraction efficiency, since it determines the size of the molecules that are able to cross the cell membrane (Saulis, 2010). Based on the assumption that the mass transfer across the cell membrane is diffusion limited, protein extraction rates were analyzed over a prolonged time period (Puc et al., 2003). Overall protein extraction rates increased with time, reaching a maximum after 24 h. Therefore, protein extraction by PEF was followed by a 24 h incubation in order to maximize protein extraction efficiency.

As the average protein concentration did not change significantly with the increasing number of pulses, the pulse number was set to two (data not shown). This parameter was the lowest possible value where no influence on the protein extraction rate was observed. These results are in agreement with literature where after a certain threshold extraction was not enhanced by increasing the number of applied pulses (Luengo et al., 2015b). Thus, the energy input could be reduced with an unaffected protein extraction rate. However, based on preliminary results, the overall protein extraction rate strongly depends on the microalgae growth state. According to Yamamoto et al. (2004), the thickness and number of cell walls changes during the autospore formation of *C. vulgaris*. Hence, *C. vulgaris* has a thinner cell wall in the early growth phase compared to later phases. It is therefore hypothesized that protein

extraction rates are higher for microalgae in the early growth phase. The influence of microalgal growth phase was analyzed by PEF treatments of microalgae cultures over the whole cultivation cycle.

3.2. Protein extraction by PEF in dependency of microalgae growth phase

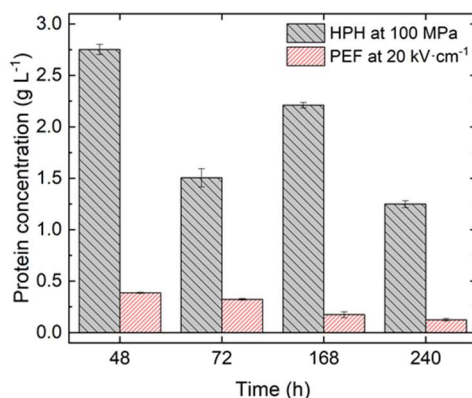
The PEF parameters were based on the obtained results with regard to overall protein extraction efficiency, set to an electric field strength of 20 kV cm^{-1} and two applied pulses. The concentration of extracted protein decreased over time (Fig. 1). Therefore, the extraction of protein from microalgae seems to be strongly dependent on their growth phase. The absolute amount of extracted protein decreased by 32.3% from the first PEF treatment after 48 h ($0.39 \pm 0.01 \text{ g L}^{-1}$) of cultivation to the last PEF treatment after 240 h of cultivation ($0.12 \pm 0.01 \text{ g L}^{-1}$). A possible reason for the decrease in protein extraction is the increased thickness of the cell wall over the growth phases (Yamamoto et al., 2004). A thicker cell wall may hamper the formation of permeable structures by PEF and hence protein diffusion, as the induced transmembrane potential is negatively affected (Marszalek et al., 1990; Teissie and Tsong, 1981). Another possible reason for the decrease in protein extraction is that the concentration of extractable protein itself may vary over time (Safi et al., 2014). However, the diffusion-driven process allows the extraction of soluble compounds while potentially insoluble compounds are concentrated within the intact microalgal cell.



M5 - Figure 1: Extractable protein concentration dependence of *Chlorella vulgaris* growth state with an electric field strength of 20 kV cm^{-1} and two applied pulses resulting in an energy input of $7.76 \pm 0.04 \text{ kJ kg}_{\text{Sus}}^{-1}$.

The change in overall extracted proteins was analyzed by comparing the PEF

treatments to a reference high-pressure homogenization treatment, which, according to Safi et al. (2015), is one of the most efficient extraction methods (Fig. 2).



M5 - Figure 2: Comparison of the overall extracted protein concentration by HPH at 100 MPa and PEF treatments at 20 kV cm⁻¹ over the cultivation cycle of *Chlorella vulgaris*.

Comparing the absolute protein extraction rates, HPH treatments appear to be superior to PEF treatments (Fig. 2). These results agree with the literature, where a low protein extraction rate by PEF treatment was found in comparison to HPH (‘t Lam et al., 2017; Carullo et al., 2018; Postma et al., 2016). However, the HPH treatment results in a complete disintegration of the microalgal cells, whereas the PEF treatment results in visually intact microalgal cells. Moreover, the supernatant after PEF treatment was transparent, whereas the supernatant after HPH treatment turned green, indicating the disruption of the chloroplast by HPH. This observation indicates that internal cell structures are not irreversibly affected by PEF, and thus, only free protein can be released from the cell. Structural proteins of membranes and organelles do not appear to be available within the chosen treatment parameters; thus, protein extraction by PEF results in lower absolute yields (Fig. 2, Table 2). However, as with the chosen parameters, mostly the outer cell membrane seems to be permeabilized, the extractable protein concentrations might differ from the absolute protein concentration (Safi et al., 2015, 2014). The initial microalgal dry weight in the treated samples was 6 g L⁻¹, with 46.46 ± 0.01% being proteins. Of these, only 30% are freely available and are therefore available for reversible PEF-based extractions (Berliner, 1986; Safi et al., 2014). With respect to the resulting free protein concentration, PEF yields extraction rates up to 96.6 ± 4.8%.

3.3. Cellular origin of PEF- and HPH-based extracted proteins

A shotgun proteomic analysis was conducted in order to investigate the cellular origin of PEF- and HPH-based extracted proteins. Overall, 1583 proteins were identified using the settings described in Section 2.7. Mostly proteins found in the thylakoid membrane of the chloroplast were significantly increased in the supernatant from HPH-treated microalgae compared to PEF-treated (Table 2). Other significantly increased proteins were from the inner mitochondrial membrane and chloroplast (Table 2). These results support the theory that only free protein can be extracted by PEF, as organelle-related and structural proteins were significantly increased after HPH processing. Comparing the absolute protein extraction efficiency, PEF processing within the chosen parameters cannot compete with HPH processing. However, considering that only 30% of the total protein content from *C. vulgaris* is freely available, reversible PEF can yield up to $96.6 \pm 4.8\%$ of this protein fraction (Berliner, 1986). Moreover, the aim of this research was not the optimization of PEF-assisted absolute protein extraction, but rather a continuous extraction of proteins from viable microalgae cultures. Therefore, an investigation of the recovery levels of PEF-treated microalgae was conducted.

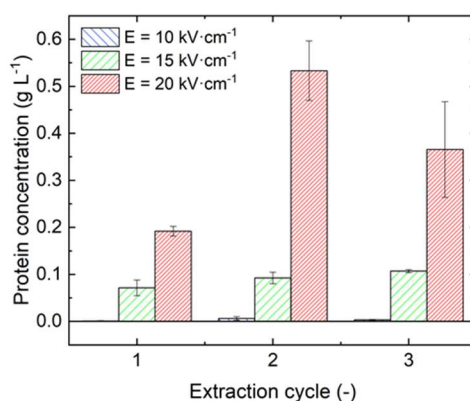
M5 - Table 2: Significantly increased proteins in the supernatant of HPH-treated *Chlorella vulgaris* in comparison to PEF-treated samples, analyzed by a proteomic shotgun analysis.

Identified proteins	p-values
Cluster of Photosystem II D2 protein OS= <i>Chlorella vulgaris</i> OX=3077 GN=psbD PE=3 SV=1 (PSBD_CHLVU)	p < 0.00010
Cluster of Photosystem II CP47 reaction center protein OS= <i>Chlorella vulgaris</i> OX=3077 GN=psbB PE=3 SV=1 (PSBB_CHLVU)	p < 0.00010
Cluster of Photosystem II protein D1 OS= <i>Chlorella vulgaris</i> OX=3077 GN=psbA PE=3 SV=1 (PSBA_CHLVU)	p < 0.00010
Cluster of Photosystem I P700 chlorophyll a apoprotein A2 OS= <i>Chlorella vulgaris</i> OX=3077 GN=psaB PE=3 SV=1 (PSAB_CHLVU)	p < 0.00010
Cluster of Photosystem II CP43 reaction center protein OS= <i>Chlorella vulgaris</i> OX=3077 GN=psbC PE=3 SV=1 (PSBC_CHLVU)	p = 0.00011
Cytochrome b559 subunit alpha OS= <i>Chlorella vulgaris</i> OX=3077 GN=psbE PE=3 SV=1	p = 0.00024
Cluster of ATP synthase subunit beta, chloroplastic OS= <i>Chlorella vulgaris</i> OX=3077 GN=atpB PE=3 SV=1 (ATPB_CHLVU)	p = 0.00024

Cluster of ATP synthase subunit alpha, chloroplastic OS= <i>Chlorella vulgaris</i> OX=3077 GN=atpA PE=3 SV=1 (ATPA_CHLVU)	p = 0.00096
Cluster of Cytochrome f OS= <i>Chlorella vulgaris</i> OX=3077 GN=petA PE=3 SV=2 (CYF_CHLVU)	p = 0.0016
Cluster of ADP,ATP carrier protein OS= <i>Parachlorella kessleri</i> OX=3074 PE=3 SV=1 (ADT_PARKE)	p = 0.00035
50S ribosomal protein L12, chloroplastic OS= <i>Chlorella vulgaris</i> OX=3077 GN=rpl12 PE=3 SV=1	p = 0.0010
30S ribosomal protein S4, chloroplastic OS= <i>Chlorella vulgaris</i> OX=3077 GN=rps4 PE=3 SV=1	p = 0.00042

3.4. Continuous microalgae cultivation with PEF-assisted protein extraction

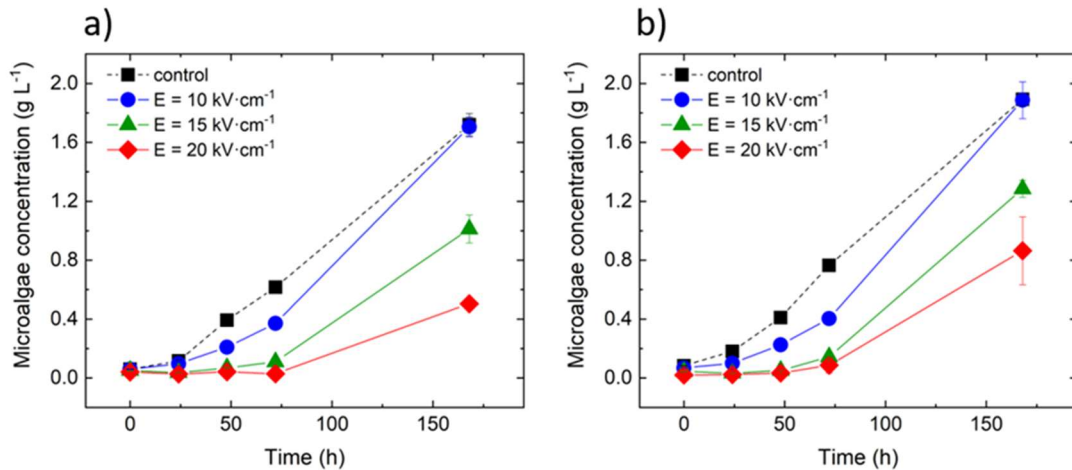
Based on the preliminary results, continuous microalgae cultivation with PEF-assisted protein extraction was analyzed for 10, 15 and 20 kV cm⁻¹. As the PEF-based protein extraction was found to be mainly electric field strength dependent, within the chosen parameter range, the number of pulses was set to two. Thereby, the energy input was minimized without affecting the protein extraction rates.



M5 - Figure 3: Protein extraction for two applied pulses at an electric field strength of 10, 15 and 20 kV cm⁻¹ resulting in 1.94 ± 0.01 , 4.37 ± 0.02 and 7.76 ± 0.04 kJ kg_{SUS}⁻¹, respectively, and three subsequent PEF treatment cycles with 168 h of cultivation in-between.

For an electric field strength of 10 kV cm⁻¹, no significant protein extraction was found. The protein extraction rate at an electric field strength of 20 kV cm⁻¹ resulted in the highest protein extraction rate. These results are in agreement with the above results for the maximum protein extraction rate. Moreover, the protein extraction rate was stable over the three cycles (Fig. 3, Table 3). The different extraction rates for 20 kV

cm^{-1} can mainly be attributed to the different recovery levels of the microalgae cultures and subsequent different growth phases prior to the treatment. The influence of the growth phase on protein extraction was elucidated in Section 3.1. The results indicate that protein extraction in an early growth phase is higher than that in later growth phases.



M5 - Figure 4: Algae recovery levels after a) the first and b) the second PEF cycle with two applied pulses at an electric field strength of 10, 15 and 20 kV cm⁻¹, resulting in 1.94 ± 0.01 , 4.37 ± 0.02 and 7.76 ± 0.04 kJ kg_{Sus}⁻¹, respectively, in comparison to the control.

The microalgae treated with an electric field strength of 10 kV cm⁻¹ fully recovered 168 h after the PEF treatments with a recovery rate of $99.5 \pm 8.3\%$ (Fig. 4a) and $93.8 \pm 6.7\%$ (Fig. 4b). PEF treatments at an electric field strength of 15 kV cm⁻¹ resulted in a recovery rate of $59.2 \pm 8.2\%$ (Fig. 4a) and $68.0 \pm 4.5\%$ (Fig. 4b) after 168 h. At an electric field strength of 20 kV cm⁻¹, the microalgae recovery rate after 168 h was $29.4 \pm 2.7\%$ (Fig. 4a) and $46.0 \pm 13.2\%$ (Fig. 4b). The free protein extraction rate and recovery rate for the investigated electric field strengths are summarized in Table 3.

M5 - Table 3: Free protein extraction and recovery rate for multiple extraction cycles at theoretical electric field strengths of 10, 15 and 20 kV cm⁻¹. The same letters indicate nonstatistical significance at a 95% confidence interval for the free protein extraction rate over the three extraction cycles.

Theoretical E [kV cm ⁻¹]	Free protein extraction rate [%] (Recovery rate [%])		
	1 st cycle	2 nd cycle	3 rd cycle
10	0.1 ± 0.1 ^a (99.5 ± 8.3)	0.8 ± 0.4 ^a (99.9 ± 8.8)	0.4 ± 0.1 ^a
15	8.6 ± 2.0 ^b (59.2 ± 8.2)	11.2 ± 1.5 ^b (68.0 ± 4.5)	12.9 ± 0.4 ^b
20	23.2 ± 1.3 (29.4 ± 2.7)	64.4 ± 7.6 (46.0 ± 13.2)	44.2 ± 12.3

^a p = 0.997., ^b p = 0.811.

The results indicate that the higher the protein extraction, the lower is the recovery level, thus the severity of PEF induced effects increases. Moreover, the lag phase after the PEF treatment is more pronounced if higher protein concentrations are extracted. Nevertheless, the results for the three cycles at 10 kV cm⁻¹ or 15 kV cm⁻¹ are not statistically significant different (Table 3), indicating a stable process and no long-term influence of PEF on microalgae recovery or composition with respect to a cultivation of 168 h between the treatments.

3.5. Influence of the incubation and treatment fluid on the protein extraction and microalgae recovery rates

To achieve matched load conditions, the PEF treatments were conducted in 151.7 mM PBS adjusted to a conductivity of 2 mS cm⁻¹ and pH = 7. Based on preliminary data indicating that the protein extraction after PEF is diffusion limited, the incubation in high conductive (10 mS cm⁻¹) DSN medium was hypothesized to increase the overall protein extraction. Moreover, as DSN medium was used to cultivate the microalgae, a physiological benefit was hypothesized, as microalgae were incubated in their respective cultivation media and therefore the recovery rate should be increased as well. In the first step, the influence of the incubation fluid on the protein extraction was analyzed.

The protein extraction was significantly higher if DSN medium was used as the incubation fluid. DSN medium as the incubation fluid resulted in a free protein extraction rate of 52.9 ± 7.1% for an electric field strength of 20 kV cm⁻¹. In contrast, PBS as the incubation fluid resulted in a free protein extraction rate of 23.2 ± 1.3%

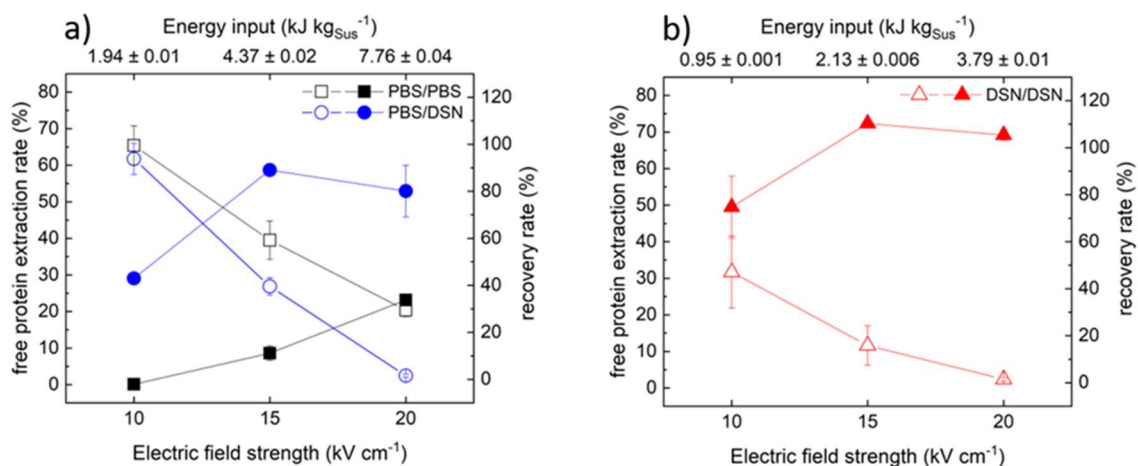
for equal PEF parameters (Table 1). With regard to the recovery rate, the same trends as for the PBS/PBS system were observed. The time-dependent recovery rate after PEF processing reached $93.8 \pm 6.7\%$, $39.6 \pm 3.7\%$ and $1.6 \pm 0.7\%$ at an electric field strength of 10, 15 and 20 kV cm^{-1} , respectively (Fig. 5).

The hypothesis of an increased protein extraction at higher ionic strengths of the incubation fluid and therefore higher diffusion gradient appears to be verified. The results indicate that high conductive incubation fluids facilitate diffusion of proteins through permeable structures, as similar electric field strengths in PBS resulted in no significant protein extraction. Therefore, the overall performance of the DSN medium was assessed using DSN as the treatment and as the incubation fluid. The higher conductivity of the DSN medium resulted in mismatched load conditions. These mismatched load conditions result in partial reflection of the applied voltage and hence lower electric field strengths than actually expected based on the initially applied voltage (Buchmann et al., 2018b). The resulting mismatched load conditions were accounted for in subsequent energy input calculations (Table 1).

The protein extraction of the DSN/DSN system was significantly higher than the extraction rate obtained for the PBS/PBS system (Fig. 5). The free protein extraction rate of the DSN/DSN system resulted in $69.2 \pm 1.4\%$ at an electric field strength of 20 kV cm^{-1} , whereas for the PBS/PBS system, at theoretical equal PEF processing parameters, it resulted in $23.2 \pm 1.3\%$. One explanation for the higher protein extraction rate is the high conductivity of the DSN medium. The increased extracellular conductivity results in an accelerated charging of the membrane (Silve et al., 2016). In addition, the increased conductivity accelerates the diffusion-driven protein extraction, and thus, a lower electric field strength is more efficient compared to low conductive suspending media. This result correlates with the results found for the PBS/DSN system.

The time-dependent recovery rates of the microalgae treated at an electric field strength of 10 and 15 kV cm^{-1} were $47.1 \pm 15.4\%$ and $15.8 \pm 8.5\%$, respectively, lower than the recovery rates of microalgae treated in PBS. The microalgae treated at 20 kV cm^{-1} did not recover at all after 168 h, with a recovery rate of $1.5 \pm 0.7\%$. Due to the correlation of increased protein extraction rate and reduced recovery rate, this trend was expected. However, the hypothesis regarding the beneficial influence of the DSN medium on the overall efficiency of the process with respect to a continuous protein extraction by PEF could

not be verified at this time. Further optimization of the PEF treatment parameters with respect to the microalgae recovery rate could support the DSN/DSN system, as the absolute protein extraction rate is superior at all investigated electric field strengths.



M5 - Figure 5: Free protein extraction rate (full) and recovery rate (hollow) for PEF treatments in a) phosphate buffered saline (PBS) and b) DSN cultivation medium, at theoretical equal PEF parameters (Table 1).

With regard to the free protein extraction efficiency, DSN/DSN performed the best, followed by PBS/DSN and PBS/PBS. However, focusing on an innovative closed-loop biorefinery concept, the recovery rates need to be taken into account as well. Assessment of the overall PEF-based extraction efficiency over multiple cycles was conducted, introducing the cyclic extraction factor as shown in Eq. (3):

$$\text{Cyclic extraction factor (-)} = \text{free protein extraction rate} \cdot \text{recovery rate.} \quad (3)$$

The cyclic extraction factor was used to correct the increased free protein concentration rate with the reduced recovery rate and thereby quantify the overall efficiency of the process (Table 4). The best overall performance is achieved at an electric field strength of $9.24 \pm 0.32 \text{ kV cm}^{-1}$ and two applied pulses. The cyclic extraction factor amounted to 0.273 ± 0.029 with an energy input of $1.94 \pm 0.01 \text{ kJ kg}_{\text{SUS}}^{-1}$. These experimental conditions resulted in a free protein extraction rate of $29.1 \pm 1.1\%$ and a recovery level of $93.8 \pm 6.7\%$ after six days. Considering the cyclic extraction factor, lower electric field strengths outperform higher field strengths, due to the disproportional decrease in the microalgae recovery rate with increasing electric field strength. In order to reach the full potential of the cyclic extraction process based on PEF further research should be conducted in e.g. a chemostat to

increase the overall performance of the process.

M5 - Table 4: Cyclic extraction factor depending on the PEF parameters as well as the treatment and incubation fluid. Specific energy inputs for the individual experiments are shown in Table 1.

PEF parameter		Cyclic extraction factor [-]		
Theoretical E [kV cm ⁻¹]	n	PBS, PBS	PBS, DSN	DSN, DSN
10	2	0.001 ± 0.001	0.273 ± 0.029	0.246 ± 0.116
15	2	0.053 ± 0.019	0.233 ± 0.028	0.115 ± 0.062
20	2	0.069 ± 0.010	0.009 ± 0.005	0.010 ± 0.005

4. CONCLUSIONS

Innovative up- and downstream processes are needed in order to increase the performance of microalgae-based biorefineries. PEF processing allowed the extraction of up to $96.6 \pm 4.8\%$ available free protein. However, the continuous PEF-based extraction showed a trade-off between a high extraction and recovery rate. Applying $1.94 \pm 0.01 \text{ kJ kg}_{\text{sus}}^{-1}$ resulted in the highest cyclic extraction factor and therefore the best process window for continuous extraction from viable cell cultures. Further research should focus on the integration of membrane technology in order to separate the extract from the microalgae cultures inline.

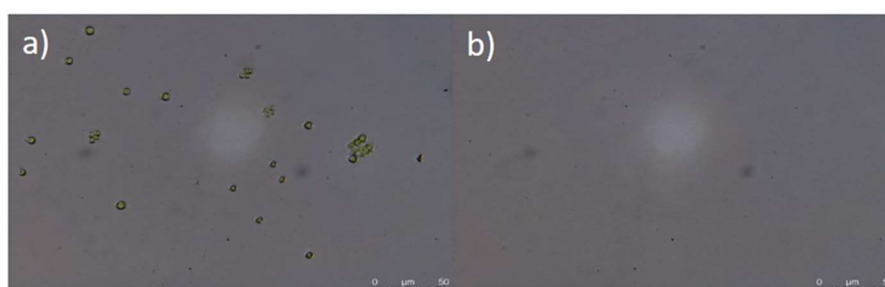
ACKNOWLEDGMENTS

The authors gratefully acknowledge support from the World Food System Center (Project “NewAlgae”, grant number: 2-72235-17); the ETH Zürich Foundation, Switzerland; and Markus Nyffeler from the Swiss Federal Office for Defence Procurement.

CONFLICT OF INTEREST STATEMENT

The authors declare that they have no known competing financial interests or personal relationships that could have appeared to influence the work reported in this paper.

APPENDIX A. SUPPLEMENTARY DATA



M5 - Supplementary Figure 1: Microscopic analysis of *Chlorella vulgaris* a) prior and b) after two subsequent high-pressure homogenization passes.

REFERENCES

1. 't Lam, G.P., Postma, P.R., Fernandes, D.A., Timmermans, R.A.H., Vermuë, M.H., Barbosa, M.J., Eppink, M.H.M., Wijffels, R.H., Olivieri, G., 2017. Pulsed electric field for protein release of the microalgae *Chlorella vulgaris* and *Neochloris oleoabundans*. *Algal Res.* 24, 181–187.
2. Alexandratos, N., Bruinsma, J., 2012. Food and Agriculture Organization, World agriculture towards 2015/2030: The 2012 Revision. ESA Work. Pap. No. 12-03, 147.
3. Becker, E.W., 2013. Microalgae for aquaculture: nutritional aspects. *Handb. Microalgal Cult. Appl. Phycol. Biotechnol.* 671–691.
4. Becker, E.W., 2007. Micro-algae as a source of protein. *Biotechnol. Adv.* 25, 207–210.
5. Berliner, M.D., 1986. Proteins in *Chlorella vulgaris*. *Microbios* 46, 199–203.
6. Bleakley, S., Hayes, M., 2017. Algal proteins: extraction, application, and challenges concerning production. *Foods* 6, 33.
7. Bradford, M.M., 1976. A rapid and sensitive method for the quantitation of microgram quantities of protein utilizing the principle of protein-dye binding. *Anal. Biochem.* 72, 248–254.
8. Brennan, L., Owende, P., 2010. Biofuels from microalgae – A review of technologies for production, processing, and extractions of biofuels and co-products. *Renew. Sustain. Energy Rev.* 14, 557–577.
9. Buchmann, L., Bertsch, P., Böcker, L., Krähenmann, U., Fischer, P., Mathys, A., 2019a. Adsorption kinetics and foaming properties of soluble microalgae fractions at the air/ water interface. *Food Hydrocoll.* 97, 105182.
10. Buchmann, L., Bloch, R., Mathys, A., 2018a. Comprehensive pulsed electric field (PEF) system analysis for microalgae processing. *Bioresour. Technol.* 265, 268–274.
11. Buchmann, L., Böcker, L., Frey, W., Haberkorn, I., Nyffeler, M., Mathys, A., 2018b. Energy input assessment for nanosecond pulsed electric field processing and its application in a case study with *Chlorella vulgaris*. *Innov. Food Sci. Emerg. Technol.* 47, 445–453.
12. Buchmann, L., Frey, W., Gusbeth, C., Ravaynia, P.S., Mathys, A., 2019b. Effect of nanosecond pulsed electric field treatment on cell proliferation of microalgae. *Bioresour. Technol.* 271, 402–408.
13. Campana, L.G., Clover, A.J.P., Valpione, S., Quaglino, P., Gehl, J., Kunte, C., Snoj, M., Cemazar, M., Rossi, C.R., Miklavčič, D., Sersa, G., 2016. Recommendations for improving the quality of reporting clinical electrochemotherapy studies based on qualitative systematic review. *Radiol. Oncol.* 50, 1–13.
14. Caporgno, M.P., Mathys, A., 2018. Trends in microalgae incorporation into innovative food products with potential health benefits. *Front Nutr* 5.
15. Carullo, D., Abera, B.D., Casazza, A.A., Donsì, F., Perego, P., Ferrari, G., Pataro, G., 2018. Effect of pulsed electric fields and high pressure homogenization on the aqueous extraction of intracellular compounds from the microalgae *Chlorella vulgaris*. *Algal Res.* 31, 60–69.
16. Chaudhary, A., Gustafson, D., Mathys, A., 2018. Multi-indicator sustainability assessment of global food systems. *Nat. Commun.* 9, 848.
17. Enzing, C., Ploeg, M., Barbosa, M., Sijtsma, L., 2014. Microalgae-Based Products for the Food and Feed Sector: An outlook for Europe JRC Scientific and Policy Reports. European Commission.
18. Goettel, M., Eing, C., Gusbeth, C., Straessner, R., Frey, W., 2013. Pulsed electric field assisted extraction of intracellular valuables from microalgae. *Algal Res.* 2, 401–408.
19. Golberg, A., Sack, M., Teissie, J., Pataro, G., Pliquett, U., Saulis, G., Stefan, T., Miklavčič, D., Vorobiev, E., Frey, W., 2016. Energy-efficient biomass processing with pulsed electric fields for bioeconomy and sustainable development. *Biotechnol. Biofuels* 9, 94.
20. Grahl, T., Märkl, H., 1996. Killing of microorganisms by pulsed electric fields. *Appl. Microbiol. Biotechnol.* 45, 148–157.

21. Grimi, N., Dubois, A., Marchal, L., Jubeau, S., Lebovka, N.I., Vorobiev, E., 2014. Selective extraction from microalgae *Nannochloropsis* sp. using different methods of cell disruption. *Bioresour. Technol.* 153, 254–259.
22. Luengo, E., Martínez, J.M., Bordetas, A., Álvarez, I., Raso, J., 2015a. Influence of the treatment medium temperature on lutein extraction assisted by pulsed electric fields from *Chlorella vulgaris*. *Innov. Food Sci. Emerg. Technol.* 29, 15–22.
23. Luengo, E., Martínez, J.M., Coustets, M., Álvarez, I., Teissié, J., Rols, M.-P., et al., 2015b. A comparative study on the effects of millisecond- and microsecond-pulsed electric field treatments on the permeabilization and extraction of pigments from *Chlorella vulgaris*. *J. Membr. Biol.* 248, 883–891.
24. Marszalek, P., Liu, D.-S., Tsong, T.Y., 1990. Schwan equation and transmembrane potential induced by alternating electric field. *Biophys. J.* 58, 1053–1058.
25. Masojídek, J., Torzillo, G., 2014. Mass Cultivation of Freshwater Microalgae. *Ref. Modul. Earth Syst. Environ. Sci.*
26. Pohl, P., Kohlhase, M., Krautwurst, S., Baasch, K.-H., 1987. An inexpensive inorganic medium for the mass cultivation of freshwater microalgae. *Phytochemistry* 26, 1657–1659.
27. Postma, P.R., Pataro, G., Capitoli, M., Barbosa, M.J., Wijffels, R.H., Eppink, M.H.M., Olivieri, G., Ferrari, G., 2016. Selective extraction of intracellular components from the microalga *Chlorella vulgaris* by combined pulsed electric field-temperature treatment. *Bioresour. Technol.* 203, 80–88.
28. Puc, M., Kotnik, T., Mir, L.M., Miklavčič, D., 2003. Quantitative model of small molecules uptake after in vitro cell electropermeabilization. *Bioelectrochemistry* 60, 1–10.
29. Safi, C., Frances, C., Ursu, A.V., Laroche, C., Pouzet, C., Vaca-Garcia, C., Pontalier, P.-Y., 2015. Understanding the effect of cell disruption methods on the diffusion of *Chlorella vulgaris* proteins and pigments in the aqueous phase. *Algal Res.* 8, 61–68.
30. Safi, C., Zebib, B., Merah, O., Pontalier, P.Y., Vaca-Garcia, C., 2014. Morphology, composition, production, processing and applications of *Chlorella vulgaris*: A review. *Renew. Sustain. Energy Rev.* 35, 265–278.
31. Saulis, G., 2010. Electroporation of cell membranes: the fundamental effects of pulsed electric fields in food processing. *Food Eng. Rev.* 2, 52–73.
32. Silve, A., Leray, I., Poignard, C., Mir, L.M., 2016. Impact of external medium conductivity on cell membrane electropermeabilization by microsecond and nanosecond electric pulses. *Sci. Rep.* 6, 19957.
33. Smetana, S., Sandmann, M., Rohn, S., Pleissner, D., Heinz, V., 2017. Autotrophic and heterotrophic microalgae and cyanobacteria cultivation for food and feed: life cycle assessment. *Bioresour. Technol.* 245, 162–170.
34. Stacey, M., Stickley, J., Fox, P., Statler, V., Schoenbach, K., Beebe, S., Buescher, S., 2003. Differential effects in cells exposed to ultra-short, high intensity electric fields: cell survival, DNA damage, and cell cycle analysis. *Mutat. Res.* 542, 65–75.
35. Teissie, J., Tsong, T.Y., 1981. Electric field induced transient pores in phospholipid bilayer vesicles. *Biochemistry* 20, 1548–1554.
36. Toepfl, S., Heinz, V., Knorr, D., 2007. High intensity pulsed electric fields applied for food preservation. *Chem. Eng. Process. Process Intensif.* 46, 537–546.
37. United Nations, 2017. *World Population Prospects: The 2017 Revision, Key Findings and Advance Tables.*
38. Yamamoto, M., Fujishita, M., Hirata, A., Kawano, S., 2004. Regeneration and maturation of daughter cell walls in the autospore-forming green alga *Chlorella vulgaris* (*Chlorophyta, Trebouxiophyceae*). *J. Plant Res.* 117, 257–264.
39. Zimmermann, U., Pilwat, G., Riemann, F., 1974. Dielectric breakdown of cell membranes. *Biophys. J.* 14, 881–899.

40. Zuñiga, C., Li, C.-T., Huelsman, T., Levering, J., Zielinski, D.C., McConnell, B.O., Long, C.P., Knoshaug, E.P., Guarnieri, M.T., Antoniewicz, M.R., Betenbaugh, M.J., Zengler, K., 2016. Genome-scale metabolic model for the green alga *Chlorella vulgaris* UTEX 395 accurately predicts phenotypes under autotrophic, heterotrophic, and mixotrophic growth conditions. *Plant Physiol.* 172, 589–602.

PERSPECTIVE

Perspective on Pulsed Electric Field Treatment in the Bio-based Industry

Leandro Buchmann and Alexander Mathys*

ETH Zurich, Department of Health Sciences and Technology, Institute of Food, Nutrition and Health, IFNH, Sustainable Food Processing Laboratory, Schmelzbergstrasse 9, Zurich 8092, Switzerland

**Corresponding author*

Frontiers in Bioengineering and Biotechnology. 7:265

Copyright © 2019 Buchmann and Mathys. This is an open-access article distributed under the terms of the Creative Commons Attribution License (CC BY). The use, distribution or reproduction in other forums is permitted, provided the original author(s) and the copyright owner(s) are credited and that the original publication in this journal is cited, in accordance with accepted academic practice. No use, distribution or reproduction is permitted which does not comply with these terms.

ABSTRACT

The bio-based industry is urged to find solutions to meet the demands of a growing world population. In this context, increased resource efficiency is a major goal. Pulsed electric field (PEF) processing is a promising technological solution. Conventional PEF and the emerging area of nanosecond PEF (nsPEF) have been shown to induce various biological effects, with nsPEF inducing pronounced intracellular effects, which could provide solutions for currently faced challenges. Based on the flexibility and continuous operation of PEF and nsPEF processing, the technology can be integrated into many existing cultivation systems; its modularity provides an approach for inducing specific effects. Depending on the treatment conditions, selective inactivation, continuous extraction without impeding cell viability, as well as the stimulation of cell growth and/or cellular compound stimulation are potential applications in the bio-based industry. However, continuous treatment currently involves heterogeneous energy inputs. Increasing the homogeneity of PEF and nsPEF processing by considering the flow and electric field heterogeneity may allow for more targeted effects on biological cells, further increasing the potential of the technology for bio-based applications. We provide an overview of existing and potential applications of PEF and nsPEF and suggest that theoretical and practical analyses of flow and electric field heterogeneity may provide a basis for obtaining more targeted effects on biological cells and for further increasing the bio-based applications of the technology, which thereby could become a key technology for circular economy approaches in the future.

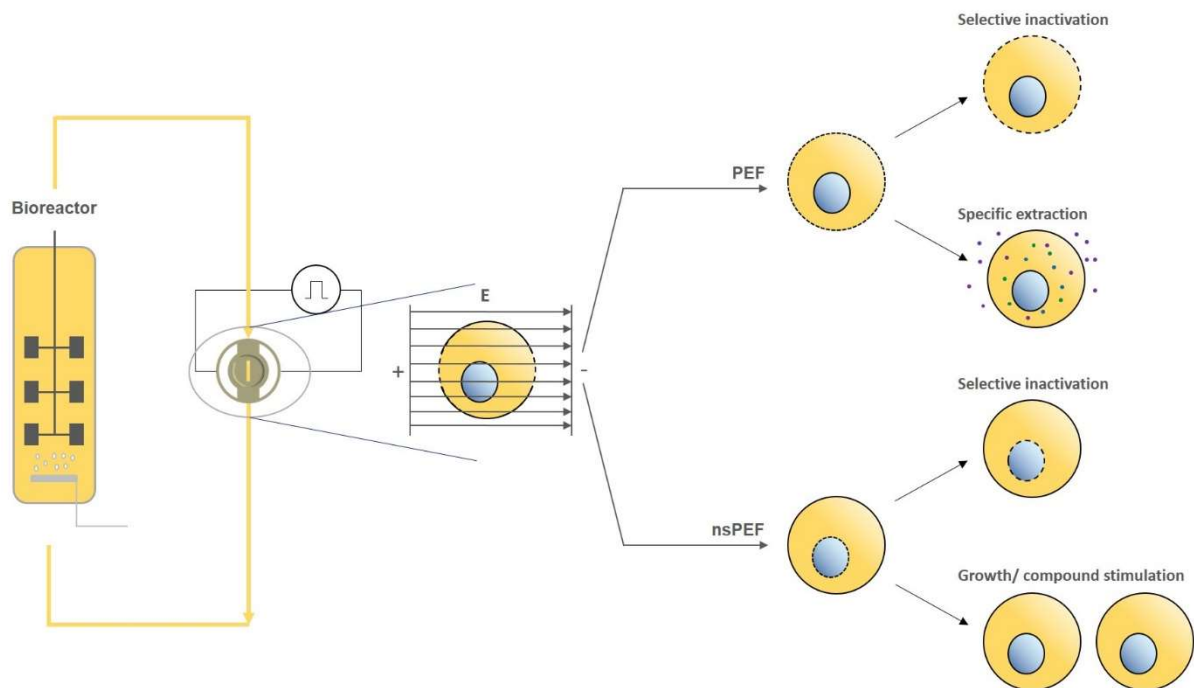
1. INTRODUCTION

Pulsed electric field (PEF) processing is a growing field in the area of electromagnetic technologies for medical, environmental, and food applications (Toepfl et al., 2006b; Miklavčič et al., 2014; Postma et al., 2016; Raso et al., 2016; Buchmann et al., 2018b, 2019c). However, knowledge transfer and applications in bio-based industries (including yeast, lactobacilli, algae, and cell tissue production systems) have been limited. Raso et al. (2016) noted that the incomplete reporting of process protocols and insufficient characterization and control of pulse parameters need to be addressed to increase the implementation of PEF processing.

The treatment is based on the formation of a potential difference across a conductive biological material between two electrodes, creating an electric field that depends on the applied electric voltage, the shape of the electrodes, and the gap between electrodes, for further information on PEF parameter interconnectivity refer to Jaeger and Knorr (2017). PEF processing can be divided into conventional PEF processing in the range of micro- to milliseconds and nanosecond (nsPEF) processing (Beebe and Schoenbach, 2005; Mahnič-Kalamiza et al., 2014), in which high electric fields ($10\text{--}100\text{ kV cm}^{-1}$) are applied for 1–300 ns. nsPEF induces intracellular effects, distinct from the pronounced effects of conventional PEF on the cell membrane (Kotnik and Miklavčič, 2006; Chopinet and Rols, 2015). Thereby, innovative applications and novel process windows are possible, while similar components for both treatments in batch and continuous mode are required (Toepfl, 2011; Buchmann et al., 2019c). In both cases, the resulting electroporation increases the mass transfer of molecules and ions (Toepfl et al., 2006b). Depending on process parameters, a reversible or irreversible effect can be induced. Most current applications are focused on irreversible electroporation, including non (minimal)-thermal pasteurization, enhanced drying rates, increased extraction yields, tissue softening as well as electrochemotherapy, and tumor ablation (Davalos et al., 2005; Toepfl et al., 2006a; Barba et al., 2015; Dermol et al., 2016; Golberg et al., 2016). Reversible electroporation is typically used in molecular biology for the introduction of specific molecules, such as plasmids and antibodies, in vivo (Smith et al., 2004; Breton et al., 2012; Casciola and Tarek, 2016). However, the mechanisms underlying the PEF/nsPEF induced effects are still the subject of intensive research (Teissie, 2017).

This perspective on PEF treatments in the bio-based industry summarizes basic

principles of electroporation by PEF/nsPEF and promising applications across different sectors (including targeted inactivation, the extraction of bioactive compounds, and the stimulation of cell growth and/or cellular compounds) (Fig. 1). Furthermore, we note that increasing the homogeneity of energy input may lead to further improvements in efficiency and a wider array of applications and therefore is a key area for future research.



P - Figure 1: Exemplary working principle of PEF/nsPEF based processing of cultivated cells and their respective effects.

2. PULSED ELECTRIC FIELD TREATMENT IN THE BIO-BASED INDUSTRY

2.1. Basic principles of pulsed electric field processing

Scale-up approaches using nsPEF technology can benefit to a great extent from experience in the domain of conventional PEF processing (Buckow et al., 2010; Toepfl, 2011). However, PEF processing requires a multidisciplinary approach, including an understanding of innovative concepts within electrical engineering, fluid mechanics, and biology (Buchmann et al., 2018a,b, 2019c). The application of PEF to biological cells is based on the principle of electroporation due to an induced transmembrane potential (Pauly and Schwan, 1959; Zimmermann et al., 1974; Schoenbach et al., 2004). The transmembrane potential difference as a function of time $\Delta\Psi_m(t)$ (V) can be derived from Equation (1) with form factor $f(-)$ (1.5 for a spherical cell), electric field strength as a function of time $E(t)$ ($V\ m^{-1}$), cell radius a_m (m), angle with respect to the direction of the electric field θ (-), treatment time t (s), and membrane charging time τ_m (s), as defined in Equation (2) with membrane capacitance per unit area C_m (F) and extracellular σ_e and intracellular conductivity σ_i ($S\ m^{-1}$).

$$\Delta\Psi_m(t) = f \cdot E(t) \cdot a_m \cdot \cos\theta \cdot (1 - e^{-t/\tau_m}) \quad (1)$$

$$\tau_m = a_m \cdot C_m \cdot (1/2 \sigma_e + 1/\sigma_i) \quad (2)$$

To induce the required effect, the extracellular conductivity is of special interest. The membrane charging time (Equation 2) is strongly influenced by extracellular conductivity, as intracellular conductivity is fixed by the cell metabolism (Teissie et al., 2005). Additionally, extracellular conductivity needs to be in a range such that Equation (3) is equal to the pulse generator's resistance and hence matched load conditions are achieved (Küchler, 2009).

$$R = 1/\sigma \cdot d/A \quad (3)$$

where R is the resistance (Ω), σ is the media conductivity ($S\ m^{-1}$), d is the electrode distance (m), and A is the electrode surface area (m^2).

To assess the load for nsPEF, Equation (3) has to be extended, as shown in Equation (4).

$$Z_{tot} = 1/(\sigma \cdot A/d + Y_c) \quad (4)$$

where the total impedance Z_{tot} (Ω) is equal to the sum of the inverse resistance and

the system's admittance Y_c (S) (Buchmann et al., 2018b).

For controlled PEF processing, the flow field distribution within chambers is an important parameter that has been neglected in energy input calculations to date (Meneses et al., 2011; Knoerzer et al., 2012; Raso et al., 2016; Buchmann et al., 2018a). The specific energy input W_s (J kg^{-1}) can be calculated according to Equation (5), with pulse width τ_p (s) and number of pulses n (-),

$$W_s = E^2 \cdot \tau_p \cdot \sigma \cdot n. \quad (5)$$

The number of pulses can be derived from Equation (6), with frequency f (Hz) and residence or treatment time t (s),

$$n = f \cdot t \quad (6)$$

From the author's perspective, the integration of the flow and electric field heterogeneities into the energy input calculation would facilitate the transferability of the results and the implementation of PEF on different scales and systems.

2.2. Microbial inactivation by PEF

The main advantage of PEF-based microbial inactivation is the ability to increase product quality while ensuring safety (Toepfl et al., 2006a; Mathys et al., 2013; Aganovic et al., 2017). PEF-based pasteurization has been widely investigated and industrialized and PEF-assisted sterilization has even been achieved under laboratory conditions (Toepfl et al., 2005; Raso et al., 2006; Reineke et al., 2015; Jaeger and Knorr, 2017). Although Aganovic et al. (2017) showed that PEF processing is actually more energy-intensive than thermal processing, its advantages could outweigh this current disadvantage, including its beneficial effects on quality due to lower thermal intensity, and therefore sustainability (Chaudhary et al., 2018; Chen et al., 2019) as well as its ability to selectively inactivate microorganisms. Nevertheless, the energy demand of PEF processing itself could actually be reduced by considering electric and flow field deviations in energy input calculations, as currently under- and overprocessed areas appear simultaneously during PEF processing resulting in overall similar inactivation rates as compared to other techniques. A more homogeneous treatment, resulting from treatment chamber modifications and subsequent experimental planning, could help to overcome this limitation and even enhance the positive attributes of PEF processing.

Bio-based industrial cultivation relies on the use of specific microbial flora to ensure stable processes. However, the conditions and boundaries of industrial production commonly result in non-axenic and non-sterile cultivation to produce high value-added functional ingredients (including pharmaceuticals or biotechnological products), food, feed, and bioenergy. Therefore, a viable cell culture and thus stable cultivation system requires measures for microbial contamination control. For conventional PEF processing, predator control within a viable microalgae culture is possible, but not yet fully understood (Rego et al., 2015; Kempkes, 2016).

Moreover, selective inactivation has been achieved by nsPEF, allowing for reduced thermal effects and broader applications of the treatment owing to the greater similarity of organisms at the level of organelles than cell membranes (Buchmann et al., 2018b). However, selective inactivation is limited by two main factors. First, interactions of prokaryotic/eukaryotic consortia are not yet fully understood, resulting in unknown target organisms for selective inactivation. Second, the specific susceptibility of biological cells to electric fields has not been fully established, unlike in thermal processing (Kessler, 2002; Álvarez et al., 2006; Gianulis et al., 2017).

However, since the entire processing principle is new, future developments in PEF/nsPEF-based culture stabilization by selective inactivation are anticipated. In addition, the concept of selective inactivation could be used to stabilize cultures after contamination, reducing bio-waste due to process failures. After the investigation of interactions in prokaryotic/eukaryotic consortia and their interdependence, specific process windows need to be established for targeted organisms in different growth phases with respect to environmental properties (pH, temperature, water activity, etc.). Despite current research on conventional PEF-based pasteurization, selective microbial control, which has enormous potential, should be a major focus of future PEF/nsPEF research.

2.3. Extraction of cellular compounds by PEF processing

PEF processing is suitable for biological applications that require gentle disintegration and extraction processes. The permeability induced by PEF processing results in increased mass transfer and thereby in higher extraction yields (Toepfl et al., 2006b; Bobinaite et al., 2015). Moreover, lower temperatures (e.g., 4°C) allow for the preservation of permeable structures without loss of cell integrity (Lopez et al., 1988). In addition, the selective nature of PEF-based extraction allows for the cascade processing of different cell-derived compounds such as carbohydrates, proteins, and lipids (Eing et al., 2013). However, PEF efficiency in terms of absolute yield and energy input is currently lower than those of other established processes (Postma et al., 2016; 't Lam et al., 2017). Two key parameters can explain the relatively low extraction yield. First, after PEF treatment, the permeable structure, which affects the cell membrane integrity, allows for the diffusion gradient assisted release of cellular compounds (Scherer et al., 2019). Second, PEF processing is able to permeabilize the cell membrane, but the lack of complete disruption, as obtained for example by bead milling, limits the extraction of membrane-bound compounds (Postma et al., 2016; Martínez et al., 2017).

Nevertheless, reversible PEF permeabilization is highly promising for selective microbial inactivation, and the concept of reversible and continuous PEF-based disintegration/extraction may have important future applications. This was demonstrated by Buchmann et al. (2019b), who showed that protein extraction without impeding growth is possible in *Chlorella vulgaris* cultures. In this system, protein extraction was highest after 24 h, resulting in a free protein extraction rate of $29.1 \pm 1.1\%$ and a *C. vulgaris* recovery rate of $93.8 \pm 6.7\%$ after 6 days. Regarding absolute yield PEF-based extraction yielded up to $96.6 \pm 4.8\%$ of the free protein fraction of *C. vulgaris*. However, high extraction yields were correlated with a reduced ability to grow after treatment in *C. vulgaris* cultures; hence, further research is necessary to identify optimal processing windows and to extend this approach to other taxonomic groups, such as yeast and bacteria.

Although initial studies have focused on proteins, permeability to various compounds, dependent on the media or solvent, should also be evaluated. Further research is necessary to identify the optimal processing window with regard to yield and growth rate. In-depth analyses of the cellular composition throughout the cultivation cycle in combination with treatment conditions favoring the extraction process are necessary.

Moreover, the application of nsPEF to extraction processing could increase yields from organelle structures due to expanding on the efficiency for organelles.

The incorporation of membrane technology can potentially allow for the inline separation of targeted compounds and viable cells, thereby the continuous PEF-based extraction could enable circular economy concepts. Accordingly, cell engineering approaches for the excretion of targeted compounds might become obsolete. The integration of downstream processing in the upstream process could overcome current limitations in the bio-based industry, such as process heterogeneity, reproducibility, energy efficiency, and application portfolio.

2.4. nsPEF induced growth stimulation

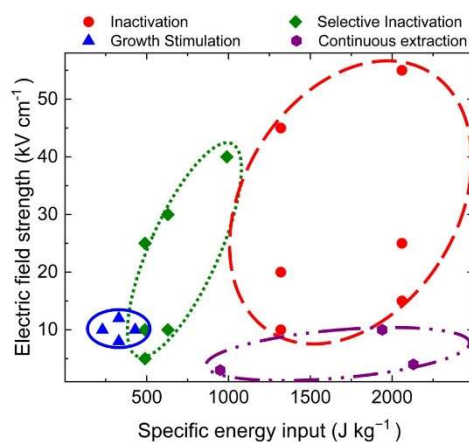
Research on growth stimulation by an electric field has a long history; positive effects have been established in fungi, soy, microalgae, and other cells (Bertholon, 1783; Lemström, 1904; Bachman and Reichmanis, 1973; Takaki et al., 1984; Costanzo, 2008; Frey et al., 2011; Gusbeth et al., 2013; Mattar et al., 2015). However, controlled and reproducible growth stimulation was currently not possible. Electric fields and PEF may have precise stimulation windows, but controllable and reliable growth and/or compound stimulation has only been achieved under nsPEF conditions. Initial studies of growth stimulation based on nsPEF processing yielded promising results for *Arabidopsis thaliana* in a batch system and different laboratories (Eing et al., 2009; Songnuan and Kirawanich, 2012). In recent experiments, the transfer from a batch system to a continuous nsPEF process was successful, resulting in a $13.1 \pm 1.6\%$ increase in *Arthrospira platensis* SAG 21.99 biomass (Buchmann et al., 2019c). Moreover, an increase of $18.8 \pm 5.5\%$ and $19.5 \pm 6\%$ in allophycocyanin and C-phycocyanin, respectively, components of the economically important blue colorant phycocyanin, was obtained. Hence, nsPEF has the potential to increase growth as well as specific cellular compounds while maintaining techno-functional properties of the remaining compounds, as demonstrated for foaming, emulsification, and color compounds (Buchmann et al., 2019a,b).

Additionally, growth stimulation has been obtained in various organisms repeatedly treated with 100 ns pulses at 10 kV cm^{-1} ; photoautotrophic *Arthrospira platensis* SAG 21.99 ($256 \pm 67 \text{ J kg}_{\text{sus}}^{-1}$) (Buchmann et al., 2019c), photoautotrophic *Chlorella vulgaris* SAG 211-12 ($360 \pm 114 \text{ J kg}_{\text{sus}}^{-1}$) (Haberhorn et al., 2019), heterotrophic *Chlorella vulgaris* CCALA 256 ($227 \pm 60 \text{ J kg}_{\text{sus}}^{-1}$) (original data), and *Saccharomyces cerevisiae* DSM 70449 ($173 \pm 55 \text{ J kg}_{\text{sus}}^{-1}$) (original data) showed increased biomass concentrations after nsPEF processing of $13.1 \pm 1.6\%$, $17.5 \pm 10.5\%$, $12.2 \pm 2.7\%$, and $20.5 \pm 3.0\%$, respectively.

In this in-depth analysis, the pulse repetition frequency was adjusted according to the flow field. Under all investigated conditions, the increased growth was observed in a narrow processing window and required thorough process characterization and control (Buchmann et al., 2018a). Thereby, these effects could potentially be enhanced by a more homogeneous treatment, increasing the fraction of cells treated with the specifically required energy input.

Moreover, successful treatment relied on the application of nsPEF at the early

exponential growth phase, as shown by Buchmann et al. (2019c). These findings support the theory that there is an increased effect of nsPEF on highly proliferating cells (Schoenbach et al., 1997). However, the specific mechanism underlying nsPEF-induced growth stimulation remains unknown. According to one hypothesis, it involves a Ca^{2+} -based abiotic stress response pathway (Buchmann et al., 2019c). In addition to plants, fungi, and bacteria, the stimulative effect of nsPEF has been shown using animal cells and stem cells (Steuer et al., 2018; Ning et al., 2019). Ultimately, the effects on growth and parallel pigment production suggest that this technique can be used to enhance heterologous protein expression. Hence, nsPEF-based growth/cellular compound stimulation could be a viable strategy for future cultivation systems and may even be combined with continuous extraction or selective inactivation. Fig. 2 summarizes a case study of the microalga *Chlorella vulgaris* SAG 211-12, illustrating treatment windows for selective inactivation, inactivation of microbial flora and *C. vulgaris*, continuous extraction of high value-added ingredients, and growth stimulation.



P - Figure 2: Case study of the microalgae *Chlorella vulgaris* SAG 211-12, illustrating treatment windows for selective inactivation, inactivation of microbial flora and *C. vulgaris*, continuous extraction of high value-added ingredients, and growth stimulation.

3. CONCLUSIONS

Currently faced challenges in bio-based industries derived from a growing world population and simultaneously limited arable land require a change in current supply chains. The presented innovative concepts based on PEF/nsPEF processing bear the potential to be key processing steps toward more sustainable and efficient supply chains. In the domain of irreversible electropermeabilization, selective inactivation could enable inline microbial control, resulting in long-term stable cultivation and low contamination-related process failure. However, further studies of interactions between target cells and surrounding flora, and particularly on PEF/nsPEF-resistance of different strains, are needed for successful selective inactivation. The integration of downstream processing into upstream cultivation via the conventional PEF-based continuous extraction of specific cellular compounds without impeding cell growth can overcome current limitations, in bio-based industries, such as process heterogeneity, reproducibility, energy efficiency, and application portfolio. Moreover, nsPEF-based growth/cellular compound stimulation has the potential to increase resource efficiency, economic viability, and the affordability of the derived products, thereby meeting the demands of a growing world population. Given that PEF and nsPEF systems can be implemented in many existing cultivation systems via a bypass, it is also possible to combine the continuous extraction process with nsPEF-induced growth/cellular compound stimulation to enhance the overall performance of bio-based systems and ensure its long-term stability by selective inactivation.

Of note, continuous PEF processing in both domains is currently based on heterogeneous treatments conditions. Therefore, modified treatment chambers by the incorporation of flow and electric field distributions are necessary for more targeted and reproducible effects within cell cultures. Increasing the homogeneity of the treatment could further increase the induced effects of PEF/nsPEF. Thus, PEF and nsPEF have the potential to become high-impact technologies and to resolve current challenges in bio-based industries.

Data availability statement

The datasets generated for this study are available on request to the corresponding author.

Author contributions

AM devised the main conceptual ideas. LB and AM discussed the ideas and commented on the manuscript. LB wrote the manuscript in consultation with AM.

Funding

This study was supported by the Coop Research Program of the ETH Zurich World Food System Center (Grant number NewAlgae 2-72235-17), the Bühler AG, and the ETH Zurich Foundation. The funders were not involved in the study design, collection, analysis, interpretation of data, the writing of this article or the decision to submit it for publication.

Acknowledgements

The authors would like to acknowledge Prof. Dr. E. J. Windhab, Daniel Kiechl, and Bruno Pfister from the Food Process Engineering Laboratory, Prof. Dr. C. Franck and Dr. M. Refaey from the High Voltage Laboratory at ETH Zurich, and Markus Nyffeler from the Institute of High Power Electromagnetics at the Swiss Federal Office for Defense Procurement for supporting this project.

Conflict of interest

The authors declare that the research was conducted in the absence of any commercial or financial relationships that could be construed as a potential conflict of interest.

REFERENCES

1. Aganovic, K., Smetana, S., Grauwet, T., Toepfl, S., Mathys, A., Van Loey, A., et al. (2017). Pilot scale thermal and alternative pasteurization of tomato and watermelon juice: An energy comparison and life cycle assessment. *J. Clean. Prod.* 141, 514–525. doi: 10.1016/j.jclepro.2016.09.015
2. Álvarez, I., Condón, S., and Raso, J. (2006). “Microbial inactivation by pulsed electric fields,” in *Pulsed Electric Fields Technology for the Food Industry - Fundamentals and Applications*, eds J. Raso and V. Heinz (Boston, MA: Springer), 97–129.
3. Bachman, C., and Reichmanis, M. (1973). Some effects of high electrical fields on barley growth. *Int. J. Biometeorol.* 17, 253–262. doi: 10.1007/BF01804618
4. Barba, F. J., Parniakov, O., Pereira, S. A., Wiktor, A., Grimi, N., Boussetta, N., et al. (2015). Current applications and new opportunities for the use of pulsed electric fields in food science and industry. *Food Res. Int.* 77, 773–798. doi: 10.1016/j.foodres.2015.09.015
5. Beebe, S. J., and Schoenbach, K. H. (2005). Nanosecond pulsed electric fields: A new stimulus to activate intracellular signaling. *J. Biomed. Biotechnol.* 2005, 297–300. doi: 10.1155/JBB.2005.297
6. Bertholon, P. (1783). *De l'électricité des végétaux*. Paris: Imprimerie de Didot Jeune.
7. Bobinaite, R., Pataro, G., Lamanaskas, N., Šatkauskas, S., Viškelis, P., and Ferrari, G. (2015). Application of pulsed electric field in the production of juice and extraction of bioactive compounds from blueberry fruits and their by-products. *J. Food Sci. Technol.* 52, 5898–5905. doi: 10.1007/s13197-014-1668-0
8. Breton, M., Delemotte, L., Silve, A., Mir, L. M., and Tarek, M. (2012). Transport of siRNA through lipid membranes driven by nanosecond electric pulses: An experimental and computational study. *J. Am. Chem. Soc.* 134, 13938–13941. doi: 10.1021/ja3052365
9. Buchmann, L., Bertsch, P., Böcker, L., Krähenmann, U., Fischer, P., and Mathys, A. (2019a). Adsorption kinetics and foaming properties of soluble microalgae fractions at the air/water interface. *Food Hydrocoll.* 97:105182. doi: 10.1016/j.foodhyd.2019.105182
10. Buchmann, L., Bloch, R., and Mathys, A. (2018a). Comprehensive pulsed electric field (PEF) system analysis for microalgae processing. *Bioresour. Technol.* 265, 268–274. doi: 10.1016/j.biortech.2018.06.010
11. Buchmann, L., Böcker, L., Frey, W., Haberkorn, I., Nyffeler, M., and Mathys, (2018b). Energy input assessment for nanosecond pulsed electric field processing and its application in a case study with *Chlorella vulgaris*. *Innov. Food Sci. Emerg. Technol.* 47, 445–453. doi: 10.1016/j.ifset.2018.04.013
12. Buchmann, L., Brändle, I., Haberkorn, I., Hiestand, M., and Mathys, A. (2019b). Pulsed electric field based cyclic protein extraction of microalgae towards closed-loop biorefinery concepts. *Bioresour. Technol.* 291:121870. doi: 10.1016/j.biortech.2019.121870
13. Buchmann, L., Frey, W., Gusbeth, C., Ravaynia, P. S., and Mathys, (2019c). Effect of nanosecond pulsed electric field treatment on cell proliferation of microalgae. *Bioresour. Technol.* 271, 402–408. doi: 10.1016/j.biortech.2018.09.124
14. Buckow, R., Schroeder, S., Berres, P., Baumann, P., and Knoerzer, K. (2010). Simulation and evaluation of pilot-scale pulsed electric field (PEF) processing. *J. Food Eng.* 101, 67–77. doi: 10.1016/j.jfoodeng.2010.06.010
15. Casciola, M., and Tarek, M. (2016). A molecular insight into the electro-transfer of small molecules through electropores driven by electric fields. *Biochim. Biophys. Acta Biomembr.* 1858, 2278–2289. doi: 10.1016/j.bbamem.2016.03.022
16. Chaudhary, A., Gustafson, D., and Mathys, A. (2018). Multi-indicator sustainability assessment of global food systems. *Nat. Commun.* 9:848. doi: 10.1038/s41467-018-03308-7
17. Chen, C., Chaudhary, A., and Mathys, A. (2019). Dietary change scenarios and implications for environmental, nutrition, human health and economic dimensions of food sustainability. *Nutrients* 11:E856. doi: 10.3390/nu11040856

18. Chopinet, L., and Rols, M. P. (2015). Nanosecond electric pulses: A mini-review of the present state of the art. *Bioelectrochemistry* 103, 2–6. doi: 10.1016/j.bioelechem.2014.07.008
19. Costanzo, E. (2008). The influence of an electric field on the growth of soy seedlings. *J. Electrostat.* 66, 417–420. doi: 10.1016/j.elstat.2008.04.002
20. Davalos, R. V., Mir, L. M., and Rubinsky, B. (2005). Tissue ablation with irreversible electroporation. *Ann. Biomed. Eng.* 33, 223–231. doi: 10.1007/s10439-005-8981-8
21. Dermol, J., Pakhomova, O. N., Pakhomov, A. G., and Miklavčič, D. (2016). Cell electrosensitization exists only in certain electroporation buffers. *PLoS ONE* 11:e0159434. doi: 10.1371/journal.pone.0159434
22. Eing, C., Bonnet, S., Pacher, M., Puchta, H., and Frey, W. (2009). Effects of nanosecond pulsed electric field exposure on *Arabidopsis thaliana*. *IEEE Trans. Dielectr. Electr. Insul.* 16, 1322–1328. doi: 10.1109/TDEI.2009.5293945
23. Eing, C. J., Goettel, M., Straessner, R., Gusbeth, C., and Frey, W. (2013). Pulsed electric field treatment of microalgae—benefits for microalgae biomass processing. *IEEE Trans. Plasma Sci.* 41, 2901–2907. doi: 10.1109/TPS.2013.2274805
24. Frey, W., Strässner, R., Eing, C., Berghöfer, T., Gusbeth, C., Flickinger, B., et al. (2011). Verfahren zur Beschleunigung der Zellproliferation. European Patent No EP2308969B1. München: European Patent Office.
25. Gianulis, E. C., Labib, C., Saulis, G., Novickij, V., Pakhomova, O. N., and Pakhomov, A. G. (2017). Selective susceptibility to nanosecond pulsed electric field (nsPEF) across different human cell types. *Cell. Mol. Life Sci.* 74, 1741–1754. doi: 10.1007/s00018-016-2434-4
26. Golberg, A., Sack, M., Teissie, J., Pataro, G., Pliquett, U., Saulis, G., et al. (2016). Energy-efficient biomass processing with pulsed electric fields for bioeconomy and sustainable development. *Biotechnol. Biofuels* 9:94. doi: 10.1186/s13068-016-0508-z
27. Gusbeth, C., Eing, C., Goettel, M., and Frey, W. (2013). “Boost of algae growth by ultra short pulsed electric field treatment,” in 2013 Abstracts IEEE International Conference on Plasma Science (ICOPS) (San Francisco, CA), 1.
28. Haberkorn, I., Buchmann, L., Hiestand, M., and Mathys, A. (2019). Continuous nanosecond pulsed electric field treatments foster the upstream performance of *Chlorella vulgaris*-based biorefinery concepts. *Bioresour. Technol.* 293:122029. doi: 10.1016/j.biortech.2019.122029
29. Jaeger, H., and Knorr, D. (2017). “Pulsed electric fields treatment in food technology: Challenges and opportunities,” in *Handbook of Electroporation*, ed D. Miklavčič (Cham: Springer International Publishing AG), 2657–2680.
30. Kempkes, M. (2016). “Pulsed electric fields for algal extraction and predator control,” in *Handbook of Electroporation*, ed D. Miklavčič (Cham: Springer International Publishing AG), 1–16.
- A. Kessler, H. (2002). *Food and Bio Process Engineering: Dairy Technology*. Munich: Kessler.
31. Knoerzer, K., Baumann, P., and Buckow, R. (2012). An iterative modelling approach for improving the performance of a pulsed electric field (PEF) treatment chamber. *Comput. Chem. Eng.* 37, 48–63. doi: 10.1016/j.compchemeng.2011.09.002
32. Kotnik, T., and Miklavčič, D. (2006). Theoretical evaluation of voltage inducement on internal membranes of biological cells exposed to electric fields. *Biophys. J.* 90, 480–491. doi: 10.1529/biophysj.105.070771
33. Küchler, A. (2009). *Hochspannungstechnik*. New York, NY: Springer International Publishing AG.
34. Lemström, S. (1904). *Electricity in Agriculture and Horticulture*. London: The Electrician Printing & Publishing Company Ltd.
35. Lopez, A., Rols, M. P., and Teissie, J. (1988). 31p NMR analysis of membrane phospholipid organization in viable, reversibly electroporated Chinese Hamster Ovary cells. *Biochemistry* 27, 1222–1228. doi: 10.1021/bi00404a023

36. Mahnič-Kalamiza, S., Vorobiev, E., and Miklavčič, D. (2014). Electroporation in food processing and biorefinery. *J. Membr. Biol.* 247, 1279–1304. doi: 10.1007/s00232-014-9737-x
37. Martínez, J. M., Luengo, E., Saldaña, G., Álvarez, I., and Raso, J. (2017). C-phycoerythrin extraction assisted by pulsed electric field from *Arthrospira platensis*. *Food Res. Int.* 99, 1042–1047. doi: 10.1016/j.foodres.2016.09.029
38. Mathys, A., Toepfl, S., Siemer, C., Favre, L., Benyacoub, J., and Hansen, C. E. (2013). Pulsed Electric Field Treatment Process and Dairy Product Comprising Bioactive Molecules Obtainable by the Process. US Patent No WO2013007620A1. Washington, DC: U.S. Patent and Trademark Office.
39. Mattar, J. R., Turk, M. F., Nonus, M., Lebovka, N. I., El Zakhem, H., and Vorobiev, E. (2015). *S. cerevisiae* fermentation activity after moderate pulsed electric field pre-treatments. *Bioelectrochemistry* 103, 92–97. doi: 10.1016/j.bioelechem.2014.08.016
40. Meneses, N., Jaeger, H., Moritz, J., and Knorr, D. (2011). Impact of insulator shape, flow rate and electrical parameters on inactivation of *E. coli* using a continuous co-linear PEF system. *Innov. Food Sci. Emerg. Technol.* 12, 6–12. doi: 10.1016/j.ifset.2010.11.007
41. Miklavčič, D., Mali, B., Kos, B., Heller, R., and Serša, G. (2014). Electrochemotherapy: from the drawing board into medical practice. *Biomed. Eng. Online* 13, 1–20. doi: 10.1186/1475-925X-13-29
42. Ning, T., Guo, J., Zhang, K., Li, K., Zhang, J., Yang, Z., et al. (2019). Nanosecond pulsed electric fields enhanced chondrogenic potential of mesenchymal stem cells via JNK / CREB- STAT3 signaling pathway. *10:45*. doi: 10.1186/s13287-019-1133-0
43. Pauly, H., and Schwan, H. P. (1959). Über die Impedanz einer Suspension von kugelförmigen Teilchen mit einer Schale. *Z. Naturforsch. B* 14, 125–131. doi: 10.1515/znb-1959-0213
44. Postma, P. R., Pataro, G., Capitoli, M., Barbosa, M. J., Wijffels, R. H., Eppink, M. H. M., et al. (2016). Selective extraction of intracellular components from the microalga *Chlorella vulgaris* by combined pulsed electric field-temperature treatment. *Bioresour. Technol.* 203, 80–88. doi: 10.1016/j.biortech.2015.12.012
45. Raso, J., Calderón, M. L., Góngora, M., Barbosa-Cánovas, G. V., and Swanson, B. G. (2006). Inactivation of *Zygosaccharomyces bailii* in fruit juices by heat, high hydrostatic pressure and pulsed electric fields. *J. Food Sci.* 63, 1042–1044. doi: 10.1111/j.1365-2621.1998.tb15850.x
46. Raso, J., Frey, W., Ferrari, G., Pataro, G., Knorr, D., Teissie, J., et al. (2016). Recommendations guidelines on the key information to be reported in studies of application of PEF technology in food and biotechnological processes. *Innov. Food Sci. Emerg. Technol.* 37, 312–321. doi: 10.1016/j.ifset.2016.08.003
47. Rego, D., Redondo, L. M., Geraldes, V., Costa, L., Navalho, J., and Pereira, M. T. (2015). Control of predators in industrial scale microalgae cultures with pulsed electric fields. *Bioelectrochemistry* 103, 60–64. doi: 10.1016/j.bioelechem.2014.08.004
48. Reineke, K., Schottroff, F., Meneses, N., and Knorr, D. (2015). Sterilization of liquid foods by pulsed electric fields—an innovative ultra-high temperature process. *Front. Microbiol.* 6:400. doi: 10.3389/fmicb.2015.00400
49. Scherer, D., Krust, D., Frey, W., Mueller, G., Nick, P., and Gusbeth, C. (2019). Pulsed electric field (PEF)-assisted protein recovery from *Chlorella vulgaris* is mediated by an enzymatic process after cell death. *Algal Res.* 41:101536. doi: 10.1016/j.algal.2019.101536
50. Schoenbach, K. H., Joshi, R. P., Kolb, J. F., Chen, N., Stacey, M., Blackmore, P. F., et al. (2004). Ultrashort electrical pulses open a new gateway into biological cells. *Proc. IEEE* 92, 1122–1136. doi: 10.1109/JPROC.2004.829009
51. Schoenbach, K. H., Peterkin, F. E., Alden, R. W., and Beebe, S. J. (1997). The effect of pulsed electric fields on biological cells: Experiments and applications. *IEEE Trans. Plasma Sci.* 25, 284–292. doi: 10.1109/27.602501
52. Smith, K. C., Neu, J. C., and Krassowska, W. (2004). Model of creation and evolution of stable electropores for DNA delivery. *Biophys. J.* 86, 2813–2826. doi: 10.1016/S0006-3495(04)74334-9

53. Songnuan, W., and Kirawanich, P. (2012). Early growth effects on *Arabidopsis thaliana* by seed exposure of nanosecond pulsed electric field. *J. Electrostat.* 70, 445–450. doi: 10.1016/j.elstat.2012.06.004
54. Steuer, A., Wolff, C.M., von Woedtke, T., Weltmann, K.-D., and Kolb, J. F. (2018). Cell stimulation versus cell death induced by sequential treatments with pulsed electric fields and cold atmospheric pressure plasma. *PLoS ONE* 13:e0204916. doi: 10.1371/journal.pone.0204916
55. 't Lam, G. P., Postma, P. R., Fernandes, D. A., Timmermans, R. A. H., Vermuë, M. H., Barbosa, M. J., et al. (2017). Pulsed electric field for protein release of the microalgae *Chlorella vulgaris* and *Neochloris oleoabundans*. *Algal Res.* 24, 181–187. doi: 10.1016/j.algal.2017.03.024
56. Takaki, K., Kanesawa, K., Yamazaki, N., Mukaigawa, S., Fujiwara, T., Takahasi, K., et al. (1984). Application of IES pulsed power generator for mushroom cultivation. *IEEE* 30, 5393–5395.
57. Teissie, J. (2017). “Critical electric field and transmembrane voltage for lipid pore formation in experiments,” in *Handbook of Electroporation*, ed. D. Miklavčič (New York, NY: Springer International Publishing AG), 25–43.
58. Teissie, J., Golzio, M., and Rols, M. P. (2005). Mechanisms of cell membrane electropermeabilization: a minireview of our present (lack of?) knowledge. *Biochim. Biophys. Acta Gen. Subj.* 1724, 270–280. doi: 10.1016/j.bbagen.2005.05.006
59. Toepfl, S. (2011). Pulsed Electric Field food treatment - scale up from lab to industrial scale. *Procedia Food Sci.* 1, 776–779. doi: 10.1016/j.profoo.2011.09.117
60. Toepfl, S., Heinz, V., and Knorr, D. (2005). “Overview of pulsed electric field processing for food,” in *Emerging Technologies for Food Processing: An Overview* (New York, NY: Elsevier Ltd.), 69–97.
61. Toepfl, S., Heinz, V., and Knorr, D. (2006a). “Applications of pulsed electric fields technology for the food industry,” in *Pulsed Electric Fields Technology for the Food Industry*, eds J. Raso and V. Heinz (Boston, MA: Springer), 197–225. 197–221. doi: 10.1007/978-0-387-31122-7_7
62. Toepfl, S., Mathys, A., Heinz, V., and Knorr, D. (2006b). Review: potential of high hydrostatic pressure and pulsed electric fields for energy efficient and environmentally friendly food processing. *Food Rev. Int.* 22, 405–423. doi: 10.1080/87559120600865164
63. Zimmermann, U., Pilwat, G., and Riemann, F. (1974). Dielectric breakdown of cell membranes. *Biophys. J.* 14, 881–899. doi: 10.1016/S0006-3495(74)85956-4

CONCLUSIONS AND OUTLOOK

The presented concepts, such as selective inactivation, cyclic protein extraction and growth and/or compound stimulation, contributed the urge of the bio-based industry to find solutions to meet the demands of a growing world population. Hence, PEF/nsPEF have the potential to become high-impact technologies and to resolve current challenges in bio-based industries. However, further optimization and investigation of PEF/nsPEF induced effects in biological cells are required.

In general, PEF/nsPEF treatment homogeneity needs to be further improved to enable the ubiquitous implementation of the presented concepts within the food- and bioprocessing industry. As shown in the thesis, the currently industrialized co-linear system was mainly optimized for its electric field homogeneity neglecting flow field inhomogeneities. However, the deviation within the electric field for the co-linear system (15.75%) was already comparable to the parallel-plate inhomogeneity incorporating flow and electric field inhomogeneities (15.87%). Thus, with regard to the spatial energy input distribution, it appeared that a parallel-plate electrode configuration would be superior to the co-linear systems. Certainly, challenges around the hygienic design of a parallel-plate treatment chamber need to be overcome in order to allow an industrial implementation of these treatment chambers. Moreover, the influence of pH and temperature changes with the respective influence of media parameters needs to be investigated for a parallel-plate treatment chamber. The pursued interdisciplinary approach to combine multiphysics simulation with non-invasive experimental validation should be applied wherever possible.

Despite the further need for an in-depth system characterization, further system optimization is needed. In order to achieve stable turbulent flow and thus increasing overall treatment homogeneity, the exploitation of Taylor-Couette flow and vortex shedding within PEF/nsPEF treatment chambers could be promising. Moreover, mixing elements prior to the treatment chamber and/or structural modifications of the wall might be valuable strategies to increase the overall treatment homogeneity.

Considering the application of selective inactivation, a case study with the microalgae *C. vulgaris* allowed total bacterial count reduction of $>1 \log_{10}$ while retaining the viability of microalgae cells. Thus, long-term stability of cellular cultivation systems might be enabled by PEF/nsPEF processing allowing for facilitated downstream processing for cellular food production systems and reduced economic and

environmental consequences due to cultivation failure as well as life support systems enabling manned interstellar missions and potentially deep space habitation.

However, a thorough microbial characterization with regard to their susceptibility to PEF/nsPEF is required in order to identify specific processing windows. Furthermore, there is a strong need for the characterization of the microbial flora, as the interaction of prokaryotic/eukaryotic consortia is not fully understood, yet. Studies around an individual, as well as mixtures of prokaryotic and eukaryotic cells within a cultivation system, will help to understand the specific response to PEF/nsPEF. Thereby, mutualistic, commensalistic and/or antagonistic relations can be further explored and in combination with on-line line flow cytometry and next-generation sequencing, the process can be optimized to specific needs, potentially enabling cumulative effects based on the interaction of target organisms with their microbial flora. The knowledge around cellular susceptibility to PEF/nsPEF treatment could be further extended to influence specific organic compounds e.g. enzymes, proteins and thus will allow targeted PEF/nsPEF treatments in the future. Thereby, microbial safety and product quality might be further optimized even for already industrialized processes.

Focusing on sub-lethal stress induction, the application of nsPEF in the early exponential growth phase within biological cells resulting in growth and/or cellular compound stimulation has been obtained in various organisms. The growth of photoautotrophic *A. platensis*, photoautotrophic *C. vulgaris*, heterotrophic *C. vulgaris* and *S. cerevisiae* was increased by $13.1 \pm 1.6\%$, $17.5 \pm 10.5\%$, $12.2 \pm 2.7\%$, and $20.5 \pm 3.0\%$, respectively. A further increase in the economically viable blue pigment complex phycocyanin by $18.8 \pm 5.5 \%$ and $19.5 \pm 6 \%$ for allophycocyanin and C-phycocyanin, respectively, was obtained for *A. platensis*. Moreover, the techno-functional properties of the soluble extracts of *A. platensis*, used as a model organism, were not impeded after the nsPEF treatment.

However, enhancing the understanding of the induced stress response and its underlying mechanisms should be the main focus for further research. Trace analysis of elements via inductively coupled plasma mass spectrometry, might allow the determination of crucial macro-/ micronutrients in the abiotic sublethal stress response and thereby, specific feeding strategies might be derived that could allow the induced effects to be amplified over the entire cultivation cycle. Furthermore, the derived hypothesis around Ca^{2+} as a crucial factor in the nsPEF induced upregulation

of cell proliferation was enforced through the response of *C. vulgaris* to the application of nsPEF, however, further research should be conducted with labeled Ca^{2+} to analyze flux as well as the relocation of the cation. In addition, monitoring of the changes occurring in the cell's proteome throughout the cultivation might reveal the underlying mode of action of nsPEF induced abiotic stress. Additionally, the integration of on-line flow cytometry might increase the resolution of the biological response, allowing for a more targeted application of the treatment. Moreover, as growth stimulation occurred in prokaryotic and eukaryotic organisms non-axenic cultivation systems with a focus on the interaction of prokaryotic/eukaryotic consortia need to be further investigated. Additionally, the approach should be further analyzed with regard to its ability to trigger specific cellular compounds within bio-based applications potentially enabling an increased production efficiency of high value/ low volume cellular compounds, without the need for genetic modification of the organisms. Growth stimulation might further be transferred to medical applications enabling efficient tissue and scaffold creation. Moreover, specific differentiation of stem cells might be achieved with a targeted abiotic sub-lethal stress induction, allowing for various application e.g. lab-grown meat and stem cell therapies.

The integration of downstream into upstream processing allowed up to $96.6 \pm 4.8\%$ of the free protein in *C. vulgaris* to be extracted by PEF. However, the cell viability after the treatment was negatively affected by the increased extraction rate. Nevertheless, a free protein extraction rate up to $29.1 \pm 1.1\%$ without a significant influence on microalgal growth after 168 h was achieved. In addition, the extraction efficiency, as well as microalgal growth, was not influenced by the repetition of the treatment. Further research in the field of cyclic extraction should focus on the selectivity of the process for specific soluble fractions e.g. extraction of pigments, proteins and bioactive substances. Thus, cascade processing of cellular biomass might be enabled within the upstream processing thereof. Further optimization of the process should focus on the best treatment window with regard to extraction rate and cell viability. Moreover, specific cultivation conditions might be suitable to increase the fraction of free proteins within the biomass, further increasing the efficiency of the process. Therefore, exclusion studies with molecules having a defined molecular weight and/or size might allow for the derivation of a relation between PEF parameters and extractable substances. This knowledge would not only be relevant

for cyclic extraction but also for applications around PEF in classical downstream processing. Thereby, the cascade processing could be further optimized and potentially allow for purification of substances within the process.

Additionally, sub-lethal stress induction via nsPEF might be a viable process to reduce the lag-phase after the cyclic protein extraction and thus bears the potential to increase the resource efficiency, economic viability, and affordability of the derived products. Furthermore, nsPEF might allow the extraction of soluble organelles' constituents into the intracellular matrix, which in turn could be extracted by subsequent PEF application focusing on the cell membrane.

Despite the promising direct applications of PEF/nsPEF shown within the presented thesis, the comprehensive system characterization and control might not only increase reproducibility and scalability of results and technology but enabling further applications within the food- and bioprocessing industry. Among these applications, the introduction of targeted molecules e.g. cryoprotectants and prebiotics and the facilitated extractability/accessibility of non-soluble substances after PEF/nsPEF treatment appear to be most relevant from the author's point of view. Moreover, PEF/nsPEF treatments could be combined with other chemical, mechanical or biological treatments increasing the efficiency and allowing for further selectivity of the process.

Hence, the presented thesis laid the foundation for promising applications of PEF/nsPEF in the bio-based industry, bearing the potential to be key processing steps toward more sustainable and efficient supply chains in order to meet the demands of a growing world population.

LIST OF FIGURES

Introduction

Figure 1: PEF parameter interconnectivity, adapted from (Jaeger, 2012). Reactor (green), electrical (yellow) and media (blue) parameters are shown. Within the whole process, all parameters are directly or indirectly linked to each other. 3

Figure 2: Electrical reference circuits and resulting pulse waveform for A) exponential decay pulse generator B) rectangular pulse generator C) Blumleingenerator and D) diode opening switch generator (Rebersek and Miklavčič, 2011)..... 4

Figure 3: The three main types of continuous PEF treatment chamber designs; parallel plate, co-axial and co-linear from left to right. The black arrows indicate the direction of the electric field whereas the white arrow indicates the flow direction (Toepfl et al., 2005). 6

Figure 4: PEF principle of action. A critical electric field has to be exceeded in order to induce permeabilization of the cells. The severity of PEF treatments depends on the difference between the critical electric field and the applied electric field (adapted from Toepfl, 2006). 16

Figure 5: Influence of pulse duration and amplitude on the induced effects ranging from electrophoresis (orange), electroporation of lipid membranes (red), dielectrophoresis (yellow) to reversible electroporation (green) and irreversible electroporation (blue) (adapted from Rebersek and Miklavčič, 2010). 17

Figure 6: Theoretical evaluation of the cells' membrane and organelles' membrane potential at different frequencies, the red area indicated the range in which the organelles' membrane potential exceeds the cells' membrane potential (adapted from Kotnik and Miklavčič, 2006). The results were obtained assuming a trapezoidal pulse shape with an electric field strength of 500 V/cm and an angle with respect to the angle of the electric field $\theta = 0$, for a cell diameter of 10 μm 18

Figure 7: Underlying cell properties explaining various cellular responses to different pulse length and amplitude configurations. A) A biological cell as an electric equivalent circuit between to electrodes. Membranes can be viewed as a capacitor whereas intra- and extracellular fluid represent a resistor (adapted from Schoenbach et al., 2004). B) Cellular properties affecting the transmembrane potential and thus PEF treatment outcome. 19

Figure 8: A case study of the microalgae *Chlorella vulgaris* SAG 211-12, illustrating treatment windows for selective inactivation, inactivation of microbial flora and *C. vulgaris*, continuous extraction of high value-added ingredients, and growth stimulation (Buchmann and Mathys, 2019). 20

Manuscript 1

M1 - Figure 1: Cuvette holder configuration with air surrounded conductive surface area (purple) of 48.80 cm^2 for the broad setup A) and 5.60 cm^2 for the narrow setup B), resulting from multiphysics simulation based optimization studies. 44

M1 - Figure 2: Voltage and current measurement obtained using the NPG-18/3500 generator with a pulse width of 5.56 ns and the broad cuvette holder configuration (Figure 1 A) using a 4 mm cuvette filled with NaCl solution I (Table 1).	48
M1 - Figure 3: Electric field strength simulated for the broad cuvette holder A) (Figure 1 A) and the narrow cuvette holder configuration B) (Figure 1 B) using electrostatic (es) physic interface in COMSOL multiphysics® simulation.....	49
M1 - Figure 4: Voltage and current measurement obtained by use of NPG-18/3500 generator with a pulse width of 5.56 ns and the narrow cuvette holder configuration (Figure 1 B) using a 4 mm cuvette filled with NaCl solution I (Table 1).	50
M1 - Figure 5: Resistance obtained by applying Ohm's law to the current and voltage measured (empty) using the narrow cuvette holder configuration compared to the theoretical resistance Eq. (2) (full). The pulses were delivered by use of the NPG 18-3500 generator with a pulse width of 5.56 ns. The values are derived for 4 mm and 2 mm electroporation cuvettes filled with NaCl solutions, as shown in Table 1, and the narrow cuvette holder configuration (Figure 1 B).....	50
M1 - Figure 6: Theoretical impedance (full) values derived by consideration of Eq. (21) compared with the measured results (empty) for 4 mm and 2 mm electroporation cuvettes filled with A) NaCl and B) KCl solutions according to Table 1 utilizing the NPG18-3500 pulse generator with a pulse width of 5.56 ns and the narrow cuvette holder configuration (Figure 1 B).....	52
M1 - Figure 7: Theoretical impedance (full) values derived by considering Eq. (22) compared with the measured results (empty) for 4 mm and 2 mm electroporation cuvettes filled with NaCl solutions, as shown in Table 1. The pulse generator FPG 10-1NL100 and pulse widths of 10 ns A), 20 ns B), 50 ns C) and 100 ns D), utilizing the narrow cuvette holder configuration (Fig. 1 B) were analyzed.....	53
M1 - Figure 8: Boxplot data for matched load conditions using 4 mm and 2 mm cuvettes filled with NaCl and KCl solutions in accordance with Table 1 for pulse widths below cutoff frequency of the RC element; the same letters indicate statistical significance ($p < 0.01$).	54
M1 - Figure 9: Resulting effects of nsPEF treatments at electric field strengths of $E_1 = 27.43 \text{ kV cm}^{-1}$ (Treatment T1), $E_2 = 39.64 \text{ kV cm}^{-1}$ (Treatment T2), and $E_3 = 49.79 \text{ kV cm}^{-1}$ (Treatment T3) of <i>Chlorella vulgaris</i> SAG 211-12. The effects were based on a 14 days revitalization ability of <i>C. vulgaris</i> according to Eq. (21) A), determination of CfU after 2 days of incubation B) and immediate vitality assessment of <i>C. vulgaris</i> , as determined by Eosin Y staining C); for figure B) the same letters indicate statistical significance ($p < 0.05$) and for figure C) no statistical significant difference was found.	56
 Manuscript 2	
M2 - Figure 1: Rheological measurement results for water and different <i>A. platensis</i> suspension concentrations, fitted with rheological equations. The viscosity increased for increasing concentrations. The suspensions exhibited a non-Newtonian, shear thinning behavior. In comparison, water showed Newtonian behavior, characterized by the horizontal line at viscosity $\mu = 0.001 \text{ Pa s}$	71

M2 - Figure 2: Relative viscosity $\mu_r = \mu/\mu_s$ of <i>A. platensis</i> suspensions as a function of their mass fractions, estimated by fitting the Krieger-Dougherty equation to the rheological data for shear rate $\dot{\gamma} = 5 \text{ s}^{-1}$, with the maximum mass fraction set to 0.43. The resulting intrinsic viscosity value $[\mu]$ equals 39.24. The relative viscosity increased exponentially as a function of its mass fraction.....	73
M2 - Figure 3: a) Ultrasonic Doppler velocity profiling (UVP) measurement and b) simulation results for water and suspensions with different <i>A. platensis</i> concentrations in the 10 mm diameter treatment chamber.....	74
M2 - Figure 4: Simulation results showing the effect of increasing inlet velocity u_0 on the velocity profiles in the parallel plate treatment chambers for a) <i>A. platensis</i> suspension of concentration 100 g L^{-1} in the 10 mm diameter parallel plate chamber and b) water in the 1 mm diameter parallel plate chamber.....	75
M2 - Figure 5: Simulation results showing the effect of increasing viscosity, according to Fig. 1, on the velocity profiles in the treatment chambers for different concentrations of <i>A. platensis</i> suspensions for the a) 10 mm and b) 1 mm diameter parallel plate chambers.	77
M2 - Figure 6: Simulated distribution of specific energy input across treatment chambers for parallel plate and co-linear geometries, both with 4 mm diameter and assuming the viscosity of water. All other parameters (inlet velocity, electric potential, pulse width, pulse repetition rate, and medium conductivity) were also kept equal for both treatment chambers (Table 2). The dotted (· ·) line represents the energy input distribution in the co-linear chamber when assuming an average or uniform flow field and only considering the nonuniform electric field. The dashed (- -) line represents the energy input in a batch parallel plate system with no flow and a uniform electric field.....	79

Manuscript 2 – Unpublished Results

M2U - Figure 1: Distribution of the specific energy input across parallel-plate and co-linear treatment chambers, all with a diameter of 4 mm. The reference simulation (parallel-plate turbulent) is thereby compared to previous simulations conducted by Buchmann et al. (2018). In all simulations, the viscosity of water (0.001 Pas) was assumed and electric potential, pulse width, pulse repetition rate, medium conductivity were kept constant. Corresponding values are listed in Table 1, column reference.	89
---	----

Manuscript 3

M3 - Figure 1: Reference 100 ns pulse as applied in the experiments.....	97
M3 - Figure 2: Percentage difference in dry substance five days after the nsPEF treatment between treated and untreated <i>Arthrospira platensis</i> solutions with varying time intervals between inoculation and nsPEF treatment. The illustrated results were obtained for an energy input of $3 \cdot 256.22 \pm 67.53 \text{ J kg}^{-1}$ as shown in Table 1 and the experimental procedure stated in Section 2.1.	103

M3 - Figure 3: Percentage difference in dry substance A) between treated and untreated <i>Arthrospira platensis</i> solutions after 5 days of cultivation. The stated energy input is only depending on the pulse repetition frequency and represents a single treatment (Table 1), which was repeated three times, with time intervals of three hours. The allophycocyanin (aPC) and C-phycoerythrin (cPC) concentration difference on the fifth day for $256.22 \pm 67.53 \text{ J kg}^{-1}$ is shown in B).	105
M3 - Figure 4: Percentage difference in dry substance after application of the same energy input by single treatment ($780.44 \pm 206.74 \text{ J kg}^{-1}$) compared to three uniform treatments ($3 \cdot 256.22 \pm 67.53 \text{ J kg}^{-1}$) performed as in Section 2.1. The single energy application was achieved by a reduction of the residence time t (s), while keeping all other parameters constant (Table 1).	106
M3 - Figure 5: Growth monitoring of <i>Arthrospira platensis</i> culture during experimental procedure, by measuring DS and OD measurement at 750 nm.....	106
M3 - Figure 6: Peak-to-baseline voltage amplitude of untreated and treated <i>Arthrospira platensis</i> cells measured between 100 kHz and 10 MHz.....	107
 Manuscript 4	
M4 - Figure 1: Process to determine bubble diameter and counts for bubble size distribution (BSD). The microscopic image a) was postprocessed b) and automatically analyzed by the software Bubble Detect c).	123
M4 - Figure 2: ζ -potential of the <i>Arthrospira platensis</i> isolate (API) extracted from commercial powder and dissolved in aliquots of 50 mM phosphate buffer ranging from pH 2 to 11 at room temperature.	124
M4 - Figure 3: Surface tension over time for the <i>Arthrospira platensis</i> isolate (API), crude <i>Arthrospira platensis</i> powder (CP) and whey protein isolate (WPI) at a concentration of 0.1% weight per volume for pH 3, pH 7 and pH 10.	126
M4 - Figure 4: Surface activity of the nanosecond pulsed electric field treated self-cultivated <i>Arthrospira platensis</i> (treated) and untreated self-cultivated <i>Arthrospira platensis</i> (control) compared to <i>Arthrospira platensis</i> isolate (API) at a concentration of 0.1% weight per volume at pH 7 and 10.....	127
M4 - Figure 5: a) Overrun and b) median d_{t_0} immediately after foaming for the <i>Arthrospira platensis</i> isolate (API), crude <i>Arthrospira platensis</i> powder (CP) and whey protein isolate (WPI) over the investigated pH range.	128
M4 - Figure 6: Bubble size distribution of crude <i>Arthrospira platensis</i> powder (CP), <i>Arthrospira platensis</i> isolate (API) and whey protein isolate (WPI) over time and at different pH values. Medians are estimated from all replicates at once and interconnected between the different time points. The box width includes all data points within the 10 th and 90 th percentiles. Time points correspond to t_0 immediately after foaming, t_{20} after 20 min and t_{60} after 60 min. The distribution for the WPI at t_{60} at pH 3 is not shown as the foam completely disappeared.	132

M4 - Figure 7. Macrostructure of foams created at pH 3, 7 and 10 at t_0 immediately after foaming, t_{20} after 20 min and t_{60} after 60 min for *Arthrospira platensis* isolate (API), crude *Arthrospira platensis* powder (CP), and whey protein isolate (WPI). A total of 10 mL algae with 50 mM phosphate buffer was foamed at a powder concentration of 1% weight per volume for 60 s using a milk frother..... 133

Manuscript 5

M5 - Figure 1: Extractable protein concentration dependence of *Chlorella vulgaris* growth state with an electric field strength of 20 kV cm^{-1} and two applied pulses resulting in an energy input of $7.76 \pm 0.04 \text{ kJ kg}_{\text{Sus}}^{-1}$ 148

M5 - Figure 2: Comparison of the overall extracted protein concentration by HPH at 100 MPa and PEF treatments at 20 kV cm^{-1} over the cultivation cycle of *Chlorella vulgaris*..... 149

M5 - Figure 3: Protein extraction for two applied pulses at an electric field strength of 10, 15 and 20 kV cm^{-1} resulting in 1.94 ± 0.01 , 4.37 ± 0.02 and $7.76 \pm 0.04 \text{ kJ kg}_{\text{Sus}}^{-1}$, respectively, and three subsequent PEF treatment cycles with 168 h of cultivation in-between..... 151

M5 - Figure 4: Algae recovery levels after a) the first and b) the second PEF cycle with two applied pulses at an electric field strength of 10, 15 and 20 kV cm^{-1} , resulting in 1.94 ± 0.01 , 4.37 ± 0.02 and $7.76 \pm 0.04 \text{ kJ kg}_{\text{Sus}}^{-1}$, respectively, in comparison to the control. 152

M5 - Figure 5: Free protein extraction rate (full) and recovery rate (hollow) for PEF treatments in a) phosphate buffered saline (PBS) and b) DSN cultivation medium, at theoretical equal PEF parameters (Table 1)..... 155

M5 - Supplementary Figure 1: Microscopic analysis of *Chlorella vulgaris* a) prior and b) after two subsequent high-pressure homogenization passes. 158

Perspective

P - Figure 1: Exemplary working principle of PEF/nsPEF based processing of cultivated cells and their respective effects. 165

P - Figure 2: Case study of the microalgae *Chlorella vulgaris* SAG 211-12, illustrating treatment windows for selective inactivation, inactivation of microbial flora and *C. vulgaris*, continuous extraction of high value-added ingredients, and growth stimulation. 173

LIST OF TABLES

Introduction

Table 1: Literature overview of pulsed electric field applications in the food- and bioprocessing industry, focused on main research areas and reported PEF parameters and different organisms within the investigated research fields of this thesis..... 22

Manuscript 1

M1 - Table 1: Resulting conductivity σ for NaCl and KCl solutions used to assess system behavior resulting from nanosecond pulsed electric field applications, based on saline concentration c differences. 44

M1 - Table 2: Resulting conductivity σ for NaCl and KCl solutions used to assess system behavior resulting from nanosecond pulsed electric field applications, based on saline concentration c differences. 46

M1 - Table 3: Electric conductivity σ and resulting relative permittivity ϵ_r for saline solutions of NaCl and KCl based on (Blüh, 1924) 52

Manuscript 2

M2 - Table 1: Values for yield stress τ_0 times shear rate $|\dot{\gamma}|^{-1}$, flow consistency index K , and flow behavior index n of *A. platensis* suspensions obtained from the Herschel-Bulkley and non-Newtonian power law fits on the rheological measurements. 72

M2 - Table 2: Parameters used for the calculation of the energy input distribution in the parallel plate and co-linear treatment chamber geometries. The electric potential U , the pulse width τ_p , the medium conductivity σ , the pulse repetition frequency f and the treatment chamber diameter D_{in} were all defined the same for both treatment chamber geometries, providing the same conditions for both chambers in order to make the results comparable. Due to the differences in geometry, the treatment chamber length L was larger for the parallel plate chamber than for the co-linear chamber. 78

Manuscript 2 – Unpublished Results

M2U - Table 1: Evaluated parameters for nsPEF system optimization focused on growth stimulation according to Buchmann et al., (2019), with reference *Arthrospira platensis* concentrations of 0, 5 and 25 g L⁻¹ as a model system according to Buchmann et al., (2018). Different scale-up scenarios were analyzed for a throughput of around ≥ 100 L h⁻¹. In addition, a Reference treatment chamber was analyzed in order to have a direct comparison to the results obtained from Buchmann et al., (2018b). 88

Manuscript 3

M3 - Table 1: Experimental parameters used in the analyzed nsPEF treatments. With electric field strength E (kV cm^{-1}), pulse duration τ_p (ns), conductivity σ (mS cm^{-1}), frequency f (s^{-1}), residence time t (s), number of applied pulses n (–), and specific energy input W_s (J kg^{-1}). The specific energy input is stated for a single treatment. 104

Manuscript 4

M4 - Table 1: Overview of the raw material name and source with the corresponding abbreviation..... 119

M4 - Table 2: Foaming characteristics of different samples at pH 3, 7 and 10 at t_0 immediately after foaming, t_{20} after 20 min and t_{60} after 60 min, ^a means significantly different from whey protein isolate (WPI), ^b means significantly different from crude *Arthrospira platensis* powder (CP) on a Scheffé corrected p-value < 0.05 after pairwise comparison with contrasts..... 129

Manuscript 5

M5 - Table 1: Resulting energy inputs for different electric field strengths and incubation fluids in PEF treatments using a 2 mm electroporation cuvette, with electric field strength E (kV cm^{-1}), conductivity σ (mS cm^{-1}), number of pulses n (–) and energy input W ($\text{kJ Kg}_{\text{Sus}}^{-1}$)..... 146

M5 - Table 2: Significantly increased proteins in the supernatant of HPH-treated *Chlorella vulgaris* in comparison to PEF-treated samples, analyzed by a proteomic shotgun analysis..... 150

M5 - Table 3: Free protein extraction and recovery rate for multiple extraction cycles at theoretical electric field strengths of 10, 15 and 20 kV cm^{-1} . The same letters indicate nonstatistical significance at a 95% confidence interval for the free protein extraction rate over the three extraction cycles. 153

M5 - Table 4: Cyclic extraction factor depending on the PEF parameters as well as the treatment and incubation fluid. Specific energy inputs for the individual experiments are shown in Table 1..... 156

CURRICULUM VITAE

Leandro Buchmann

Born 14 December 1991 from Hinwil ZH, Switzerland

Education

- 2017-2020 **Doctor of Science in Sustainable Food Processing**
Laboratory of Sustainable Food Processing
Institute of Food, Nutrition and Health
Department of Health Sciences and Technology
ETH Zurich, Switzerland
Awards:
MERCATOR POSTER PRIZE (2017) at the World Food System
Centre Symposium
GNT YOUNG SCIENTIST AWARD (2018) at the 32nd EFFoST
International Conference
- 2015-2017 **Master of Science ETH in Food Science**
Major Food Processing, Minor Food Biotechnology
Department of Health Sciences and Technology
ETH Zurich, Switzerland
Master Thesis:
*Development of a high voltage nanosecond pulsed electric
field reactor for sub-lethal cell stress applications*
- 2011-2015 **Bachelor of Science ETH in Food Science**
Department of Health Sciences and Technology
ETH Zurich, Switzerland
- 2004-2010 **High School Diploma**
Bündner Kantonsschule, Chur

Publications

1. Buchmann, L., Mathys, A., 2019. Perspective on Pulsed Electric Field Treatment in the Bio-based Industry. *Front. Bioeng. Biotechnol.* 7, 265.
<https://doi.org/10.3389/fbioe.2019.00265>
2. Haberkorn, I., Buchmann, L., Hiestand, M., Mathys, A., 2019. Continuous nanosecond pulsed electric field treatments foster the upstream performance of *Chlorella vulgaris*-based biorefinery concepts. *Bioresour. Technol.* 293, 122029.
<https://doi.org/10.1016/j.biortech.2019.122029>
3. Buchmann, L., Bertsch, P., Böcker, L., Krähenmann, U., Fischer, P., Mathys, A., 2019. Adsorption kinetics and foaming properties of soluble microalgae fractions at the air/water interface. *Food Hydrocoll.* 97, 105182.
<https://doi.org/10.1016/j.foodhyd.2019.105182>
4. Buchmann, L., Brändle, I., Haberkorn, I., Hiestand, M., Mathys, A., 2019. Pulsed electric field based cyclic protein extraction of microalgae towards closed-loop biorefinery concepts. *Bioresour. Technol.* 291, 121870.
<https://doi.org/10.1016/j.biortech.2019.121870>
5. Buchmann, L., Frey, W., Gusbeth, C., Ravaynia, P.S., Mathys, A., 2019. Effect of nanosecond pulsed electric field treatment on cell proliferation of microalgae. *Bioresour. Technol.* 271, 402–408.
<https://doi.org/10.1016/j.biortech.2018.09.124>
6. Buchmann, L., Bloch, R., Mathys, A., 2018. Comprehensive pulsed electric field (PEF) system analysis for microalgae processing. *Bioresour. Technol.* 265, 268–274.
<https://doi.org/10.1016/j.biortech.2018.06.010>
7. Buchmann, L., Böcker, L., Frey, W., Haberkorn, I., Nyffeler, M., Mathys, A., 2018. Energy input assessment for nanosecond pulsed electric field processing and its application in a case study with *Chlorella vulgaris*. *Innov. Food Sci. Emerg. Technol.* 47, 445–453.
<https://doi.org/10.1016/j.ifset.2018.04.013>
8. Hörmansperger, J.T., Buchmann, L., Merz, S., Schmitt, R., Beyrer, M., Windhab, E.J., 2016. Microbial decontamination of porous model food powders by Vacuum-Steam-Vacuum treatment. *Innov. Food Sci. Emerg. Technol.* 34, 367–375.
<https://doi.org/10.1016/j.ifset.2015.12.027>